UC Davis

UC Davis Electronic Theses and Dissertations

Title

Decoding the mechanisms of MAP kinase-mediated dynamic signaling for control of cellular processes

Permalink

https://escholarship.org/uc/item/060969hk

Author

Ram, Abhineet Rajnal

Publication Date

2023

Peer reviewed|Thesis/dissertation

Decoding the mechanisms of MAP kinase-mediated dynamic signaling for control of
cellular processes

By

ABHINEET RAJNAL RAM
DISSERTATION

Submitted in partial satisfaction of the requirements for the degree of

DOCTOR OF PHILOSOPHY

in

Biochemistry, Molecular, Cellular, and Developmental Biology

in the

OFFICE OF GRADUATE STUDIES

of the

UNIVERSITY OF CALIFORNIA

DAVIS

Approved:

_____

Dr. John Albeck, Chair

_____

Dr. Ken Kaplan

_____

Dr. Chang-il Hwang

Committee in Charge

2023

To those who prove that success is not solely a product of innate abilities but is cultivated through resilience, unyielding spirit, and a bit of luck.

Contents

List of Figures

Decoding the mechanisms of MAP kinase-mediated dynamic signaling for control of
cellular processes

Abstract

Extracellular-signal regulated kinase (ERK) has long been studied as a key molecule in cellular homeostasis. ERK is a driver of essential cellular processes and is often dis-regulated in human diseases. A persistent question has been how a single pathway is able to direct multiple cell behaviors, including growth, proliferation, and death. Modern biosensor studies have revealed that the temporal pattern of ERK activity is highly variable and heterogeneous, and critically, that these differences in dynamic signaling mediate cell fate. This dissertation discusses the current understanding of dynamic activity in the ERK pathway, how it regulates cellular decisions, and how these outcomes lead to tissue regulation and pathology. Furthermore, I address the question of how the ERK pathway exerts distinct and context-specific effects on multiple processes. In brief, the dynamics of ERK activity induce selective changes in gene expression programs which induces subsequent changes in cellular behavior. In my research study, I combine an ERK biosensor approach with multiplexed measurement of downstream target proteins to ask how well ERK activation correlates to protein expression at the single-cell level. This analysis produces a model that can distinguish different classes of ERK dynamics within a heterogeneous population, providing a tool for assaying ERK dynamics within fixed tissues. By understanding the dynamic mechanisms involved in ERK signaling, there is potential for improving detection of oncogenic behavior, and adopting pharmacological strategies that not only inhibit ERK, but also restore functional activity patterns and improve disease outcomes.

Acknowledgments

I would like to express my gratitude and appreciation to my amazing mentor, Dr. John Albeck. His unwavering support, insightful advice, and constant encouragement were the cornerstone of my success in this program. I am also incredibly thankful to my lab-mates, who have been an essential source of inspiration and motivation throughout this journey. I am grateful for their input on my work and the engaging conversations we shared, which pushed me to explore new ideas and perspectives. In particular, Dr. Michael Pargett, Dr. Taryn Gillies, Dr. Carolyn Teragawa, and Dr. Alex Davies have been invaluable mentors and collaborators, whose guidance and expertise have helped me navigate the challenges of my research. My friends Devan Murphy and Emel Akdoğan provided academic, scientific, and moral support which greatly influenced my mental health throughout graduate school. I would like to extend my heartfelt gratitude to my parents, Yogendra and Geeta Ram, and my brother Abishek Ram. I could not have achieved this without their constant support. Furthermore, I would like to express my appreciation to my partner, Hisani Stenson, for her incredible support and belief in me. Her encouragement has been a source of constant inspiration, and I am deeply grateful for her love.

Chapter 1

Introduction

1.1 Preface

This introductory chapter provides a brief, broad, and layperson's overview of the biology of MAP Kinase signaling. The aim of this chapter is to educate readers who are not well versed in biology and to explain the basic concepts needed to understand the entirety of this dissertation.

1.2 Abstract

Cells are the basic unit of life and how they are maintained is crucial to human health. Maintenance involves multiple cellular processes which have to be precisely timed and regulated. These processes involve movement, creating new cells, or using different cell types for various functions. One of the most important molecules for these processes is Extracellular signal-regulated kinase (ERK). This chapter discusses how ERK is at the center of these cellular functions and provides a brief background into the research presented in the subsequent chapters.

1.3 Cells use signaling pathways for homeostasis

The human body is composed of cells that coordinate together to allow us to breath, move, heal, and think. Not only do cells work together, they must also function independently to maintain themselves or sense changes in the body. This process is referred to as maintaining "homeostasis." One of the main questions that this work seeks to address is how do cells maintain homeostasis? Cells must grow, multiply (proliferate), or die in a precisely regulated manner, which allows for the body to function normally. In other words, if there is damage to the body (e.g. a cut on the skin), the skin cells will grow to heal the wound. Alternatively, if a cell is damaged, it must kill itself to prevent further problems. These are complicated cellular processes that cells execute by using signaling pathways (Lodish et al. 2000).

1.4 What are signaling pathways?

Cells are made of molecules, sugars, and fats which all contribute to how a cell functions. A specific type class of molecules are called proteins. There are many different types of proteins, and they play a critical role in the structure and function of cells. Proteins can be enzymes which break down sugars or catalyze other types of biochemical reactions, they can replicate DNA, and can even generate force to move other proteins around the cell. Proteins are the core components of signaling pathways. There are different types of proteins within these pathways, however, the most essential parts are receptors, enzymes, and transcription factors. Receptors are proteins that reside on the outer surface of the cell, and allow the cell to sense its surroundings. There are many types of receptors, each of which can uniquely identify different molecules that surround the cell. Once a receptor attaches to (binds) another molecule (ligand), this is perceived as a signal and other proteins will react to this message. Each receptor is wired to its own specific set of downstream proteins. Once a signal

is perceived, a set of proteins will interact with each other, and carry (transmit) the signal into different parts of the cell, hence why this is referred to as a signaling pathway. Enzymes help transmit the signal from the receptor by modifying other proteins. In many cases, several enzymes sequentially act on other enzymes, where one enzyme modifies another, and so on. Ultimately, the signal will be transmitted into the nucleus of the cell, where transcription factors will trigger the creation of other proteins (transcription). Once these new proteins are completely synthesized (translation), they will go on to execute their specific tasks. Signaling pathways consist of unique sets of proteins that act as controllers of other proteins, thereby regulating specific cellular functions (Alberts et al. 2014).

1.5   The central dogma

To better comprehend the work presented in this dissertation, it is important to understand a few core principles of biology. Firstly, cells are bags of proteins. While there are many other parts of a cell, proteins provide structure and function to a cell. Proteins reside in three main parts of a cell, the membrane, the nucleus, and the cytoplasm. The cellular membrane separates the outside of the cell from the inside, keeping unwanted molecules out, and letting wanted molecules in (i.e. oxygen and nutrients). The cytoplasm is the fluid-like substance inside of the cell containing nutrients, proteins, and other components of the cell (organelles). Finally, the nucleus is an organelle that is itself a bag within the cell; it houses the DNA.

Deoxyribonucleic acid (DNA) is often described to non-biologists as "the blueprint of life." To be more specific, DNA is the blueprint for proteins. Each protein has its own design written in DNA, which is known as a gene. Humans have over 20,000 genes; therefore, there are over 20,000 different proteins. Proteins originate from DNA, and there are steps that involve reading the blueprint, and building each protein from smaller molecules. When

synthesizing a new protein, other proteins read DNA and create simpler blueprints called mRNA molecules. This process is deemed DNA transcription. mRNA is similar to DNA; however, it is much smaller and can be transported outside the nucleus. Once mRNA is transcribed, a new protein is produced by reading the mRNA molecule; this is referred to as mRNA translation. The central dogma of biology explains the process of turning DNA into mRNA, and turning mRNA into proteins. These steps are also known collectively as gene expression (Lodish et al. 2000).

1.6 The Ras/MAP Kinase pathway

The research conducted in this dissertation focuses on one of the most important signaling pathways in cell biology: the Ras/MAP Kinase pathway or the Ras/ERK pathway. This pathway is essential for cells and a functioning organism because it mainly controls cell division (proliferation) and cell survival. Furthermore, the Ras/MAP Kinase pathway is unique due to its role in additional cellular processes such as cell death, or turning one cell type into another (cell differentiation). The ability to control multiple, different processes is another reason why this pathway is highly studied. The core proteins of the pathway are named Epidermal Growth Factor Receptor (EGFR), Ras, RAF, MEK and ERK. EGFR is a receptor that recognizes extracellular molecules that may be secreted from other cells. Another important protein, Ras, is a molecular switch which turns on when EGFR is bound to a molecule such as Epidermal Growth Factor (EGF). Once Ras is switched on, it will lead to a specific chemical modification in RAF known as a phosphorylation. RAF, along with MEK and ERK, are enzymes that switch into active enzymes when they are phosphorylated. Interestingly, these enzymes will modify other proteins by phosphorylating them. Hence, they are switched on by phosphorylation, and will phosphorylate other proteins; these proteins are known as kinases. Overall, the pathway activates once the receptor binds a ligand,

Ras becomes activated which in turn activates RAF, then RAF phosphorylates MEK, MEK phosphorylates ERK, and ERK phosphorylates many other proteins. These proteins include transcription factors, which are proteins that help begin the transcription of genes (Alberts et al. 2014).

1.7   ERK is the main character

ERK is the most important kinase of the pathway because it directly phosphorylates over 1000 different proteins, depending on the signal at the initiation of the pathway and the state of the cell. This seemingly allows the pathway to control several cellular processes with just one central kinase. A fundamental question in the Ras/ERK field is how ERK regulates different cellular outcomes, and how ERK decides which process to initiate. This question is discussed in depth in the subsequent chapters of this dissertation. Broadly, the current understanding is that different ERK targets are phosphorylated depending on the stimulus that activates the pathway. ERK can rapidly switch between active and non-activated states, which becomes a mechanism to control the rate of production of different genes. Importantly, the strength of ERK activation is also dependent on the initial stimuli. By varying the strength of activity, genes become produced at varying amounts. Certain extracellular stimuli trigger specific patterns of ERK activation, which leads to different sets of genes being produced in the cell. Subsequently, these genes continue on to control unique cellular processes (Lavoie, Gagnon, and Therrien 2020).

The most classic example of this signal transmission was shown by giving rat cells (grown in plastic dishes) two different growth factors, Epidermal growth factor (EGF) or Nerve growth factor (NGF). Cells treated with NGF undergo a long and sustained activation of ERK, while EGF triggers only a short burst of ERK activation. As a consequence of sustained ERK, cells differentiate into a different cell type (Gotoh et al. 1990; Nguyen et

al. 1993; Traverse et al. 1992). In contrast, the transient ERK activation by EGF causes cells to divide instead of differentiate (Marshall 1995). The sustained ERK activation causes accumulation of the proteins: c-Fos, c-Jun, and others which subsequently leads to cell differentiation (Eriksson, Taskinen, and Leppä 2007; Murphy et al. 2002). It was previously thought that only EGF and NGF were stimulating different pathways to induce the two cell fates. However, the above work demonstrates that the growth factor signal is encoded by different patterns of ERK activation.

1.8   Why study the ERK pathway?

ERK drives cell proliferation, and mutations in ERK or other parts of the pathway lead to uncontrolled cell division. This is the basis of cancer and why the Ras/MAP Kinase pathway is highly researched. Understanding the biology of the pathway in both normal and cancer cells has helped develop many drugs that target specific proteins in the pathway. Furthermore, there are several developmental disorders that ERK plays a role in. These disorders are known as RASopathies and studying them will help identify better prevention and treatments (Tidyman and Rauen 2009).

1.9   How ERK mediates several cell processes

As previously stated, a core question this work answers is how ERK controls cellular processes. This question is addressed with two chapters that cover previous work on this topic, and another chapter which presents new research conducted with cutting edge methods. Firstly, ERK undergoes intricate patterns of activation as a mechanism to create different signals depending on the context of the cell. While there are many reviews that discuss this process, few emphasize research that conducts mathematical modeling, which involves

representing the Ras/MAP kinase pathway as equations and quantitatively describing the interactions in the system. Chapter 2 provides an in depth review of the history of ERK biology, specifically describing ERK behavior and how it can undergo complex patterns of activation. One of the more recent advances in the field of ERK biology is the use of single-cell biosensors. These are tools that allow researchers to measure ERK activation in live cells over time. Chapter 2 also discusses the different forms of ERK activation patterns that have been observed using biosensors.

In the past decade, live-cell biosensors have revealed dynamic patterns of ERK signaling that occur in many different cells and tissues. These ERK patterns are associated with changes in gene expression, and chapter 3 provides an in depth description of this topic. Additionally, chapter 3 describes how ERK alters cellular processes and regulates tissues. This chapter also discusses how ERK is dysregulated in cancer and developmental diseases. Finally, chapter 4 is a research study on the effect of ERK activation on eight genes that are directly or indirectly regulated by ERK. No study to our knowledge has measured live-cell ERK signaling and measured the protein levels of many genes downstream of ERK in the same, individual cell. Furthermore, activation of the ERK pathway is typically assayed by measuring phosphorylated ERK. Live-cell biosensors have made measurements more accurate, but are not always feasible. Therefore, we set out to find other proteins that capture ERK dynamics, which can serve as alternative measurements to assay ERK activity. These results will improve detection of abnormal ERK behavior in disease settings.

1.10 Appendices

The appendix of this dissertation contains three projects related to the Ras/MAP Kinase pathway. Appendix A displays preliminary results showing the c-Jun, a target of several MAP Kinases, is highly dynamic in basal settings. It demonstrates oscillations in its ex-

pression, an observation that has not previously been shown. Appendix B, is a commentary article written about a recent study from the lab of Olivier Pertz. This study investigates the spatial patterns of ERK observed during embryonic development. Finally, appendix C is a methods chapter describing how to quantitatively investigate paracrine signaling in the Ras/MAP Kinase pathway.

Chapter 2

Models and Mechanisms Driving Intricate Patterns of ERK Activity

2.1 Preface

This chapter was originally submitted to *The Biochemical Journal* on May 30th, 2023, as part one of a two part review on ERK dynamics: Abhineet Ram, Devan Murphy, Nicholaus DeCuzzi, Madhura Patankar, Jason Hu, Michael Pargett, and John Albeck. A Guide to ERK Dynamics, part 1: Models, Mechanisms, and Mayhem.

J.A. conceptualized and the review and contributed to the text. A.R., D.M., N.D., MaP., contributed to the writing and editing the text. Mi.P. assisted with reviewing sections of the text. J.H. created all figures.

The article has been modified to satisfy the formatting requirements of this dissertation.

2.2 Abstract

Extracellular-signal regulated kinase (ERK) has long been studied as a key driver of both essential cellular processes and disease. A persistent question has been how a single pathway is able to direct multiple cell behaviors, including growth, proliferation, and death. Modern biosensor studies have revealed that the temporal pattern of ERK activity is highly variable and heterogeneous, and critically, that these differences in dynamic signaling mediate cell fate. This two-part review discusses the current understanding of dynamic activity in the ERK pathway, how it regulates cellular decisions, and how these outcomes lead to tissue regulation and pathology. In part 1, we cover the optogenetic and live-cell imaging technologies that first revealed the dynamic nature of ERK, as well as, current challenges in analysis of the resulting data. While hurdles still remain, it is clear that higher temporal and spatial resolution provides mechanistic insights on pathway circuitry. We also discuss the mathematical models that describe ERK dynamics, including receptor-level regulation, negative feedback, cooperativity, and paracrine signaling. Alongside improvements in experimental capabilities are the advancement of computation models that arise from this type of data. Exciting new algorithms and advanced computational tools enable quantitative measurements of single-cell ERK activation, which in turn inform better models of pathway behavior. However, the fact that current models still cannot fully recapitulate the diversity of ERK responses calls for a deeper understanding of network structure and signal transduction.

2.3 Introduction

The extracellular signal regulated kinase (ERK) pathway (2.1) plays a widespread role in the development and physiology of animals (Lavoie et al., 2020). ERK is a member of the mitogen-activated protein kinase (MAPK) family, which is found in all eukaryotes. Among
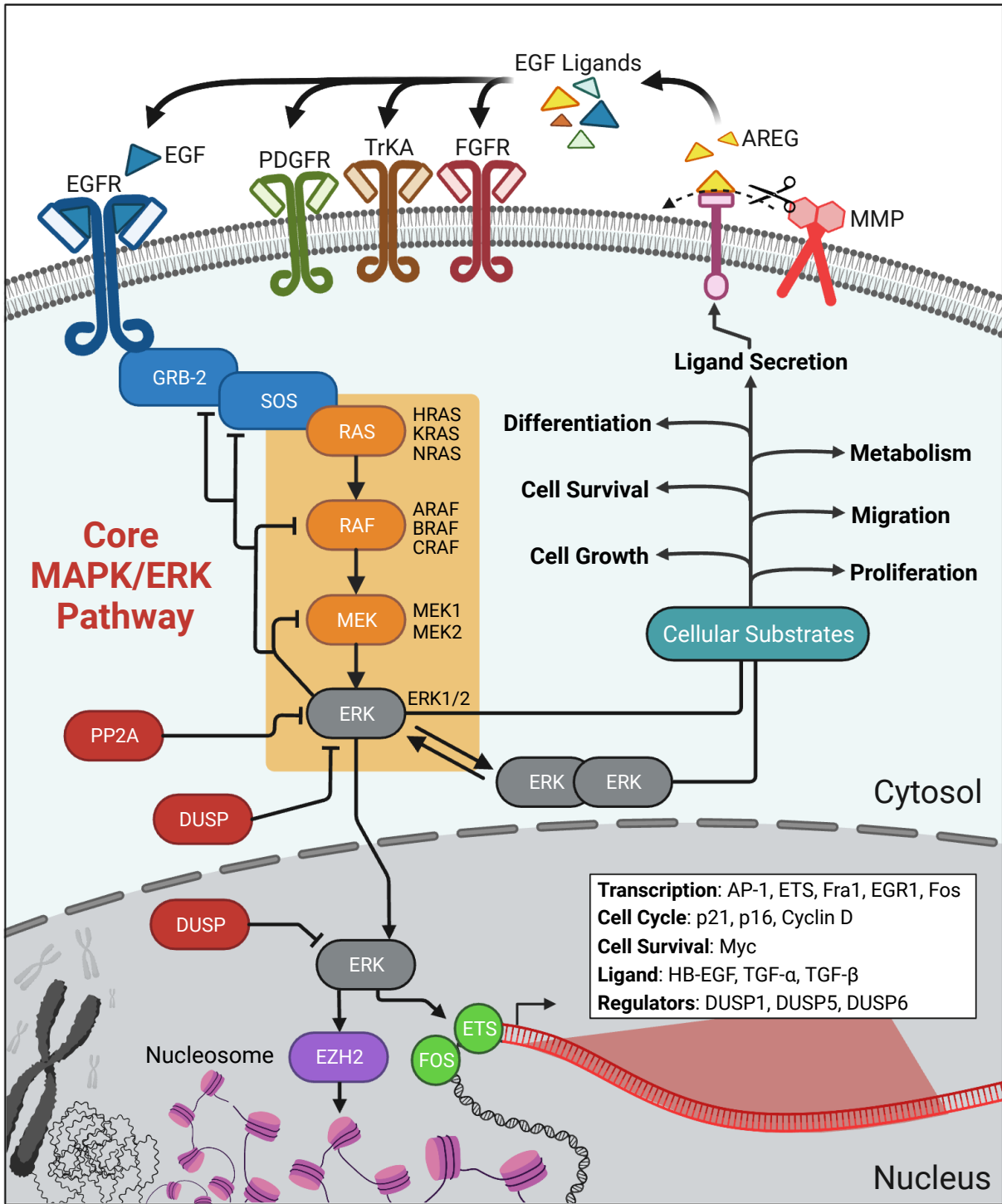
Figure 2.1 The central ERK signaling pathway

Figure 2.1: The central ERK signaling pathway **a** Initiation of the MAPK/ERK pathway begins with ligand binding of tyrosine receptor kinases (RTKs). This begins the phosphorylation cascade and activation of the core MAPK/ERK pathway consisting of RAS, RAF, MEK, and ERK (blue box, individual isoforms are listed). Active ERK either translocates to the nucleus where it stimulates gene expression, or dimerizes and phosphorylates cytoplasmic substrates. Depending on ERK dynamics, several gene programs are activated including cell cycle, cell survival, pathway regulation, and ligand production (pathways bolded and specific genes listed in the box within the nucleus). Outside the nucleus, ERK regulates cytoplasmic proteins involved in cell growth, metabolism, and differentiation. Pathway termination is regulated by numerous phosphatases (PP2A and DUSPs), as well as several negative feedback loops. For a more comprehensive illustration see Lavoie review (Lavoie et al., 2020). This complex network regulates ERK dynamics and is responsible for driving many cellular behaviors.

the MAPK family, ERK has received a disproportionate amount of attention, owing to its essential involvement in many processes that impact human health. ERK activity is required for the proliferation of cancer cells, the formation of memory by neurons, and morphological changes in development, among many other examples. Compared to its close MAPK relatives, JNK and p38, ERK shows a unique propensity for dynamic fluctuations in activity over time (Regot et al., 2014). These dynamics arise from the regulatory topology of the pathway, which includes numerous feedback loops. It has been recognized for two decades that the frequency, duration, and amplitude of ERK activation are important in determining its effect on the cell (Ebisuya et al., 2005).

Several early studies laid the conceptual groundwork for understanding the importance of ERK dynamics. In the 1990s, observations from several groups first established a relationship between ligand stimulation, the timing and duration of ERK activity, and cell fate (Wells et al., 1990). Manipulating ERK activation patterns by different growth factors, receptor expression levels, or oncogenic mutants led to alternate cell fates (Marshall, 1995). In parallel, Ferrell *et al.* showed that MAPK activation occurs in a highly switch-like manner in individual Xenopus oocytes (Ferrell and Machleder, 1998). These results demonstrated that a pathway's output does not necessarily operate as a simple linear response to stimuli,

but instead is shaped heavily by feedback, especially when viewed at the single-cell level (C. Y. Huang and Ferrell, 1996). Finally, it was found that the regulatory structure for a number of ERK target genes can make them sensitive to the duration of ERK activity (Cook et al., 1999; Murphy et al., 2002, 2004). Together, these concepts form the overarching framework for dynamics-based information encoding and decoding by the ERK pathway. In this review, we focus on the unique dynamic behavior observed for ERK and examine how it arises from the biochemical organization of the pathway. In a companion review (Insert reference to jointly submitted manuscript), we look further into the impact of ERK dynamics on downstream processes and cell phenotypes.

Mathematical models have played an essential role in the study of ERK, providing a way to test questions that are not accessible experimentally and to explore possible mechanisms for dynamic behavior. In general, the flux of protein-protein interactions and modifications in the pathway can be represented as a system of ordinary differential equations (ODEs), which simulate pathway dynamics under different conditions. Historically, Ferrell and colleagues used such models to understand how MAPK pathways could exhibit the observed non-linear responses without explicit cooperativity and positive feedback (C. Y. Huang and Ferrell, 1996). This behavior is termed zero-order ultrasensitivity and occurs for MAPK systems when both the kinase and the competing phosphatase are limited enough to be saturated (Ferrell and Ha, 2014). Subsequently, the question of how transient ERK behavior arises under constant stimuli led to an expansion of MAPK models. Early evidence implicated the internalization of the EGF receptor (Wiley et al., 1991), but it was also argued that transient assembly of signaling complexes at the EGF receptor could explain the observed transient kinetics (Kholodenko et al., 1999). Multiple models then began to explore the possibility of oscillations in activity due to feedback phosphorylation (Brightman and Fell, 2000; Kholodenko, 2000). Orton and colleagues elegantly summarize the early mathematical models of MAPK signaling (Orton et al., 2005), and the field of MAPK modeling continues to

evolve, exploring the complex effects of feedback and more subtle concepts such as buffering of ERK by its substrates (Ahmed et al., 2014). The concepts of transient, oscillatory, and excitatory behavior remain actively studied, especially with regard to distinguishing between the roles of true oscillations of the MAPK pathway and of pulsatile responses excited by fluctuating external stimulus. Throughout this review, we discuss the relevant mathematical models that can be used to understand the dynamic operation of the ERK pathway.

2.4   Forms of dynamic ERK activity

Experimentally observed ERK dynamics can be grouped into several major categories (Box 1), including sustained, transient, peak with sustain, oscillatory, sporadic, and complex. These categories are not rigid but provide a useful framework for discussing ERK activity over time. In early studies, the PC-12 rat pheochromocytoma cell line served as a useful model system, as it responds with ligand-specific ERK dynamics: sustained activity to NGF stimulation and transient activity to EGF (Cowley et al., 1994). Importantly, these dynamics have phenotypic consequences resulting in cell proliferation and differentiation, respectively. At the time, population-level assays, such as immunoblots, were only able provide rough estimates of ERK patterns, such as, sustained activation lasting several hours, or transient activation peaking at about 20 minutes before returning to baseline (Marshall, 1995; Muroya et al., 1992; Nguyen et al., 1993; Wells et al., 1990). More complex ERK dynamics such as oscillations were postulated (Kholodenko, 2000), but were only clearly observable with the development of fluorescent ERK biosensors (Green and Alberola-Ila, 2005; Harvey et al., 2008). These reporters are briefly summarized in the following section and have been reviewed in depth elsewhere (Nakamura et al., 2021).

Using live-cell reporters, Pertz and colleagues re-examined the classic PC-12 system, confirming the original findings from Marshall et al., but also uncovering substantial cell-to-cell

Box 1. Field Guide to Dynamic ERK Signaling
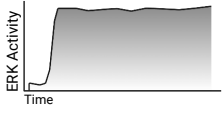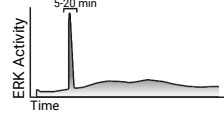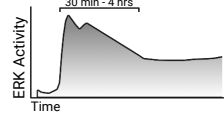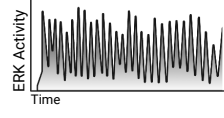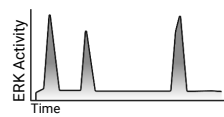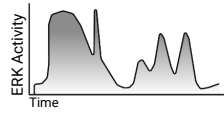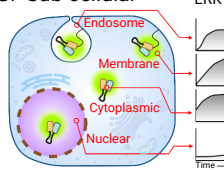
A. Sustained - Long Term

Sustained - Long Term: Continuous, near-maximal activation of ERK in response to a stimulus.

Pheochromocytoma PC-12 cells treated with 50 ng/mL NGF [5,24,52]

H1666 Cells treated with 10 ng/mL EGF [52,134]

TrkA expressing MCF10A treated with 50 ng/mL NGF [5,24,18,41]

WT HRAS expressing MEF cells treated with bFGF [73]

Possible Mechanisms: Stimulation of receptors with low internalization and weak negative feedback; activating oncogenes in the RAS/RAF/MEK cascade

B. Single Transient Peak

Short-Term Transient Peak: A single 5–20-minute ERK response to ligand-stimulation with minimal or no subsequent ERK activity for the duration of stimulation.

Pheochromocytoma PC-12 cells treated with 1 ng/mL EGF [5,24,52]

NIH 3T3 cells treated with 50 ng/mL Anisomycin [2]

WT HRAS expressing MEF cells treated with 100 ng/mL PDGF or IGF-1 [73]

Possible Mechanisms: Stimulation of receptors with high internalization rate or strong negative feedback.

C. Peak with Sustain

Peak with Sustain: A strong initial ERK activation peak that gradually decays to a steady-state.

Simulated HeLa cells treated with 0.5 ng/mL EGF [64]

A431 cells treated with 5nM EGF [62]

Pheochromocytoma PC-12 cells treated with 50 ng/mL NGF [24]

WT HRAS expressing MEF cells treated with 0.1 - 10 ng/mL EGF [73]

Possible Mechanisms: Stimulation of receptors with intermediate internalization and negative feedback strength.

D. Oscillatory

Oscillatory: Regular transient ERK activations, or "pulses" of ERK with a fixed period.

Simulated generic MAP Kinase [14,100]

NIH 3T3 cells treated with 25ng/mL bFGF [135]

184A1 cells treated with 1ng/mL EGF [25]

Mouse Embryonic Stem Cells exposed to 20ng/mL FGF [136]

Possible Mechanisms: Combination of positive cooperativity and negative feedback.

E. Sporadic Pulsing

Sporadic Pulsing: Intermittent pulses of ERK activity with similar amplitudes but irregular spacing, whose frequency increases with the concentration of stimulus.

MCF10A cells treated with 10-100 pg/mL EGF [26]

NRK-52E cells in normal culture medium (DMEM+10% FBS) [27]

Mouse epidermis in vivo, localized to regions where cell division events occur [92]

C. elegans vulval precursor cells during differentiation [137]

Serum starved MCF10A cells adjacent to a cell that undergoes apoptosis [138]

Possible Mechanisms: Paracrine signaling between cells via secreted EGFR ligands or other cytokines.

F. Complex Peaks

Complex Peaks: Dynamic ERK activity consisting of pulses with varying duration and amplitudes.

H1395 cells that obtained G469A BRAF mutation have aberrant ERK "off" kinetics, resulting in irregular dynamics compared to wt BRAF cells. [139]

HMT-3255 S1 cells treated with 100 ng/mL AREG [112]

MCF10A cells after induction of Oncogenic BRAF (V600E) [43]

Primary Mouse Keratinocytes, complete or growth factor-free media [140]

Possible Mechanisms: High levels of paracrine secretion; oncogenic mutations.

G. Sub-cellular

Sub-cellular ERK Dynamics: ERK activity can vary depending on the sub-cellular region where the activity is measured within the cell.

HEK293T cells expressing Plasma Membrane localized ERK reporter or Cytoplasmic localized ERK ERK reporter treated with EGF. Plasma Membrane ERK activity was sustained whereas cytoplasmic ERK activity was transient [31].

HEK293T expressing SNAP-β2AR and either cytoplasmic, plasma membrane, or endosome localized ERK reporter. When treated with 10uM adrenaline transient, none, and sustained ERK activity was observed for each reporter, respectively [141].

<u>Legend</u>

 Simulation   Biosensor   Western Blot   *C. elegans* Model   Mouse Model

Figure 2.2: Box 1: A field guide to ERK dynamic behaviors

variation (Ryu et al., 2015). This variation is extremely broad; Ryu *et al.* found both sustained and transiently responding cells at different proportions within any population of PC-12 cells, regardless of EGF or NGF stimulation. Further intricacies were revealed in the form of oscillations (Shankaran et al., 2009) and sporadic pulses (Albeck et al., 2013; Aoki et al., 2013) in growth factor-stimulated cells. The cell-to-cell variation also found in these systems made it clear why these diverse ERK activity forms were not measurable in immunoblot studies; because they occur asynchronously between cells, they are irrevocably blurred in the average of thousands of cells in an immunoblot sample. In addition to distinguishing single-cell variation, live-cell assays also provide much greater time resolution, allowing dynamics to be closely tracked on the scale of minutes for many hours or even days, in contrast to the small number of time points typically captured in an immunoblot.

The subcellular distribution of active ERK within a cell is also an important facet of ERK dynamics. ERK sequestration to different subcellular regions can be a mechanism to regulate interactions between ERK and its substrates, altering the subset of targets that are phosphorylated (Nakakuki et al., 2010; Wortzel and Seger, 2011). This is highlighted by the requirement of ERK translocation from the cytoplasm to the nucleus for the phosphorylation of transcription factors such as Elk1 and their subsequent induction of gene expression (Brunet et al., 1999). ERK biosensors localized to the plasma membrane and endosomes have begun to uncover examples of distinct subcellular ERK activity patterns. For example, activity at the plasma membrane can be sustained, in contrast to the transient activation observed in the cytosol and nucleus (Keyes et al., 2020). However, complexities in the subcellular milieu remain yet to be fully resolved. ERK translocation is not necessarily required for the phosphorylation of ERK substrates within the nucleus (Raman et al., 2007; Wilson et al., 2017). It is possible for ERK to interact with and phosphorylate its substrates irrespective of their bulk localization because of shuttling between compartments on the scale of minutes. Even with the biosensors now available, further work will be needed to understand

the full temporal and subcellular features of ERK activity dynamics (Kholodenko et al., 2010).

2.5 Advances in measuring ERK activity and remaining challenges

ERK dynamics are most easily detected by fluorescent protein-based ERK activity reporters (i.e., biosensors) which have recently been reviewed in detail (Nakamura et al., 2021). The main categories of reporter include FRET-based (EKAR series), translocation-based (ERK-KTR; ERK-FP fusions), and degradation-based (FIRE) (outlined in Table 1). While the FRET-based ERK sensor has undergone many generations of improvements, the ERK-KTR, ERK-FP and FIRE reporters remain essentially unchanged (Table 1). Furthermore, as each reporter type has advantages and disadvantages, the choice of reporter used is critical when studying live-cell ERK activity. For instance, FRET-based ERK reporters are spectrally limited to FPs capable of FRET, such as CFP/YFP for their function. Alternatively, translocation-based reporters use only a single FP of any color, providing much more flexibility to combine with other reporters or fluorescent markers (Kudo et al., 2018; Regot et al., 2014). Additional markers to distinguish the nucleus from cytosol are still needed to quantify translocation reporters, and cells with complex three-dimensional or dynamic shapes can be a significant challenge to accurately quantify. Reporters also vary in the timescale of ERK activity changes they can detect, with FRET reporters showing the fastest responses, followed closely by translocation-based reporters, and degradation reporters being the slowest. While rapid reporter responses are needed to accurately distinguish closely grouped pulses of ERK activity, the slow responses of a degradation-based reporter can be very useful for measuring the integrated activity of ERK over time (Albeck et al., 2013; Benary et al., 2020; Brandt et al., 2019).

In most cases, the specificity of ERK reporters is high, as judged by the ability of either MEK or ERK inhibitors to eliminate their signal. However, one notable exception is the tendency of FRET and translocation-based reporters to show a non-ERK-specific increase in activity late in the cell cycle. This non-specific response is attributable to the fact that the ERK substrate sequences used in many of the existing reporters can also be phosphorylated by cyclin-dependent kinases (CDKs) that are most active in that G2 and M phases (Aoki et al., 2013), causing a slow increase in reporter signal that is resistant to MEK or ERK inhibitors and rapidly disappears following cell division (Gerosa et al., 2020). In our experience, the onset of this non-specific activity varies between cell lines; some cells show an increase in non-specific signal 1-2 hours prior to mitosis while others show a much longer period of accumulation. A recent set of FRET-based reporters derived from the EKAR-EV reporter, EKAR-EN4 and EKAR-EN5, addressed this problem by mutating two residues in the target phosphorylation sequence to eliminate the CDK affinity (Ponsioen et al., 2021).

An ongoing challenge for accurate reporter readouts lies in quantifying the intensity of ERK activity. This is an inherently difficult problem, as "ERK activity" at any given time is not a uniform parameter across the cell. In addition to spatial variability, different endogenous substrates can be phosphorylated to different extents, depending on the affinity of the substrate-kinase interaction (Burkhard et al., 2011). Thus, any individual reporter is inherently limited to a single "perspective" on ERK activity, while the set of endogenous ERK substrates represent multiple perspectives. Combining multiple ERK reporters in the same cell has been a useful exercise to show how the same pulse of ERK activity can be received differently by alternate targets (Aikin et al., 2020; Gillies et al., 2017; Sparta et al., 2015). These studies show that FRET and translocation ERK reporters agree in large part, but they also reveal subtle differences in on-rate and off-rate. Another key difference is in the measured amplitude of ERK activity. Dual readouts highlight systematic differences in dynamic range between reporters. For example, the FRET reporter EKAR3 shows greater

18

sensitivity than ERK-KTR to small ERK activity changes but saturates easily (Gillies et al., 2017). While the dynamic range of FRET-based reporters has increased (Ponsioen et al., 2021; Vandame et al., 2014), a head-to-head comparison between the newest FRET reporters and translocation reporters to assess their relative advantages has not yet been performed. Altogether, these differences emphasize the caveat that the amplitude of ERK reporter signals must be interpreted with caution and not as an absolute linear measurement. We discuss these quantitative issues in more depth in Box 2.

Another current challenge lies in extracting meaningful information from the hundreds or thousands of cells that are interrogated in a typical live-cell imaging experiment. The first step in this process is the extraction of ERK activity "traces" from image datasets, which can now be performed automatically using various segmentation and tracking algorithms (Blum et al., 2017; Bray and Carpenter, 2015; Pargett et al., 2017). While this step was often rate-limiting in the past, advances in computational image analysis have made it routine. In particular, machine learning software such as StarDist and CellPose have greatly increased the reliability of automated cell recognition (Schmidt et al., 2018; Stringer et al., 2021). Tracking algorithms, such as uTrack (Jaqaman et al., 2008) and EllipTrack (Tian et al., 2020), link cells from one image frame to the next, creating a time-series vector for each cell. Typically, it is possible to track over 90% of cells in each experiment; however, tracking efficiency is reduced by abnormal cell morphology, over-confluency, fast migration, or cell death. Despite these limitations, recent studies have used data from thousands or even hundreds of thousands of cells to draw statistically well-supported conclusions. Subsequent challenges emerge in the analysis of high-content time-series data, which we briefly discuss in Box 2.

2.5.1 Box 2: Rigor and Challenges in Quantification and Analysis

Reporter Calibration

For true quantitative measurements of ERK activity, two problems must be dealt with. First, the reporter signal itself must have its linear range of response characterized. This can be done by western blotting, to relate the fraction of the reporter in their phosphorylated form to its readout detected by FRET (Gillies et al., 2020; Kosaisawe et al., 2021). When performed carefully, reporter signals can be interpreted quantitatively, relative to the maximal signal, and any nonlinear regions of the readout can be identified. Second, the reporter readout must be linked to the level of ERK activity in the cell. This calibration can be approached by relating ERK FRET readouts to immunoblots on parallel samples that measure the fraction of ERK phosphorylation or endogenous ERK substrate phosphorylation. However a crucial caveat is that ERK reporters indicate not simply ERK activity, but instead the balance of ERK activity relative to any phosphatase activity on the reporter's ERK target site. The rapid reversibility of reporter signals upon ERK inhibition indicates high cellular phosphatase activity, and it seems reasonable that these phosphatases are the same ones that act on endogenous ERK substrates. However, this assumption has not been established experimentally. Any change in this phosphatase activity will affect the relationship between ERK activity and the observed reporter signal. This complicating factor can be approached by mathematically modeling both ERK and phosphatase effects on the reporter, or by empirically determining the relationship between phosphorylated ERK and the reporter signal (Gillies et al., 2020). While often overlooked, phosphatase activity may be one of the main drivers of heterogeneity in observed ERK readouts, both within and between cell types.

Quantifying features in time series data

Once live-cell data is collected, one must choose the appropriate technique to mathematically describe, or "featurize", the time-dependent signal of ERK activity. Several mathematical methods are available to extract information from time series data (Fulcher and Jones, 2017). Pulse detection algorithms identify peaks of signal activity and then quantify parameters such as signal amplitude, pulse duration, or frequency (2.3A) (Pargett and Albeck, 2018; Foreman and Wollman, 2020). Other methods include Fourier and wavelet transformation (Kobrinsky et al., 2005; Geva-Zatorsky et al., 2010), which decompose time series measurements into simpler components (which, added together, reconstruct the original signal). With any of these methods, the challenge lies in identifying the information that is most relevant for the cellular process under study, whether it be the amplitude, duration, average, or another aspect of ERK activity. Typically, it is necessary to experiment with more than one method to quantify the relationship of interest.

Clustering cells by dynamics

Parsing cells with similar reporter activity is often necessary as a first step during analysis. This task is not trivial as cellular kinetic data frequently have overlapping distributions, and thus determining the appropriate number of clusters is often arbitrary. A critical consideration is whether to predefine the number of clusters or allow the algorithm to determine the final number of groupings. There are many clustering functions to choose from, including K-means clustering, hierarchical clustering, K-nearest neighbor, principal component analysis, and other deep learning-based methods. Another important consideration is which distance metric to use; dynamic time warping has proved to be one useful approach, which allows signals that are similar in shape but have different timing to be grouped together (Strasen et al., 2018). Each of these approaches require significant user input which must be guided

by awareness of algorithm limitations and the structure of the data. As a result, clustering can be challenging to implement in exploratory research.

Deep learning and neural networks offer a more sophisticated approach to classify dynamic signaling behaviors. Rather than directly breaking down signals into unique characteristics, neural networks are trained to recognize distinguishing features in the data. A recent example of this is CODEX, which can recognize dynamic "prototypes" for signal behavior that can be used to group similarly behaving cells (Jacques et al., 2021). This method allows a computer to learn which classifiers patterns distinguish signal activity between specified categories, such as treatment conditions. Although these methods allow for analysis of large, multidimensional datasets, it can be difficult for humans to understand the abstract patterns that the algorithms learn. CODEX resolves this issue by providing prototypical time trajectories for each of the cell categories it identifies. An additional advantage is that CODEX can be used on datasets where multiple biosensors are measured in the same cell. Thus, with the increasing size and complexity of reporter datasets, deep learning methods provide an attractive tool to facilitate data interpretation.

2.6   Modeling the mechanisms driving dynamics

The question of how different forms of ERK dynamics are generated at the molecular level has captured scientific interest for at least 30 years (Wells *et al.* 1990). Approaches to this question have spanned structural analysis, subcellular localization, and mass-action kinetic modeling (Sasagawa *et al.* 2005; Filippi *et al.* 2016; Markevich, Hoek, and Kholodenko 2004; Sturm *et al.* 2010; Nakakuki *et al.* 2010; Lemmon *et al.* 2016; Freed *et al.* 2017). Many mechanistic details can shape the dynamic behavior of ERK, and here we group these mechanisms into several overarching concepts and discuss the evolution of mathematical models that explore these factors. Computational models play an increasingly essential role

in this question because the complexity of multiple layers of regulation make it difficult or impossible to predict system behavior from intuition alone. A major caveat that applies across these studies is that many mathematical models pre-date the ability to track ERK activity in live cells. Consequently, many published models, although intended to represent a prototypical cell, have been fit only to population-average data, which does not always accurately represent the true behavior of any individual cell. Thus, conclusions from models must be interpreted with caution in cases where it is unknown how single cells differ from the mean.

2.6.1   Predominance of RTKs in setting ERK dynamics

From the earliest studies of ERK signaling, it was observed that ligands for different RTKs can specify distinct activity kinetics (Muroya, Hattori, and Nakamura 1992). These receptor-specific patterns can be attributed either to differential binding of adaptor and RAS-family G proteins to the receptor (Kao *et al.* 2001), or to differences in the kinetics of receptor dimerization, internalization, degradation, and recycling (Sorkin and Goh 2008; Wells *et al.* 1990). EGFR dimers perform autophosphorylation of their partner receptors, which targets them for internalization by both clathrin-mediated and clathrin-independent mechanisms (Sigismund *et al.* 2008). Although the receptor may continue to signal from endosomal compartments of the cell, this internalization ultimately results in EGFR inactivation and transient ERK activation (**??**B) (Burke, Schooler, and Wiley 2001; Sorkin and Goh 2008). Numerous mathematical models of ERK signaling have incorporated the mechanisms of receptor processing as a focus of regulation (W. W. Chen *et al.* 2009; Kleiman *et al.* 2011; Schoeberl *et al.* 2002; Hendriks *et al.* 2005; H. Steven Wiley, Shvartsman, and Lauffenburger 2003; Sasagawa *et al.* 2005; Santos, Verveer, and Bastiaens 2007; Richard J. Orton *et al.* 2005; Starbuck and Lauffenburger 1992). These models enabled exploration of how receptor internalization rates determine the duration of ERK activity and predict responses

to different EGF levels.

The importance of receptor kinetics is underscored by converging evidence that ERK activity tracks very closely with RTK activity. When ERK activity is stimulated by light-induced optogenetic constructs upstream of RAS, the activity follows the intensity of light stimulation with very little lag or adaptation (Toettcher, Weiner, and Lim 2013; Dessauges *et al.* 2022b). This "memoryless" behavior is surprising given that several downstream negative feedback loops (detailed in the next section) are operative under these conditions and would be expected to complicate the signal dynamics. However, a strong correlation between upstream initiation and ERK output has been observed in multiple systems, regardless of whether the signaling is initiated at the level of RAS or the intracellular domain of RTKs (Dessauges *et al.* 2021). Further corroborating this concept are data showing that ERK activity terminates within seconds to minutes upon RTK inhibition (Kleiman *et al.* 2011; Sparta *et al.* 2015), and that ERK activity tracks dynamically with receptor phosphorylation across different receptors (Kiyatkin *et al.* 2020).

Another line of evidence for the importance of receptors in dynamics is that oncogenic or activating mutations in proteins downstream of the receptor, including RAS, RAF, or MEK generally promote more sustained ERK activity in single cells (**??**A) (Gillies *et al.* 2020; Aikin *et al.* 2020). Together, these data argue that tendency toward transient or sustained activity of ERK is primarily a reflection of the activation and deactivation of the ligand-bound receptor, in at least several commonly studied cell types. However, under more atypical experimental conditions, the regulation of EGFR internalization can result in surprising behavior. Under conditions in which EGF is slowly ramped to high concentrations, receptors become downregulated and fail to activate ERK (Krause *et al.* 2021). This adaptation persists for hours, and even withdrawal of EGF for several hours and subsequent re-stimulation does not elicit ERK activation. Thus, receptor-level regulation also acts as a noise filter to reduce spurious ERK activity in the face of incremental or gradual ligand
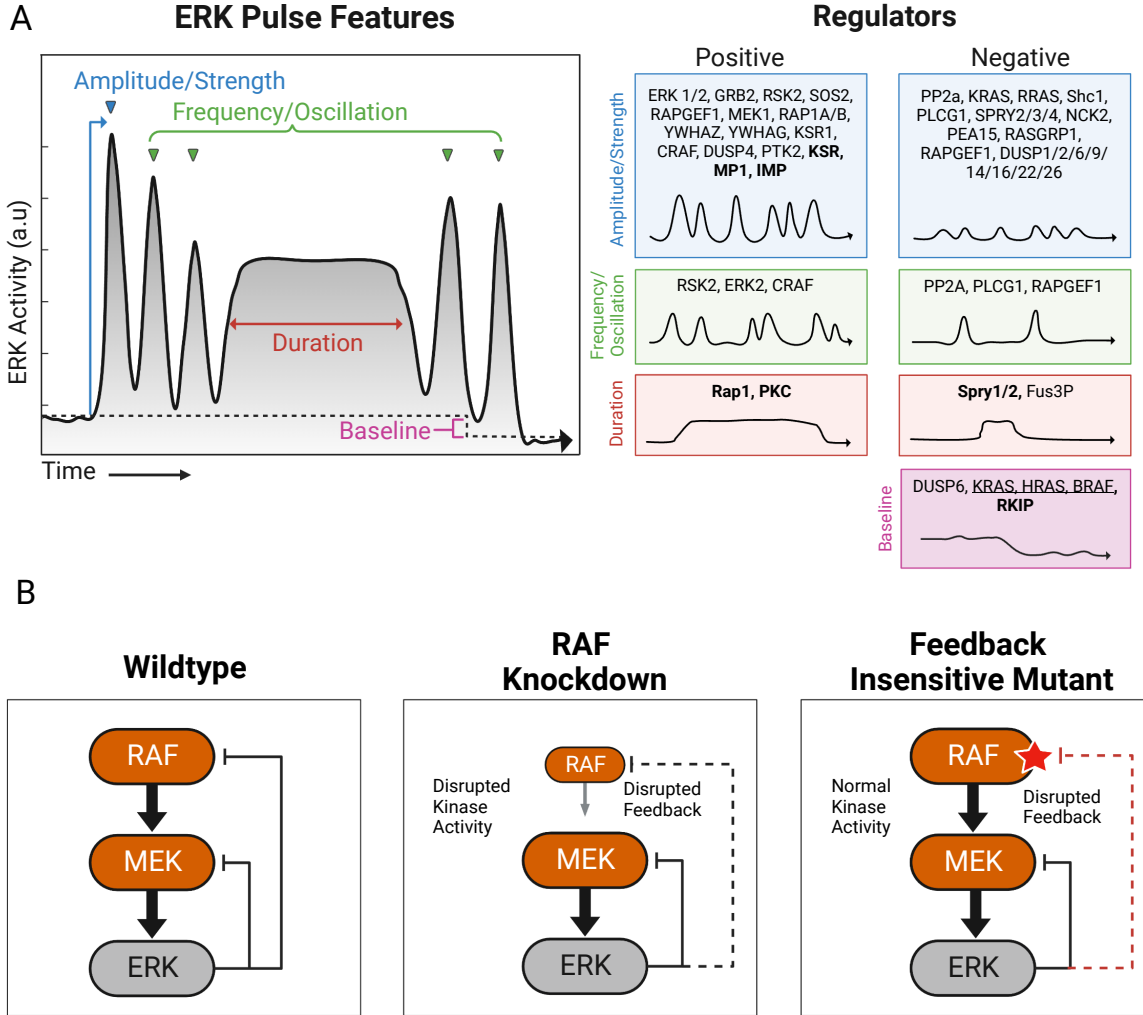
Figure 2.3: **A** Comparison of experimental techniques to investigate the strength of negative feedback. Left: ERK inhibits both MEK and RAF. Middle: Experimental knockdown of Raf weakens negative feedback from ERK; however, signaling from RAF to MEK will also be disrupted. Right: Feedback insensitive mutants only weakens the negative feedback from ERK, and allows for wild type RAF to MEK signaling. **B** List of genes that have been shown to positively or negatively regulate unique features of ERK activity. This list is curated from experiments where ERK activity features were measured after knockdown or knockout (KD/KO) of respective genes. KD/KO of positive regulators resulted in decreased features of ERK activity. KD/KO of negative regulators resulted in increased features of ERK activity. Most experiments were performed at single-cell resolution (Dessauges *et al.* 2022b), or from western blot experiments (indicated in bold).

changes. The additional complexities that occur when more complex, but likely physiologically relevant, stimulation patterns that deviate from simple bolus treatments will be an important area in which to refine models of EGFR internalization and feedback.

2.6.2 Additional regulation by downstream negative feedback

Another essential feature of ERK regulation is an intricate negative feedback structure. Active ERK can negatively regulate several upstream targets, including EGFR (X. Li *et al.* 2008), MEK1 (Catalanotti *et al.* 2009), RAF (Ritt *et al.* 2010) or SOS (Corbalan-Garcia *et al.* 1996; Kamioka *et al.* 2010). Still another level of negative feedback is the ERK-mediated transcriptional induction of phosphatase genes, such as the dual specificity phosphatases (DUSPs) and MAPK phosphatases (MKPs) (Amit *et al.* 2007). Increased expression of DUSPs and MKPs leads to dephosphorylation of the MAP kinases, reducing their activity. The net result of these seemingly redundant negative feedback mechanisms is a strong tendency of ERK activity to fall sharply within 15-30 minutes after its peak activation, even independently of the receptor internalization described above, to enforce the transient pulse shape observed in many cell types (**??**B). In contrast, systems with weaker collective negative feedback show sustained signaling (**??**A) (Sasagawa *et al.* 2005; Brightman and Fell 2000; Kao *et al.* 2001). Studies combining both modeling and experiments have built a consensus that negative feedback loops vary in their relative importance, explaining the diverse ERK dynamics found across different cell types (Cirit, Wang, and Haugh 2010; R. J. Orton *et al.* 2008; W. W. Chen *et al.* 2009).

One of the most thorough efforts to deconvolve feedback mechanisms in ERK dynamics was a pathway-wide RNAi screen of 50 MAPK genes (Dessauges *et al.* 2022b). With its large scale and detailed analysis employing optogenetic stimulation at different points in the pathway, this landmark study provided two important conclusions. First, a number of subtle changes in ERK dynamics resulted from knocking down certain genes, including

CRAF, RSK2, PP2A, PLCG1 (2.3A), several of which are involved in negative feedback. Some of these knockdowns led to increased oscillatory behavior, while others moderately increased ERK amplitude. Second, this study underscores the remaining challenge of disentangling highly redundant signaling systems. In many cases, ERK activation was not affected by knockdown of core pathway genes such as ERK2, GRB2, or SOS2, likely because additional isoforms of these proteins maintained their function. Perhaps most strikingly, the authors found that even this extensive dataset was still insufficient to fully specify a multi-feedback computational model. Thus, redundancy of negative feedback loops continues to be a formidable challenge for both experiments and modeling.

While computational models can capture basic ERK kinetics using one or more of these feedback loops (W. W. Chen *et al.* 2009; Kocieniewski and Lipniacki 2013; H. Steven Wiley, Shvartsman, and Lauffenburger 2003; Boris N. Kholodenko 2000), it is difficult to verify that these models capture the underlying biology. Due to the redundancy of feedback circuitry (2.3B, left), isolating single feedback loops is experimentally difficult. Simple knockdown or overexpression experiments are often limited in their ability to test feedbacks, because they would change both the forward and the feedback effects of the protein within the loop (2.3B, middle). Ideally, feedback nodes could be isolated experimentally by replacing the proteins involved with feedback-insensitive versions (2.3B, right). This requires either editing multiple sequences in endogenous genes or expressing a mutated protein while simultaneously knocking out the endogenous protein, both of which would be highly time-intensive. The closest examples to date ablate specific feedback loops via phopho-insensitive RAF (Ritt *et al.* 2010; Brummer *et al.* 2003; Dougherty *et al.* 2005) or SOS mutations (Saha *et al.* 2012; Corbalan-Garcia *et al.* 1996). Current computational models may suffer from overfitting due to the large number of components and limited experimental controls to constrain these parameters. Future experiments aimed at accurately disentangling individual feedback nodes, without altering the protein's forward signaling activity, will refine models

and improve prediction performance.

In addition to simply terminating pathway activation, negative feedback plays an important role in producing linear ERK responses that are robust to noise (Nunns and Goentoro 2018; Sturm *et al.* 2010). Because ERK inhibits upstream pathway components, the system takes on the topology of a negative feedback amplifier, a design frequently used in engineering to stabilize system output and reduce sensitivity to environmental perturbations. Acting in this fashion, pathway inputs that would normally saturate ERK output instead show a graded linear response over a wide range of stimuli (Sturm *et al.* 2010; Nunns and Goentoro 2018). Finally, another function of negative feedback is that it can render the amount of ERK activity output insensitive to the total ERK protein level (Fritsche-Guenther *et al.* 2011). Together, these studies highlight the importance of negative feedback in setting the system-level input-output properties of ERK activity and the need for models to represent the multiple feedback loops accurately. A simplified interpretation that reconciles many of the existing observations is that negative feedback loops within the RAF-MEK-ERK cascade act on the scale of seconds or minutes and provide linearity and robustness to the input-output behavior of this module, while feedback at the receptor level varies the input to the cascade on a longer time scale, creating the overall form of the dynamics. However, this concept has yet to be fully tested, both computationally and experimentally.

2.6.3 Pulsatile and oscillatory behavior due to cooperativity

In many systems, the ERK cascade exhibits evidence of cooperativity - that is, a steeply nonlinear response curve to ligands that tends toward full activation once stimulated (Das *et al.* 2009; Altan-Bonnet and Germain 2005; C. Y. Huang and Ferrell 1996). In experiments using single-cell assays, ERK activity often transitions rapidly from fully off to maximally active, with few intermediate responses observed (Aoki *et al.* 2013; C. Y. Huang and Ferrell 1996). Cooperativity is important in allowing the ERK pathway to act as an excitable system in

which activity can propagate spatially, either within a cell or from cell to cell. This form of activity is referred to as a trigger wave, and has been observed in various types of monolayer cultures, both *in vitro* and *in vivo* (De Simone *et al.* 2021; Hiratsuka *et al.* 2015; Lin *et al.* 2022; Ogura *et al.* 2018). In the slime mold Dictyostelium, the RAS-linked signaling network displays excitability that allows regions of RAS activity to propagate within individual cells (C.-H. Huang *et al.* 2013).

The most comprehensive study of cooperative MAPK behavior has been carried out in Xenopus oocytes, where cooperative activation is driven by positive feedback from MAPK to the MAPKKK Mos (J. E. Ferrell Jr and Machleder 1998; J. E. Ferrell Jr 1999). However, in other systems, the source of cooperativity has been more difficult to identify definitively. It has been suggested that the requirement for dual phosphorylation of MEK and ERK enables cooperative behavior of the cascade, and modeling of these effects shows that they are sufficient to create switch-like behavior or oscillations in ERK/MAPK activity (e.g., ??D) (Markevich, Hoek, and Kholodenko 2004). Another potentially important positive feedback occurs at the level of SOS, a guanine nucleotide exchange factor that mediates RAS activation by RTKs (Gureasko *et al.* 2008; Margarit *et al.* 2003). SOS has two binding sites for RAS - one at which it catalyzes guanine nucleotide exchange on RAS, and one at which GTP-bound RAS binds and allosterically enhances exchange activity at the first site. This allostery creates a positive feedback loop, which has been proposed as the source of cooperative ERK activation in mammalian cells (Das *et al.* 2009). However the observations that optogenetic stimulation either at the receptor level or the SOS level fail to elicit cooperative activation of ERK suggest that these mechanisms alone are insufficient for cooperativity (Dessauges *et al.* 2021). Thus, similar to the situation of redundant negative feedbacks, there remains substantial difficulty in unambiguously establishing contributions of individual positive feedback mechanisms in most cell types examined to date.

Despite ambiguity in the molecular mechanism, it is likely that some combination of

negative feedback and cooperativity underlies the oscillatory or highly pulsatile behavior that has been observed for ERK in various systems (Shankaran *et al.* 2009; Shankaran and Wiley 2010). The first demonstration of such a possibility used a model in which high cooperativity (also known as ultrasensitivity) was coupled to negative feedback from ERK to RAF to produce oscillatory behavior (Boris N. Kholodenko 2000). A number of other models have confirmed that such combinations can produce oscillatory behavior. In a more recent example, Kochańczyk *et al.* constructed a MAPK pathway model with one positive feedback from Ras to SOS, and three negative feedbacks from ERK acting on MEK, RAF, and SOS (Kochańczyk *et al.* 2017). They found that the positive feedback from Ras to SOS allows for bistable pathway activation, and the negative feedback from ERK to SOS then refashions the network's bistable behavior into oscillatory patterns of ERK activation. In this model, negative feedback from ERK to MEK and RAF primarily modulates the shape of ERK activity pulses. Finally, similar models are supported by additional work from Arkun and Yesemi, who argue that bistability and switch-like behavior arises from positive feedback from Ras to SOS, but add that internal negative feedback from phosphatases allow for dampened oscillations (Arkun and Yasemi 2018).

2.6.4 Autocrine and paracrine signaling as a source of sporadic pulses

While feedback and cooperativity can explain regular oscillations in ERK activity, irregular patterns of pulses (??E, F) indicate a strong source of variability. Several lines of evidence suggest that autocrine and paracrine signaling through EGFR plays a dominant role in driving irregular pulsatile dynamics. Epithelial cells secrete numerous EGFR ligands (Shi *et al.* 2016), each eliciting distinct ERK activities. For example, high-affinity ligands, such as TGF-alpha rarely escape capture by the secreting cell's own receptors, and thus act primarily

as an autocrine signal (DeWitt *et al.* 2002). Lower-affinity ligands such as AREG can diffuse more broadly to stimulate surrounding cells. Release of these ligands is controlled by matrix metalloproteinases (MMPs) on the cell surface that cleave the membrane anchor motif to release the soluble mature forms into the extracellular space (Loffek, Schilling, and Franzke 2011). MMPs are in turn stimulated by ERK activity, which effectively forms a positive feedback loop that operates across intracellular and extracellular compartments (Aoki *et al.* 2013). In addition to canonical EGFR ligands, other growth factors, including those from the fibroblast growth factor (FGF) and G-protein coupled receptor (GPCR) families, stimulate ERK and act in a paracrine fashion (Chavez-Abiega *et al.* 2022; Tany *et al.* 2022; Simon *et al.* 2020). The combination of these different ligands and irregular timing of their release create a dynamically evolving microenvironment for the neighboring cells. An additional layer of complexity arises from the fact that different EGFR ligands can trigger distinct patterns of ERK activity even though they signal through the same receptor. Freed *et al.* examined ligand-specific EGFR dimer interactions and found that high-affinity ligands such as EGF or TGF-beta create highly stable EGFR dimers, whereas low affinity ligands such as Epiregulin and Epigen (EREG and EPGN) form weakly bound asymmetric dimers (Freed *et al.* 2017). The varying stability of these complexes results in differences in internalization rate, effectively altering the strength of a key negative feedback. Strong EGFR binders (e.g. heparin binding-EGF like growth factor, betacellulin) target all EGFRs for lysosomal degradation and attenuate signal (Roepstorff *et al.* 2009). As a result, EGFR molecules bound to EREG and EPGN are less subject to internalization and drive more sustained ERK signaling (Roepstorff *et al.* 2009). Furthermore, differences in ligand dissociation from internalized EGFR allows the receptors to be recycled to the plasma membrane surface rather than broken down, permitting rapid re-activation by ligand and potential for sustained ERK activation (Waterman *et al.* 1998; Roepstorff *et al.* 2009). This diversity of activation mechanisms further diversify the ERK responses that result from paracrine stimulation.

In *in vivo* imaging studies, some form of dynamic ERK pulses, resembling those described in cell culture, have been observed in every case where single-cell resolution was available. The patterns of pulses vary depending on the tissue and organism. Examples of focal points of ERK activity that radially spread to neighboring cells include the mouse epidermis (Hiratsuka *et al.* 2015) and Drosophila embryonic epithelium (Valon *et al.* 2021). In some cases, ERK activity only travels limited distances (3-4 cell diameters), suggesting that propagation is limited by diffusion of the ligand. However, in regenerating fish scales, wound healing, or cultured MDCK epithelial cells, waves of ERK activation travel much farther, spreading out across dozens of cell layers. In these cases, ERK activity causes shedding of EGFR ligands via MMPs, allowing for continued propagation of the wave (Lin *et al.* 2022; De Simone *et al.* 2021; Hiratsuka *et al.* 2015; Aoki *et al.* 2017). Other cell systems show rapid, sporadic patterns of well-defined pulses with limited spatial correlation, suggesting multiple overlapping sources (Aoki *et al.* 2013; Albeck, Mills, and Brugge 2013). At the extreme end of this continuum, cells containing oncogenic mutations show a complex and seemingly stochastic pattern of ERK activity without clearly separated pulses, which has been linked to increased secretion of amphiregulin, a paracrine EGFR ligand (Davies *et al.* 2020; Ponsioen *et al.* 2021; Aikin *et al.* 2020). In nearly all of these cases, EGFR inhibition eliminates ERK pulses, confirming the importance of receptor-level regulation of these patterns and dynamics. Thus, paracrine ligand secretion underlies a variety of highly dynamic ERK behavior.

Several mathematical models have been developed to simulate the propagation of ERK activation between cells (Aoki *et al.* 2013). For instance, a spring model was used to investigate ERK-driven collective cell migration. In this model, ERK activity increases the length of each cell and subsequently changes in cell density and decreases myosin light chain (MLC) phosphorylation. The model indicates that as ERK waves propagate through cells, MLC dephosphorylation is sufficient for collective cell migration in the opposite direction

of the ERK wave, whereas cell density is not sufficient (Aoki *et al.* 2017). This model was restricted to observations in a one-dimensional monolayer. Therefore, the spring model was transformed into a continuum model, which allows for a two dimensional analysis that accurately represents the 2D epithelial cell movement. The continuum model averages the heterogenous and noisy properties of individual cells in order to successfully recapitulate tissue-level dynamics driven by single cells (Asakura *et al.* 2021). Finally, biophysical models further our understanding of how monolayer mechanics coupled to ERK translate to polarity changes and active cell migration (Boocock *et al.* 2020).

2.6.5   Cell states create variability in ERK responses

Another prominent feature of ERK activation revealed by biosensors is cell-to-cell variation in activity patterns. Such variation is found even in cases where genetically identical cells with controlled spatial differences in stimulating ligands often have substantial divergence in the timing and intensity of ERK activation. Studies investigating this phenomenon have found that the variation can be accounted for by pre-existing differences in cell state, also termed "extrinsic noise", rather than true stochastic behavior of the pathway, or "intrinsic noise" (Selimkhanov *et al.* 2014). This finding is consistent with the findings in several signaling pathways (Cheong *et al.* 2011) and confirmed by a recent study measuring dozens of cell state parameters, including local cell density, cell shape, and expression of various non-pathway markers (Kramer, Sarabia del Castillo, and Pelkmans 2022). The latter study demonstrated that factors such as calreticulin, Sec13 levels, and cell density may exert an even larger effect on a given cell's ERK activation (as well as for many other signaling pathways) as compared to different concentrations of EGF. This concept helps to explain a disparate set of findings that ERK pathway activation depends strongly on actin cytoskeletal protrusions (J.-M. Yang *et al.* 2018), the presence of caveolin pits in the plasma membrane (Kortum *et al.* 2014), and the rate of glycolysis (Peeters *et al.* 2017). If all of these "non-

canonical" mechanisms each impact ERK activation, the pathway can be considered not only as output of growth factor stimulation, but also as an integrated index of both intracellular and extracellular factors.

2.7 Conclusion

The diversity of ERK dynamics helps to explain how this ubiquitous pathway plays a variety of cell-specific roles in controlling cell proliferation, differentiation, and migration. Collectively, the work highlighted here demonstrates that ERK activation dynamics are well positioned to provide acute sensing of the extracellular microenvironment, allowing cells to respond in unique ways to paracrine signals, cell density, and extracellular matrix. When connected to pathway outputs, such as gene expression, that are selectively responsive to different dynamic patterns, the ERK pathway makes it possible for the cell to continuously adjust its state and behavior based on its physical context. In the companion review, we delve into the "output" side of this function, exploring how dynamics regulate gene expression. We also examine the potential for pharmacological inhibitors of the ERK pathway to promote different cellular functions depending on how they affect ERK dynamics.

Fully understanding and exploiting the ERK signaling code will depend on accurate quantitative models. The rich history of pathway models that we discuss here have provided an excellent start in capturing the main mechanisms driving dynamic ERK activity. Nonetheless, as the most recent work shows, a complete model that accurately predicts the effects of pharmacological and genetic perturbations remains some distance away (Dessauges *et al.* 2022b). While the existing models provide the conceptual building blocks to understand how dynamic behaviors arise, many cell systems contain several of these mechanisms operating together. As noted above, predictive models of highly redundant systems are challenging to validate, especially when relatively few experiments perform a careful dissection of the com-

ponent mechanisms. Furthermore, even in the absence of mutations, genetically identical cells can diverge in their dynamics due to variation in the copy numbers of pathway proteins (Niepel, Spencer, and Sorger 2009). Such differences explain the observed differences between cell types in an organism and the heterogeneity of cells within the same tissue. Fully modeling these differences would require information on the hundreds of parameters (i.e. protein concentrations) that vary between contexts, which remains experimentally challenging.

The new technologies highlighted here, including improvements in biosensors, image processing, and large dataset analysis, will likely be critical in overcoming the remaining obstacles. Machine learning is an exploding field that has rapidly expanded into biology. From predicting protein structure, cell segmentation, and improving CRISPR guide RNA design, neural networks have pushed the boundaries of many fields (Jumper *et al.* 2021; Meijering 2012; H. K. Kim *et al.* 2018). Recently, convolutional neural networks have been used to identify ERK patterns and characterize signaling motifs in single cells (Jacques *et al.* 2021; Dessauges *et al.* 2022a). These newer models are able to recognize objective and abstract patterns in large-scale data; therefore, they are an approach that may fully connect signaling, gene expression, and cell fates. Future work should be aimed at creating a model that connects network topology and the functional and phenotypic consequences of signal propagation. Specifically, how do the positive regulators of the pathway shape the spatial and temporal activation and deactivation of ERK? What features of the pathway are most important for regulation, and which are redundant? Furthermore, how important is the pathway topology for generating dynamic patterns of gene expression? Although it is unlikely there will be one universal model that represents all aspects of the pathway, a future computational model may be able to capture the entire network circuitry and generate the various pulsatile behaviors of ERK.

2.7.1 Funding

2.7.2 Acknowledgements

Chapter 3

The control of gene expression and physiological outcomes by ERK

3.1 Preface

This chapter was originally submitted to *The Biochemical Journal* on May 30th, 2023, as part two of a two part review on ERK dynamics: Abhineet Ram, Devan Murphy, Nicholaus DeCuzzi, Madhura Patankar, Jason Hu, Michael Pargett, and John Albeck. A guide to ERK dynamics, part 2: Decoding the control of gene expression and physiology.

J.A. conceptualized and the review and contributed to the text. A.R., D.M., N.D., MaP., contributed to the writing and editing the text. Mi.P. assisted with reviewing sections of the text. J.H. created all figures.

The article has been modified to satisfy the formatting requirements of this dissertation.

3.2 Abstract

Signaling by Extracellular signal regulated kinase (ERK) controls many cellular processes including cell division, differentiation, and death. In the second installment of this two-part review, we address the question of how this single pathway exerts distinct effects on multiple processes. We discuss how ERK activation leads to changes in gene expression and the mechanisms that further diversify the transcriptional output of ERK signaling. With a focus on single-cell, biosensor-based studies, we summarize four major functional modes for ERK signaling in tissues: adjusting the size of cell populations, gradient-based patterning, wave propagation of morphological changes, and diversification of cellular gene expression states. These modes of operation are disrupted in cancer and other related diseases and therefore represent potential targets for therapeutic intervention. By understanding the dynamic mechanisms involved in ERK signaling, there is potential for pharmacological treatment to not only simply inhibit ERK but to restore functional activity patterns and improve disease outcomes.

3.3 Introduction

The extracellular signal regulated kinase (ERK) pathway regulates many aspects of cellular physiology, including cell growth, proliferation, differentiation, and death. Since the identification of the pathway's core components, which are found in all eukaryotes, it has served as a paradigm for how signal transduction pathways convey information from the cell surface to the nucleus, driving cell fate decisions (Lavoie, Gagnon, and Therrien 2020). Activation of ERK also plays an essential role in tissue development, homeostasis, and cancer. As with many signal transduction pathways, ERK controls multiple cellular effects, which raises the fundamental question of how specific cellular outcomes are determined in a given context

(Vasudevan and Soriano 2016). Two basic types of explanation can be proposed. First, unique cellular responses could be determined by contextual cues, such as the coincidence of ERK activation with other signaling activities or cell type-specific gene regulation (Vasudevan *et al.* 2015). Alternatively, changes in the amplitude, duration, or timing of ERK activity - collectively referred to as "dynamics" – could specify distinct downstream behaviors. Both of these modes contribute to cellular regulation (Vasudevan and Soriano 2016; J.-Y. Chen *et al.* 2012), but dynamics-based encoding poses a unique challenge for cell biology (Boris N. Kholodenko, Hancock, and Kolch 2010), in part because standard methods are not well suited to study this type of information processing.

In this review, we focus specifically on the dynamic modes of ERK signaling. We explore the concept that information about the identity and strength of extracellular stimuli is carried (or encoded) not only in the identity of the intracellular molecules activated, but in the specific timing of their activation and deactivation (Marshall 1995; Jones and Kazlauskas 2001). In the past 10 years, long-standing challenges in rigorously evaluating the role of dynamics have become tractable through new tools including optogenetics, biosensors, microfluidics, and computational models. These developments have revealed a surprisingly elaborate array of dynamic behaviors of the ERK pathway, which may act as a "code" to specify cellular behaviors. In a companion review (2), we survey the observations of dynamic activity and mechanistic models for the cell-specific operation of this ubiquitous pathway. Here, we explore the concept that specific patterns of ERK activity define its downstream effects on gene expression and tissue behavior.

The concept of temporal coding is already well appreciated in neural circuits, where the timing and frequency of action potentials can transmit specific information between neurons. Activation of signaling pathways is typically less discretized and occurs on a slower time scale (minutes) than action potential firing (milliseconds). Nonetheless, it is now established that many signaling pathways show highly dynamic activity, featuring pulses that

occur repeatedly on a time scale relevant to pathway function (Antebi, Nandagopal, and Elowitz 2017; Levine, Lin, and Elowitz 2013). Beyond the ERK pathway, there are several examples of signal transduction pathways in which dynamic activation figures prominently, including NF-kB (Hoffmann *et al.* 2002; Tang *et al.* 2021), p53 (Purvis *et al.* 2012; Hafner *et al.* 2017), and Msn2 (Hansen and O'Shea 2013). There is already an expansive field investigating communication by intracellular calcium dynamics, which have been accessible at the single cell level for decades through fluorescent dyes (Giorgi *et al.* 2018; Kraus *et al.* 2000; Dolmetsch *et al.* 1997). Elegant work in each of these systems has established that downstream gene expression patterns are indeed strongly influenced by the temporal pattern of pathway activity. In the Msn2 pathway in particular, the experimental power of yeast genetics has enabled a careful quantitative analysis of the pathway's temporal coding capacity (Hansen and O'Shea 2015; Hansen, Hao, and O'Shea 2015), culminating in the demonstration that four distinct expression programs can be determined by different input patterns of Msn2 activation (Hansen and O'Shea 2016).

These findings establish the importance of dynamic encoding in the ERK pathway, which influences many cell fate decisions. Because these cell fates ultimately control tissue homeostasis and repair, the physiological function of the ERK pathway – to shape tissues during development or regeneration – depends on its temporal activation profile. The dysfunction of the pathway in diseases such as cancer is closely tied to changes in its temporal activity profile (Bugaj *et al.* 2018; Davies *et al.* 2020). In the sections that follow, we explore how dynamic regulation of ERK defines its downstream effects on gene expression and tissue behavior, with implications for its dysfunction and drug responses in disease.
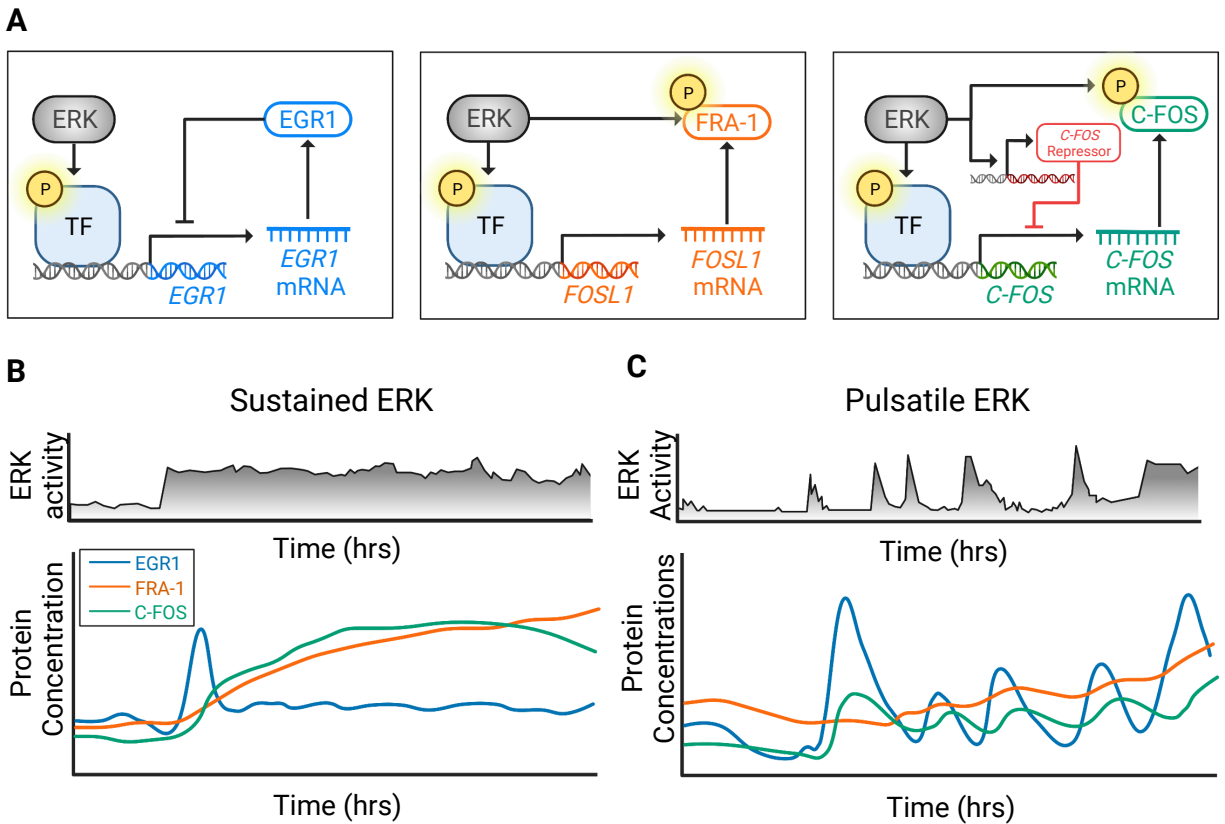
Figure 3.1: Differential gene expression responses to ERK signaling **A** Differential regulation of Egr-1, Fra-1, and c-Fos. Egr-1 protein binds to its promoter, inhibiting further transcription. ERK initiates Fra-1 transcription and also stabilizes Fra-1 protein. ERK initiates c-Fos expression, and sustained ERK activation induces a c-Fos repressor. **B** Sustained signaling generates high concentrations of Fra-1 and c-Fos. Subsequently, c-Fos repressor inhibits further expression of c-Fos. After the initial peak of Egr-1 levels, Egr-1 represses its own transcription (auto-inhibition), thus returning to an equilibrium with low baseline expression. **C** Pulsatile signaling generates short bursts of Egr-1 levels. Since Egr-1 transcription is brief, auto-inhibition does not persist. This allows Egr-1 levels to oscillate. Conversely, pulsatile signaling weakly induces Fra-1 and c-Fos because sustained signaling is required for protein stabilization. Figure adapted from Davies *et al.* 2020.

3.4 Effects of ERK dynamics on gene expression

The cellular effects of ERK dynamics are exerted largely through regulation of gene expression. ERK has over 1000 identified target genes (Ünal, Uhlitz, and Blüthgen 2017), many of which are themselves involved in transcriptional regulation, allowing ERK to exert widespread influence on the expressed genome. ERK activity can stimulate cell proliferation, differentiation, metabolism, and cancer drug resistance, through numerous target genes including Cyclin D1, c-Fos, c-Myc, and Fra-1. ERK target genes have been categorized into rapidly responding immediate-early genes (IEGs), immediate-late genes (ILGs) and delayed early genes (DEGs) based on their timing of expression following ERK activation (Uhlitz *et al.* 2017). Here we discuss how dynamic ERK activation can lead to selective target gene expression, which provides a mechanism to induce distinct cellular processes.

ERK activity modulates gene expression at multiple levels. First, ERK directly phosphorylates transcription factors, including ETS family members such as Elk-1, inducing allosteric changes that increase DNA binding and increase transcriptional activity (Q.-J. Li *et al.* 2003; S.-H. Yang *et al.* 1999). Once mRNA is produced, prolonged ERK activity increases mRNA half-life for certain genes, including so-called "late response genes" (EGFR, DUSP6), but not early (EGR1, FOS) or mid (PHLDA1) response genes (Nagashima *et al.* 2015). For many of these genes, the synthesized proteins can also be phosphorylated by ERK to protect them from degradation (Ferrara *et al.* 2003). Such stabilizing phosphorylations are present in Fra-1, c-Fos, and other AP-1 family members (3.1a) (Ferrara *et al.* 2003; Gomard *et al.* 2008). Furthermore, ERK activity regulates chromatin modifiers, such as EZH2, and RNA splicing factors, like DAZAP1, which can together modulate the transcriptional productivity of many loci (Choudhury *et al.* 2014). As we discuss below, these overlapping mechanisms enable significant opportunity to build gene regulatory circuits that are sensitive to different spatial and temporal patterns of ERK activity.

3.4.1 Persistence detection in Immediate Early Genes

The parallel regulation of multiple steps in the gene expression process by ERK creates a feedforward regulatory motif. In principle, this configuration can make target gene expression sensitive to the duration of ERK activity (Murphy *et al.* 2002; Murphy, MacKeigan, and Blenis 2004). Because stimulation of transcription and protein stabilization both require active ERK but are separated in time, short periods of ERK activity can be unproductive because they stimulate RNA production but do not persist for long enough to phosphorylate and stabilize the newly translated protein. Conversely, persistent ERK activity permits both gene transcription and stabilization of proteins. Mathematical modeling of this feedforward motif confirms that it can in fact act as a "persistence detector" that preferentially responds to longer durations of ERK activity, allowing genes such as c-Fos to be selectively induced by growth factors such as HRG that stimulate prolonged, rather than transient ERK activity (Nakakuki *et al.* 2010).

Additional modeling analysis has added depth to this concept, demonstrating that persistence detection depends critically on the kinetic parameters of RNA induction and degradation (Gillies *et al.* 2017). Effective persistence detection by a gene requires that mRNA and protein production be very low in the unstimulated state, because any pre-existing pool of protein can be directly phosphorylated and stabilized by ERK, bypassing the feedforward requirement for ERK duration. Consequently, strong persistence detection can be difficult to achieve. Analysis of Fra-1 expression using a knock-in fluorescent tag revealed that it has a significant basal rate of production and does not require a threshold duration of ERK activity (Gillies *et al.* 2017). Instead, Fra-1 production integrates total ERK activity over time, regardless of its duration. Thus, ERK target genes vary in their capacity for persistence detection and their responses to ERK activity dynamics.

3.4.2 Gene expression as a filter for ERK dynamics

Expression of IEGs, which include c-Fos and Egr-1, increases within minutes following ERK activation (Uhlitz *et al.* 2017). Models indicate this response profile is due to mRNA kinetics, whereby genes with short half-life have a higher transcription rate, quickly reach high mRNA levels, and quickly decay in the absence of ERK activity. c-Fos and Egr-1 fit into this category as they are sensitive to rapid changes in ERK activity; however, they are insensitive to long-term ERK activity since they quickly reach their maximal mRNA levels. Although c-Fos and Egr-1 do not integrate signals as effectively as Fra-1, their high basal expression allows for rapid responses to ERK (H. Steven Wiley 2017; Gillies *et al.* 2017). Overall, mRNA half-life appears to be a critical factor, as the short-half lives of IEGs allow responsiveness to ERK duration while long-half lives of ILGs and DEGs integrate both ERK duration and amplitude. These gene properties, combined with transcriptional control and post-translational modification, allow for differential gene expression in response to ERK dynamics (3.1b) (Davies *et al.* 2020).

An extension of this concept is that gene expression output can respond to the frequency of ERK activity pulses. Frequency modulation of ERK is sufficient for cell behaviors, like proliferation (Albeck, Mills, and Brugge 2013), however, how ERK encodes frequency into gene expression is still unknown. One hypothesis is a logic gate, referred to as a "band-pass" filter, that allows target genes to respond to different frequencies of ERK signaling (Wilson *et al.* 2017). In this framework, each gene has a different sensitivity of its promoter to ERK pulses. For example in fibroblasts, c-Fos and other IEGs can be maximally induced by intermediate frequencies of ERK stimulation, but longer or shorter pulse frequencies lead to lower protein expression (Wilson *et al.* 2017). Interestingly, they found that negative feedback to be essential for band-pass filtering, however mRNA stability was not needed, which directly contrasts Uhlitz, *et al.* findings.

Recently, mathematical modeling has also been used to design synthetic genes that can selectively respond to pulsed but not constant ERK activity (Ravindran *et al.* 2022, 2020). These gene designs were experimentally tested in cells and confirmed to respond preferentially to pulsatile ERK activation; it is not yet clear whether natural examples of this type of behavior exist. The closest candidate for this type of regulation so far is Egr-1, a protein with a short half life, that inhibits its own transcription (3.1a) (Cao *et al.* 1993). Data-driven modeling indicates that Egr-1 selectively decodes pulsatile ERK activity, compared to c-Fos (3.1b) (Saito *et al.* 2013). These results imply that genes which can encode ERK frequency likely have similar characteristics as Egr-1 – fast responding yet short-lived.

Despite the large body of work mechanistically linking ERK dynamics to gene expression, we postulate that ERK dynamics do not reliably guarantee specific gene expression profiles, but rather shift probabilities towards certain outcomes. Several studies have developed reporter cells in which both ERK activity and the expression of a target gene can be measured, by using CRISPR-based tagging of endogenous genes with fluorescent protein fusions at genomic loci (Gillies *et al.* 2017; Wilson *et al.* 2017). These systems allow continuous monitoring of ERK and its target gene expression in the same cell. Data from these experiments are useful to examine the fidelity and precision of the process by which ERK drives the expression of IEGs such as FOS or FOSL1. There is a striking degree of variability; in Gillies, *et al.* ERK activity only explained 35% of the variation in Fra-1 expression in single cells (Gillies *et al.* 2017). Thus, ERK activity can be strictly required for IEG expression but paradoxically show a low correlation at the single cell level. This observation can best be explained by the existence of unmeasured factors that also impact expression, such as epigenetic regulation of IEG loci, or metabolic changes that impact transcription or translation rates. Another explanation is that IEG expression may only respond to ERK stimulation in a subpopulation of cells, perhaps due to chromatin modification (Jena, Yu, and Toettcher 2021). In general,the effect of ERK on gene expression at single-cell resolution

is not as clear as classical bulk measurements report; therefore, future studies will require careful analysis of how ERK activation affects the distribution of its target gene expression within a cell population. Furthermore, there is yet to be a comprehensive quantification of the effects of ERK dynamics on the transcriptional and translational response of many ERK target genes in an individual cell.

3.4.3 ERK dynamics in the nucleus vs. cytoplasm as a mechanism for transcriptional diversification

Sub-cellular compartmentalization provides another mechanism to generate distinct downstream responses to ERK. Nuclear import of ERK is necessary for proliferation (Brunet *et al.* 1999) and activation of stress pathways (Sebastien Cagnol and Chambard 2010). On the other hand, cytosolic sequestration of ERK promotes expression of differentiation factors that drive myogenesis, suggesting a link between cytosolic signaling and differentiation (Michailovici *et al.* 2014; Marenda *et al.* 2006). Cytosolic ERK signaling is also linked to growth arrest and autophagy (Sebastien Cagnol and Chambard 2010). Control of nuclear and cytosolic ERK localization and phosphorylation is achieved through differentially localized DUSPs, or anchoring proteins (i.e. PEA-15) which sequesters ERK in the cytosol (Formstecher *et al.* 2001; Maik-Rachline, Hacohen-Lev-Ran, and Seger 2019). Spatially regulated ERK activity within the cytosol and the nucleus is another mechanism to diversify gene expression and cellular responses. In MCF-7 cells for example, either epidermal growth factor (EGF) or heregulin (HRG) can induce transient nuclear ERK activity; however, only HRG causes a sustained cytoplasmic ERK response. This sustained ERK activity in the cytoplasm stabilizes the c-Fos protein in HRG treated cells (Nakakuki *et al.* 2010). The transient nuclear activity is largely due to the negative feedback system in which ERK activity induces DUSP4 transcription, which targets nuclear ERK activity, while cytosolic

p-ERK remains constant (Wilson *et al.* 2017). This logic can be applied to the opposite scenario where ERK is only active in the nucleus; nuclear targets such as MYC, Jun, ETS may be phosphorylated while cytosolic targets (RSK1, cPLA2, PDE4, BIM) may not. The complex effects of nuclear versus cytoplasmic ERK activity is not fully examined, and more studies are needed to understand how different transcriptional programmes can arise from compartmental control of ERK.

3.5 ERK dynamics in tissue regulation

Gene knockout studies in roundworms, fruit flies, zebrafish, and mice have established the genetic requirement for ERK in many developmental and physiological systems. However, knockouts reveal little about the timing and dynamics of ERK activation needed to control tissue function. Recent work with optogenetic tools has begun to address this question by making it possible to create custom spatiotemporal patterns of ERK activation in a Drosophila embryo (Johnson *et al.* 2017; Johnson and Toettcher 2019). These new tools make it possible to understand when and where ERK activity is required during development. Live-cell reporters also demonstrate transient, localized ERK activation involved in adult tissue homeostasis and wound healing (Valon *et al.* 2021; Hiratsuka *et al.* 2015). Here, we describe four main roles for ERK dynamics within tissues (3.2).

3.5.1 Setting cell fate probabilities by integrated signal strength or duration

The most basic function of ERK within tissues is as a rheostat for mitogenic activity, where ERK activity controls cell division (3.2A). The average frequency of entry to S-phase can be modulated by increasing or decreasing ERK activity through growth factors, pharmacological compounds, or cell density (J.-Y. Chen *et al.* 2012; Fan and Meyer 2021; Min *et al.* 2020).
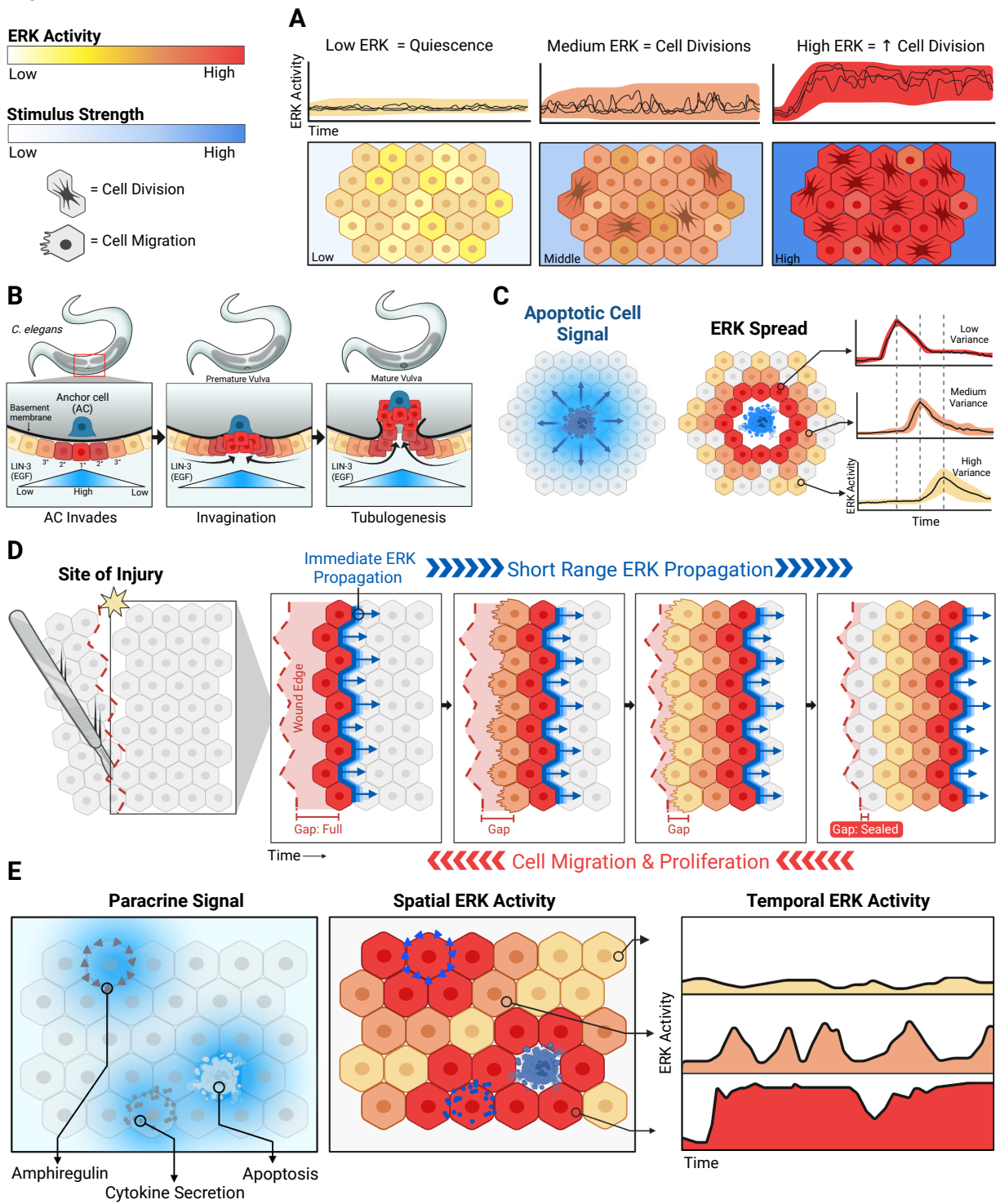
Figure 3.2 ERK Dynamics During Development and Tissue Homeostasis

Figure 3.2: ERK Dynamics During Development and Tissue Homeostasis **A** Increasing ERK activity increases the probability of cell division within the population on average. Schematic of single-cell ERK activity within a population (top panel) exposed to different EGF concentrations (bottom panel). Variations in signal activity indicated by different colors of cells. **B** Spatially restricted ERK activity is essential during development. Within the *C. elegans* gonad, the anchor cell (AC) is the point source for EGF ligand secretion. This creates a gradient to cells beneath the basement membrane around the AC (blue triangle below cells). Cells closest to the anchor cell receive the most stimulation (individual cell colors, with 1' cell being red), and thus show highest ERK activity leading to increased division and migration up through basement membrane to create the mature vulva. **C**. An apoptotic cell secretes EGF-like ligands, which creates a radial gradient from the dying cell. Cells closest to the center show high ERK activity, which conveys a survival advantage. Cells farther away from the dying cell see lower concentration of ligand (blue halo in left panel) resulting in slower and lower ERK activity and incomplete responses within the cell layer. Individual ERK activity traces shown to the right, color shading indicates variability within the population. Figure adapted from Gagliardi *et al.* 2021. **D**. During tissue injury, ERK activity provides both directional and migratory signals. Initially, cells adjacent to the injury have high ERK activity (first row, red cells) and secrete a short range ERK stimulus gradient that activates its neighbors (abutting gradient, blue). Once the neighbors are activated, the ERK activity in the previous cell layer decays, ultimately creating a wave of ERK activity (second through fourth panel). ERK activation waves repeatedly propagate from the site of injury. This directs cells to migrate towards the site of injury (red arrows below) resulting in gap closure and wound healing. **E** Altogether, many processes that cause ERK activity happen simultaneously within biological systems. Cells that are actively shedding EGF-like compounds such as apoptotic ligands, cytokines, and amphiregulin, create microenvironments (blue gradients) within the larger tissue. This is in contrast to subfigure A in which all stimuli are uniform. Due to the wide range of stimuli across a tissue, ERK activity will be heterogeneous. These complex and overlapping microenvironments allow diverse gene expression within a population, however it also makes predicting the behavior of a single-cell difficult.

Canonically, ERK acts primarily at a point in the cell cycle, termed the restriction point, by inducing Cyclin D transcription. Cyclin D enables CDK4/6 activity, promoting Rb phosphorylation and a concerted switch in kinase activities and gene expression that commits cells to enter S phase (Albanese *et al.* 1995; Weinberg 1995; Meloche *et al.* 1992). However, an important question remains to be fully answered, as to which features of ERK activation are essential for activating this transition. Earlier studies suggest that ERK activity timing is crucial during discrete time windows, in cells re-entering the cell cycle after serum starvation (Jones and Kazlauskas 2001; Zwang *et al.* 2011). However, in cells that are continuously cycling, the probability of S-phase entry for a newly-divided cell is proportional to ERK activity throughout the cell cycle of the mother cell (Min *et al.* 2020; Spencer *et al.* 2013). A further surprise revealed by this quantitative single-cell analysis is that ERK activity directs the rate of cell cycle entry by setting an overall translational capacity of the cell, and not simply by inducing Cyclin D expression. An important caveat in many studies of cell cycle regulation is that they employ cells exposed to high levels of growth factor or serum, or cells that are starved and then restimulated with a large bolus of serum or growth factors. These conditions drive rapid cell cycle times (¡20 hours) and abrupt transitions in metabolism that are unusual within most adult tissues, where cells experience intermittent stimulation by low concentrations of growth factors and cell cycle durations range from days to weeks.

Further complicating ERK's as a cell cycle driver, high levels of ERK activity can induce cell cycle arrest or senescence, especially when driven by oncogenes (Michaloglou *et al.* 2005; Deschênes-Simard *et al.* 2013). In an *in vivo* RAS-driven mammary tumor model, immediate induction of high RAS/ERK activity induced senescence rather than tumorigenesis, and effective tumor growth was only stimulated if RAS activation was initiated at low levels (Sarkisian *et al.* 2007). Conversely, human fibroblast cultures showed very low ERK activity linked to senescence (Tresini *et al.* 2007). In both stem cells and non-tumor cell line modes,

pulsatile activity is linked to cycle progression whereas sustained ERK activation correlates with cell cycle arrest (Aikin *et al.* 2020; Hiratsuka *et al.* 2020). While these results are context dependent, a compelling model suggests ERK is a non-monotonic driver of cell fates like proliferation and arrest (Deschênes-Simard *et al.* 2013). Using population and single-cell methods, a recent study reports that low and high levels of ERK activation induce arrest, whereas intermediate levels lead to maximal proliferation (J.-Y. Chen *et al.* 2023).

A similarly complicated situation is found in the regulation of cell death by ERK. Apoptosis in both normal and cancer cells occurs via the release of mitochondrial pro apoptotic factors including cytochrome c to the cytoplasm, which promote activation of initiator and effector caspases. While ERK is often regarded as a pro-survival signal that suppresses BIM to prevent cytochrome c release (Craxton *et al.* 2005; Sheridan, Brumatti, and Martin 2008), other studies have demonstrated a pro-apoptotic role in inducing caspase-8 activation which stimulates cytochrome c release mediated by Protein Kinase B (AKT) activation (S. Cagnol, Van Obberghen-Schilling, and Chambard 2006; H. Li *et al.* 2007). Paradoxically, both MEK inhibitors and active forms of MEK/ERK/RAF/RAS pathway have been associated with apoptosis induction (Sebastien Cagnol and Chambard 2010). A recent study used an improved ERK biosensor to clarify the role of ERK in apoptosis and necroptosis in murine fibrosarcoma cells. (Sipieter *et al.* 2021). In response to cell death-inducing ligands, cells demonstrated strong ERK signaling, including an increase in amplitude and duration during early stages of apoptosis compared to necroptosis. During later stages of cell death, the signaling characteristics of apoptosis and necroptosis were similar, except apoptosing cells displayed higher amplitudes (Sipieter *et al.* 2021). Interestingly ERK inhibition delayed TNF induced necroptosis while it sensitized cells to hFas ligand induced apoptosis, bolstering the context dependent role of ERK as both a pro-death and pro-survival regulator.

Thus, while ERK is a major regulator of quiescence, senescence, proliferation, and cell death, we still lack a comprehensive model of how its activity decides between these cell

fates. Developing such a model remains challenging due to the difficulty in accurately measuring the intensity of ERK activity, as well as differences between cell types. As noted above, the context of ERK activity is also very important; several studies emphasize cooperative interactions between ERK activity and other kinases such as PI3K/AKT for cells to enter into S-phase (Benary *et al.* 2020; J.-Y. Chen *et al.* 2012). Furthermore, cooperation between ERK and c-Jun-N-terminal kinase (JNK) is required to initiate DNA damage induced-senescence (Netterfield *et al.* 2022). Given the above examples, a comprehensive model will be dependent on the cell type and the context of each cell fate.

3.5.2   Providing a spatial cue for patterning and maintaining tissues

In many of its physiological roles, ERK activity is localized to certain cells, serving as a spatial cue. A classic example of this function is the differentiation of vulval precursor cells (VPCs) in *C. elegans* (3.2B). Development of this tissue is regulated by each cell's proximity to the EGF-releasing anchor cell (AC). Cells closest to the AC (i.e. VPC P6.p) show increased frequency of ERK pulses throughout development compared to VPCs that are farther away (Barkoulas *et al.* 2013; de la Cova *et al.* 2017). Critically, any disruption in this EGF gradient and resulting ERK dynamics disrupts normal vulval development. Furthermore, the dynamics of ERK activity in the Drosophila embryo play a role in driving cell fates (Gabay, Seger, and Shilo 1997; Lim *et al.* 2015; Grimm *et al.* 2012). One hour of ERK signaling is required to drive gut-endoderm-like gene expression, while a 30-minute pulse initiates an ectodermal neuroblast cell fate (Johnson and Toettcher 2019). The Drosophila embryo is less sensitive to the dose and more perceptive to the spatial distribution and timing of ERK activation (Johnson *et al.* 2017). In mouse blastocysts, spatially graded ERK pulses differentiate polar versus mural lineages, and pluripotent blastocysts exhibit opposing levels

of basal ERK activity compared to primitive endoderm (Simon *et al.* 2020).

Localized ERK signals can also be found in adult organisms, where they help to maintain tissue homeostasis. As noted in part 1 of this review, spatial propagation of radial ERK activity distribution, or SPREADs, have been observed in live mice (Hiratsuka *et al.* 2015). Similar patterns are also found in organotypic cultures of epithelial cells, where SPREADs occur preferentially in the outer layer of cells and reduce their propensity for apoptosis, relative to inner cells (Ender *et al.* 2022). In monolayer cultures, apoptotic cells trigger radially propagating waves of ERK pulses, which prevents apoptosis in the surrounding cells (3.2C) (Gagliardi *et al.* 2021). By preventing large numbers of adjacent cell deaths, these waves help to maintain integrity of the epithelium (Valon *et al.* 2021). In contrast, tissue compaction during Drosophila pupal notum development leads to downregulation of ERK signaling. In this context, ERK maintains tissue homeostasis by upregulating pro-apoptotic genes and driving excess cell elimination (Moreno *et al.* 2019).

3.5.3 Driving morphogenesis via wave-like activation

In some systems, the wave-like activity of ERK plays a specialized role in rapid structural changes needed for tissue morphogenesis. Importantly ERK regulates cell motility on the scale of hours (Mendoza *et al.* 2015, 2011). For example, coordinated effects on motility have been reported in 3D mammary epithelial cell cultures (Gagliardi *et al.* 2021) and immune cells (Kamioka *et al.* 2012; Zhang *et al.* 2016). Elevated ERK activity can also drive collective migration, a phenomenon crucial for tissue morphogenesis and wound repair (3.2D) (Aikin *et al.* 2020; Aoki *et al.* 2017; Matsubayashi *et al.* 2004). Cell-cell relay of ERK activity across contracting tissues drives proper invagination in the Drosophila tracheal placode. In this process, cells are activated in a sequential manner with a positive feedback from EGFR to Rho acting as a switch cooperatively triggers high ERK activity that is then relayed to the next cell (Ogura *et al.* 2018). Spatiotemporal patterns of ERK activity

drive base to apex multicellular flow in the developing murine inner ear. This suggests that ERK-driven helical collective cell movement mediates the spiral morphogenesis of the inner ear (Ishii *et al.* 2021). This type of tissue behavior is thought to be a product of a mechanical feedback loop where cell extension triggers ERK activation subsequently leading to cell contraction and pulling neighbor cells into an elongated and ERK activated form (Hino *et al.* 2020). In a similar manner as gradient based spatial activation, zebrafish scale regeneration is triggered by oscillating waves of ERK activity through the regenerating tissue. The wave-like activation is important for their optimal growth as sustained, non-wave-like ERK pattern impairs regeneration times (De Simone *et al.* 2021). These examples clearly demonstrate the importance of dynamic ERK signaling in regulating cell motility and tissue morphology.

3.5.4 Diversification of cell states

Cell fate decisions are often thought of as deterministic responses to a given stimulus, but emerging lines of evidence point to a more probabilistic view. In many of the examples above, the cell fates driven by ERK occur only in a subset of stimulated cells. Yet, this heterogeneity may often be an advantage in physiological tissues. Diversification of cellular behaviors allows a population of cells to adjust its responses over a wider range of stimuli strength and to behave more robustly (Suderman *et al.* 2017; Albeck, Pargett, and Davies 2018). An interesting possibility is that ERK dynamics may actively facilitate such cellular heterogeneity. The properties of ERK-mediated signaling and gene induction make it well suited to increase the diversity of gene expression within a cell population (3.2E) (Davies *et al.* 2020). In comparison to other signaling pathways examined via live-cell imaging, ERK activation is especially sensitive to local environmental stimuli (Regot *et al.* 2014), and it can amplify small changes in local growth factor ligands into high dynamic range pulses (Gillies *et al.* 2017). As noted above, these pulses trigger disparate patterns of IEG expression,

and because IEGs are transcriptional regulators themselves, this variation can translate into diversified expression profiles across the entire genome (Davies *et al.* 2020). Other data corroborate this idea; for instance, during developmental plasticity, autocrine ligands may provide deciding ability to cells by adjusting their fate in response to changing environmental signals (Shvartsman, Muratov, and Lauffenburger 2002). Reversible regulation of transcriptional enhancer activity by ERK may explain this concept: sustained ERK activity induces AP-1 proteins to bind DNA and displace pluripotency transcription factors from genes such as Nanog, while fluctuating ERK activity can allow for continued expression of pluripotency network factors (Hamilton *et al.* 2019). In this context, sporadic ERK signaling contributes to plasticity, allowing cells to maintain multi-fate potential.

In the *C. elegans* vulval system, variability of cell fate induction can have deleterious morphological effects that reduce organismal fitness. Careful quantitative experiments have delimited the range of variation in EGF expression that is compatible with wild type morphology. Expression of EGF above or below this range results in variable cell fates and mutant phenotypes (Barkoulas *et al.* 2013). While ERK signaling has been observed to be variable even within the wild-type range (de la Cova *et al.* 2017), the potential phenotypic outcome of this variation is suppressed by Notch signaling (Barkoulas *et al.* 2013). Thus, EGF-ERK signaling can be an enhancer of cellular heterogeneity in multiple systems, with either functional or deleterious effects, depending on the system.

3.6 ERK dynamics in disease, therapeutics, and pharmacology

ERK dynamics are intertwined with its roles in tissue homeostasis, regeneration, cancer progression, and drug resistance. Sporadic mutations in EGFR, RAS or RAF that steer ERK activity are strongly associated with cancer development, while somatic mutations in path-

way genes cause RASopathies, a family of syndromes that share overlapping developmental abnormalities (Rauen *et al.* 2015). However, the details of how ERK signaling dynamics are altered in mutant cells have only recently been examined. Cells with differences in amplitude, intensity, or duration of ERK signaling in single cells can still appear identical in a cell population when measured by immunoblot (Albeck, Pargett, and Davies 2018), which may help to explain why bulk measurements of ERK phosphorylation do not correlate with phenotypes in some models, such as RAS-driven tumor induction (Tuveson *et al.* 2004). Furthermore, different forms of inhibition, including EGFR or MEK inhibitors, can differentially alter patterns of ERK activity while appearing to produce similar degrees of suppression at the population level (Albeck, Mills, and Brugge 2013). Distinguishing single-cell behaviors is critical in diseases such as cancer where small treatment-resistant subpopulations can exert a disproportionately large effect on disease progression (Hirata *et al.* 2015; Gerosa *et al.* 2020). Thus, it is critical to understand how ERK activity dynamics are altered in diseases, and how they can be modulated for therapeutic benefit.

3.6.1 Differences in ERK activity dynamics in cancer and related diseases

Recent work has begun to examine the distinction between ERK dynamics in normal and cancer cells. This question is complicated by the fact that cancer cells contain hundreds of mutations that can affect pathway function, some of which directly alter the function of the pathway proteins, and others that exert indirect effects by changing contextual factors such as gene expression or cell shape. To help restrict this variation and simplify the comparison of RAS/ERK signaling properties between cancer cells, Bugaj *et al.* used an elegant strategy of activating RAS optogenetically at the level of RAS and simultaneously monitoring ERK activation via the nuclear translocation of FP-tagged ERK (Bugaj *et al.* 2018). This study

revealed that tumor cells carrying RAS pathway mutations have reduced temporal resolution in the transmission of the input light stimulus to the output of ERK (3.3A). In particular, cells with RAF mutations had a slower off-rate when the input was deactivated, preventing them from distinguishing sequential pulses of input. This loss of fidelity impacted gene expression, as Egr-1 showed lower expression levels when pulsatile input signals were blurred at the level of ERK in mutant cells, while Cyclin D1 and c-Jun expression increased, due to the extended active period of ERK (Bugaj *et al.* 2018).

Impaired stimulus resolution is also found in other examples of RAS/ERK pathway mutations. When mutant RAS isoforms were compared to wild type RAS within an isogenic "RAS-less" background, the major change in ERK dynamics driven by RAS mutants was a higher baseline activity that reduced the amplitude of ERK activity upon growth factor stimulation (3.3B) (Gillies *et al.* 2020). Additionally, a series of MEK mutants found in RASopathies were analyzed in embryonic Drosophila and zebrafish models (Goyal *et al.* 2017; Jindal *et al.* 2017). While these disease-associated mutants varied in whether they increased or decreased ERK activity, a shared feature was a reduction in the dynamic range of ERK activation gradients within each embryo. Finally, in a structural study of mutant EGFR forms found in glioblastoma, these variants showed a reduced difference in their response curve to strong and weak affinity ligands (Hu *et al.* 2022). Together these studies suggest a general feature of RAS/ERK pathway mutations in limiting cells' ability to generate ERK responses with distinct amplitude and duration to inputs. Interestingly, computational models of the RAS mutants revealed that although the dynamic range of ERK signaling was reduced, it was still much greater than would be expected based on the known biochemical properties of RAS mutants (Gillies *et al.* 2020). This observation suggests that the RAS/ERK pathway resists changes in its dynamic range, potentially through feedforward regulation of phosphatases. Theoretical work on signaling pathways supports the idea dynamic range is a key parameter for signaling pathways that can be made robust by certain pathway structures
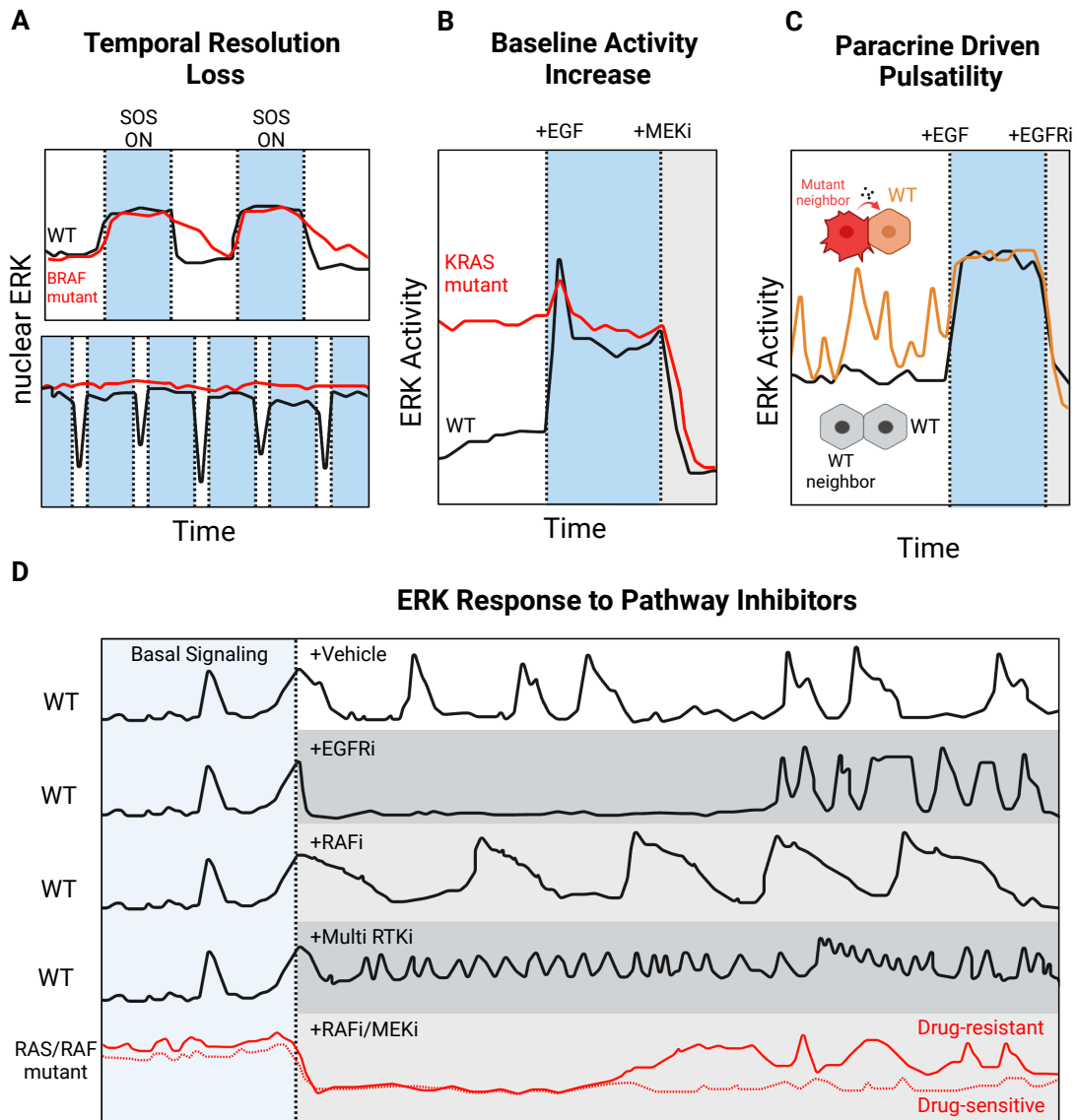
Figure 3.3: Alterations in ERK dynamics as a result of oncogenic mutations **A** Wildtype (WT) ERK undergoes fast activation and deactivation in response to optogenetic stimulation of SOS. BRAF G491A mutation leads to slower deactivation time (top). As a consequence, highly pulsatile ERK become elongated into sustained activity (bottom), leading to aberrant ERK signaling and transcriptional regulation (Bugaj *et al.* 2018). **B** KRAS and other mutations lead to increased baseline ERK activity and rescaled maximum stimulation levels (Gillies *et al.* 2020). **C** Mutant/malignant cells release paracrine signals that cause neighboring wild-type cells to become more pulsatile (Davies *et al.* 2020, Aikin *et al.* 2020). **D** Comparison of the ERK response to different inhibitor targets. EGFR inhibition quickly prevents ERK activation; however, pulsatile signaling later emerges (Gillies *et al.* 2020) . RAFi inhibitors paradoxically increase RAF activity resulting in long, low frequency ERK pulses. Non-EGFR receptor tyrosine kinase inhibitors result in high frequency pulses of ERK. (Goglia *et al.* 2020). Oncogenic mutations lead to decreased sensitivity of cells to inhibition, leading to heterogeneous reactivation of ERK activity (Ponsioen *et al.* 2021).

(Andrews *et al.* 2016; Janes, Reinhardt, and Yaffe 2008).

A second theme found in models of disease-associated ERK signaling is increased paracrine signaling, which results in greater spatial or temporal variability between cells in a population. Expression of EGFR, RAS, and RAF mutants in a non-tumor epithelial cell line led to increased amphiregulin (AREG) secretion that activated ERK in neighboring cells and triggered increased proliferation, migration, and cell extrusion activities (Aikin *et al.* 2020). In another mammary epithelial cell model, non-tumorigenic cells were selected *in vitro* and *in vivo* for highly invasive behavior. At the single-cell level, these malignant variants exhibit disordered pulses of ERK activity, which is driven by secreted AREG (3.3C) (Davies *et al.* 2020). In this model, the paracrine AREG signaling drives temporally dynamic ERK activation in neighboring cells, which as noted in section 2, can increase the variation of cellular transcriptional states.

Connecting the differences in mutation-driven ERK signaling to the gene expression outputs discussed above suggests two models for how mutations can drive malignant cell behavior. In the first model, the higher baseline ERK activity will drive increased average expression of genes such as Fra1 or Cyclin D1 that tend to accumulate regardless of the dynamics of ERK activity (Gillies *et al.* 2017; Min *et al.* 2020). This aberrant expression of Fra1 has been linked to cancer stem cells and clonal selection of resistant phenotypes in cancer (Tam *et al.* 2013; Dhillon and Tulchinsky 2015). In the second model, increased paracrine signaling drives a greater degree of time-varying heterogeneity, which may allow individual cells under stress to evade death by modifying their transcriptional profile. In any given tumor, both models could play a role, at different points in time or space. In addition to the simple paracrine signals modeled by *in vitro* systems, ERK activity in cancer cells is likely affected by a mixture of cell-cell, matrix, and nutrient signals from the complex microenvironment, convolved with the blurring effects of activating pathway mutations (Davies and Albeck 2018).

3.6.2 Manipulating ERK dynamics pharmacologically

Many ERK pathway inhibitors are now available, including small molecule inhibitors of EGFR and other receptor tyrosine kinases (RTKs), certain RAS variants, RAFs, MEKs, and ERKs. The development of these drugs was driven by the hope they would effectively target cancers with RTK, RAS, and RAF mutations. However, the history of clinical usage for these drugs is complex, with some proving effective as combination therapies and approved for clinical use in certain cancers, while other candidates were less successful. One explanation for varied performance of ERK inhibitors is the extensive feedback-driven buffering of ERK activity that we discuss in the companion review (Chapter 2). Although stability is important for physiological homeostasis, it adds complexity to pharmacological blocking activity. Mathematical models and *in vitro* cell-based studies are influenced by intact versus broken feedback systems resulting in varied ERK activity hence creating a need for targeting the protein outside of the feedback system, or using a combination of inhibitors to successfully disrupt the feedback loops (Sturm *et al.* 2010).

A data-driven approach based studies addressed how different inhibitors impact ERK dynamics. Such large scale screens allow identification of which drugs are potent ERK inhibitors and which are not. Such large scale screens are useful to quickly identify which drugs are likely to be effective candidates for ERK inhibition or to rule out compounds that work counterintuitively, such as the BRAF inhibitors that increase ERK signaling (Poulikakos *et al.* 2010). A systematic study compared the effects of 429 known kinase inhibitors and related compounds (Goglia *et al.* 2020) using keratinocyte cells with pronounced pulsatile ERK activity as baseline behavior. Several compounds showed altered pattern of ERK activity classified into three classes: EGFR or MEK inhibitors suppresses strong ERK activity, B-Raf "paradox activators" that slowed ERK pulsing, and non-ERBB RTK inhibitors, which increased pulsatile behavior of the keratinocytes (3.3D).

Despite the clinical successes of MAPK inhibitors, some fail as therapeutic candidates due to the robust wiring of this pathway. Even with increasing specificity and potency of drugs, complete inhibition of the pathway is difficult to achieve and a small portion of dividing cells remain (Albeck, Mills, and Brugge 2013; C. Yang *et al.* 2021). As ERK is inhibited, so too are the negative feedback mechanisms it activates. This has far reaching consequences, such as upregulation of drug insensitive protein isoforms (i.e. B/CRAF dimers), reactivation receptor-level signaling, and relaxing of phosphatase activity on ERK (3.3D) (Lito *et al.* 2012; Nazarian *et al.* 2010). Live-cell imaging confirms that cells progressing through the cell cycle after BRAF inhibition are not due to mutations, but rather incomplete suppression of the pathway and sporadic re-entry into the cell cycle (Gerosa *et al.* 2020; C. Yang *et al.* 2021). Interestingly, while both authors found upregulation of ERK targets in persister cells, Gerosa *et al.* found a spatial clustering of these cells while Yang *et al.* did not. This may reflect the differences in mechanisms of resistance, with receptor reactivation showing paracrine activity and distinct groups of ERK activity, while alternate mechanisms, such as stress adaptation, do not locally cluster drug resistant cells. Importantly, these different mechanisms of resistance yield distinct ERK activity patterns, which can be utilized to formulate personalized treatment plans (Goglia *et al.* 2020). Ultimately, the power of these biosensor tools lies in the ability to profile patient derived tumor organoids based on dynamic ERK activity and identify effective treatment regimes (Ponsioen *et al.* 2021; Muta *et al.* 2018). A major caveat to these studies is that dynamics in isolated tumor cells alone are not reflective of all the possible origins of resistance. ERK dynamics are influenced by numerous other factors including cell density (Fan and Meyer 2021), substrate stiffness (Farahani *et al.* 2021), cell type (Lebedev *et al.* 2022), and the tumor microenvironment. ERK biosensor studies in mouse models of melanoma show that extracellular matrix from cancer associated fibroblasts creates less sensitized tumor cells that escape pathway inhibition within 12 hours of treatment (Hirata *et al.* 2015). Future work must address other mechanisms altering

61

ERK dynamics in order to overcome the multifactorial nature of resistance.

Heterogeneity further complicates ERK targeting efficacy because each cell or subpopulation within a tumor may have different drug sensitivities. Within melanomas, differentiated melanocytic cells are sensitive to BRAF and ERK inhibitors, while dedifferentiated cells that have lost their lineage markers (SOX10 and MITF) are drug-resistant (Tsoi *et al.* 2018; Sun *et al.* 2021). This cell-to-cell variation can be due to differences in signaling pathway activities. Variation MAPK activation within a population of cells may lead to differential expression of AP-1 transcription factors which results in changes in heterogeneity and plasticity. In studies with patient-derived melanomas, transcriptional variation is well correlated with drug resistance (Shaffer *et al.* 2017). Single-cells expressing high levels of EGFR prior to vemurafenib inhibition were more likely to become resistant, and this resistant state included increased AP-1 expression. Corroborating these findings, AP-1 expression levels have been found to determine the diversity of states of BRAF-mutant cell lines upon MAPK inhibition. Specifically, cells with high c-Fos levels correlate with melanocytic and transitory states, whereas Fra-1/2 and c-Jun levels correlate with undifferentiated cells. Furthermore, knockdown of AP-1 factors lead to changes in differentiation state markers, suggesting that targeting AP-1 factors may render cells more vulnerable to pharmacological treatment (Comandante-Lou, Baumann, and Fallahi-Sichani 2022; Niepel, Spencer, and Sorger 2009). Unfortunately, heterogeneity and adaptive tendencies within highly mutated carcinomas continues to be a challenge for pharmaceutical industries.

Modulating the ERK pathway has great potential in treating RASopathies. One of the most prevalent RASopathy is neurofibromatosis type I, which affects individuals with mutations in the NF1 gene. NF1 normally down-regulates the ERK pathway by inactivating RAS, and individuals carrying a heterozygous loss of function of NF1 allele develop numerous neurofibroma tumors throughout their life (Amaravathi, Oblinger, and Welling 2021). Plexiform neurofibromas (pNFs) cause morbidity and can progress to malignant peripheral

neural sheath tumors (PNSTs). Sustained treatment with the MEK inhibitor selumetinib has shown substantial effectiveness at reducing the growth of pNFs, demonstrating that a sustained reduction in signaling activity over the course of time can counteract the increased ERK activity which primarily arises from NF1 loss (Gross, Dombi, and Widemann 2020; Gross *et al.* 2020). Further investigations are needed to determine the potential of similar strategies against different RASopathies, and also to decipher if they harbor distinct forms of ERK activity amplification requiring different patterns of inhibition.

3.6.3 Harnessing ERK activation dynamics for stem cells and re-generation

While the primary focus of most therapies in cancer and RASopathies remain to inhibit ERK, here we explore other ways in which manipulating ERK dynamics can be used in regenerative therapies. One emerging tool is the use of stem cells to repair injured tissues. ERK plays a multifaceted role in stem cell pluripotency and cell fate choices, which makes pharmacological targeting of the pathway a potential route for controlling differentiation. ERK activation, typically through Fibroblast Growth Factor (FGF), leads to differentiation of Embryonic stem cells (ESCs) (Kunath *et al.* 2007; Lanner and Rossant 2010; Hamilton and Brickman 2014; Hamilton *et al.* 2019). In fact, cultured ESCs can only be maintained in their naive, fully pluripotent state if ERK activity is strongly suppressed (Ma, Chen, and Chen 2016). To maintain their pluripotency, culture media dubbed "2i" and "3i" have been developed. 2i media includes inhibitors for both MEK and GSK3, with the MEK inhibitor suppressing ERK activity and the GSK3 inhibitor activating the transcription factor beta-catenin, while 3i additionally includes an FGFR inhibitor. Live-cell imaging revealed substantial heterogeneity in ERK activity ESCs following removal of 2i media, which coincided with loss of expression of the pluripotency factor Nanog over time (Deathridge *et*

al. 2019). Further study of ESCs revealed that they respond with a unique form of ERK activity: periods of high-frequency oscillations that are more regularly spaced and have a much shorter period (7 minute) than pulses found in epithelial cells (Raina *et al.* 2020).

The precise control of stem cell differentiation by ERK is still an ongoing area of research. An extensive study of biosensor dynamics in hematopoietic stem cells and multipotent progenitor cells reveals that the fate of adult stem cells involves ERK signaling (Wang *et al.* 2021). Live-cell imaging of these primary cells revealed differential responsiveness to different cytokines, as well as strong variation in ERK response between cells of the same type. Importantly, the specific pattern of ERK activity in individual cells predicted the future emergence of differentiation markers, suggesting that heterogeneity in ERK dynamics plays a role in setting the proportions of cells of different cell fate. However, the specific effect of ERK activity on gene expression is context dependent. Deathridge *et al.* surprisingly found a weak correlation between ERK activity and Nanog expression in ESC differentiation, while a study in blastocyst development found a negative correlation (Deathridge *et al.* 2019; Pokrass *et al.* 2020). Therefore, ERK activity likely controls cell fate by biasing gene expression and driving differentiation of cells in a proportional manner (Raina *et al.* 2021). These data provide important insights into engineering stem cells and controlling differentiation programs (Yu *et al.* 2018; Zarrabi *et al.* 2018), which is shown to be beneficial in treating a wide range of diseases.

Along with stem cell therapies, directly altering ERK signaling within injured tissue can be used to improve healing. As previously discussed, waves of ERK activity coordinate epithelial migration close wound gaps (Aoki *et al.* 2017; Matsubayashi *et al.* 2004). Additionally, ERK activity also helps direct movement of immune cells (Kamioka *et al.* 2012; Zhang *et al.* 2016) and fibroblasts, which produce the scaffolding, that are necessary for reepithelialization (Sepe *et al.* 2013). Live-cell imaging in zebrafish also indicates that sustained ERK activity is required for angiogenesis (Okuda *et al.* 2021). Transient epithelial-

mesenchymal transition (EMT) is thought to be an important part of this process (Kalluri and Weinberg 2009; Stone *et al.* 2016), whereby ERK facilitates the temporary phenotypic changes that result in loss of cell-cell contacts, increased cell motility, and increased expression of matrix proteins (Janda *et al.* 2002; Navandar *et al.* 2017; Shin *et al.* 2019; Zheng *et al.* 2022; Lamouille, Xu, and Derynck 2014). ERK activation leads to epigenetic remodeling and expression of transcription factors that facilitate global gene expression changes (Navandar *et al.* 2017; Beisaw *et al.* 2020). Single-cell modeling indicates that pathways are not rewired during EMT, but rather signaling dynamics are altered during cells transition from epithelia to mesenchyme (Wade *et al.* 2020). While the exact ERK dynamics driving EMT are still unclear, one study by Aikin *et al.* showed sustained ERK activity via BRAF and MEK mutations induced increased motility and decreased epithelial cell markers consistent with an EMT-like phenotype (Aikin *et al.* 2020). Time resolved signaling data would greatly contribute to our understanding of wound healing. It is clear ERK is necessary for initial wound healing and is maintained during healing by various growth factors released at the site of injury. Inhibition of ERK activity prolongs wound closure and could result in scar tissue (Tomasso, Bartscherer, and Seifert 2022; Matsubayashi *et al.* 2004). Conversely, ERK also promotes aberrant EMT and fibrosis (Jeng *et al.* 2020; S.-J. Kim *et al.* 2020; Madala *et al.* 2012). Resolving the timing and amount of ERK necessary for proper wound healing will allow for rational design of therapies for faster healing with minimal scar tissue (Escuin-Ordinas *et al.* 2016).

3.7 Future directions for dynamic ERK encoding

ERK is a powerful and flexible communication system that has been adapted to many biological functions. While early models envisioned deterministic signaling programs triggered by distinct growth factors that encoded discrete outcomes, single-cell studies have provided

a much more nuanced view. In other words, the relationship between ERK activation, gene expression, and cell fate is not perfectly correlated in individual cells. Despite the complexity of this behavior, the emerging principles discussed in this review help to make some sense of the intricate patterns and their biological functions. These concepts bring us closer to understanding the "code" of ERK dynamics that determines cell behavior, and they also bring remaining challenges into focus.

The first challenge is capturing spatiotemporal ERK dynamics in more *in vivo*, and clinically relevant models (i.e. patient derived tissues). While live-cell biosensors are becoming standard in studies of ERK dynamics, incorporation of these sensors are not always practical in clinical settings. We imagine a model that allows for highly accurate inference of ERK dynamics in patients without the use of biosensors. We have discussed the ways in which ERK signals are encoded into gene expression and cell fates. Therefore, future models should be able to decode gene expression and cell fates into ERK signals, providing the ability to predict or infer a patient's ERK history profile from simple measurements like fixed tissue staining. In the clinic, knowledge of this history is crucial for assaying for oncogenic activity and also pharmacologic efficacy. Models that can precisely recapitulate ERK histories using more feasible methods will greatly benefit therapeutic success.

Second, the most important actions of ERK occur not in single cells but in groups. There is ample evidence that collective cell behaviors and gene expression profiles can be strongly influenced by different forms of ERK dynamics. For example, MDCK cells migrate against the direction of intercellular ERK activity waves during wound healing (Moreno *et al.* 2019). In this instance, the aggregate pulsatile ERK signaling drives the behavior of a group of cells. A similar process occurs during scale regeneration where wave propagation is crucial for proper ring-like growth of the tissue (De Simone *et al.* 2021), or during mechanical feedback of ERK signaling on mouse ear development (Ishii *et al.* 2021). Although ERK is activated at the single cell level, it is the aggregate signaling that results in changes in

morphology (Potey *et al.* 2019). This is crucial for tissue homeostasis, where collective cell behavior is more important than that of an individual cell.

Finally, ERK is a strong causal driver of tissue-level cell behavior, but its actions at the single cell level are imprecise. Even for the most directly regulated genes, detailed measurements of a cell's ERK activity provides only limited predictive power for a given gene. The majority of this literature points to an essential interplay between signaling and contextual factors rather than the dynamics alone. The information provided by ERK dynamics must be interpreted in light of the status of other pathways within each cell. Thus, precise ERK responses and downstream effects are not the driving principle in most physiological settings, and the same is true for any signaling pathway. While we often study signaling pathways in isolation, each cell - and even an individual gene within the cell - responds to many inputs simultaneously. Viewed from this perspective, each signaling pathway is only a piece of the puzzle in determining cell behavior. A key question for future work will be to understand how much information about signaling status would be needed to predict cell behavior with high confidence. Lessons from the ERK pathway will need to be integrated with similar insights from other pathways such as NF-kB, p53, and cyclin regulation for which similarly extensive fields have developed. New methods will be needed to interrogate pathways with less dynamic information available, such as metabolic regulation, and to monitor multiple pathways simultaneously within each cell.

3.7.1 Funding

3.7.2 Acknowledgements

All figures were created with BioRender.com.

Chapter 4

Deciphering the History of ERK Activity from Fixed-Cell Immunofluorescence Measurements

4.1 Preface

This chapter was the originally submitted to Nature Communications on February 10th, 2023: Abhineet Ram, Michael Pargett, Yongin Choi, Devan Murphy, Markhus Cabel, Nont Kosaisawe, Gerald Quon, John Albeck. Deciphering the History of ERK Activity from Fixed-Cell Immunofluorescence Measurements.

A.R., M.P., and J. A. conceptualized the study, interpreted data, and wrote the manuscript. A.R. conducted the imaging experiments and data analysis. M.P. created the ordinary differential equation model and the subsequent scripts that allowed for gene simulations. Y.C. trained the convolutional neural networks. D.M. assisted with western blot and image registration. M.C. assisted with cell culture. N.K assisted with data analysis.

The article has been modified to satisfy the formatting requirements of this dissertations.

4.2 Abstract

The Ras/ERK pathway drives cell proliferation and other oncogenic behaviors, and quantifying its activity in situ is of high interest in cancer diagnosis and therapy. Pathway activation is often assayed by measuring phosphorylated ERK. However, this form of measurement overlooks dynamic aspects of signaling that can only be observed over time. In this study, we combine a live, single-cell ERK biosensor approach with multiplexed immunofluorescence staining of downstream target proteins to ask how well immunostaining captures the dynamic history of ERK activity. Combining linear regression, machine learning, and differential equation models, we develop an interpretive framework for immunostains, in which Fra-1 and pRb levels imply long term activation of ERK signaling, while Egr-1 and c-Myc indicate recent activation. We show that this framework can distinguish different classes of ERK dynamics within a heterogeneous population, providing a tool for annotating ERK dynamics within fixed tissues.

4.3 Introduction

The RAS/ERK pathway directs multiple cellular behaviors and regulates tissue homeostasis (Lavoie *et al.* , 2020). The terminal kinase in this pathway, Extracellular Signal-Regulated Kinase (ERK), is essential for cellular decisions to enter the cell cycle, migrate, or differentiate. Elevated ERK activity drives cancer and other diseases, and the quantitative strength and timing of ERK signaling play a critical role in disease progression and treatment. For example, individual cell fates can be altered by minor interruptions in ERK activity (Min *et al.* , 2020). Additionally, residual ERK activity following targeted kinase inhibitor treatment determines therapeutic efficacy (Bollag *et al.* , 2010), showing that proper measurement of pathway activation is an essential clinical parameter. Measuring phosphorylated ERK

within patient tissue samples is a widely used diagnostic for cancer drivers and treatment potency. However, such methods to assay ERK activation are limited in their spatiotemporal resolution and quantitative accuracy.

The complexity of measuring ERK activity arises from the fact that the duration and amplitude of ERK activation influence the cellular interpretation of its signal. The pattern of activity influences expression of numerous target genes (ETGs), including the Immediate Early Genes (IEGs), both by activating mRNA production and by enhancing protein stability (Cook *et al.*, 1999; Murphy *et al.*, 2002, 2004; Nakakuki *et al.*, 2010; Uhlitz *et al.*, 2017). Advances in live-cell imaging and CRISPR tagging have allowed a higher-resolution view of how patterns of activation and deactivation (ERK dynamics) correlate with ETG expression at the single-cell level. Dynamic features of the ERK signal have been shown to differentially drive its target genes. ERK amplitude and duration are integrated over time by stabilization of Fra-1 protein levels, whereas c-Fos, Egr-1, and other genes are reported to respond maximally to intermediate frequencies of activation (Gillies *et al.*, 2017; Saito *et al.*, 2013; Wilson *et al.*, 2017). In some systems, ERK pulsatility also correlates with proliferation and protection from apoptosis, while sustained activity correlates with cell cycle arrest (Aikin *et al.*, 2020; Ender *et al.*, 2022). These results highlight that the dynamic nature of ERK signaling can differentially activate genes, and therefore control cellular processes.

Current assessments of Ras/ERK pathway activation measure levels of phosphorylated ERK (pERK) using antibody-based assays (Bollag *et al.*, 2010; Escobar-Hoyos *et al.*, 2020; Flaherty *et al.*, 2010). However, a more informative measure of ERK activity would capture its dynamic history, enabling the observer to distinguish between cells with long-term constitutive activity or intermittent activation. Live-cell reporters provide a method to achieve this resolution in experimental settings, but cannot be used in humans and are often inaccessible in animal models. Furthermore, phospho-ERK concentration does not neces-

71

sarily capture its activity within the cell, given the variable role of competing phosphatases (Gillies *et al.* , 2020), and changes in ERK phosphorylation can occur rapidly within the cell, especially during pharmacological inhibition of the pathway or tissue isolation (Kleiman *et al.* , 2011). Therefore, detection of pERK is an unreliable indicator of the longer-term activation history of ERK (Albeck *et al.* , 2013). In this study, we explore the feasibility of estimating past ERK activity using antibody-based measurements of ETGs. Previous work has demonstrated that synthetic ETGs can capture ERK dynamics (Ravindran *et al.* , 2022). While incorporation of such biosensors remains impractical, endogenous ETGs have a range of different sensitivities to dynamic ERK activity (Davies *et al.* , 2020; Wilson *et al.* , 2017), which could potentially be used to infer pathway activation history using fixed-cell measurements only. Such inferences could be used in biopsy tissues to infer the dynamic nature of ERK activity within tumor tissue. Oncogene induced ERK activation has been shown to be distinct from normal physiological patterns, and is often sustained (Aikin *et al.* , 2020; Bugaj *et al.* , 2018), thus knowledge of the types of signaling found in a tissue can be informative about the source of stimulating activity. Moreover, the duration of signaling suppression by inhibitors is of high interest, therefore this could be a way of assessing the efficacy of a treatment over a long window of time.

To date, most studies of ETGs have considered how changes in ERK signaling dynamics impact the expression of a given ETG. We pose the reverse question: can an individual cell's ETG expression profile be decoded to infer the history of ERK activation? Furthermore, what are the best quantitative indicators of ERK activation, and how can the strength, duration, and frequency of ERK activation be predicted? To investigate these questions, we used a live-cell biosensor of ERK in combination with cyclic immunofluorescence for ETGs and other proteins regulated by ERK, including the canonical ETGs Egr-1, Fra-1, c-Jun, c-Myc, c-Fos, and phosphorylated proteins such as pERK, pc-Fos, and pRb (a downstream marker of ERK-dependent cell cycle entry; for convenience we collectively refer to all of these

markers as ETGs). Using statistical models and machine learning to predict ERK activity features based on the expression of each protein, we find that each gene product reports ERK history with a different memory span. Of the measurements used, long-term, average ERK activity is predicted best by levels of Fra-1, while short term, recent ERK activation is predicted best by levels of Egr-1 and c-Myc. Lastly, we tested the limits of our method by mathematical simulations of ERK driven gene expression, finding that in theory, static immunofluorescence measurements can well recapitulate dynamic activation history with as few as 16 targets.

4.4   Results

4.4.1   A dataset linking live-cell ERK activity to ERK target immunofluorescence

To create a dataset that enables correlation of ERK activation to downstream target expression and modification, we first collected live ERK activity measurements in response to differential activation of the RAS/MAP Kinase pathway. We used EKAR 3.5, a calibrated, FRET-based biosensor of ERK activity, to measure single-cell activation in MCF10A mammary epithelial cells (Fig. 4.1a, 4.7a-d). With a series of Epidermal Growth Factor (EGF) concentrations, ERK activity was stimulated in a dose-dependent manner (Fig. 4.1b, 4.7e). To increase the diversity of activity patterns, we added MEK inhibitor (MEKi) at varying times after EGF stimulation, and included treatments where EGF was added at different timepoints of the experiment (Fig. 4.1c, 4.7e, Supplementary Table 1). The combination of MEKi treatments and the dose curve of EGF led to a broad spectrum of ERK signaling behaviors, with pulsatile activity varying in both duration and amplitude (Fig. 4.1d). Consistent with previous studies (Gillies *et al.* , 2017; Ryu *et al.* , 2015), we found that ERK

73

activation is heterogenous from cell to cell within each dose of EGF stimulation.

Immediately following live-cell data collection, we fixed the cells, and conducted cyclic immunofluorescence (4i) staining to measure levels of eight targets downstream of ERK (Fig. 4.1a, e, Supplemental Movie 1). This protocol was adapted from Gut *et al.* (Gut *et al.*, 2018), and validated for our 96-well plate experiments (Fig. 4.8a-d). After quantifying antibody staining intensities, we found that most targets were dose responsive to EGF and suppressed by MEKi treatment (Fig. 4.1f, 4.7e). The one exception was c-Jun, which increased moderately with both MEK inhibition and EGF concentration, suggesting that its expression is not directly regulated by ERK activity in these cells.

We then analyzed the correlation between ERK activity and the expression of each target. To link live-cell ERK activity measurements with the respective 4i data for each cell, we aligned the corresponding image datasets and generated a heatmap arranged by the mean ERK activity measurement in each cell (Fig. 4.2a). While both ERK activity and 4i targets were variable across the data set, most of the 4i targets exhibited some discernible correlation with mean ERK activity, which was especially strong for Fra-1 and pRb. We calculated the Pearson correlation between ERK pulse features, such as frequency and duration for each cell, and each ETG measurement (Fig. 4.2b, c). The strongest correlations were between the sum of pulse duration to Fra-1 and pRb. Interestingly, Egr-1 was uniquely correlated with the average derivative of ERK activity, supporting the previous notion that Egr-1 selectively decodes pulsatile ERK activation (Saito *et al.*, 2013). Of note, c-Jun had little to no correlation with any feature of ERK activation, implying again that its expression is not directly controlled by ERK in these cells and providing a useful negative control for subsequent analyses. We also performed a more granular time-sensitive analysis by calculating the Pearson correlation between each target and the EKAR FRET measurement at each timepoint of the live-cell movie (Fig. 4.2e). The correlation of Fra-1 and pRb was distributed across most of the time series ($r \approx 0.5$, 0.4, respectively) from the initial stimulus,
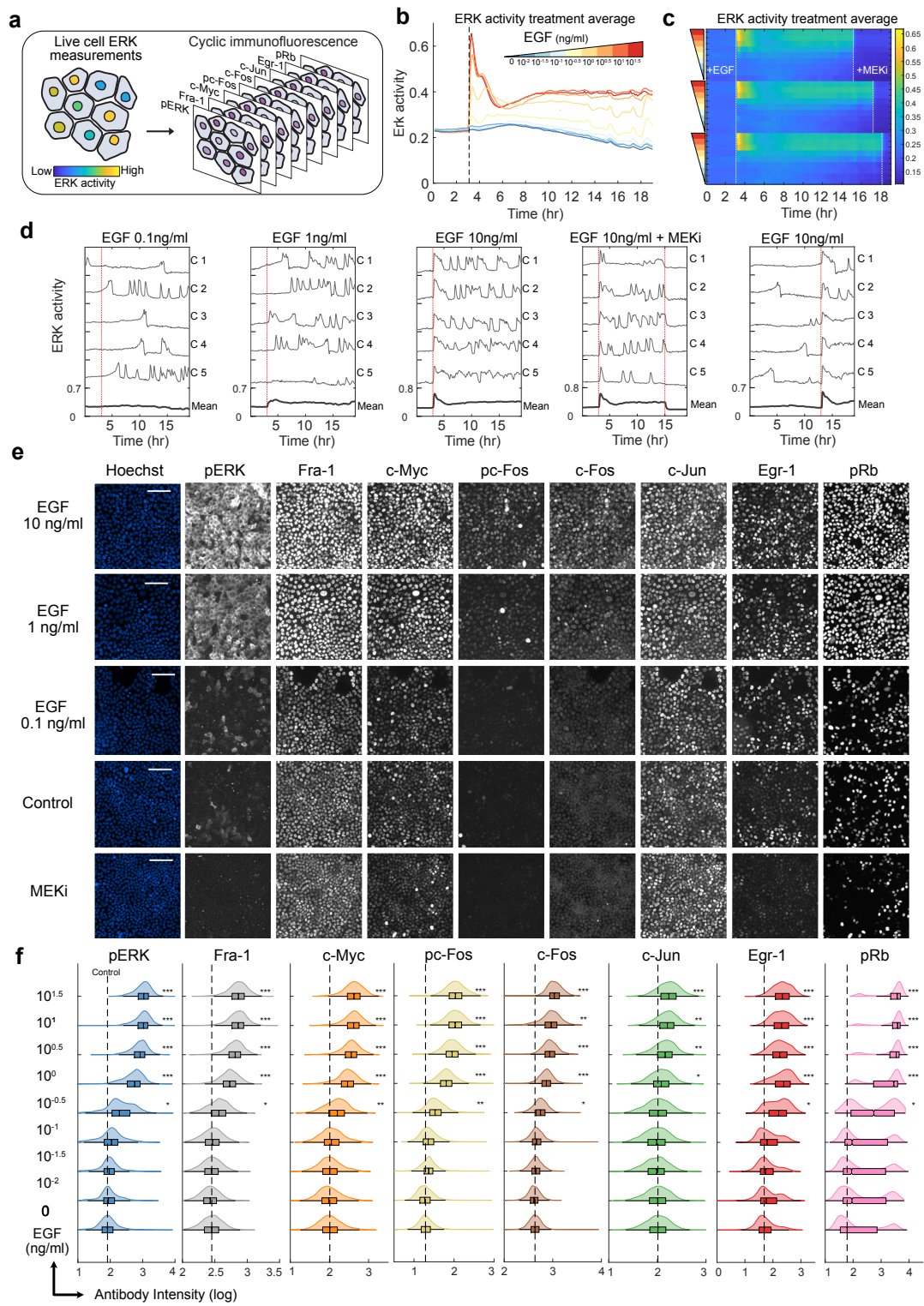
Figure 4.1 ERK activity and target genes are dose-responsive to Epidermal Growth Factor

Figure 4.1: ERK activity and target genes are dose-responsive to Epidermal Growth Factor **a** Schematic of the experimental method. Live cells were imaged in 96-well plates for 19 hours and immediately fixed. Plates were subsequently stained for antibody-based measurements. **b** Treatment average response measurements for live-cell ERK biosensor (EKAR) with increasing concentrations of EGF. Data are presented as the mean of each treatment ($n_{wellreplicates}$ = 9-11 for each dose of EGF, 21 for control). **c** Treatment average response measurements depicted as a heatmap. Each row is the treatment average EKAR measurement (FRET measurements are indicated by color). EGF concentration indicated by colored triangles from Fig. 1b. MEKi = MEK inhibitor PD0325901 (100nM) ($n_{wellreplicates}$ = 2-4 for each treatment). **d** Single-cell response plots to indicated treatment. Bold line indicates the average of all cells in one well of the treatment. **e** MCF10A cells immuno-stained with cyclic immunofluorescence. Each row depicts the same group of cells. Scale bar = 100 um. **f** Quantification of cyclic immunofluorescence measurements from listed EGF treatment. Dashed line indicates median of vehicle control condition (0 ng/ml EGF). Variance corrected t-tests were conducted by comparing each EGF treated condition to vehicle control $n_{replicates}$ = 3. * p-val <0.05, ** p-val <0.005, *** p-val <0.0005.

apart from a period where ERK activity is weakest, about 2 to 4 hours after EGF addition. In contrast, c-Myc, c-Fos, and pc-Fos mildly correlate to ERK activity about 5 hours from prior to fixation ($r \approx 0.3$), and the correlation is highest ($r \approx 0.55$) during the last hour before fixation. As expected, pERK most correlates to ERK activity immediately prior to fixation ($r \approx 0.6$). Finally, Egr-1 correlates only to ERK activities 30 minutes to 1 hour prior to fixation ($r \approx 0.5$).

To visualize spatial correlations of ERK-ETG signaling within the dataset, we plotted a spatial heatmap of signaling and gene expression, where cells within a single image are clustered in a heatmap visualization by proximity to one another (Fig. 4.2d). This analysis shows spatial ERK activation of groups of cells throughout the experiment. Interestingly, recent activation events are typically marked by strong Egr-1 expression within a local group of cells (Fig. 4.2f).
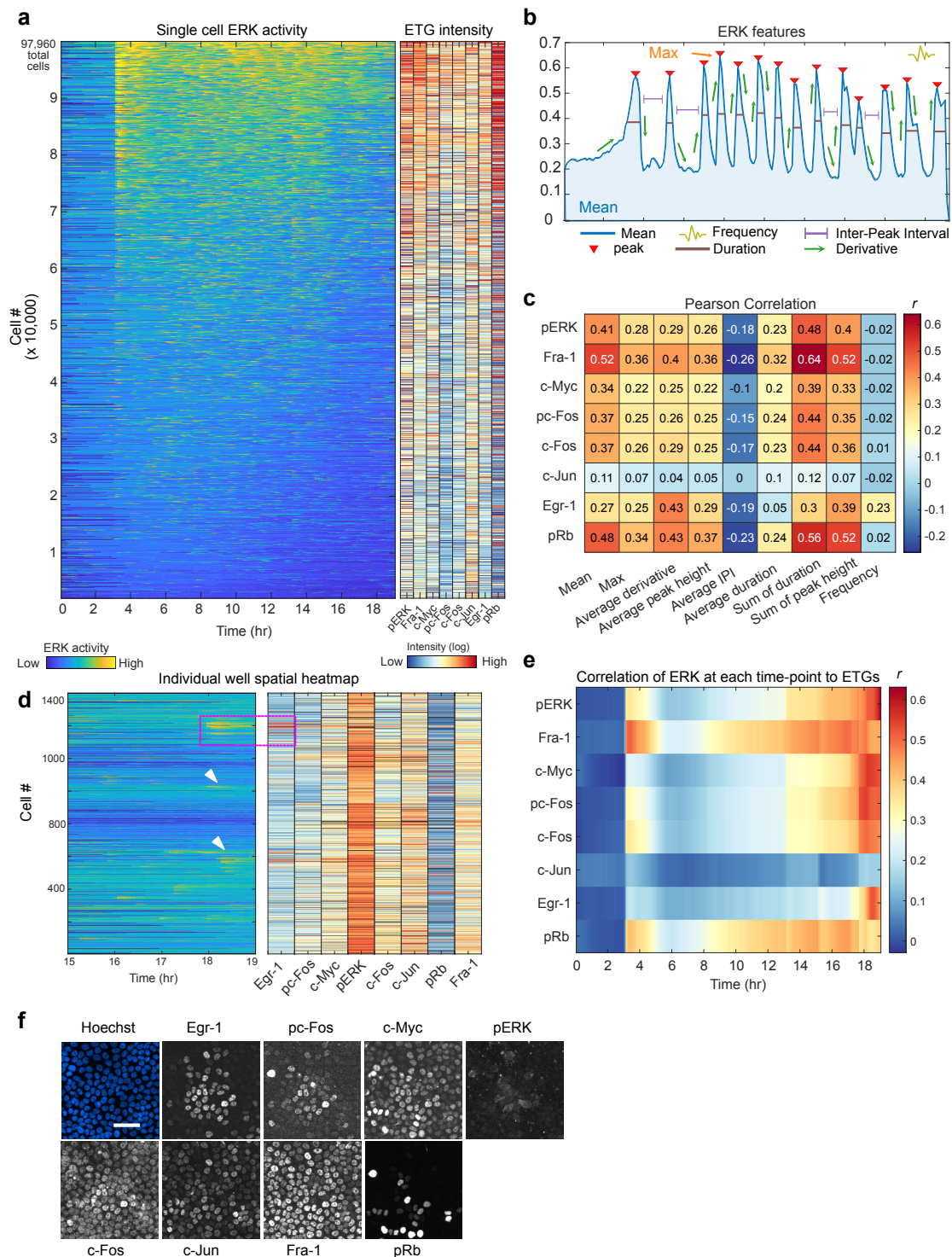
Figure 4.2 ERK target gene expression moderately correlates with features of ERK dynamics

Figure 4.2: ERK target gene expression moderately correlates with features of ERK dynamics **a** Single-cell heatmap for EKAR FRET measurements and corresponding ETG intensity, each row represents one cell (ncells = 97,960, $n_{replicates}$ = 3). ETG expression colored by log of antibody intensity from immunofluorescence measurements. **b** Features of ERK dynamics analyzed. Frequency was also calculated by estimating the mean normalized frequency of the power spectrum of the EKAR FRET measurement time series for each cell. **c** Pearson correlation (r) between each ERK feature and each cyclic immunofluorescence measurement, where single-cell values were used. **d** Spatial heatmap of EKAR (left) and ETG (right) measurements from a single well (control condition). Heatmap is organized by proximity of cells to each other so that neighboring cells in the well are plotted closer to each other in the heatmap. Magenta box indicates cells in f. White arrows indicate cells that recently activated ERK which resulted in higher Egr-1 expression (right). **e** Pearson correlation (r) between single-cell ETG measurements and the EKAR FRET measurement at each timepoint from the live-cell experiment. **f** Corresponding cells from magenta box in Fig. 4.2d. Scale bar = 50um.

4.4.2 Regression modeling of the ERK-ETG relationship predicts features of ERK dynamics

For a rigorous statistical analysis of the relationship between ERK activity and ETG expression, we performed cross-validated linear regression using the 4i measurements as predictors and ERK pulse features as response variables. We first created single predictor models to assess how well each target individually predicts each ERK feature in an individual cell. Analysis of the variance explained (R^2) for each model confirms the results from the Pearson correlation analysis. Fra-1 and pRb best predict the sum of duration of ERK pulses ($R^2 =$ 0.42, 0.31, respectively), and the average ERK activity in each cell (R^2 = 0.28 and 0.23) (Fig. 4.3a, b., 4.9a). These results suggest the duration of ERK activation seems to have a stronger influence on gene expression than the strength of the activation.

To assess whether the prediction models can be improved by considering multiple stains simultaneously, we generated several multiple linear regression (MLR) models using all 4i measurements as predictors at once (Fig. 4.3a, c). The ERK parameter with the highest variance explained was the sum of duration (R^2 = 0.52) The models for derivative benefited

the most from the multivariable models, however, they still only explained 33% of the variation in the data. c-Jun again served as a negative control, as those models did not explain any of the variation in ERK activity.

We then investigated which antibody combinations are most important in the MLR models. For each ERK feature, we created models that successively added predictors, and measured the resulting R^2, and test-set error for each new predictor (Fig. 4.3d, 4.9b). For most ERK features, we found that the maximum R^2 values can be achieved with just 2 to 3 predictors, where adding Fra-1 and pRb typically caused the highest improvement in R^2 values and decrease in test-set error. The best model for the average derivative of ERK had a similar R^2 with the model for the ERK mean ($R^2 = 0.36$, 0.33, respectively). The main distinction for the average derivative model is the strong contribution from Egr-1. To understand why adding more predictors does not improve models, we calculated the pairwise correlation between each 4i target, and found that many targets were moderately correlated with each other (Fig. 4.9c). The slight co-linearity between the predictors suggests that they share mutual information and thus explains why only a few predictors are needed to achieve the best possible models. These results indicate that ERK strength and duration are best inferred using Fra-1 and pRb, while ERK variability (derivative) are best inferred using Egr-1 and pRb. The fact that pRb predicts both long term ERK activation and variability suggests that Rb phosphorylation (cell cycle entry) is sensitive to different types of ERK activity (Min *et al.*, 2020; Zwang *et al.*, 2011).

We repeated the regression analysis on treatment averages to explore the difference between population and single-cell models. To calculate the treatment average for each measurement, we simply grouped cells with similar treatment conditions, and averaged their respective 4i measurements and ERK features. Overall, bulk models were superior to the single-cell models, as Fra-1 and pRb individually were excellent predictors for ERK dynamics (R^2 ¿ 0.7, Fig. 4.3e, f). Treatment average MLR models notably improved the predictions for

average inter-peak interval, average duration, and frequency ($R^2 = 0.85$, 0.72, 0.39, respectively). Fra-1 and pRb retained the most consistent relationship to ERK dynamics and were the most important predictors in all models. These results further solidify the importance of Fra-1 and pRb as markers for ERK activity. Furthermore, population average models reconcile the modest predictive power of the single-cell models and confirm the classical view that ERK determines gene expression.

Both the regression analysis and Pearson correlation indicate the pERK was not strongly correlated to long-term ERK activation in single cells. The poor relationship is partly due to the treatments that inhibit MEK at varying times after EGF addition, which lead to the virtually no pERK signal. When we remove these treatments from the analysis, the regression models notably improve for pERK, and slightly improve for other 4i measurements (Fig. 4.9d). These results indicate that pharmacological inhibition renders pERK an unreliable predictor of ERK histories, and that relying solely on pERK staining can lead to misinterpretations of pathway activation. Many studies assess the effect of pathway inhibitors using pERK staining; consequently, we argue other markers should be used. The Fra-1 and pRb models are robust to MEKi treatments, and therefore are the best predictors of long-term ERK activation.

4.4.3 Neural network-based models of the ERK-ETG relationship reveals non-linear time dependence of ERK dynamics

While the previous models of featurized ERK activity provide interpretable correlations that help to understand the underlying biological process, they assume linearity and may not capture more complex relationships in the data. Additionally, some ERK parameters are correlated with each other, and other features of the time series may be missed. To examine the importance of the timing of ERK activation and identify which timepoints have
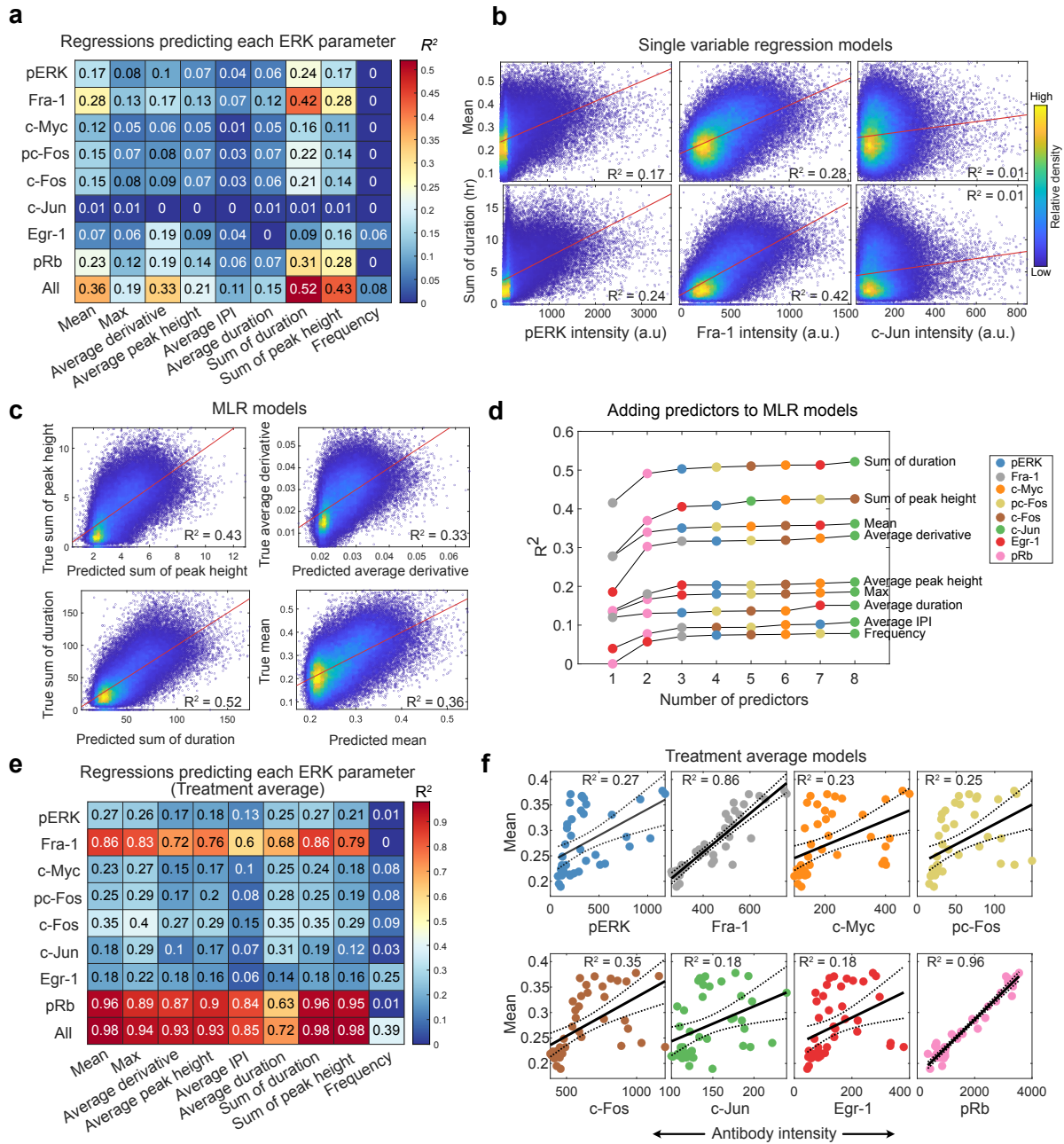
Figure 4.3 ERK target gene expression predicts history of ERK activation

Figure 4.3: **a** Single-cell regression showing the coefficient of determination (R^2) of linear regression models which use ETGs to predict each ERK feature. 10-fold cross-validation was conducted to retrieve the best test-set model. This model was then fitted on the full dataset. **b** Scatter plots of single-cell regression models showing line of best fit. Color indicates relative density of the data. **c** Scatter plot showing each cell's predicted (x-axis) vs true (y-axis) value in the multiple linear regression (MLR) models. **d** Results of adding predictors to MLR models. Color of each point indicates which predictor was added at each step. **e** Average values were calculated for all cells with the same treatment. These values were then used to fit regression models that predict each ERK feature using ETGs. **f** Scatter plots showing line of best fit and confidence intervals for treatment average regression models.

the greatest impact on final expression levels, we trained a convolutional neural network (CNN) to use the ERK activity time series to predict expression levels of each ERK target in individual cells (Fig. 4.4a, top). As a comparison to the CNN, we also fit linear regression models (TS linear) using the values at each timepoint of the ERK time series as individual variables to predict final ERK target levels (Fig. 4.4a bottom left). Finally, we compared the performance of these time series-based models with that of ERK dynamics feature-based models (Featurized linear). These feature-based models used all nine featurized ERK measurements (i.e. mean/duration/frequency) to predict the expression of each ERK target (Fig. 4.4a bottom right).

We found that the CNN achieved the highest performance in predicting all ERK targets, except for pERK (Fig. 4.4b). To account for overfitting, we calculated the mean squared error (MSE) on unseen data (test set) and the CNN exhibited the least error for all targets, except for pERK (Fig. 4.4b bottom). Although the CNN yielded better performance for most targets, a significant amount of variance is still not captured by the model (Fig. 4.4c). Notably, the CNN models for Egr-1 and pRb explained much more variance than linear regression models of other targets, implying that Egr-1 and pRb likely respond to ERK activation with significant non-linearity. Finally, for many 4i targets, the featurized linear models underperformed the other two methods, both in R^2 and test set error, indicating that the featurization method often does not capture important aspects of ERK signaling

that influence gene expression.

We then used the CNN model parameter weights (feature importance) to investigate which timepoints most influenced the final expression of each target. However, feature importance across much of the time series was overshadowed by a strong correlation to the initial stimulus response, which likely reflects a correlation with the treatment delivered rather than direct biochemical regulation of ETGs (Fig. 4.10a). Therefore, we limited the model to using only time points more than 5 hours after the initial treatment when training our time series models, which resulted in a minimal decrease of the CNN performance (Fig. 4.10b). A CNN trained on fewer time points further confirms our regression results, and captures nuances of the ERK-ETG relationship (Fig. 4.4d). The findings reinforce the observations from the linear regression analysis, and highlight the importance of considering both the timing and intensity of ERK activation in understanding how gene expression is regulated. Fra-1 is influenced by a wide time span with peak influence starting as early as 12 hours prior; the most recent two hours have little effect. c-Fos and pc-Fos are also influenced by time spans of more than six hours, but focused on the last two to four hours. Egr-1 is strongly influenced by ERK activation within the last two hours, while pERK, c-Myc and pRb are influenced strongly by the last hour of ERK activation. This alternate modeling approach confirms that each ETG is differentially sensitive to timing of ERK activity, and that in some cases, this relationship is not well characterized as a linear relationship.

4.4.4 Classification models uncover prototypical patterns of ERK signaling with distinct gene expression profiles

Thus far, we have trained models that predict several continuous variables that represent ERK history; however, the application of these models is limited by the challenge of concurrently visualizing the predictions. Therefore, we demonstrate here how spatiotemporal ERK
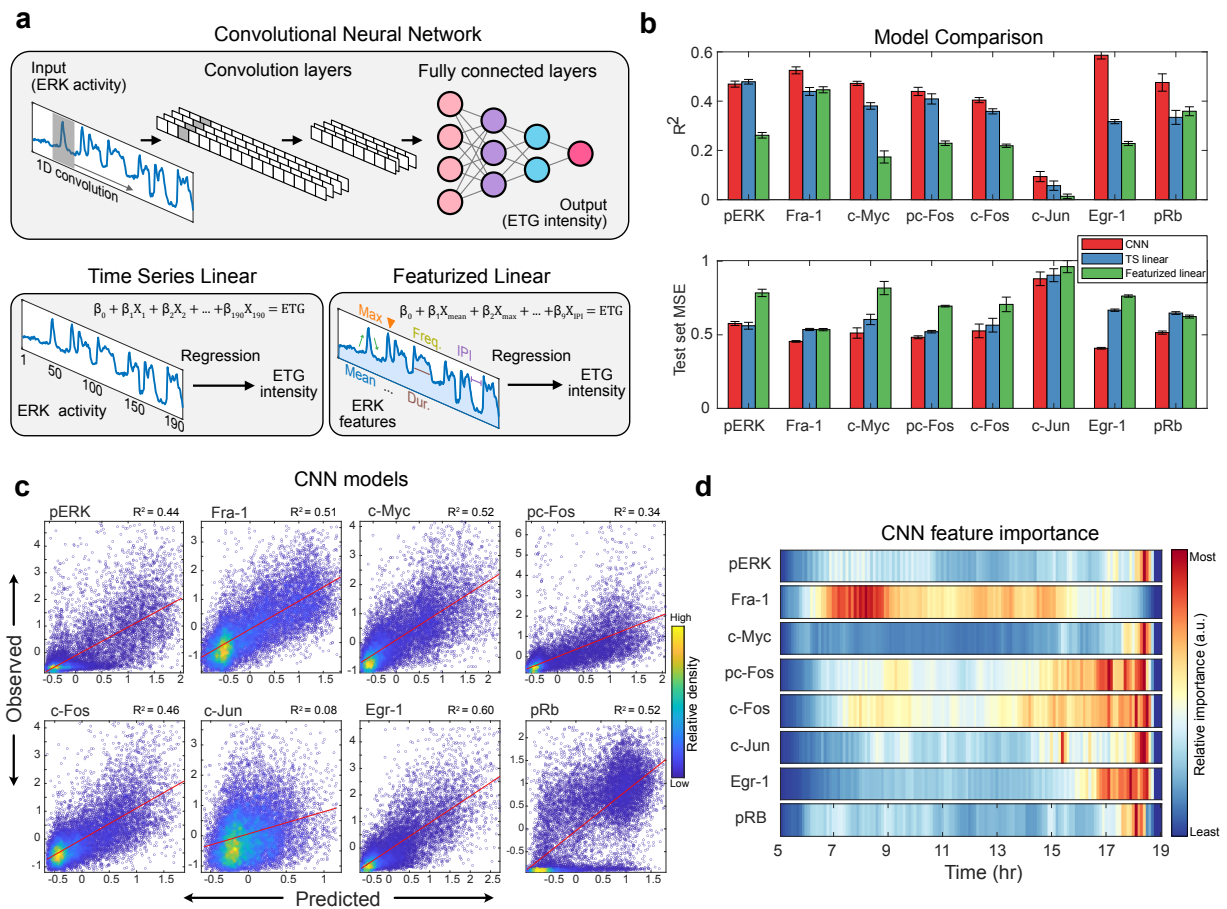
Figure 4.4: Convolutional neural network identifies non-linear signal transmission. **a** For each ETG, three types of prediction models were separately trained. Top: Simplified schematic of convolutional neural network architecture containing two convolutional layers and three fully connected layers. Bottom left: Multiple variable regression where ERK activity at each time point is considered as a predictor variable (TS linear). Bottom right: Multiple variable linear regression where nine features of ERK activity are considered as predictor variables (Featurized linear). **b** Top: Bar plot indicating R^2 for three models used to predict ETG levels. Bottom: Bar plot indicating mean square error for three models used to predict ETG levels. Error bars represent standard error calculated using values from each fold of the 5-fold cross-validation partitions. **c** Scatter plot of the predicted and observed values of the CNN trained on all 190 timepoints (19 hours). The data represent standardized (z-scored) values. **d** Feature attribution heatmap showing the importance of each timepoint in the CNN model trained on 150 timepoints (15 hours). Color map represents relative values within each row.

a Cluster average ERK signaling

b Cluster average ETG expression

c Decision tree model confusion matrix

d ROC curve for classification

e Predicted signaling histories using ETG measurements
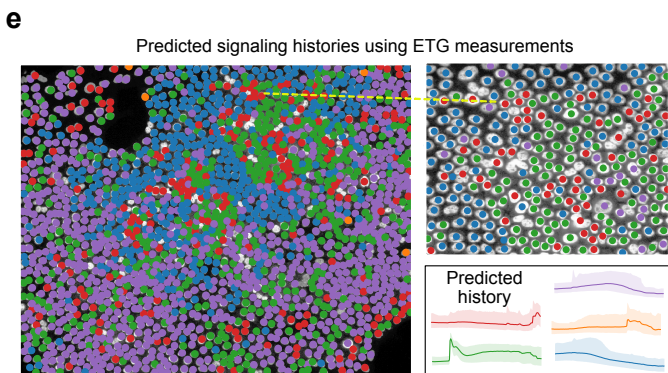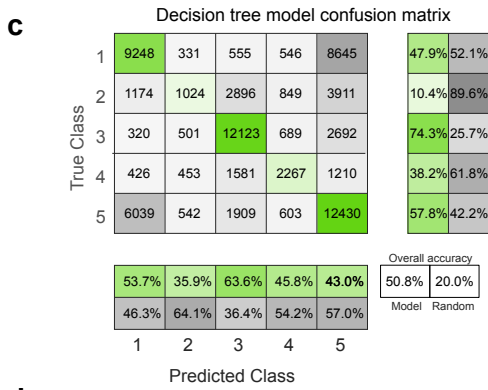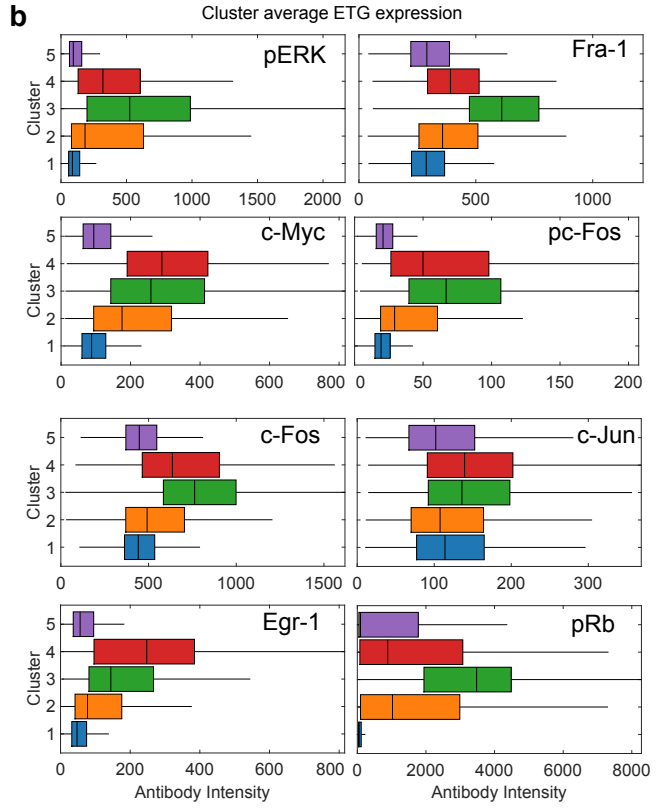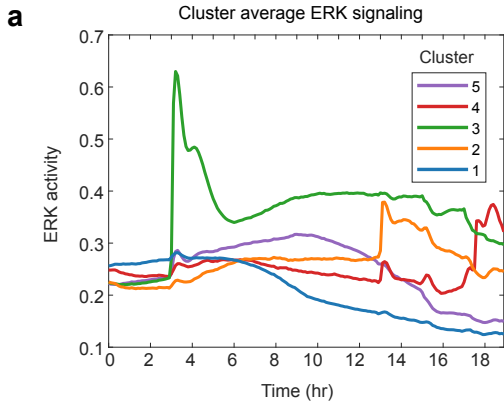
Figure 4.5: Annotating spatiotemporal ERK patterns in images using Decision Tree model. **a** Average ERK activity in each cluster identified by k-means clustering of EKAR time series data. Cells per cluster: C_{119325}, C_{29989}, C_{316325} ,C_{46244}, C_{521523}. **b** Box plot showing median, quartiles, and range of ETG intensity in each cluster. **c** Confusion matrix showing the amount of accurate (green) and misclassified (gray) cells in each class. Decision tree leaf size was optimized by cross-validation and collecting the leaf size with the minimum test-set error (129). **d** Receiver operating characteristic curves for each class in the decision tree model. **e** MCF10A cell stained with Hoechst (gray) overlayed with predicted signaling histories. Dark lines indicate the mean ERK activity for each cluster (as in **a**), and shaded regions indicate 25th and 75th percentiles.

predictions can be represented in a concise and intuitive manner. To do so, we first used k-means clustering to group cells into similar response classes, or prototypes, of ERK activity. We clustered cells into five classes: low activation (cluster 1), recent deactivation (cluster 2), long term activation (cluster 3), mid-term activation (cluster 4), and recent activation (cluster 5) (Fig. 4.5a, 4.11a). Analysis of the 4i target expression levels in each cluster was consistent with our previous statistical models (Fig. 4.5b). Long-term activation led to the highest expression of pERK, Fra-1, and pRb, while low activation displayed the lowest for all targets. Cells with recent activation highly expressed Egr-1 and c-Myc.

We next trained a decision tree classifier that predicts prototypes of ERK signaling history using ERK target expression levels (Fig. 4.5c, d). The overall prediction accuracy of our model was 51% (compared to 20% for random selection), while individual class predictions varied in accuracy. Long-term activation class predictions were the most accurate (64%), and mid-term activation classifications were the least accurate (36%). These /findings indicate that long term and recent activation result in distinct patterns of the expressed genes we measured, while mid-term activation produces the highest variability in gene expression. The residual confusion in the classifier reflects that some classes are not well separated in the dataset, and that individual cells vary quite widely in their ERK activity (Fig. 4.5d, 4.11a). For classification, the predictor importance ranked pc-Fos as the most important predictor, followed by Fra-1 and pRb (Fig. 4.11b). This result indicates that, while pc-Fos may not

explain a high amount of variance in ERK history, it carries particularly useful information for distinguishing among the five classes identified here. Finally, to simulate a potential use case with fixed tissue samples, we then used our classifier to predict ERK activity classes, and therefore histories, in cells from a single well in our dataset (Fig. 4.5e). Our analysis effectively quantifies the distinctiveness in gene expression associated with different ERK signaling prototypes and illustrates the utility of ETG stains in predicting the spatiotemporal signaling history of individual cells.

4.4.5   Dynamical systems modeling of ERK-driven gene expression

To investigate the theoretical limits of predicting ERK dynamics from ETG levels, we extended an ordinary differential equation (ODE) model representing the regulation of ETGs (Davies *et al.* , 2020; Gillies *et al.* , 2017) (Fig. 4.6a). For a given ERK activity time series, the model simulates the mRNA and protein levels of a hypothetical ERK-responsive gene (sim-ETG). We constructed 1,000 hypothetical sim-ETGs by randomly assigning each one with different parameters values for mRNA degradation rate, protein degradation rate, phosphorylated protein degradation rate, protein dephosphorylation rate, negative feedback half-max concentration, and fractional expression at baseline (Fig. 4.6c, Supplementary Table 2). These 1,000 gene parameter configurations survey the parameter space with the goal of identifying sim-ETGs that capture different aspects of ERK signaling. Using 10,000 randomly selected live-cell ERK activity measurements from our experimental data, we simulated responses of all 1,000 sim-ETGs for each cell (Fig. 4.6b, 4.12A). Using the end point sim-ETG protein values (representing a fixed-cell 4i measurement of the hypothetical protein), we applied single variable regression modeling to characterize each sim-ETG's capacity to predict ERK dynamics features. For predicting average ERK activity throughout the experiment, we found that 49% of sim-ETGs exhibited a R^2 above 0.5 and over 100 were excellent predictors (R^2 ¿ 0.8) (Fig. 4.6d). For predicting the maximum activation and

average pulse height, only 12% of sim-ETGs exhibited a R^2 above 0.5, with a maximum R^2 around 0.6 (Fig. 4.12c). Models for predicting dynamic ERK features like the frequency or the average derivative were overall worse than integrative features like the mean or sum of duration, reflecting that sim-ETGs under this model are variations on an integrator of ERK activity (Fig. 4.12c).

To visualize the gene expression response, we plotted a single cell's ERK signal along with the response of the top five predictors of the mean (Fig. 4.6f). These response profiles show that both genes activated by or inhibited by ERK can serve as reliable predictors of ERK activity. While our experimental ETG measurements were selected based on known positive responders to ERK, 20% of sim-ETGs were negatively regulated by ERK (Fig. 4.12b); experimental prediction of ERK activity would likely be improved by including genes that are inhibited by ERK (Yamamoto *et al.* , 2006). We then analyzed which gene parameters most influence how well an individual sim-ETG predicts mean ERK activity by examining the weights from a MLR model of sim-ETGs (Fig. 4.12d, e). Consistent with the known behavior of Fra-1, slow mRNA and phosphorylated protein degradation rates allow for accurate recording of the average ERK history.

Our 4i data analysis determined that while Fra-1 predicts long-term history, Egr-1 and c-Myc predict recent history. To examine this distinction in sim-ETGs, we calculated the correlation between the ERK activity at each timepoint and end-point protein expression (analogous to the experimental data in Fig. 2e). As expected, genes that predict mean ERK activity tend to be correlated with ERK activity over a wide time span, similarly to Fra-1. Those that are less effective at predicting mean are correlated with recent activation, behaving more like Egr-1 or c-Myc (Fig. 4.6e). Notably, no sim-ETG under this model was specifically predictive of intermediate timescales of activation (i.e. 5-10 hours prior to fixation).

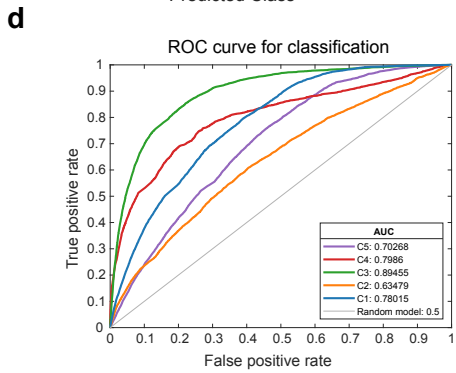Finally, to investigate how many gene measurements are required to accurately predict
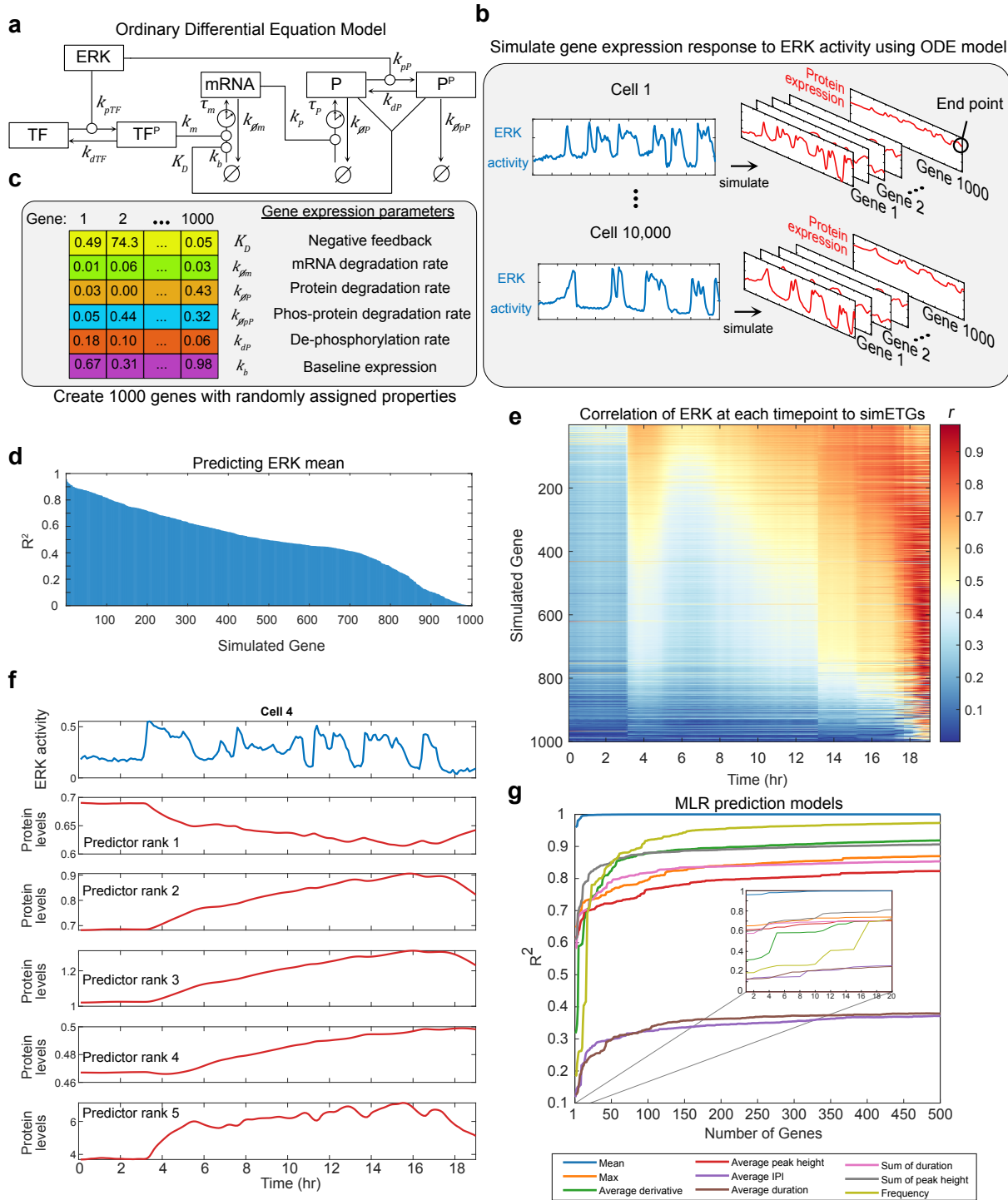
Figure 4.6 Annotating spatiotemporal ERK patterns in images using Decision Tree model

Figure 4.6: Mathematical model identifies limits of ERK activity prediction method. **a** Ordinary differential equation model representing ERK-dependent modification of a transcription factor (TF), expression of mRNA, and expression of a protein (P) product. Superscript P denotes phosphorylation of a molecule. Lowercase k's indicate rate parameters, uppercase K indicates a dissociation constant for feedback effects. Clock icons indicate a time delay (τ). **b** 10,000 cells were randomly picked from our main dataset. We simulated the gene response of 1000 genes for each cell using our experimentally collected EKAR measurements. **c** 1000 simulated genes (sim-ETGs) were randomly assigned the listed rate parameters while other rate parameters in the model remained constant. **d** Coefficient of determination (R^2) of single variable linear regression models using each sim-ETG to predict the average ERK activity in each cell. **e** Pearson correlation (r) between each sim-ETG (rows) measurement and the EKAR values at each timepoint from the live-cell experiment. **b** Top: one ERK activity trace from one cell in the dataset. Rest: gene expression response of the top 5 predictors of the mean ERK activity. **g** Multiple regression models fit to predict each ERK feature. For each ERK feature prediction model, a single sim-ETG was added as a predictor at each step. To determine the order of sim-ETGs to add, we performed single regression and ranked sim-ETG by their ability to individually predict each feature.

the different aspects of ERK signaling, we created MLR models which used many sim-ETGs at once to predict multiple ERK pulse features. These models greatly improved our predictions, as most explained 75 to 99% of the variance in the dataset (Fig. 4.6g). Of note, the derivative and frequency model predictions drastically improved as the number of predictors increased. This result was not obtained through overfitting, as the test set error of the models also decreased with more sim-ETGs (Fig. 4.12f). For most ERK features, between 16 to 20 sim-ETGs are required for obtaining good models (R^2 0.7) (Fig. 4.6g inset). From an experimental standpoint, these results demonstrate that predicting dynamic features of ERK is highly feasible, and depends largely on which gene products are measured. From a practical standpoint, measuring for 20 proteins using a multiplex staining protocol is readily achievable (Comandante-Lou *et al.* , 2022; Stallaert *et al.* , 2022). In all, the ODE model indicates that our ERK activation inference method is a feasible solution for fixed tissue analysis, and will benefit from further exploration of potential endogenous gene products to measure.

4.5 Discussion

Here, we provide proof of principle that end-point ETG staining can be used to infer key aspects of long-term ERK activity within fixed cell samples. While differences in ETG activation by ERK were previously known, our analysis formalizes these differences and shows how quantitative models can be used to infer ERK's activity history with single-cell resolution. The ETG measurements in these experiments provide information about two broad types of ERK behavior, long-term and short-term activation. Additionally, our model analysis of simulated ETGs demonstrates that additional measurements could even more finely resolve signaling patterns, such as intermittent pulses. The experimental and biological limits of these predictions remain to be established; however, this model framework can be used to estimate properties of ETGs that would optimally improve the measurement set.

While the main characteristics of ERK activity are captured by our models, a significant amount of unexplained variance in ERK activity in our analysis prompts the question of what other parameters can be used to improve ERK history predictions. While our dynamical systems modeling suggests that other direct ERK targets could be used, a recent study identified orthogonal markers of cellular state, such as Sec13 (a nuclear pore component) and Calreticulin (an Endoplasmic Reticulum-resident protein), that correlate highly with phosphorylated ERK (Kramer *et al.* , 2022). These results imply that intrinsic cellular factors modify ERK signaling, and that these markers can improve our ERK prediction models. Furthermore, other cell state measurements that may improve predictions include protein translation rates, chromatin accessibility, or transcription factor availability.

The statistical models in this study were trained on data from diploid non-tumor mammary epithelial cells. Generalizing these methods for use in other cell lines or tissues will require similar datasets from a broad array of cellular settings because there are reported

differences in some ETG responses among various cell types. For example, B-Raf inhibition disrupts signal transmission and alters the transcriptional response of c-Jun, Egr-1, and Cyclin-D1 (Bugaj *et al.* , 2018). Additionally, different mutations in B-Raf can lead to induction or suppression of c-Jun (Comandante-Lou *et al.* , 2022). Accordingly, prediction models should be trained on cell-line specific data, especially from cancer cells with different MAPK pathway mutations. Potentially, a much larger scope of experiment is needed to train a model to simultaneously capture many cell lines, for example by identifying either ETGs whose responses remain consistent, or additional targets that sufficiently reflect the cellular context. However, it is also possible that a small set of well-chosen measurements may be sufficient to generate a broadly useful model (Janes *et al.* , 2005).

In the dataset presented here, phosphorylated-Rb was a surprisingly good predictor of both long term and short term signaling in both single-cell and population-level models. An important caveat about these results is that ERK biosensors (EKAR and ERK Kinase translocation reporter) have some sensitivity to cyclin-dependent kinases (CDKs). EKAR 3.5 in particular is sensitive to CDK1 during mitosis (Hirashima, 2022). Though mitotic events are typically much rarer than changes in ERK activity, some of the variation in our EKAR measurements likely arises from this CDK1 activity. Since EGF increases mitotic activity, pRb levels, and EKAR measurements, there will be some correlation between EKAR and pRb that is an artifact. This serves as a reminder that co-variance, or cross-talk, among measurements will bias these types of machine learning analyses, and should be carefully evaluated.

The results of this study suggest that the duration of signaling plays a stronger role in protein expression than the integrated activity. Such an effect could arise from saturation of a particular gene's response to ERK, or from differences among genes in phosphatase specificity or other competing regulators. An alternative explanation for this result is that our ERK biosensor fails to capture the high ranges of ERK activation. However, we resolved

this by calibrating the reporter to provide a linear readout of ERK substrate phosphorylation (Gillies *et al.*, 2020). This leads to the possibility that ERK target genes have been selected for duration responders rather than signal integrators. Nonetheless, a fundamental question remains to be further explored: What is the biological resolution of strength, duration, and other features of ERK activity, with respect to gene expression? Our analysis provides some quantitative answers to how ERK activation patterns specify a subset of gene expression. Finally, the method can be employed further to more closely investigate the effect of ERK signaling on cell fate changes rather than gene expression.

Our method could be used to provide important details of ERK signaling within fixed tissue samples in a clinical setting. The ability to infer the long-term patterns of ERK activity in samples from patients treated with MEK, EGFR, or other targeted pathway inhibitors would provide a more reliable indication of the effectiveness of long-term ERK activity suppression, helping to reveal areas of drug resistance. By analogy, measurements of hemoglobin A1C provide a reliable indication of a patient's time-averaged blood sugar that is useful in the clinical management of diabetes. We propose that inferring the longer-term characteristics of ERK activity will be of similar use in managing tumors that rely on aberrant signaling in this pathway. This strategy can further be applied to other dynamically regulated pathways implicated in disease such as metabolic, inflammatory, or stress response signaling. Both generalized and patient-specific models would allow for more accurate diagnoses and improve personalized medicine.

4.6 Methods

4.6.1 Reporter cell line generation

For these experiments, two stable cell lines were created by electroporating MCF10A 5e cells with the EKAR 3.5 construct on the piggyBAC transposase system (Pargett *et al.* , 2017). Cells were selected with neomycin (250 μg/ml 2 weeks) until they were resistant to selection (2 weeks).

4.6.2 Cell culture and media

All experiments were conducted with MCF10A 5e (Janes *et al.* , 2010). Cells were maintained in DMEM/F12 supplemented with 5% horse serum, 20 ng/ml EGF, 10 μg/ml Insulin, 500 ng/ml hydrocortisone, and 100 ng/ml cholera toxin. 10cm plates were passaged approximately every four days and re-plated at a 1:10 dilution. Imaging experiments were conducted in custom DMEM/F12 lacking phenol red, riboflavin, and folate. This "imaging media" was supplemented with 500 ng/ml hydrocortisone, 17.5 mM glucose, 1 mM sodium pyruvate, 2 mM glutamine, 50 μg/ml Penicillin/Streptomycin. Before plating cells for imaging experiments, 5 μl of Rat tail collagen was added to the middle of each well of a glass bottom 96-well plate (Cellvis) and incubated for 45 mins at 37°C. Cells were typsinized, plated at 6000 cells per well, and then incubated at 37°C for 45-60 mins. Growth media was then added, and the plate was left overnight in the incubator. The next day, immediately before the imaging experiment, the plate was washed 3x with imaging media, and the media was changed to imaging media. The experiment began one hour after this media change.

4.6.3   Live cell microscopy and data acquisition

Prepared 96-well plates were imaged on a Nikon Ti-E inverted microscope with a stage-top incubator (37°C, 5% CO2). Coordinates within each well of the 96-well plate were imaged at 6 minute increments which were automated by the Nikon Elements AR software. Images were captured using an Andor Zyla 5.5 scMOS camera and a 20x/0.75 NA objective. Chroma #49001 (ET-CFP) and #49003 (ET-YFP) excitation/emission filter cubes were used for mTurquoise2 and YPet measurements, respectively. Further details are described in (Pargett *et al.* , 2017). Coordinates of each acquisition area were saved for future imaging of immunostaining experiments.

4.6.4   Cyclic immunofluorescence

Immediately after the final acquisition of the live cell experiment, cells were fixed in freshly prepared 12% paraformaldehyde for 10 min. Cells were then permeabilized with fresh, cold methanol for 10 mins (2 times total). Cells were then ready for iterative rounds of staining using a protocol adapted from (Gut *et al.* , 2018). Briefly, the iterative protocol involves rounds of elution, blocking, primary staining, secondary staining, Hoechst staining, and finally image acquisition in a specific imaging buffer. Recipes for buffers are as follows: Elution buffer (0.5M Glycine, 3M Urea, 3M Guanidinium Chloride, 70mM TCEP), Blocking buffer (200mM NH4Cl, 300mM Maleimide, 2% BSA in PBS), primary/secondary staining buffer (200mM NH4Cl, 2% BSA in PBS), Hoechst-33342 stain (1:10,000 in PBS), and 4i imaging buffer (700 mM N-Acetyl Cysteine). Antibodies were incubated 24 to 48 hours from varying concentrations recommended by the manufacturer. The protocol was validated during the first replicate experiment to ensure that antibodies were properly eluted, data is shown in Fig. 4.8b-d. For the second and third replicate experiment, a visual inspection was completed prior to each round of staining to ensure proper antibody elution.

4.6.5   Phos-tag western blotting

MCF10A 5e cells were plated on 6-well dishes the day before lysing. Cells were treated with EGF, PD0235901, or imaging media and lysed at the indicated timepoints. This procedure involved rinsing each well twice with ice cold PBS, cell scraping, and lysis with RIPA buffer (Sigma) with Halt protease inhibitor cocktail and 1 μM DTT. Cells were lysed at 80-90% confluency with a 50 μl of lysing buffer per well. 2 μl of each sample was then loaded in pre-cast phos-tag gels (Wako-Chem) and ran at 100V for 3 hours. The gel was chelated two times with transfer buffer and 10 mM EDTA for 15 minutes each and rinsed once more with just transfer buffer. Proteins were transferred overnight at 50V. The membrane was blocked with Li-COR Odyssey blocking buffer and blotted with anti-GFP antibody (24 hr incubation). The membrane was then blotted with Li-COR 800 anti-Mouse secondary antibody and imaged using a fluorescent scanner (Sapphire-Azure Biosystems). Intensities of the resulting phosphorylated EKAR 3.5 reporter and total EKAR 3.5 bands were measured in ImageJ.

4.6.6   Image processing

Imaging data were saved as .nd2 files and accessed using the Bio-Formats toolbox for MAT-LAB (available from www.openmicroscopy.org/bio-formats), and processed with a custom MATLAB cell segmentation pipeline (Pargett *et al.* , 2017). The procedure identified each cell's nucleus using either EKAR 3.5 (live-cell) or Hoechst 33342 (IF) as a nuclear marker. The cytoplasm was defined as a ring around each cell's nucleus. Background signal intensity was measured by imaging a well with no cells, but containing live-cell imaging media or 4i imaging buffer. Cell position tracking and linking was performed using uTrack 2.0 (Jaqaman et al,. 2008). The resulting single-cell data was filtered to remove cells with less than 15 hours of tracking data. FRET measurements of ERK activity for each cell were calculated

with 1 – ((CFP/YFP) / R_p), where CFP and YFP are the intensities of Cyan and YFP channels measured in each cell, respectively. R_p is the ratio of total power collected of CFP over YFP where the power of each channel is the integral of the spectral product of excitation intensity, filter transmittances, exposure time, fluorophore absorption and emission properties, and quantum efficiency of the camera (detailed in appendix of (Gillies *et al.* , 2020)).

4.6.7 Batch effect correction

To correct for batch effects in the immunofluorescence measurements across three replicates, we scaled measurements in logspace. For each 4i target, we calculated the median value for each treatment and matched identical treatments across replicates. These treatments included all EGF doses at timepoint 30, MEKi at timepoint 30, and imaging media control. We then took the log10 of these values and fit a linear model 4.1

$$Intensity_{replicate3} = \beta_1(Intensity_{replicate_n}) + \beta_0 \qquad (4.1)$$

Where $Intensity_{replicate_n}$ represents log10 median values for either replicate 1 or replicate 2, $Intensity_{replicate3}$ represents the corresponding log10 median values for the third experimental replicate, and β_0 and β_1 are the scaling factors. These scaling factors were then used to correct all single-cell values for replicate 1 and 2. The corrected values were then returned to the linear scale by exponentiating.

4.6.8 EKAR 3.5 Calibration

FRET measurements were calibrated to deliver a quantitative linear readout of ERK activity, as described previously (Gillies *et al.* , 2020). Briefly, we used Phos-Tag immunoblotting to quantify the fraction of the EKAR 3.5 reporter that is phosphorylated in 3 concentrations of

EGF (15 mins), phosphorylation inhibited (MEKi for 2 hours), and control conditions. These values were then linearly fit against the average EKAR 3.5 signal for the same conditions (4.2).

$$\frac{\text{EKAR}^A}{\text{EKAR}^T} = (K_{AU} + K_{AP})\frac{\text{EKAR}^P}{\text{EKAR}^T} \tag{4.2}$$

Where $\frac{\text{EKAR}^P}{\text{EKAR}^T}$ represents the phos-tag ratio between phosphorylated and total reporter, and $\frac{\text{EKAR}^A}{\text{EKAR}^T}$ represents the average FRET measurement in the corresponding condition.). (K_{AU} and K_{AP} represent fractions of EKAR in the "associated" state when completely un-phosphorylated and when completely phosphorylated, respectively. Single-cell FRET measurements (fA) were then used to estimate the concentration ratio of active ERK to the competing phosphatase(s) (4.3). This ratio is the quantitative measure of ERK activity in a cell ($\frac{\text{ERK}^A}{\text{PPASE}^A}$).

$$\frac{\text{ERK}^A}{\text{PPASE}^A} = \frac{f_A - K_{AU}}{K_{AP} - f_A} \tag{4.3}$$

4.6.9   Data analysis and regression modeling

Cells with less than 15 hours of data were removed prior to analysis, and cells out of the expected range of the FRET measurements were removed. FRET measurements were then adjusted using the reporter calibration model created from the phos-tag experiments. Thus, statistical models were created on cells that had complete EKAR and ETG measurements. Models were created using 10-fold cross validation. The data was randomly assigned to 10 groups, in which the 10th group was held out of the model fitting procedure. The model was then tested against the 10th group (test-set) to collect the test error (residual mean squared error, RMSE). This procedure is repeated for a total of 10 times to collect RMSE values from 10 test sets. The model that produced the lower test-set error was then refitted to the entire dataset to calculate the reported RMSE values.

4.6.10 Pulse analysis and peak detection

The findpeaks function in MATLAB was used to find local maxima (peaks) for each cell's ERK activity. Pulse features were then calculated based on the identified peaks. Frequency was calculated using the meanfreq function in MATLAB.This function estimates the mean normalized frequency of the power spectrum of each ERK activity trace.

4.6.11 Statistical tests

For single-cell immunofluorescence data, each statistical comparison was made by t-test with unequal variances, and false discovery rate was controlled within each dataset via the Benjamini and Hochberg Step-Up procedure ($\alpha = 0.05$). The variance for each experiment was determined from single-cell samples and added to variance across experiments. This corresponds to a linear error model: $\epsilon_i = \epsilon_{\text{cell}} + \epsilon_{\text{exp}}$, where the error (from the mean) of an individual cell ϵ_i equals the sum of the errors arising from cell-to-cell variation ϵ_{cell} and from experiment variation ϵ_{exp}.

4.6.12 Spatial heatmap generation

Each cell's time averaged coordinates were used to calculate the average Euclidean distance between each pair of cells within each well of the 96-well plate. Hierarchical clustering was performed on this distance matrix. The optimal leaf order was calculated by maximizing the sum of the similarity between adjacent leaves by flipping tree branches and without dividing the clusters. This order was then used to sort and display the live-cell and fixed-cell data.

4.6.13   ETG prediction models and evaluation

For convolutional neural networks, we trained a CNN per ETG prediction. Each model consisted of 1) feature learning module and 2) prediction module. Feature learning module consists of 2 convolutional layers (16 channels and kernel size of 16) followed by an FC layer with size of 192 to match the initial input size. Prediction module consists of 2 FC layers (each size of 64 with relu activations) followed by a final linear FC layer that outputs a single ETG prediction. We trained one model per ETG for 100 epochs using Adam optimizer with learning rate of 0.001 and L2 regularization of 0.001. For the linear model, linear regression was implemented using sklearn python package with default parameters. The inputs were either the raw or featurized ERK activity for linear model or featurized linear model respectively. Evaluation on the model was performed using 5-fold cross validation with each fold roughly having the same representation from each well of origin and treatment.

Identification of significant input timepoints

For feature attribution approach, we used feature attribution, specifically Integrated Gradient (Sundararajan *et al.* , 06–11 Aug 2017), to identify input timepoints that the model considers significant to prediction of ETG. Integrated Gradient was implemented using the python package Captum (Kokhlikyan *et al.* , 2020). Feature attribution outputs score from each input time point to ETG per cell, which was averaged across cells for summarized visualization in the form of heatmap.

Backwards feature selection with timepoints after stimulation with CNN

To test the importance of the timepoints after the initial stimulation, we trained new CNN models to only use timepoints 2 hours after stimulation for ETG prediction. This model was trained on 15 hours of ERK activity data. The model and training setup used is identical

to the setup used for the model with all the time points (19 hours of ERK activity data).

4.6.14   Decision Tree Classifier

EKAR time series data were clustered into five groups using k-means clustering. Each group was assigned its class label. An optimized decision tree was fit using 8 ETG measurements to predict class labels of each cell. Leaf optimization was done by fitting multiple cross validated models and recording test-set error. This was done using MATLAB's fitctree function. The model with the lowest test set error was chosen. Predictor Importance was estimated by summing the changes in the risk due to splits on every predictor and dividing the sum by the number of branch nodes–MATLAB predictorImportance function.

4.6.15   Ordinary Differential Equation Modeling

The ODE model was adapted from Davies *et al.* 2020. The model of ERK dependent gene expression (Equations 4.4, 4.5, 4.6, and 4.7) was constructed from a mass action approximation. This process is modeled in four steps (Eq. 4.4) phosphorylation of a transcription factor by ERK (TFP), (Eq. 4.5) transcription of target mRNA (mRNA), (Eq. 4.6) translation of target protein (P), and (Eq. 4.7) potential stabilization of target protein by ERK-dependent phosphorylation (PP). A regulatory term is included in the transcription process allowing negative feedback from target protein onto its own production. The model is formulated as a delay differential equation to account for the effective lag times of transcription and translation without explicitly addressing the complex processes involved.

$$\frac{d}{dt}\text{TF}^P(t) = k_{\text{pTF}} \times \text{ERK}(t) \times (\text{TF}^T - \text{TF}^P(t)) - k_d\text{TF}^P(t) \qquad (4.4)$$

$$\frac{d}{dt}\text{mRNA}(t) = \frac{k_b + k_m \text{TF}^P(t - \tau_m)}{\left(\frac{P(t-\tau_m)+P^P(t-\tau_m)}{k_D}\right)^v + 1} - k_{\emptyset m} \times \text{mRNA}(t) \tag{4.5}$$

$$\frac{d}{dt}\text{P}(t) = k_P \times \text{mRNA} \times (t - \tau_P) + k_{dP} \times \text{P}^P(t) - (k_{\emptyset P} + k_{PP}) \times \text{P}(t) \tag{4.6}$$

$$\frac{d}{dt}\text{P}^P(t) = k_{pP} \times \text{ERK}(t) \times \text{P}(t) - (k_{\emptyset PP} + k_{dP}) \times \text{P}^P(t) \tag{4.7}$$

4.6.16   Acknowledgements

4.7   Supplementary Figures
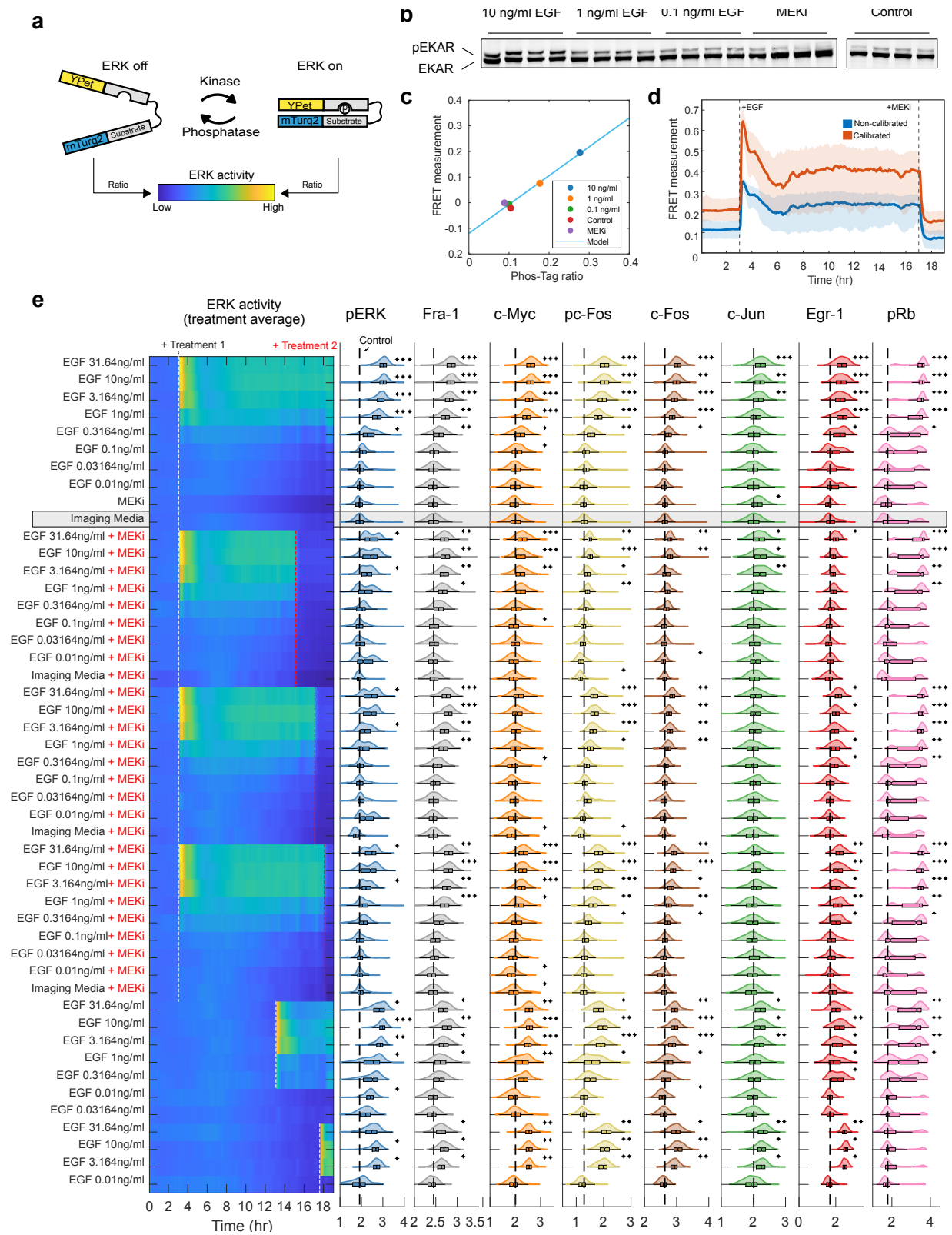
Figure 4.7 Live cell measurements with a calibrated ERK reporter followed by immunofluorescence

Figure 4.7: Live cell measurements with a calibrated ERK reporter followed by immunofluorescence. **a** Schematic of EKAR 3.5 FRET-based reporter. When ERK is inactive, mTurquoise2 and Ypet are distanced from each other. Active ERK binds the reporter substrate and induces a conformational change, bridging the two fluorescent proteins together. This causes a change in the ratio of mTurquoise2 and Ypet fluorescence intensities. **b** Phos-Tag immunoblot for phospho-EKAR 3.5 under 4 conditions that span the full range of ERK activity levels. Samples treated with EGF for 15 minutes, or MEKi for 2 hours. $n_{wellreplicates}$ = 4 for each treatment. **c** Quantified ratio of the phosphorylated EKAR 3.5 over total EKAR 3.5 immunoblot intensities (x-axis). Y-axis represents the average live-cell FRET measurement in all cells within each treatment. FRET measurements were calculated at 15 minutes after EGF treatment, or 2 hours after MEKi. Each point represents the average of the 4 replicates. Model indicates the line of best fit. **d** Slope and intercept of the Phos-Tag model were used to calibrate the live-cell FRET measurements. **e** Left: Treatment average responses of EKAR biosensor data. Right: Histogram and box plot showing immunofluorescence quantifications for each treatment corresponding to the biosensor data. Box plot indicates median, quartiles, and range of the data. Dashed line indicates the median of the control (imaging media). Variance-corrected t-tests were conducted by comparing each EGF treated condition to vehicle control (imaging media) ($n_{replicates}$ = 3). * p-val <0.05, ** p-val <0.005, *** p-val <0.0005., *** p-val <0.0005.
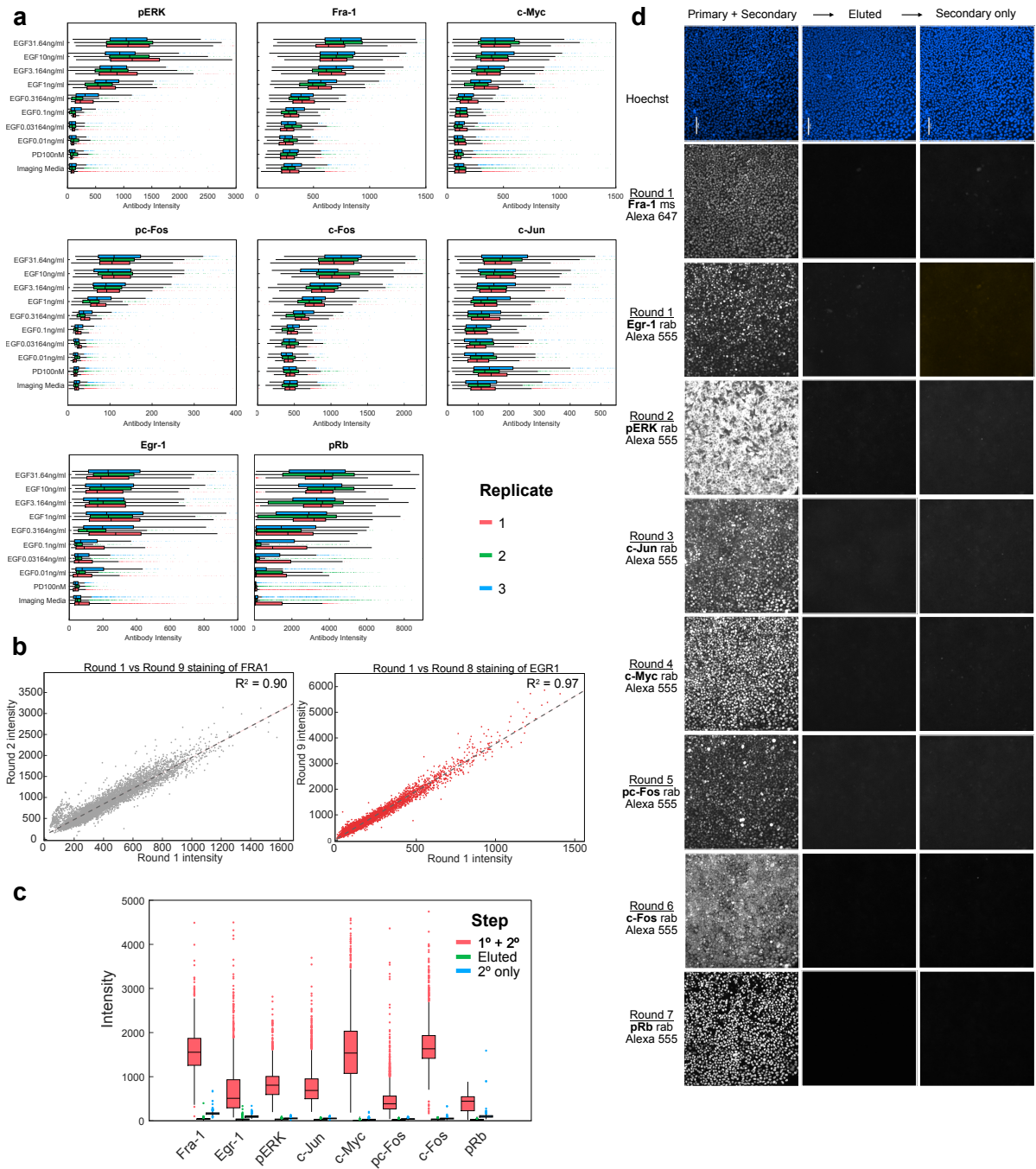
Figure 4.8 Batch effect correction and cyclic immunofluorescence protocol validation

Figure 4.8: Batch effect correction and cyclic immunofluorescence protocol validation. **a** Box plot showing immunofluorescence quantifications for each treatment in each replicate experiment. Box plot indicates median, quartiles, and range of the data. Dots indicate outliers. $n_{replicates} = 3$. **b** Scatter plot of Fra-1 (left) and Egr-1 (right) intensity in the first round of staining vs. the ninth round from replicate plate 1. Data includes cells treated with EGF (all doses), imaging media, or MEKi. $n_{wellreplicates} = 2$ for each treatment. **c** Quantification of pixel intensities of cells in d. Box plot indicates median, quartiles, and range of the data. Dots indicate outliers. **d** Images of cyclic immunofluorescence rounds of staining. Cells were incubated with primary+secondary, eluted, and re-incubated with secondary only to ensure proper elution of the primary. Egr-1 and Fra-1 antibodies were both incubated together in round 1. Rab: anti-rabbit primary. Ms: anti-mouse primary. Cells treated with 31.64 ng/ml EGF. $n_{wellreplicates} = 1$. Five other wells treated with lower concentrations of EGF were also imaged and validated for proper elution (data not shown).
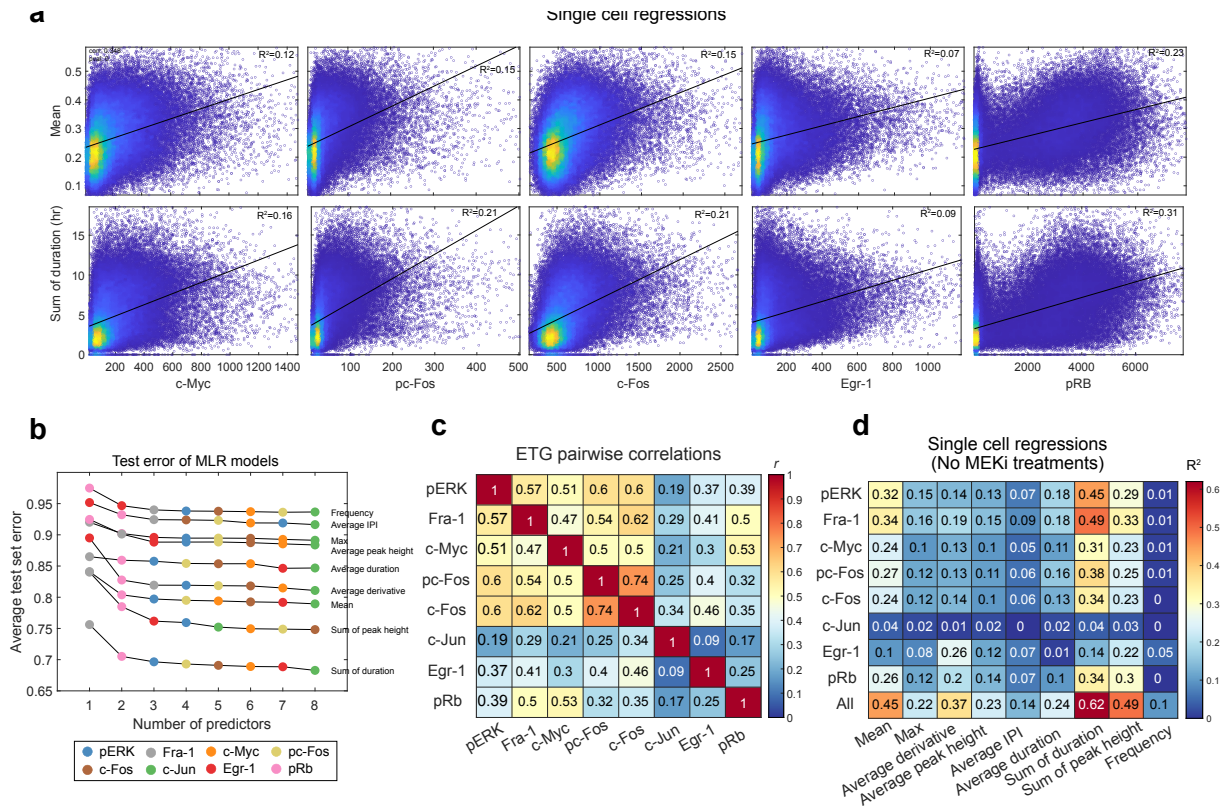
Figure 4.9 Regression modeling of ERK and ETGs

Figure 4.9: Regression modeling of ERK and ETGs. **a** Scatter plots and line of best fit for ETGs and ERK features. Color indicates relative density of data. **b** Test error (RMSE) of MLR models where additional predictors were added at each step. **c** Pearson correlation between each ETG. **d** Single variable regression models using single-cell data, cells treated with MEKi were removed from this analysis.
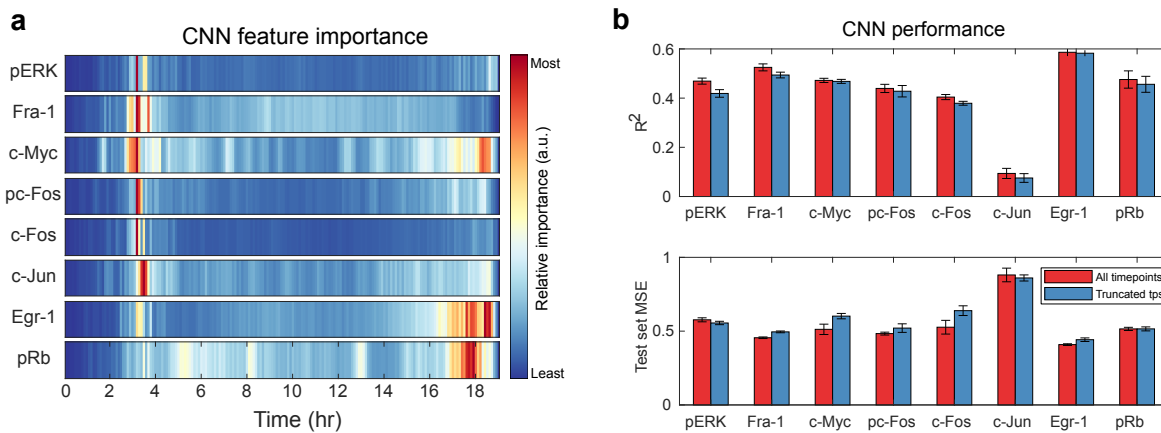
Figure 4.10 CNN feature importance is overshadowed by initial response

Figure 4.10: CNN feature importance is overshadowed by initial response. **a** Convolutional neural net feature importance of each timepoint in predicting levels of each ETG. Color map represents relative values within each row. **b** Comparing CNNs trained on 190 timepoints (19 hr) or 150 time points (15hr). Top: Bar plot of $R^2 =$ value for predicting each ETG using k-fold cross-validation (k=5). For each ETG, data was partitioned into 5 groups. Within each k-fold, a training, test, and final set were created. Bar represents the average final set $R^2 =$ value across all 5 groups. Error bars (Standard error) were calculated by dividing the standard deviation of $R^2 =$ values for each ETG by the square root of five. Bottom: Test set mean squared error values for each ETG. Bar height and error bars were calculated as described above.
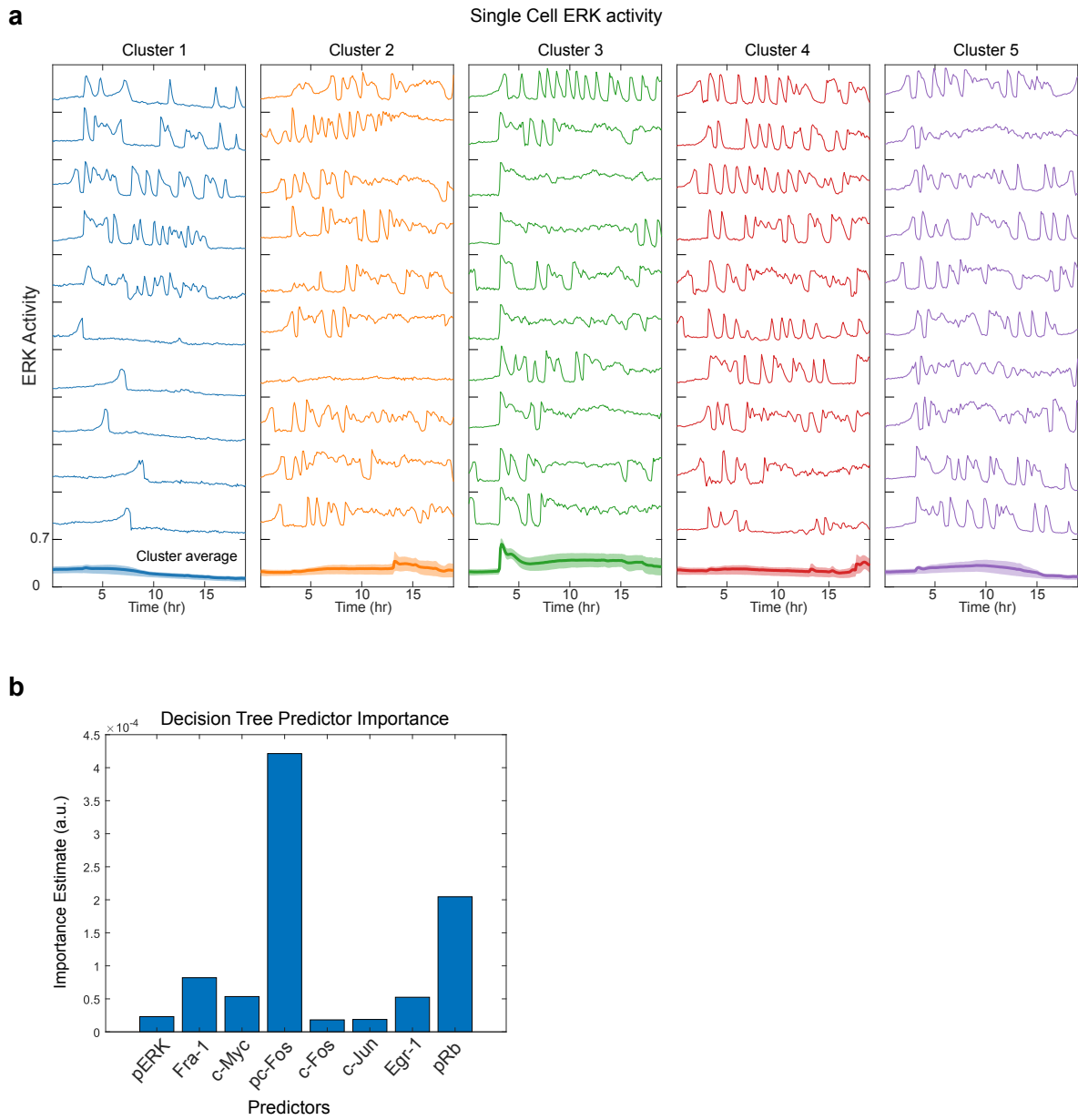
Figure 4.11 Single-cell variation with clusters

Figure 4.11: Single-cell variation with clusters. **a** ERK activity of 20 individual cells from each cluster identified by k-means clustering. Bottom line represents the cluster average, and the shading represents the 25th and 75th percentiles. **b** Predictor importance estimates for the decision tree classification model
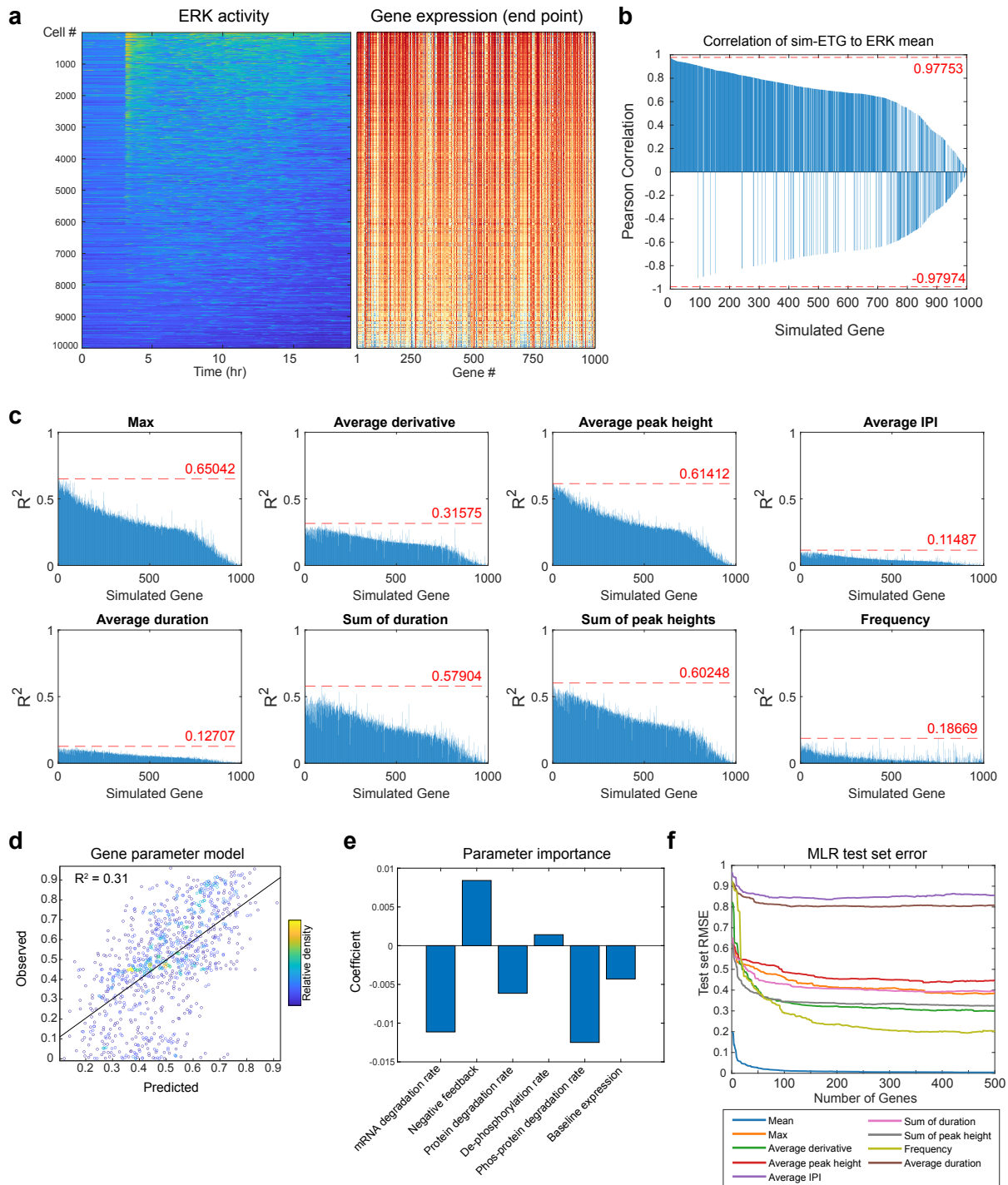
Figure 4.12 Ordinary differential equation modeling

Figure 4.12: Ordinary differential equation modeling. **a** Left: single-cell ERK activity heatmap sorted by the mean of each cell (highest mean at the top). Right: Corresponding sim-ETG end point values. Color represents the relative expression within each column. ncells = 10,000. ngenes = 1,000. **b** Pearson correlation between mean ERK activity and end-point gene expression. **c** R^2 = of single variable models using end point values of each sim-ETG to predict each ERK feature. Dashed line represents the maximum value. **d** Linear regression using gene parameter values to predict how well each gene tracks with average ERK activity. The model uses the negative feedback rate, mRNA degradation rate, protein degradation rate, phosphorylated protein degradation rate, de-phosphorylation rate, and fraction baseline to predict the R^2 = value from Fig. 6d. **e** Coefficient weights for linear regression in Fig. 4.12d. **f** Test set error (residual mean squared error) for each newly added gene in the prediction model.

Treatment1	T1 Time (hr)	Treatment2	T2 Time (hr)	Well replicates	Experimental replicates (days)
EGF 0.01ng/ml	3			11	3
EGF 0.03164ng/ml	3			11	3
EGF 0.1ng/ml	3			9	3
EGF 0.3164ng/ml	3			10	3
EGF 1ng/ml	3			11	3
EGF 3.164ng/ml	3			11	3
EGF 10ng/ml	3			11	3
EGF 31.64ng/ml	3			11	3
PD 100nM	3			21	3
Imaging media control	3			32	3
EGF 0.01ng/ml	3	PD 100 nM	18	2	2
EGF 0.03164ng/ml	3	PD 100 nM	18	3	3
EGF 0.1ng/ml	3	PD 100 nM	18	3	3
EGF 0.3164ng/ml	3	PD 100 nM	18	3	3
EGF 1ng/ml	3	PD 100 nM	18	3	3
EGF 3.164ng/ml	3	PD 100 nM	18	3	3
EGF 10ng/ml	3	PD 100 nM	18	3	3
EGF 31.64ng/ml	3	PD 100 nM	18	3	3
EGF 0.01ng/ml	3	PD 100 nM	17	2	2
EGF 0.03164ng/ml	3	PD 100 nM	17	3	3
EGF 0.1ng/ml	3	PD 100 nM	17	3	3
EGF 0.3164ng/ml	3	PD 100 nM	17	3	3
EGF 1ng/ml	3	PD 100 nM	17	3	3
EGF 3.164ng/ml	3	PD 100 nM	17	3	3
EGF 10ng/ml	3	PD 100 nM	17	3	3
EGF 31.64ng/ml	3	PD 100 nM	17	3	3
EGF 0.01ng/ml	3	PD 100 nM	15	3	3
EGF 0.03164ng/ml	3	PD 100 nM	15	4	3
EGF 0.1ng/ml	3	PD 100 nM	15	4	3
EGF 0.3164ng/ml	3	PD 100 nM	15	4	3
EGF 1ng/ml	3	PD 100 nM	15	4	3
EGF 3.164ng/ml	3	PD 100 nM	15	4	3
EGF 10ng/ml	3	PD 100 nM	15	4	3
EGF 31.64ng/ml	3	PD 100 nM	15	4	3
Imaging media control	3	PD 100 nM	18	4	3
Imaging media control	3	PD 100 nM	17	2	1
Imaging media control	3	PD 100 nM	15	2	1
EGF 31.64ng/ml	17.5			2	2
EGF 10ng/ml	17.5			1	1
EGF 0.01ng/ml	17.5			1	1
EGF 3.164ng/ml	17.5			1	1
EGF 0.01ng/ml	13			1	1
EGF 0.03164ng/ml	13			1	1

Supplementary Table 1: List of treatments/conditions along with the number of replicate wells and replicate experiments.

Parameter	Description	Unit
TF^T	Total transcription factor concentration	nM
k_{pTF}	ERK-dependent transcription factor phosphorylation rate	nM^{-1}min^{-1}
k_{dTF}	Transcription factor de-phosphorylation rate	min^{-1}
k_b	Baseline target mRNA transcription rate	nM/min
k_m	ERK-dependent target mRNA transcription rate	min^{-1}
$k_{\emptyset m}$	Target mRNA degradation rate	min^{-1}
τ_m	Transcription delay	min
K_D	Negative feedback half-maximal concentration	nM
ν	Feedback Hill Coef.	-
k_P	Target protein translation rate	min^{-1}
$k_{\emptyset P}$	Target protein degradation rate	min^{-1}
τ_P	Translation delay	min
k_{pP}	ERK-dependent target phosphorylation rate	nM^{-1}min^{-1}
k_{dP}	Target protein de-phosphorylation rate	min^{-1}
$k_{\emptyset pP}$	Phosphorylated target degradation rate	min^{-1}

Supplementary Table 2: List of gene parameters in the ordinary differential equation model.

Reagent or Resource	Source	Identifier/RRID
Antibodies		
Anti-Fra-1, clone C-12	Santa Cruz Biotechnology	sc28310; AB_627632
Anti-Egr-1, clone 44D5	Cell signaling	4153; AB_2097035
Anti-phospho-ERK p44/42 clone D13.14.4E	Cell signaling	4370; AB_2315112
Anti-cJun clone 60A8	Cell signaling	9165; AB_2130165
Anti-c-Myc clone D84C12	Cell signaling	5605; AB_1903938
Anti-phospho-c-Fos clone D82C12	Cell signaling	5348; AB_10557109
Anti-c-Fos clone	abcam	ab190289; AB_2737414
Anti-phospho-Rb (Ser807/811) clone D20B12	Cell signaling	8516; AB_11178658
Goat anti-Mouse IgG Alexa Fluor 647	ThermoFisher	A-21235
Donkey anti-Rabbit IgG (H+L) Alexa Fluor 555	ThermoFisher	A-31572; AB_162543
IRDye 800CW Donkey anti-Mouse IgG	Licor	926-32212; AB_621847
Chemicals, Peptides, and Recombinant Proteins		
Epidermal growth factor	Peprotech	AF-100-15
PD0325901	Selleck Biochemicals	S1036
Cholera Toxin	Sigma-Aldrich	C8052
Hydrocortisone	Sigma-Aldrich	H0888
Insulin	Sigma-Aldrich	I9278
Bovine Serum Albumin	Sigma-Aldrich	A7906
Heat Inactivated Horse Serum	Life Technologies	26050
DMEM/F-12 1:1	Life Technologies	11320
Neomycin		
Collagen I, rat tail	Life Technologies	A10483-01
l-Glutamine	Life Technologies	25030-081
Penicillin streptomycin	Life Technologies	15070-063
0.25% Trypsin-EDTA	Life Technologies	25200-056
Tris Base	Fisher	BP152
Glycine (Crystalline Powder)	Fisher	BP381
Ponceau S solution, suitable for electrophoresis, 0.1% (w/v) in 5% acetic acid, 1L	Sigma-Aldrich	P7170-1L
Bromophenol blue	Sigma-Aldrich	B5525

Supplementary Table 3: List of materials, software, and reagents used in the study.

Dithiothreitol	Fisher	BP172
Ammonium chloride	Sigma-Aldrich	254134
Maleimide	Sigma-Aldrich	129585
N-Acetyl-L-cysteine	Sigma-Aldrich	A7250
TCEP hydrochloride	ApexBio	B6055
Hoechst-33342	Life Technologies	H3570
Odyssey Blocking Buffer (PBS)	Licor	927-40000
Urea	Fisher	U15-500
Guanidinum Hydrochloride	Fisher	BP178-500
Phosphate-buffered saline,	Fisher	BP399-1
Paraformaldehyde	ThermoFisher	043368.9M
Glycine	Fisher	BP381-500
Tween-20	Fisher	BP337100
Halt Protease inhibitor cocktail	ThermoFisher	1861278
Experimental Models/Cell Lines		
Human: MCF-10A, clone 5E	Joan Brugge, Harvard Medical School	RRID:CVCL_0598
Recombinant DNA		
Plasmid: pPBJ-EKAR3.5nls-neo	Sparta et a. 2015	Addgene # forthcoming
Software and Algorithms		
NIS-Elements AR ver. 4.20	Nikon	RRID:SCR_014329
Bio-Formats ver. 5.1.1 (May 2015)	OME	RRID:SCR_000450
uTrack 2.0	(Jaqaman et al., 2008)	http://www.utsouthwestern.edu/labs/danuser/software/
MATLAB 2020a	Mathworks	SCR_001622
ImageJ (1.52p)	National Institues fo Health	RRID:SCR_003070
Python (3.8.16)	Python Software Foundation	RRID:SCR_008394
Proofreading software		
Grammarly	Grammarly, Inc	www.grammarly.com/
ChatGPT	OpenAI	www.openai.com
Other		
Glass Bottom Plates, #1.5 cover glass	In Vitro Scientific	P24-1.5H-N, P96-1.5H-N
SuperSep Phos-tag gels (50 µmol/l), 12.5%, 17 wells	Wako-Chem	195-17991

Supplementary Table 3 (continued): List of materials, software, and reagents used in the study.

Chapter 5

Conclusions and Future Directions

5.1 Abstract

This dissertation discusses how ERK signaling mediates homeostasis. We cover the mechanisms of how signals are encoded into cellular processes, which in turn regulate tissues. Much of this regulation is done through gene expression. A key question that remains to be elucidated is how are other genes regulated by ERK at the single-cell level. Answering this question will lead to enhanced tools for ERK diagnostics in cancer.

5.2 Summary of work

ERK is responsible for homeostasis, and mutations in ERK signaling lead to disease. Given its biological and clinical significance, understanding ERK's exact role in controlling cells will be highly beneficial. Decades of research clearly indicates that ERK is one of the main regulators for several cellular processes, and we have discussed the mechanisms that allow ERK to mediate these tasks. The Ras/MAP Kinase pathway contains many feedback loops that allow for highly dynamic activation and deactivation patterns of ERK. Depending on the

context, the pattern of ERK activity determines the fate of cells. ERK activity is different in dividing cells, growth arrested cells, and dying cells. Since ERK activates transcription, gene expression is likely driving the differences in these cellular events. To test how well ERK activation correlates with gene expression we measured live-cell ERK activity along with protein expression of eight canonical ERK targets. We found that on average, ERK drives gene expression; however, the correlation at the single-cell level is mild to moderate. Importantly, the correlation is dependent on the timing of ERK activity. Fra-1 and pRB correlate to long-term sustained ERK activity while Egr-1 and c-Myc correlate to recent ERK activation. This information demonstrates that clinical assays of ERK activation can be improved by measuring optimal ERK targets instead of phosphorylated ERK.

5.3   Conclusions

A major conclusion of this dissertation is that ERK activation in an individual cell is only moderately correlated with ERK target gene expression. While this is partly due to measurement noise, single-cell studies show an unexpectedly lower correlation between ERK activity and gene expression (Gillies et al. 2017). This result is in contrast to early work that hypothesized a more deterministic relationship. Nonetheless, our study showed a high correlation in bulk measurements, suggesting that the average behavior within a group of cells may be more important. This notion is supported by the role of ERK in collective movement, regeneration, and tissue development. The behavior of all cells on average that drive these processes in order to maintain homeostasis.

Chapter four provides a strong proof of concept for a method to enhance the ERK activation diagnostics. In many studies, Ras/MAP kinase pathway activation is simply assayed by immunostaining-based measurement of phosphorylated ERK (p-ERK). However, this requires the assumption that phosphorylated ERK is continuing signal transmission into its

targets. While this is a sound assumption, ERK can be phosphorylated and dephospho-rylated quickly. Therefore, a single time point measurement of phosphorylated ERK only provides a snapshot of its behavior. We hypothesized there is more information about ERK that can be extracted. Our models demonstrate that ERK targets can be used for spatiotem-poral predictions of the history of ERK activity. Phosphorylated-ERK measurements have had a significant impact on basic and translational cancer biology. Here we show that ERK targets provide more information than p-ERK, and therefore, this strategy can be used to improve pathway activation assays.

5.4   Future Directions

We observed a very low correlation between ERK activity and c-Jun expression. This obser-vation led us to further investigate the relationship between these two canonical connected proteins. Appendix A discusses preliminary data which measures endogenous, live-cell c-Jun expression. Surprisingly, we show that c-Jun exhibits oscillatory behavior, revealing several new questions about its regulation.

A natural next step of our prediction method is to improve the accuracy of our ERK history predictions. Training improved models requires optimal predictors of ERK activity. While we show that Fra-1, pRB, Egr-1, and c-Myc are better predictors than p-ERK, a larger screen is needed to find optimal proteins. We show that in theory, ERK prediction models can be highly accurate with at least 16 different predictors. Therefore, the natural next step is to find the most informative set of proteins to measure in a feasible and inexpensive manner. From a biological perspective, finding sets of proteins that report different ERK histories will answer the question of how ERK encodes differential gene responses. Future studies will quantitatively connect ERK signaling, gene expression, and cell fates at the single-cell level.

Once optimal genes are chosen, continuation of our approach will require repeating data collection in various models, including other (cancer) cell lines, patient derived tissues, or even *in vivo* mouse studies. The goal of which is to collect enough data to train more cell type specific models that can be used in the clinic. We imagine a tool where images of stained patient tissue can be uploaded to software which will then use pre-trained cell-type specific models to annotate the images. The automatic, model based predictions of spatiotemporal ERK history would facilitate a robust and quantitative analysis of tissues, and remove the need for subjective visual annotations. Ultimately, these tools will enhance diagnostic accuracy and lead to more effective treatments for patients with cancer.

Appendix A

Regulation of c-Jun is heterogeneous and oscillatory

A.1 Abstract

c-Jun plays an important role in cell cycle progression, survival, apoptosis, and cancer. The transcriptional and translational control of c-Jun affects cellular phenotype in response to extracellular stimuli. Here we measured endogenous levels of c-Jun using CRISPR-based knockins in mammary epithelial cells. We reveal that c-Jun undergoes oscillatory patterns of expression with a periodicity of 5 to 10 hours. These results suggest that c-Jun is dynamically regulated by upstream MAP kinases. Furthermore, we show that initial levels of c-Jun may affect the changes of survival in response to cell stressors. These new insights show that targeting c-Jun may increase the sensitivity of cells to chemotherapy.

A.2 Introduction

Cell to cell variability in gene expression results in differences in phenotype and can affect responses to extracellular stimuli. While genetic heterogeneity allows cells in tissues to be adaptable to different stimuli, it can lead to drug resistance, posing a significant challenge to chemotherapy. Heterogeneity arises from multiple sources, including variability in epigenetic modification, paracrine signals, or stochastic gene expression (Niepel, Spencer, and Sorger 2009). Intrinsic noise is a major driver of stochastic gene expression and is caused by the inherent noise in transcription and translation (Elowitz *et al.* 2002). Subtle fluctuations in intracellular biochemical reactions can have long term consequences for the cell. For example, naturally occurring differences in the expression of proteins regulating apoptosis affects the timing and probability of cell death (Spencer *et al.* 2009). Additionally, cell-cell variability of p21 expression in response to chemotherapeutics alters the drug response (Hsu, Altschuler, and Wu 2019). Another source of heterogeneity is cellular state. In an asynchronous population, cells may be in different stages of the cell cycle or exist in different metabolic states (Kosaisawe *et al.* 2021). For example, levels of cyclins oscillate through stages of the cell cycle (Evans *et al.* 1983). Furthermore, genes that exhibit rapid response to extracellular signals are ideal targets for the identification of heterogeneously expressed genes within a population of cells. Accordingly, the search for other variable genes is critical to addressing drug resistance in cancer.

c-Jun is an AP-1 transcription factor that responds to various extracellular stimuli and is also associated with the cell cycle. Several upstream kinases are shown to regulate c-Jun, including Extracellular signal regulated kinase (ERK), p38 MAP Kinase, and Jun N-terminal Kinase (JNK) (Dérijard *et al.* 1994; Humar *et al.* 2007; Pulverer *et al.* 1991). The combined regulation by multiple kinases allow c-Jun to respond to growth factors, DNA damage, and other stress signals. Additionally, c-Jun is required for progression through the G1 phase of

the cell cycle, and it plays a role in the survival response to stress (Wisdom, Johnson, and Moore 1999; Hettinger *et al.* 2007). Due to its role in the cell cycle, dysregulation of c-Jun is characteristic of many cancers (Eferl and Wagner 2003).

Here we used a CRISPR-based GFP knockin strategy to monitor endogenous levels of c-Jun in response to basal and stress conditions in MCF10A cells. Surprisingly, c-Jun displays oscillatory behavior in basal conditions, and responds quickly to the c-Jun-N-terminal Kinase (JNK) activator anisomycin. WIth high anisomycin treatment, many cells undergo cell death, yet the survivors upregulate c-Jun. This is consistent with previous reports of c-Jun's pro-survival role. Interestingly, the levels of c-Jun at the time of treatments may affect the survival of cells responding to high stress conditions. These results reveal a previously unobserved regulatory behavior of c-Jun and suggest that targeting c-Jun heterogeneity may lead to higher fractional killing in chemotherapy.

A.3 Results

c-Jun-mVenus knockin cells were stimulated with imaging media control, EGF, or anisomycin and imaged for 16 hours (Figure 1a). In control cells, c-Jun exhibits a striking oscillatory pattern of expression where cells range from one to three peaks per cell (Figure 1b). EGF triggers a slight increase in c-Jun signal, while anisomycin results in a rapid, dose dependent response (Figure 1c). With 50 ng/ml anisomycin, cells begin to undergo cell death within one hour of treatment, and further cell death continues until 10 hours post-treatment. Interestingly, survivors immediately begin to express c-Jun-mVenus. In high anisomycin treated wells, c-Jun expression in survivors is high and sustained while a lower concentration produces an intermediate level of c-Jun. Interestingly, cells with a lower dose of anisomycin reach a peak of c-Jun and subsequently undergo smaller oscillations over time. To investigate whether the levels of c-Jun prior to anisomycin treatment affects cell survival, we binned
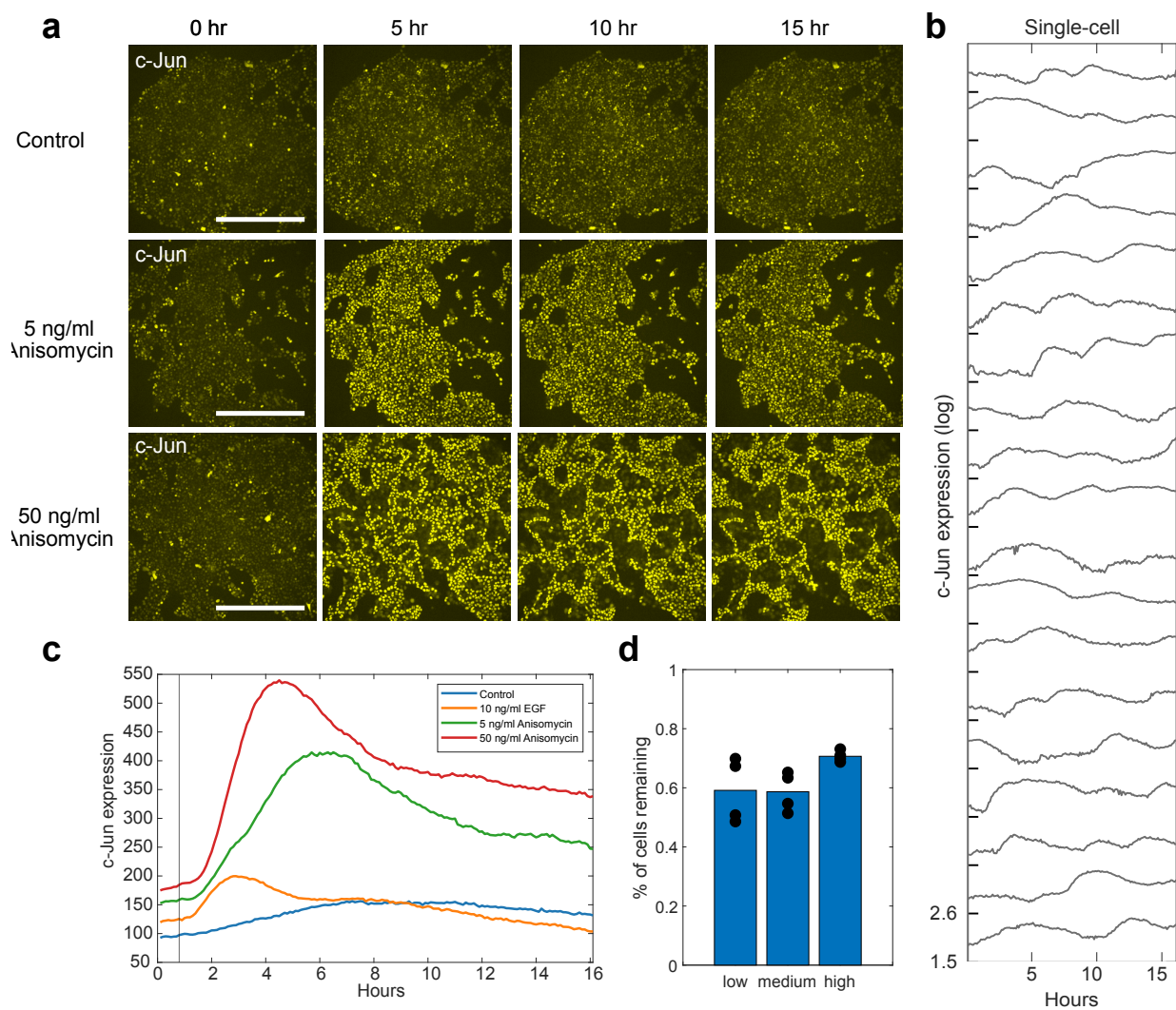
Figure A.1: Endogenous tagging of c-Jun reveals dynamic regulation **a** a MCF10A c-Jun-mVenus knockin cells treated with control, Epidermal growth factor (EGF), or Anisomycin. Scale bar = 500 um. **b** Single-cell measurements for 19 cells in control wells. **c** Average measurements of c-Jun for all cells treated with the indicated stimulus. **d** Percent of remaining cells were quantified by considering dead cells as an initially tracked (live) cell with a scalar YFP signal which then displayed a NaN value after 2 hours of treatment. Dots represent the percent remaining in 4 separate wells treated with 50 ng/ml anisomycin.

cells into three groups (low, medium, or high). These bins represent the level of c-Jun at the time of anisomycin treatment. After two hours of anisomycin, cells with initially high levels of c-Jun survived slightly longer than cells with low or medium levels (Figure 1d). These results indicate that prior expression of c-Jun may prevent cells from quickly inducing cell death under stress-response conditions.

A.4 Discussion

The data presented here reveal the highly variable nature of c-Jun expression in single-cells. While previous reports have proposed that c-Jun may accumulate and degrade throughout the cell cycle (Wei *et al.* 2005), our observed oscillations occur in periods shorter than the cell cycle. Many cells display two to three pulses within a 16 hour time frame. These results suggest that c-Jun regulation is highly dynamic and may be subject to other periodic cellular states (i.e. metabolism). Alternatively, regulation from ERK, JNK, or p38 could explain why c-Jun is highly variable. Further work will seek to address the sources of these oscillations.

We show that initial levels of c-Jun may mediate the cell death/survival response. Therefore further studies should investigate whether this is the case in other settings such as DNA damage, hypoxic stress, or chemotherapy. If such is true, treatments that limit the heterogeneity in c-Jun may be used in combination with chemotherapeutics to prevent cells from averting cell death.

A.4.1 Limitations of this study

These experiments were conducted in 4 separate, unvalidated CRISPR knockin cell lines. Further work is needed to confirm proper incorporation of mVenus into the endogenous c-Jun locus and to demonstrate that the knockin does not alter endogenous regulation.

Additionally, these experiments were conducted in non-clonal cell lines; therefore, the heterogeneity we observe may be due to clonal differences. Future experiments should be done with a clonal line.

A.5   Methods

The Eflute CRISPR knockin system was used to generate knockin cell lines (Stewart-Ornstein and Lahav 2016). Briefly, two different gRNAs were used to target Cas9 to the genomic c-Jun locus. Cells were electroporated with gRNA/Cas9 plasmid and a homology arm template containing mVenus/p2a/blasticidin DNA sequences. Cells were then treated with blasticidin for two weeks to select for cells with homology donor incorporation. These cells were imaged as described in chapter 4 of this dissertation.

Appendix B

ERK signaling dynamics: Lights, camera, transduction!

B.1 Preface

This chapter was published in *Developmental Cell* as a commentary piece on Gagliardi *et al.* "Spatiotemporal control of ERK pulse frequency coordinates fate decisions during mammary acinar morphogenesis" *Developmental Cell* 2022:

The article has been modified to satisfy the formatting requirements of this thesis.

B.2 Abstract

Three-dimensional mammary epithelial acini are a model for understanding how microenvironment-driven signaling coordinates cell behavior and tissue morphogenesis. In this issue of Develop-

mental Cell, Ender *et al.* use live-cell imaging to capture dynamic spatiotemporal patterns of ERK activity that instruct cell migra-tion and survival fates in developing acini.
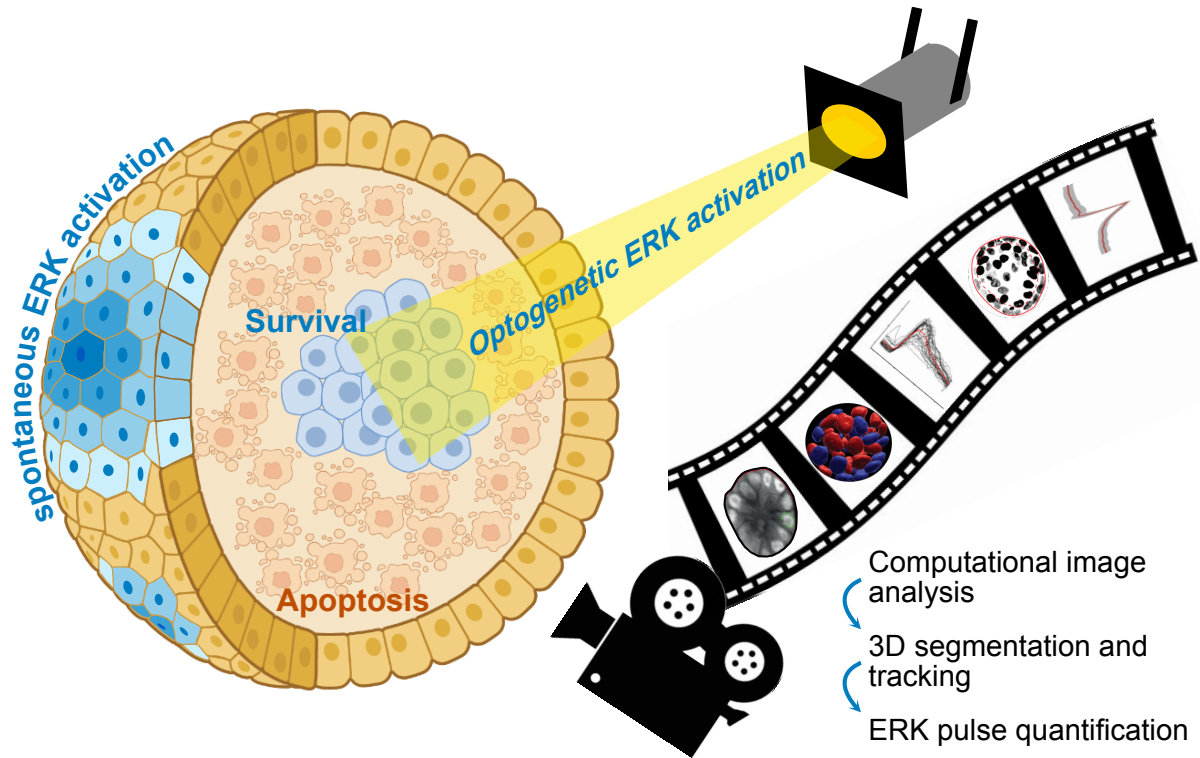
BioRender Clipartlibrary Clipartmax

Figure B.1: A cinematic view of signaling dynamics in 3D cell culture **a** Ender *et al.* combine live-cell biosensor imaging, optogenetic activation, and computational image analysis to reveal the inner workings of a classic organotypic model.

B.3 Commentary

Development and homeostasis depend on the orchestration of cell fates within tissues. Cell fates such as proliferation and apoptosis are determined by signaling and gene regulatory networks that respond to the local cellular environment. A major goal of modern biology is to understand how these fate "decisions" are made at the molecular level, and how they affect physiological functions at the tissue level. The gold standard is to establish these answers

within a living tissue. However, many experiments cannot be done in an organismal context, especially those requiring intensive intervention or questions specific to human biology. To address such challenges, organotypic cell culture has emerged as an important tool for *in vitro* manipulation of tissue like-structures retaining some authentic elements of the cellular microenvironment and cell-cell interactions. In this issue, Ender et al elegantly exploit a widely used mammary epithelial organotypic system to bring a new level of spatio-temporal resolution to cell fate determination. Employing advanced engineering tools, including 3D live-cell tracking of activity biosensors and optogenetic activators, they uncover intricate 3D dynamics in growth factor signaling. Importantly, they also document the impact of transient signaling activity on cell death events that shape the overall organotypic structure.

The MCF10A acinus model has been used for over 20 years to study how cells interact within an extracellular matrix (ECM) to generate three dimensional structures (Muthuswamy *et al.* 2001). This model helped catalyze awareness that traditional two-dimensional cell culture, where cells adhere to a stiff plastic surface, is limited in its ability to capture physiological cell behavior. The acinus system begins with single MCF10A mammary epithelial cells suspended in Matrigel, an ECM secreted by cultured tumor cells. As the cells divide to form spherical cell masses, they undergo heterogeneous activation of signaling pathways and changes in gene expression (Debnath and Brugge 2005). Within 6 days, the outer layer of cells polarizes, attaching to the surrounding ECM, while the inner cells, without a strong ECM attachment, begin to die by apoptosis. By 10-14 days, a single-layered hollow sphere develops and reaches a stable size due to an equilibrium between cell deaths and divisions. Disrupting cell signaling during acinar development, for example by expressing active forms of the ErbB2 receptor or perturbing their metabolic state, leads to phenotypes ranging from increased acinus size to uncleared acini and multi-acinar structures.

All of this prior work sets up MCF10A acini as an ideal *in vitro* setting where the molecular states of cells can be carefully manipulated and connected to the phenotype of the

larger structure they build. Previous studies have approached this question by looking at the gene expression profiles of MCF10A cells in developing acini, identifying transcription factors that control morphogenesis (Janes *et al.* 2010). However, these approaches have the drawback that they provide only fixed snapshots in time. A similar caveat extends to gene expression profiling in other organoid and tissue systems. Although transitions between expression states can be inferred computationally, there is much that is overlooked by focusing only on fixed mRNA measurements.

Ender et al bring several important new tools to this question, focusing on the ERK pathway that plays an important role in acinar morphogenesis (Fig. 1). They employ a biosensor that reads out ERK activity in living cells, a tool used previously to show wave-like activation patterns in cell culture and intact tissues (Nakamura *et al.* 2021; Hiratsuka *et al.* 2015). As in other systems, Ender *et al.* observe that ERK activity in acini occurs in pulses and waves that propagate from cell to cell. With optogenetic techniques, they also test specific ERK pulse timings on the acini. Key to using these methods effectively is sophisticated 3D image analysis software they developed for tracking and quantification of all cells within the acinus. This combination of tools enables an impressive new level of precision to define the regulatory processes that shape the developing acinus.

With all these tools in place, a deeper look into ERK's functions in acinar morphogenesis produced some action-packed movies. A persistent question in the signaling field is how information is "encoded" by ERK activity dynamics and "decoded" to determine specific cellular responses. Ender *et al.* first note that during the early stages of morphogenesis, high motility of cells is driven by frequent pulsatile ERK activity. When optogenetic stimulation is used to induce synchronous ERK activation during this stage, migration speeds decrease. In later stages, cell motility slows and ERK pulses become less frequent, changing from a motility cue to an anti-apoptotic signal. This switch confirms that the "meaning" of ERK activity pulses is specific to particular periods of developmental activity.

In the later stages of morphogenesis, Ender *et al.* found that ERK wave propagation occurs at a rate of about six cells per hour, with variable numbers of cells participating in the wave. Previous work (Gagliardi *et al.* 2021) has shown that such transient activation of ERK can protect cells from apoptosis, and the authors further this concept, finding that cells require a minimum of one 20-minute pulse every 0.5 to 4 hours to survive. Probing further, they find that the frequency of ERK pulses, rather than the integrated activity, regulates the survival fate. An important next question is to understand what mechanisms set this frequency threshold for survival. One possibility lies in the dynamics-dependent expression of ERK target genes. For example, Egr1 is an ERK target gene that is highly sensitive to dynamics (Davies *et al.* 2020) and has been implicated in cell death regulation. ERK also protects against cell death in acini by phosphorylating the cell death activator Bim, and the survival threshold could be linked to the rate of Bim dephosphorylation following an ERK pulse.

MCF10A acini have long been a tool for investigating the phenotypes of oncogenic mutants, and Ender *et al.* extend this analysis to the signaling dynamics level. In cells carrying a mutation in Phosphoinositide 3-kinase (PI3K), the shape of ERK pulses remains the same but the frequency of ERK pulses is increased, especially in inner cells. This upregulation correlates with a decrease in apoptosis, leading to a defect in acinar lumen clearance, while PI3K inhibitors reduce the number of pulses. These findings argue that signaling dynamics are an important but often overlooked mechanism underlying the actions of mutations and drugs. Relatively subtle changes in average signaling levels can belie much more dramatic changes in single-cell dynamics.

Ender *et al.* contribute not only to the growing appreciation of ERK signaling dynamics in epithelial morphogenesis, they pioneer new technical capabilities to make spatio-temporal regulation accessible in a 3D system that is already a mainstay in cancer cell biology. With similar methods also being pioneered in other *in vivo* model systems (Johnson *et al.* 2017;

Nakamura *et al.* 2021), this quantitative approach to signaling promises to provide detailed insight into increasingly complex ex vivo and *in vivo* models of tissue function. An important future challenge still lies in connecting signaling dynamics to gene expression states of individual cells. In MCF10A acini it will be particularly interesting to determine whether pulsatile ERK signaling, which is a potent generator of gene expression heterogeneity (Davies *et al.* 2020), plays a role in setting up the gene expression variants that arise in the early stages of morphogenesis as acinar cells self-organize (Janes *et al.* 2010). Also important will be to investigate how multiple signaling pathways collaborate to determine cell behaviors, for example by combining multiple biosensors with gene expression measurements within the same cell. The next films in this series promise to be as interesting as the latest installment.

B.3.1 Declaration of interests

J.G.A. has received research funding from Kirin Corporation. A.R. declares no competing interests.

Appendix C

Live-Cell Sender-Receiver Co-cultures for Quantitative Measurement of Paracrine Signaling Dynamics, Gene Expression, and Drug Response

C.1   Abstract

Paracrine signaling is a fundamental process regulating tissue development, repair, and pathogenesis of diseases such as cancer. Herein we describe a method for quantitatively measuring paracrine signaling dynamics, and resultant gene expression changes, in living cells using genetically encoded signaling reporters and fluorescently tagged gene loci. We discuss considerations for selecting paracrine "sender-receiver" cell pairs, appropriate reporters, the use of this system to ask diverse experimental questions and screen drugs blocking intracellular communication, data collection, and the use of computational approaches to model and interpret these experiments.

C.2 Introduction

Intercellular communication is a core process regulating normal development and pathological states such as cancer [1,2,3,4,5]. However, understanding the precise spatial and temporal aspects of intercellular signaling is challenging. *in vivo*, one must be able to track cell signaling responses over time and geographically within a tissue. Technical limitations make these studies challenging to perform, and the *in vivo* setting limits perturbations that can be made to quantitatively define signaling dynamics, gene expression, and cell fate. Additionally, *in vivo* signaling represents a composite effect from multiple signals, arising from multiple cell types that converge on individual "receiver" cells. Thus, an *in vitro* system that uses a reductionist approach to study intercellular communication, in a simple and controllable environment, represents an attractive model to perform "sender" to "receiver" cell interaction studies. Herein we describe such an approach that allows detailed exploration of sender-receiver relationships and has been used successfully to study this relationship between malignant and adjacent nonmalignant cells [5]. Implementation of this approach allows for detailed spatial and temporal profiling of signaling, gene expression, and cell fate in living cells with single cell resolution and yields quantitative information that can inform computational model development. Importantly, this system is adaptable to multiple signaling pathways and cell types. Therefore, it can be used to answer questions focused on tissue development, wound healing, and other relevant biological problems coordinated by intercellular signaling.

During development and homeostasis, intracellular signaling is known to spatially and temporally orchestrate cell fate changes or behaviors resulting in the generation or maintenance of organized tissue systems [2, 3, 6,7,8]. One such example occurs during postnatal mammary gland development. At puberty, rising systemic estrogen levels induce mammary luminal epithelial cells to produce and secrete the epidermal growth factor receptor

(EGFR) ligands, including amphiregulin (AREG), in a paracrine manner, creating a sender-receiver cell relationship between epithelial and surrounding myoepithelial and stromal cells, respectively [9,10,11]. Gradients of AREG are received by proximal myoepithelial cells and fibroblasts resulting in induction of gene expression programs that regulate mammary gland invasion and morphogenesis [11]. Establishment of such a sender-receiver relationship between mammary epithelial cells and the surrounding stromal cells is an essential step in functional gland development. However, this process is hijacked in some tumors of the breast. Breast cancer cells spontaneously gain the ability to secrete AREG, independent of estrogen signaling, leading to the establishment of a dysregulated sender-receiver system between individual tumor cells and between tumor and stromal cells [4, 12, 13]. Secreted AREG is bound by receiver cell EGFR, resulting in stimulation of the downstream MAPK terminal signaling effector, ERK, stimulating tumor cell proliferation, and reprogramming of the surrounding nonmalignant cell types [4, 13]. Consequently, in this specific case, the basic AREG sender-receiver cell relationship can drive normal morphogenesis, or when dysregulated, aberrant tissue function-organization relationships.

Adding complexity to the sender-receiver system, recent advances in light microscopy and reporter technologies have revealed that signaling is dynamic and varies both spatially and temporally at the single cell level. Implementation of genetically encoded reporters has allowed such detailed study using several methodologies and targeting multiple pathways. The majority of these approaches utilize Förster resonance energy transfer (FRET) or kinase translocation-based reporters. For extensive review of these reporters, see [15, 16]; FRET reporters are composed of a donor and acceptor fluorophore (typically cyan fluorescent protein (CFP) and yellow fluorescent protein (YFP) variants, respectively) separated by a linker sequence, docking, phosphorylation site for a kinase of interest (e.g., ERK), and a phospho-amino acid binding domain. Following phosphorylation by the kinase, the phosphorylated residue and binding domain interact, reorienting the donor-acceptor pair into close proximity
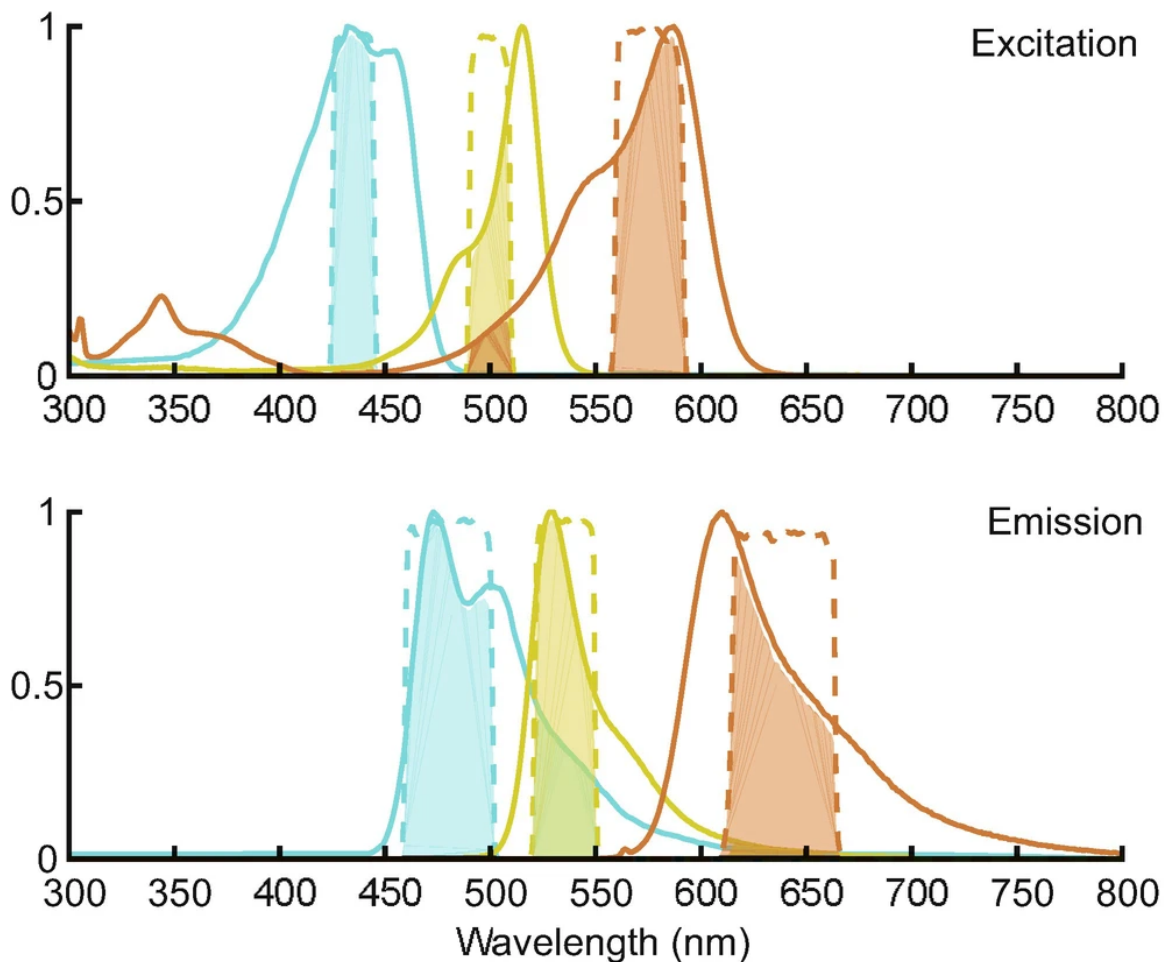
Figure C.1: Spectral comparison example for multiple fluorescent proteins. Shown as solid lines are the excitation (upper) and emission (lower) spectra for mTurquoise2 (cyan, left), YPet (yellow, center), and mCherry (red, right). Dashed lines show filter transmission bands, for example, CFP, YFP, and RFP filter sets (colored and ordered spectrally). The relative intensity of light passing from a fluorophore through a filter can be assessed by the shaded overlap areas. The net channel intensity through a filter set is proportional to the product of the shaded areas for excitation and emission of that color. Unwanted cross-talk between channels can be evaluated by the shaded areas where a fluorophore spectrum overlaps a differently colored filter. For example, the YFP emission filter overlaps the mTurquoise2 spectrum significantly (green shading, center of lower graph). However, in the excitation graph, these spectra overlap negligibly (center of upper graph). The product of these two cross-talk areas is very small compared to that for the YFP channel, resulting in well-separated channels

resulting in FRET when the CFP is excited. Kinase activity can be measured by the ratio of CFP to YFP in fluorescent microscopy or by fluorescence lifetime imaging microscopy (FLIM). Kinase translocation reporters, or KTRs, contain a tandem nuclear import and export sequence that is also a kinase substrate. Phosphorylation of the reporter by a kinase suppresses shuttling from nucleus to cytoplasm. As a result, kinase activity can be measured as the ratio of cytosolic (C) to nuclear (N) fluorescence. KTRs have been designed for a number of signaling pathways including ERK, Akt, JNK, and others [16]. For a more extensive discussion of basic translocation reporter use and analysis, we suggest reading Pargett *et al.* (2017), Pargett and Albeck (2018), and Kudo *et al.* (2018) [17,18,19]. One benefit of KTRs is the utilization a single fluorophore resulting in the ability to use and discriminate different reporters (e.g., ERK and Akt reporters), in a single cell, based on discrete emission wavelengths (Fig. 1). Additionally, because the tandem import/export and kinase substrate sequences can be fused to different fluorophores, one can use the same reporter to measure kinase activity and to discriminate different cell types, for example, an ERK reporter fused to a different fluorophore in each different cell type. As described in this protocol, this feature allows different cell types to carry the same functional reporter with spectrally distinct fluorophores (e.g., mVenus or mTurquiose2) to easily distinguish the signaling dynamics of sender and receiver cells with single cell resolution (Fig. 2).

With the advent of CRISPR-technologies, we are now able to tag genes of interest with fluorescent proteins at their endogenous loci. This allows one to track both signaling dynamics using genetically encoded reporters and the expression of downstream target genes, such as ERK target gene Fra-1, in living cells over time. Utilization of this approach allows determination of both signaling and resultant gene expression under varying conditions (Fig. 2) [20]. In this protocol, we describe the use of this approach to simultaneously measure the effects of sender cell growth factor secretion on receiver cell signaling and gene expression.

Making full use of reporters requires an analysis pipeline able to track single cells over
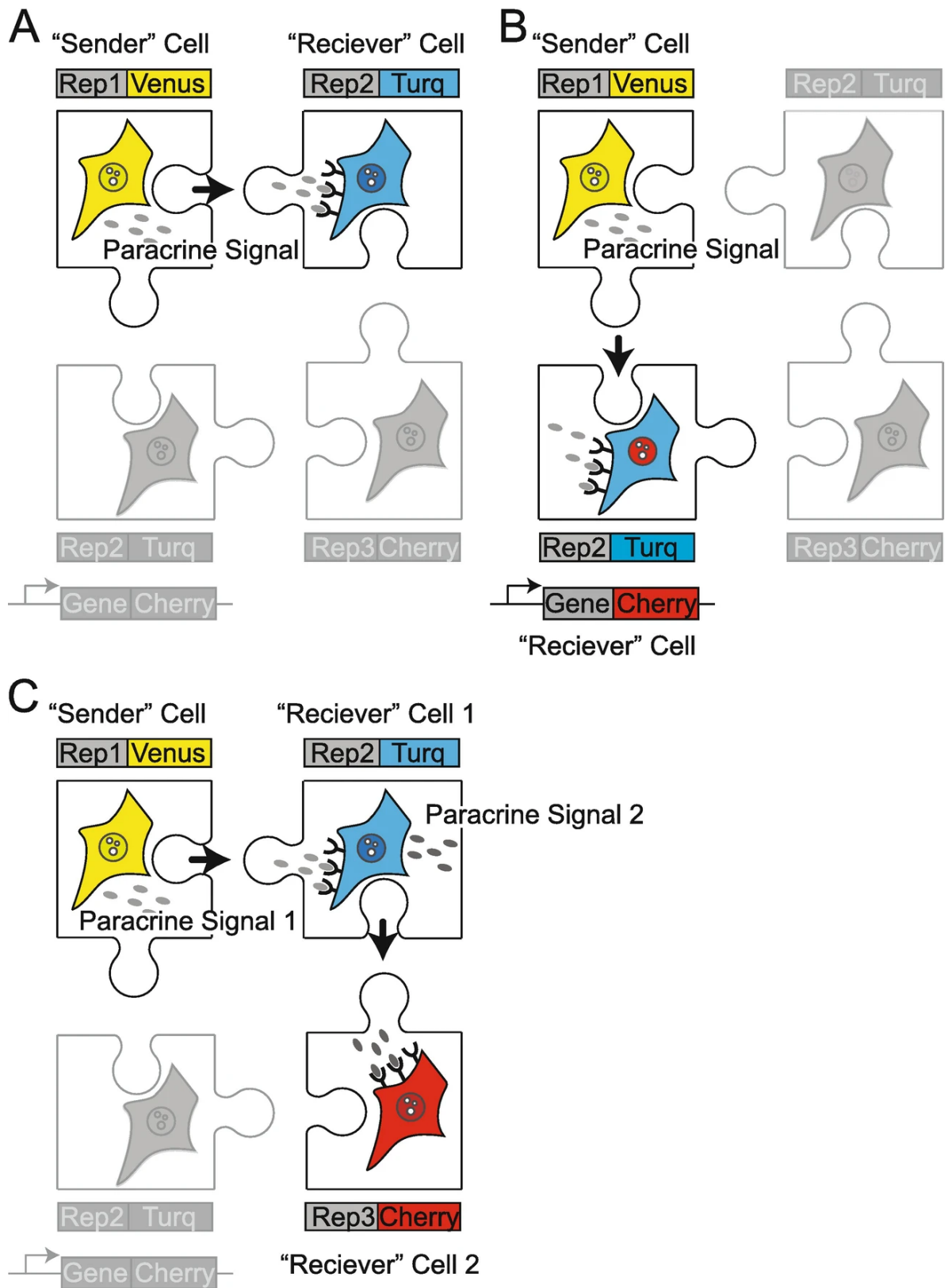
Figure C.2 Modular construction of sender-receiver cell cultures

Figure C.2: Modular construction of sender-receiver cell cultures. Sender-receiver pairs, analogous puzzle pieces, can be combined in various ways and are limited only by available spectra, suitable cell pairs, and analysis capabilities. **a** In the simplest form, a sender-receiver pair is constructed using the same reporter ("Rep1" and "Rep2," e.g., ERK KTR) fused to different fluorescent proteins (e.g., mVenus (yellow) or mTurquoise2 (blue) allowing visual and computational deconvolution of the data. **b** Using this same approach, receiver cells can be generated that co-express a reporter construct (blue) and another reporter or CRISPR-based fluorescent protein-gene fusion, represented here as a mCherry fusion (red). **c** A more complex assay can be created using cell lines multiple spectrally distinct sender-receiver combinations (mVenus, mTurquoise2, and mCherry fused reporter constructs; yellow, blue, and red, ("Rep1-3"), respectively), where, for example, the sender cell engages receiver cell 1 and receiver cell 1 acts as a sender for receiver cell 2.

time and measure the signal intensity of multiple reporters and/or tagged genes with high fidelity. With the expansion of live-cell markers, several computational methods have been developed to fill this need. Such software is able to automatically analyze time-lapse images, identifying and tracking individual cells over time. Software implementations are increasingly available and are now largely approachable without writing custom code. However, while some of these software provide visualization and plotting tools, handling and analysis of the time series data are often performed with custom code via scripting software (e.g., MATLAB, Python, and R).

In the following protocol, we provide an approach based on experiments reported in Davies *et al.* (2020) that can be adapted to explore intracellular signaling biology generally, or used for other purposes, such as screening for drugs that block tumor-microenvironment signaling interactions [5]. This system is also highly adaptable to many types of sender-receiver relationships such as tumor-immune signaling, three-dimensional cultures, and tissue explants in a manner dependent upon available reporters, the appropriate microscope, environmental control equipment, and a suitable computational analysis pipeline.

C.3 Materials

C.3.1 Cell Lines

1. 293FT cells for packaging of viral vectors (Thermo Fisher, #R70007).

2. Sender and receiver cells of interest (see Note 1 Choice of Cell Lines). This approach applies to a wide variety of cell lines and primary cell types. For the example outlined here, we utilize the isogenic HMT-3522 malignant progression series, pairing the nonmalignant S1 cells with the malignant T4-2 cells. HMT-3522 cell lines are available commercially through Millipore Sigma (98102210, 98102212, respectively); however, the cells described here were sourced from the original lineages and only available upon request [21,22,23].

C.3.2 Cell Culture Reagents

Reagents 1–9 are required for replicating the experiments in Davies *et al.* (2020), if other cell types are to be utilized, adjust cell culture reagents as required.

1. Prolactin from sheep pituitary gland (Millipore Sigma L6520).

2. Insulin (Millipore Sigma I6634).

3. Sodium selenite (Millipore Sigma S5261).

4. Beta-estradiol (Millipore Sigma E8875).

5. Hydrocortisone (Millipore Sigma H0888).

6. Transferrin (Millipore Sigma T8158).

7. Recombinant human epidermal growth factor (Peprotech AF-100-15).

8. DMEM/F12 containing bicarbonate buffer (Gibco 11320082).

9. DMEM/F12 phenol-free media for imaging (Gibco 11039047).

10. DMEM high glucose containing HEPES (Gibco 12430112).

11. OptiMEM (Gibco #31985088).

12. Fetal bovine serum (Gemini Biosciences 100-106).

13. 0.25% trypsin solution (Gibco 25200056).

14. Antibiotic selection agents corresponding with reporter plasmid selection marker expression (e.g., puromycin).

C.3.3 CRISPR Tagging and Validation Reagents

Adapted from Ornstein *et al.*

1. Cas9/gRNA delivery plasmid (e.g., px330 Addgene #42230).

2. Homology template plasmid backbone (e.g., pENTR, pAAV, TOPO).

3. Custom gRNA PCR primers.

4. Custom homology arm PCR primers.

5. Fluorescent protein template sequence.

6. High fidelity PCR polymerase, dNTPs, and associated standard PCR reagents.

7. Thermocycler.

8. Restriction enzymes (BbsI).

9. T4 polynucleotide kinase.

10. Gibson Assembly Master Mix.

11. PCR or gel purification kits.

12. Competent E. coli.

13. Plasmid isolation kit.

14. Transfection reagents (see Subheading 2.5 for reference).

15. Standard immunofluorescence reagents, including paraformaldehyde, permeabilization buffer (e.g., % Trition X-100 diluted in PBS), blocking buffer (e.g., 2% BSA diluted in PBS containing 0.1% Triton X-100), and wash buffer (e.g., 0.1% Triton X-100 in PBS).

16. Primary antibody specific for CRISPR tagged gene(s) of interest.

Secondary antibody with a distinct emission spectrum as compared to reporters and tagged genes. We prefer Alexa Fluor (Life Technologies) tagged secondaries as they are available in a wide range of emission wavelengths.

C.3.4 Genetically Encoded Reporter Constructs

1. Multiple reporter constructs are available via Addgene corresponding with the published literature or by request from individual investigators. In the protocol discussed here, the original ERK-KTR reporter from Regot *et al.* (2014) was cloned into the pLJM1-puromycin (Addgene #19319) lentiviral vector followed by the mTurquoise2 or mVenus fluorescent protein coding sequence [16]. For a discussion on selection of reporters, see Note 2 Choice of Genetically Encoded Reporters.

2. If genetically encoded nuclear tracking markers are required, we recommend using histone H2B tagged with mCerulean, mRuby, or iRFP with the specific choice dependent upon the spectrum of other reporter(s) to be used (Addgene #90234, #90236, #90237, respectively). If a genetically encoded marker is not required, we recommend the cell permeable nuclear dye Hoechst 33342.

C.3.5 Viral Production Reagents

Ensure proper virus handling safety protocols are in place.

1. Sterile tissue culture dishes (6-well plate suggested).

2. Sterile 15 mL conical tubes.

3. Polybrene (Millipore Sigma TR-1003).

4. Poly-D-Lysine (Millipore Sigma P6407).

5. Fugene HD (Promega E2311) or JetPRIME (PolyPlus Transfection 114-01).

6. 5 mL syringe.

7. 0.45 uM sterile filter.

8. Viral packaging vectors – third-generation lentiviral compatible (e.g., psPAX2 Addgene #12260, and pMD2.G Addgene #12259).

C.3.6   Live Cell and Fixed Imaging Materials and Reagents

Plating conditions must be optimized on a per cell line basis.

1. Laminin-111 (Thermo Fisher 23017015).

2. Laminin working stock (prepared immediately before use): Laminin-111 50 μg/mL with 20 mM sodium acetate pH 4 and 1 mM CaCl2.

3. Rat tail collagen I coating solution (Gibco A1048301).

4. Rat tail collagen I working stock: 50 μg/mL rat tail collagen dissolved in 0.02N acetic acid.

5. 10× Phosphate Buffered Saline.

6. Bovine Serum Albumin (BSA).

7. Triton X-100.

8. Multi-well glass bottom imaging plates (e.g., CellVis P96-0-N).

9. Single and multichannel pipettors.

10. Reagent reservoirs.

11. Hoechst 33342 (Thermo Fisher 62249) or genetically encoded marker (e.g., H2B mCerulean).

12. Recombinant human epidermal growth factor if using ERK-KTR, or another growth factor capable of stimulating the pathway of interest (Peprotech AF-100-15).

13. MEK inhibitor (e.g., PD0325901, Selleck Chemicals S1036) if using ERK-KTR, or another inhibitor capable of suppressing the pathway of interest.

C.3.7 Live Cell Microscopy Equipment

Ensure proper laser safety procedures are in place.

1. Stage top environmental chamber capable of maintaining 5% CO_2 and 37 °C for over 12–24 h, such as OkoLabs Bold Line or Tokai Hit STX systems used in our laboratory.

2. Automated microscope capable of taking serial xy images at predetermined time points for 12–24 h. We utilize a Nikon Ti2E with automated stage and NIS-Elements software.

3. Fluorescence excitation source (e.g., Lumencor Sola II), filter sets corresponding with the chosen fluorescent reporters, and an image capture device (e.g., Photometric Prime 95B).

C.3.8 Image Processing and Modeling

1. Computer with at least a 2 GHz CPU and 8 GB RAM (though many software can operate on lesser systems). Depending on software, a dedicated GPU may be required, often with at least 2 GB video RAM.

2. MATLAB software and Image Processing Toolbox or comparable (see Note 3 Image Processing Software).

C.4 Methods

C.4.1 CRISPR Gene Tagging

CRISPR-Cas9 systems are widely used to generate gene knock-in cell lines and model systems [20, 24, 25]. The revolutionary method enables endogenous labeling of proteins of interest (POI) with fluorescent tags, allowing for careful investigation of expression, localization, and dynamics. This section will describe an effective protocol to generate knock-in cell lines. There are several techniques for endogenous tagging that differ in type of Cas9 protein,

number of guide RNA (gRNA), length of homology arms, and delivery of each component to the target cell line [24, 26,27,28]. This protocol uses a human codon optimized Streptococcus pyogenes Cas9 nuclease in a chimeric guide RNA expression cassette (e.g., px330). The homology repair template is cloned into any desired plasmid vector (pENTR, pAAV, TOPO) [29]; however, it can optionally be delivered as a PCR product. Because CRISPR gene tagging can be technically challenging, we recommend generating edited cell lines first, then freezing down stocks prior to adding genetically encoded reporters (Subheading 3.3). See Note 4 for considerations prior to gene knock-in studies.

1. Preparation of guide RNA and homology repair template plasmid constructs. Use online tools to search for 20 nucleotide gRNA sequences followed by PAM (NGG) motifs. The gRNA will target the Cas9 protein to the cleavage site; therefore, the sequence should be close to (within 100 base pairs) or directly over STOP codon of the gene of interest. Most online tools also provide efficiency and off target effect predictions. Consider which is most important for the proposed study and chose the top three to five gRNA sequences for cloning. The Broad Institute or Benchling websites host useful gRNA design tools.

2. If the gRNA sequence does not start with a guanine, add a G to the beginning (5' end) of the sequence to facilitate U6 promoter transcription. Then design a complementary sequence to be used for annealing and restriction cloning. Add CACC base pairs to the 5' end of the forward sequence. Then add AAAC base pairs to the 5' end of the complementary sequence. This will make the ends compatible for BbsI restriction cloning. An example of annealed primers is shown below.

Forward primer 5' CACCGNN..NN   3'

Reverse primer 3'   CNN..NNCAAA 5'

3. Order and anneal each pair of oligos together. Digest the px330 plasmid with BbsI, and ligate it with each annealed gRNA. A detailed px330 cloning guide can be found on Addgene.com.

4. When designing the homology repair template, ensure the following: (1) introduce silent mutations in the guide RNA recognition sequence of the homology region so that the Cas9 protein does not continue its nuclease activity after homology-directed repair (HDR). (2) Insert a flexible linker between the POI and fluorescent protein; this is important for stability of the fusion protein [30]. We recommend a 3–5× repeating sequence of Gly-Ala [24] or Gly-Gly-Ser [31] for the linker domain. (3) Ensure there is a STOP codon at the end of the fluorescent protein to terminate translation of the fusion protein. (4) Each homology arm (HA) encompasses 1.4 kb-sized base pairs on each side of the target gene stop codon. An example is shown below.

Native gene locus:

$ATG_{start}...GCGGC...TAGAC_{1.4kb}TAG_{stop}$ ...CTGGA...$TGACGA_{1.4kb}$

Repair template:

GCGGC...$TAGAC_{1.4kb}$– Linker domain – Fluorescent Protein – STOP –

...CTGGA...$TGACGA_{1.4kb}$

5. Design PCR primers for a four-piece Gibson assembly of the left homology arm, fluorescent protein, right homology arm, and the desired plasmid backbone. The linker domain DNA sequence can be inserted directly into the overhanging region of the PCR primers. PCR the homology arms from the target cell line genomic DNA, and PCR the fluorescent protein from its template plasmid. Assemble the final plasmid and amplify. This cloned plasmid will be used as the homology repair template. The template can be optionally delivered as a PCR product instead by using a primer pair flanking each homology arm.

6. Transfect the homology repair template, and the Cas9/gRNA plasmid into your target cells using optimal transfection methods for each specific cell line.

7. Monitor cells after the transfection to ensure normal growth and proliferation.

8. Positive knock-in cells can be isolated through fluorescence-activated cell sorting (FACS) or limited dilution cloning. If the cell line is tolerant of single cell plating, con-

duct single cell FACS into a 96-well dish or perform limited dilution cloning. If the POI is regulated by the cell cycle, consider synchronizing the cells into the stage with highest POI expression before cell sorting. See Note 5.

C.4.2 Validation of CRISPR Gene Editing

1. Validate expression of tagged proteins. Correct integration of the fluorescent protein can be checked via western blotting for the POI. Use standard protocols suited to the cell line. This validation step may require stimulation experiments (i.e., if the POI is not constitutively expressed) using the knock-in (tagged) cell line and negative control (non-tagged) cells. See Note 6.

2. Validate accurate genomic insertion of tags. Following standard protocols, extract genomic DNA from knock-in and non-tagged cell lines, and PCR the edited gene locus using primers flanking the homology region of the gene (both homology arms). Analyze PCR products for size by gel electrophoresis, and validate the fidelity of the insertion by sequencing. See Note 7.

3. Validate intracellular localization of tagged proteins. For the highest confidence that knock-in cell lines are good representations of the parental lines, cells can be fixed and stained for immunofluorescence (using standard protocols for the cell line, see Note 8). Compare the fluorescence of antibodies directed at the POI with that of the fluorescent protein marker (or from antibodies against that marker).

C.4.3 Establishing Reporter Cell Lines

The first step is to select appropriate sender-receiver cell lines based on pathways of interest. For example, in Davies *et al.* (2020) we utilized the HMT-3522 malignant progression series lines composed of nonmalignant breast epithelial S1 cells and their isogeneic T4-2 malignant

counterparts [5]. S1 and T4-2 cells form an excellent sender-receiver pair because T4-2 have acquired the ability to secrete the epidermal growth factor ligand, amphiregulin (AREG), whereas S1 cells do not. Additionally, S1 cells express the epidermal growth factor receptor (EGFR) allowing them to receive AREG paracrine signals from T4-2 cells. See Note 1 for important considerations of cell line selection.

Kinase translocation reporters such as ERK-KTR are an advantageous tool for studying live, single-cell signaling and can be multiplexed with other biosensors for multiple kinase activity measurements from the same cell making them suitable for sender-receiver studies (Fig. 2) [16, 32]. An important consideration is choosing the ideal fluorescent protein that serves as the readout for the reporter. Several labs have taken advantage of different color fluorescent proteins for their experiments; these include mClover, mCherry, mVenus, and mTurquoise2 [2, 5, 33]. If multiplexing with other reporters, confirm spectral compatibility by analyzing the excitation/emission spectra of the fluorescent proteins (Fig. 1). Additionally, ensure that the microscope florescence filter cubes have proper excitation wavelengths and emission filters that will allow for accurate measurement of the reporter(s). Regardless of the reporter chosen, careful selection is warranted before proceeding. This is because some receptor ligand interactions can stimulate multiple downstream pathways of interest, for example, EGFR is capable of stimulating ERK, AKT, STAT, and other signaling pathways for which reporters exist. Considering the pathway, or pathways, of interest is therefore critical depending upon the goals of a particular experiment.

A clear nuclear marker must be used for proper computational nuclear and cytoplasmic segmenting. A common method facilitating accurate nuclear segmentation is to stably integrate a fluorescent protein fused to histone 2B (H2B) [16]. This fluorescent protein must be a different color than the ERK-KTR reporter. A more convenient method is to stain cells with Hoechst before the live-cell imaging experiment. These compounds can be visualized with fluorescence microscopy, have low toxicity, and can be used in live cells for several days.

1. For further discussion on selecting of sender-receiver cells, see Note 1.

2. For further discussion on selecting of reporters, see Note 2.

3. Thaw and culture 293T cells for transfection in DMEM supplemented with 10% FBS until 70–80% confluent.

4. Coat 6-well cell culture dish with 1 mL Poly-D-Lysine.

5. Incubate at 37 °C for 20 min.

6. Seed 293T cells at a density of 500,000–750,000 cells per well. Resuspend cells thoroughly so that there are no cells attached together.

7. Incubate overnight at 37 °C and 5% CO_2.

8. Transfect 293FT cells. Transfection reagents may vary; efficient chemical transfection reagents include FuGENE® (Promega) and jetPRIME® (PolyPlus) transfection reagent. Transfection protocol depends on the reagent and follows manufacture instructions. Each reaction should contain 1 ug of the lentiviral reporter plasmid of your choice, 1 ug of the viral packaging plasmid (psPAX2), and 100 ng of the viral envelope plasmid (pMD2.G).

9. After transfection, incubate cells for 12 h at 37 °C and 5% CO_2.

10. Change media to fresh growth media and incubate for another 24 h. If desired, you can inspect transfection rates by using a fluorescence microscope. High transfection rates will leave many cells visibly expressing the reporter construct.

11. Begin to collect virus using appropriate techniques and personal protective equipment. After the previous 24-h incubation step, the media will begin to contain viral particles. Collect this media and replenish wells with fresh media. Store collected media at 4 °C.

12. If desired, this collection step can be repeated every 24 h for 3–4 days after the initial transfection step.

13. After the desired amount of virus is collected, sterile filter the virus using a 0.45 uM filter. Create 500 μL aliquots of virus containing media, and proceed to transduction step or store aliquots at -80 °C. Aliquots may be stored at 4 °C up to 2 weeks; however, this may

result in decreased transduction efficiency.

14. Prepare target cell line to be transduced by seeding cells at a density of 100,000 cells per well in a 6-well tissue culture dish, and incubate overnight to allow cells to attach. Include one well that will not be infected with virus; this will serve as a control for future antibiotic selection. Cell culture media should be prepared as appropriate for the cell line chosen. If using the HMT-3522 cell lines, refer Weaver *et al.* (1997) and Briand *et al.* (1987) for a detailed description of media composition and cell handling [22, 23].

15. After 24 h, replace media with 1 mL fresh media containing polybrene at a concentration of 12 μg/mL. After virus addition, the final concentration of polybrene will be 8 μg/mL. Depending on the cell line, optimal concentration of polybrene may be within 1–10 μg/mL.

16. Add 500 μL of virus containing media dropwise to each well and gently swirl the plate.

17. Incubate for 24 h at 37 °C and 5% CO2.

18. Replace virus containing media with fresh media, and allow cells to divide for another 24 h.

19. 48 h after transduction, begin antibiotic selection, and continue for 2 weeks. Transduction rates can be assessed using a fluorescence microscope. The construct should be visibly expressed in cells.

20. (Optional) If reporter expression levels are heterogenous within the population, fluorescence-activated cell sorting (FACS) may be conducted to isolate high reporter expressing cells or cells expressing multiple reporters. Alternative single cell cloning techniques may be employed to establish clonal populations (see Note 9 Selection of Reporter Cells for discussion of options).
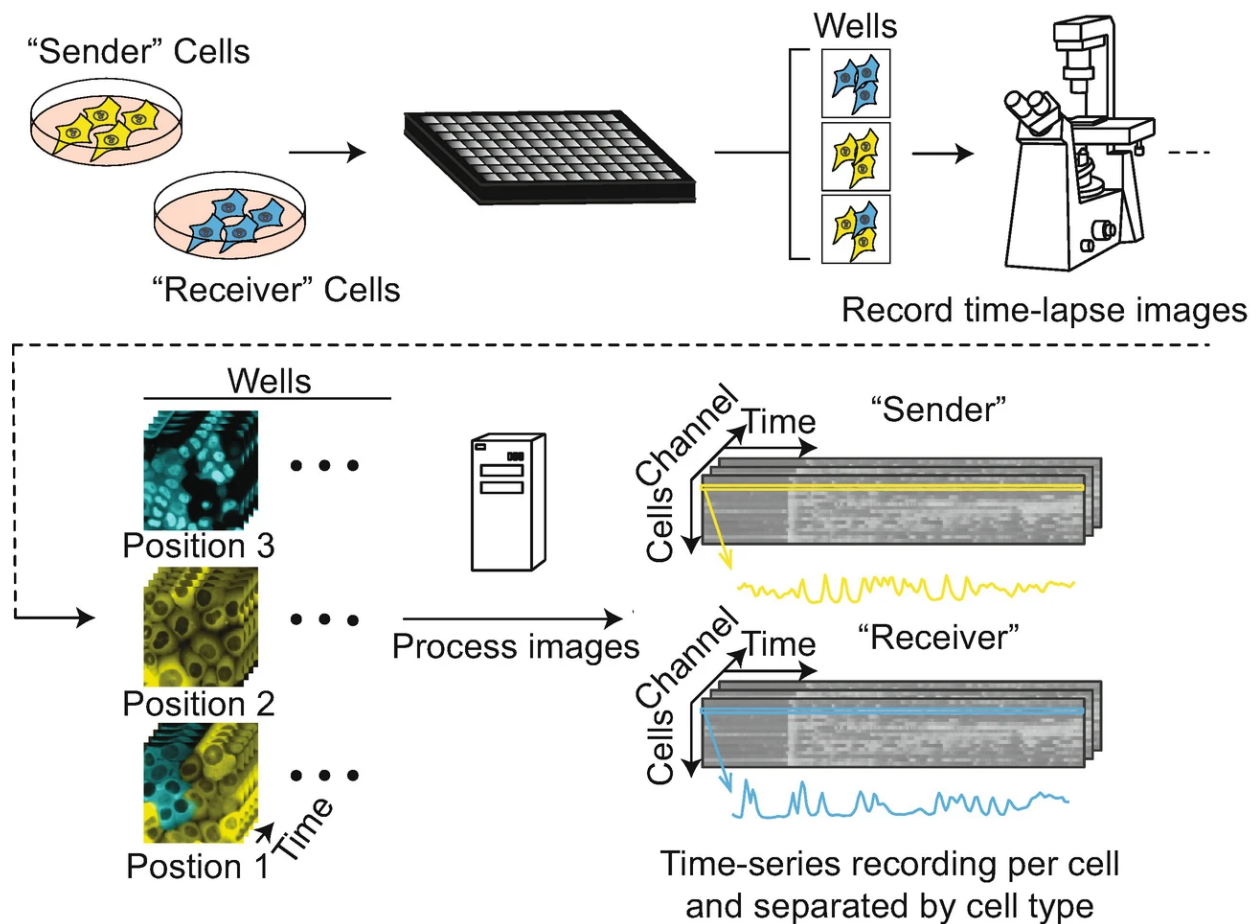
Figure C.3: Schematic example of major protocol steps. The complete experiment consists of (1) acquiring or producing DNA constructs for reporters, (2) inserting constructs into desired cell lines, (3) mixing "sender" and "receiver" cells in the desired experiment format (4) imaging co-cultured cells under desired treatments, (5) processing image data, and (6) analyzing time-series data according to the co-culture conditions used.

C.4.4 Imaging Experiment Preparation

This section provides a basic outline of imaging plate preparation that can be utilized to validate cell lines, establish co-culture conditions, and conduct sender-receiver experiments. As basic diagram is provided in Fig. 3 and will be expanded upon in the following sections.

1. Prepare imaging plate by coating 96-well glass bottom cell culture plate with extracellular matrix. For a discussion of extracellular matrix selection choice, see Note 10 Extracellular Matrix Choice.

2. If rat tail collagen is chosen, apply 3 μL of 50 μg/mL collagen solution (see Subheading 2) to the center of a well. Incubate at 37 °C for 30 min. After the incubation, add 100 μL of PBS into each well to wash out unbound collagen; see Note 11 Plating Technique for a discussion of spotting technique versus whole well plating.

3. If laminin-111 is chosen, apply 3ul of 50 μg/mL laminin solution as prepared according to MATERIALS. Incubate at 37 °C for overnight. After the incubation, add 100 μL of PBS into each well to wash out unbound laminin.

4. Trypsinize cells in accordance with the requirements of your chosen cell lines. Neutralize trypsin, and centrifuge cells.

5. Prepare cell culture media. If using the HMT-3522 cell lines, refer to a detailed description of media composition and cell handling [21, 23].

6. Resuspend and count cells using a hemocytometer. Dilute cells to 1000–3000 cells per μL in media. Optimal seeding density depends on cell line.

7. Aspirate the PBS from each well of the imaging plate, and ensure that collagen or laminin spot is not aspirated or dried.

8. Pipette 3 μL of cell suspension directly onto the spot. For best results, aspirate PBS and immediately pipette cells onto each spot. This is best done by aspirating 5–10 wells at a time and pipetting cells with a multi-channel pipette.

9. Incubate the plate at 37 °C and 5% CO2 for 1 h.

10. Gently add 200 μL of media to each well, and incubate overnight.

11. Cells should be growth factor starved for at least 12 h before conducting and experiment. For example, starvation will decrease activity of ERK and allow for robust stimulation upon growth factor treatment.

12. If there is no nuclear marker stably expressed (e.g., H2B mCerulean), dilute Hoechst 33342 in imaging media to a concentration of 0.1–1 μg/mL (see Note 12 Imaging Media).

13. Replace media with 200 μL of Hoechst containing imaging media, and incubate for 1 hour.

14. Place plate on automated stage, and begin time course experiment, image Hoechst, and ERK-KTR reporter every 6 min for several hours (typically 12–24 h). The microscope stage must be equipped with a 37 °C and 5% CO2 environmental chamber to maintain healthy, viable, cells.

C.4.5   Validation of Reporter Cells

Once reporter cell lines are generated, one must validate the function of the reporter in both sender and receiver cultures. In the case of ERK-KTR, we utilized EGF to stimulate signaling and establish the maximal and dose-dependent response for the reporter. Conversely, we verified the maximal reporter suppression that can be achieved by inhibiting the activation of ERK-KTR using a MEK inhibitor. The combination of stimulus and inhibitor use allows one to (1) establish the dynamic range and response characteristics of a particular reporter in the cell(s) of interest, (2) establish the baseline signaling activity of a signaling pathway within the receiver cells, and (3) evaluate the expression of a CRISPR tagged gene under these conditions, if present. See Note 13 for a discussion of baseline signaling activity verification.

1. Prepare your experiment, and begin imaging as outlined in Subheading 3.4.

2. Collect at least 3 h of images before adding growth factor or inhibitors. This will reveal

baseline ERK-KTR activity after starvation and allow cells to equilibrate to the imaging conditions.

3. Conduct a dose curve stimulation using EGF to activate ERK if using the ERK-KTR reporter. Final EGF concentrations in the media should range from 0.01 to 100 ng/mL and include a vehicle-only treatment. If using another reporter, choose the appropriate growth factor or stimulus. Add 10 μL of the treatment directly into the media for minimal perturbation of the cells. This 10 μL "spike in" should be 21$\times$ the desired final concentration; the final volume in each well will be 210 μL.

4. After 6–12 h of growth factor treatment and imaging, spike in the MEK inhibitor PD0325901 to reach a final concentration of 100 nM. This treatment will fully deactivate ERK signaling. Image for an additional 2 h. If using another reporter, choose the appropriate inhibitor and dosage.

5. After completing the experiment, visually inspect the images collected for nuclear translocation. The ERK-KTR construct should exit the nucleus after activation and enter the nucleus after inhibition.

6. Conduct cell tracking and segmentation using the nuclear marker. ERK-KTR activity can be calculated as the ratio of cytoplasmic/nuclear intensity at each timepoint then dose-dependent activation and deactivation visualized and quantified (see Subheading 3.7 Image Processing for details).

C.4.6   Establishing Co-culture Conditions

Establishment of optimal co-culture conditions is an essential step in this protocol because it directly effects sender-receiver dynamics (Fig. 4) and the quality of data obtained by these assays. To begin, one must consider the optimal seeding density, which will vary by cell line, since some cell lines prefer a high density to grow effectively and thus may need to be plated as such. However, this could lead to overcrowding and layered growth which can impede

tracking of individual cell signaling behaviors. Therefore, careful optimization is required to achieve adequate density which promotes a uniform monolayer (unless utilizing confocal microscopy). One must also consider the properties of the sender-receiver relationship. For example, because AREG has a moderate affinity for EGFR, it distributes widely throughout the culture to reach receiver cells. Higher (or lower) affinity ligands may distribute with different kinetics, necessitating that sender-receiver plating ratios be optimized relative to the goals of a particular experiment. A stepwise discussion of our considerations is as follows:

1. Follow general cell plating steps as outlined in Subheading 3.4.

2. Design an optimal plating density experiment. We suggest starting with a range of 1000–4000 cells per μL with increments of 500 cells per μL. For our experiments, we found 3500 cells per μL to give optimal plating density with appropriate monolayer formation. Lower cell densities tended to result in round cell morphology forming balls on the plate surface with reduced ERK activity. High cell densities resulted in crowding, layered growth, and impeded segmentation and tracking.

3. Establishing sender-receiver cell mixing ratios. For our experiments, we choose to optimize over a range from 10:90 to 90:10 sender-receiver cell ratios, respectively (see Fig. 4). We found an optimal ratio of 70:30 sender to receiver cells which gave dynamic ERK activity in both cell types with comparable signaling frequency and amplitude. Increasing the sender cell ratio resulted in decreased ERK activity, whereas increased sender cell ratios had no appreciable effect beyond a 70:30 fraction. When using this protocol, you will have to determine the optimal cell ratios based on the properties of the cell types used and the particular hypothesis being tested.

C.4.7 Image Processing

This section provides an overview on the extraction of single-cell data from time lapse microscopy images and distinguishing between nuclear and cytoplasmic subcellular compart-
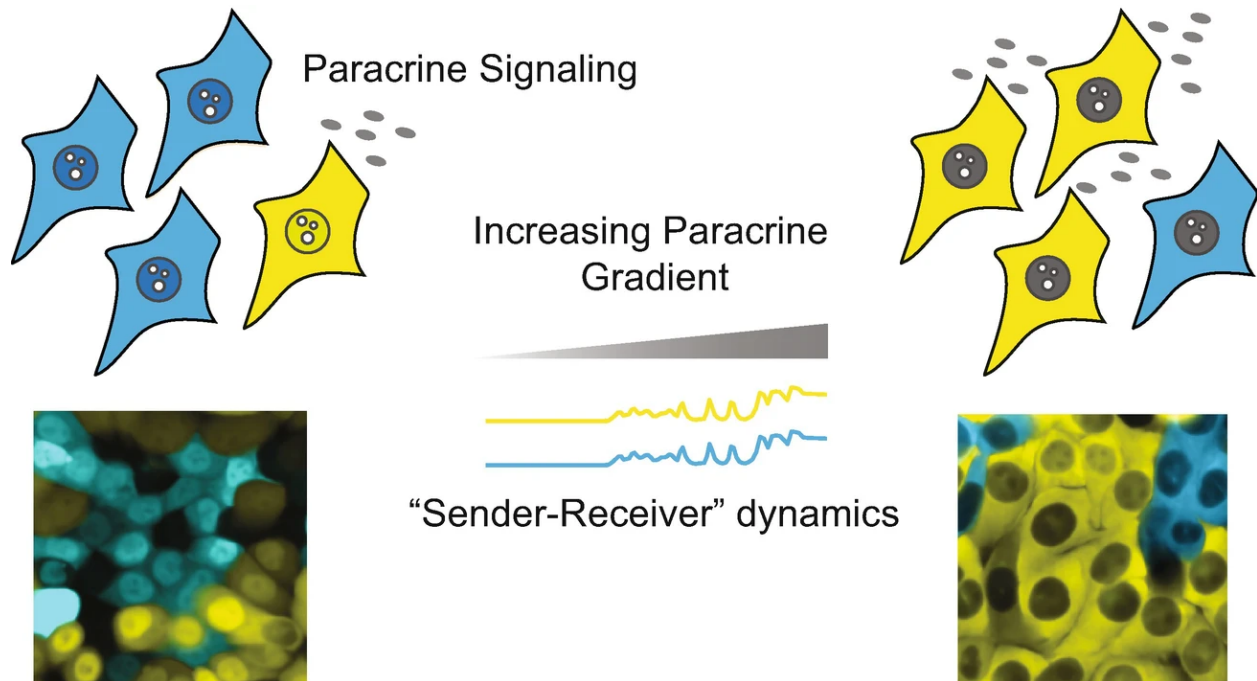
Figure C.4: Co-culture conditions dictate sender-receiver signaling dynamics. Left to right, increasing ratios of sender to receiver cells result in a progressive increase in both sender (autocrine mechanism, yellow cells) and receiver cell (paracrine mechanism, blue cells) signaling dynamics. Such dynamics correspond with increasing ligand abundance that is proportional to sender cell density.

ments. As this protocol is focused on issues specific to co-cultures, we assume a working knowledge of processing time-lapse imagery. The procedure is largely unaffected by the presence of different cell types in culture, but there are several important considerations. For protocols detailing lower level details of single-cell image analysis, see Pargett *et al.* 2017 [18]. While custom processing software is often used, there are a variety of accessible software tools to perform this processing, many of which include documentation (see Note 3 for comments on software availability).

1. Import or access data with software of choice. Microscope software stores data in a variety of formats, often specific to a manufacturer. However, most bio-image processing software is designed to access many of these formats, often using the Bioformats software tool (www.openmicroscopy.org/bio-formats/) [34]. See software user guides for details.

2. Segment cell nuclei. This is performed for every image, using the color channel detecting a reporter or dye localized to the nucleus or cytoplasm. There are several widely used techniques broadly split between thresholding and machine learning. Thresholding is simpler and useful for images with clearly defined nuclei. Machine learning requires human interaction to "train" the algorithm by manually marking out nuclei in sample images. It is particularly useful when the images are highly complex and nuclei are not clearly distinct from the rest of the image (see Note 14). In our recent work, we achieved reliable segmentation using a thresholding approach for images with Hoechst-stained cell nuclei. Different cells in co-culture were identified by the presence of a particular color of ERK-KTR reporter (see Note 15 on the use of differentially colored segmentation markers).

3. Estimate cytoplasm regions around each nucleus. Some machine learning approaches estimate the entire region of a cell's cytoplasm, given an adequate membrane stain. However, in practice, it is typically sufficient to sample a ring surrounding the nuclear mask, which is the methods used in Davies *et al.* (2020) (see Note 16) [5].

4. Track nuclei over time. With cells identified in each frame, the software will link them

from frame to frame, forming a time series. A variety of different algorithms are employed, each with differing strengths, but basic tracking is consistently well handled. See software user manuals for any details. Problems in tracking can often be mitigated at the experimental level, for example, optimizing cell density such that each cell is easily delineated. For detailed culture and imaging conditions that facilitate this process, see Subheading 3.6.

5. Collect and store times series data per tracked cell. Extract the single-cell time series data from the processing software to analyze with software of your choice (typically a scripting language, like Python, MATLAB, and R). The quantity extracted should clearly reflect the underlying feature measured by the markers or reporters used. In many cases, the average intensity in each mask is appropriate, but other use cases exist. For example, if the reporter forms puncta, the average intensity of puncta only, or the number of puncta per mask area, may be more appropriate. Ultimately, the best metric depends on the nature of the reporter expressed or dye used (see Note 17).

C.4.8 Analysis of Co-culture Signaling and Gene Expression Responses

This section describes analyses of particular importance when assessing signaling between cell types in co-culture. Reporters for both signaling (e.g., ERK-KTR) and gene expression (e.g., CRISPR knock-ins) are handled equivalently. The only processing differences between reporter types occur in how they are initially interpreted (typically, gene expression is recorded as the average fluorescent intensity, while some reporters require additional interpretation, as with the nuclear-to-cytoplasmic ratio of ERK-KTR). A wide array of analyses is possible once the co-culture data can be reliably acquired. Those highlighted here represent a sampling of the most basic and widely applicable. Overall, these analyses allow one to quantitatively attribute differences in signaling and cellular responses to the quan-

tity of different cell types present and to investigate the mechanism of intercellular signal transmission, for example, using drugs to block shedding of particular ligands.

1. Separate tracks from different cell types. To distinguish the differences between multiple cell types in culture, the tracks must be separated according to the marker profile of each cell line. If cells were segmented in separate runs, this is already complete and can be validated as needed. If cells were segmented in a single run, determine the cell type of each track by its marker profile (e.g., with a cyan and a yellow marker, cells will be either high cyan/low yellow or high yellow/low cyan). The best metric to distinguish will depend on the exact marker profiles but is typically straightforward. In the cyan versus yellow example, the ratio of cyan to yellow will show two distinct clusters, one high and one low. Below, we provide sample MATLAB code to set up an index identifying two cell types, assuming a 3D data array, Cells x Time x Channel.

```matlab
cyan = mean(celldata(:,:,idx_cyan),2); %Get mean of cyan
    intensity for each cell
yellow = mean(celldata(:,:,idx_yellow),2); %Get mean of yellow
    intensity for each cell
cy_ratio = cyan ./ yellow; %Get ratio of cyan to yellow
%If markers are similar in intensity range, the cell identity
    can be called based on cy_ratio being greater or less than
    one. i.e. iscyan = cy_ratio > 1;
%To be more robust, but a clustering algorithm
[cluster_id, c] = kmeans(cy_ratio, 2); %Get cluster assignments
    .
%Make index vector identifying cyan vs. yellow cells.
if c(1) > c(2) %If first cluster has the larger ratio, assign
    as cyan, otherwise cyan is cluster 2.
```

```
iscyan = cluster_id == 1;

else

iscyan = cluster_id == 2;

end
```

2. Estimate average density per cell type. While the ratio of cell types is known at the time of plating, it is good practice to check the status at the time of imaging (typically days later). Calculate this estimate as the ratio of average cell number in the frame(s) for each cell type (see Note 18).

```
%Estimate the fraction of cells that are cyan vs. yellow

fraction_cyan = sum(iscyan)./numel(iscyan);

fraction_yellow = 1 - fraction_cyan;
```

3. Analyze the effect of relative density on signaling. In our experience, high concentrations of receiver cells can result in low ERK activity because, as the fraction of sender cells decrease, so too does the effective concentration of ligand in the media. Correspondingly, the reporter activity of both sender and receiver cells is reduced. For our experiments, we defined the optimal ratio of sender to receiver cells at 70:30, resulting in roughly equivalent dynamic ERK activity in both cell types. In each new experimental setting, the sender/receiver ratio (either from original plating, or final estimates of relative density) can be compared with signaling and expression differences (with or without additional stimulus). Because single-cell data have been collected, not only response means, but their distributions (variance, skewness, any bi-modality, etc.) can be compared with the mixing ratios. Because signaling data are taken in a time series in this procedure, time-dependent features may also be compared, such as oscillations or other variability over time (see Note 19)

4. Calculate cross-correlation and time lag between cell types. On an average basis, the cell-type-specific responses to a stimulus can be compared, both for how they correlate in

time. This is especially useful in a scenario where a receiver cell type may be responding to the activity of a sender cell type. For this average analysis, it is important to deliver a stimulus that synchronously activates one (or both) cell types. Cross-correlation delivers two values: the maximum correlation between the signals and the lag time between them (e.g., how much later the receiver cells respond, after the sender cells activate).

```
[rho, lag] = xcorr(sender_avg, receiver_avg);
[rhomax, idx_rhomax] = max(rho); %Get maximum correlation
lagmax = lag(idx_rhomax); %Get lag corresponding to maximum
    correlation
```

5. Estimate the dependence of cellular responses on the spatial organization of cells. Knowing the position of each tracked cell in the culture, it is possible to investigate if signaling appears dependent on which other cells are nearby. One approach is to compare each cell's signaling trace with its proximity to other cells of each type. If there is a cell-type-specific interaction, cells surrounded by their own cell type would be expected to respond differently from those surrounded by other cell types. On a per cell basis, estimate the local density of each cell type, for example, as the number of tracked cells of each type within a chosen radius (see Notes 20 and 21).

```
%Calculate average signal for each cell
avg_signal = mean(celldata(:,:,reporter_idx),2);
%Calculate average local density around each cell
cellxy = mean(celldata(:,:,[x_idx, y_idx]),2); %Get average x,
    y location values per cell
for s = 1:size(,1)
cell_dist = sqrt(sum((cellxy(s,:) - cellxy).^2,2)); %Distance
    to each other cell
```

160

```
nearby_cells = cell_dist <= local_radius; %Flag each cell as
    local or not
ldens(s,1) = sum(nearby_cells(iscyan)); %Count local cyan cells
ldens(s,2) = sum(nearby_cells(isyellow)); %Count local yellow
    cells
end
%Correlate signal with local density
[rho, pval] = corr(avg_signal, ldens)
```

6. Extensions to mathematical modeling. The data gathered with this protocol open a wide range of options to inform and extend mathematical modeling studies. While these applications are outside the scope of this protocol, we briefly discuss the potential. A typical scenario would involve a paracrine signaling model, describing the receiver response to a ligand shed by sender cells in the culture, potentially including expression of a downstream gene product. Dynamic signaling models may take a variety of forms, from more generic ARMAX (auto-regressive moving average exogenous) models to detailed ODEs (ordinary differential equations), or even spatial PDEs (partial differential equations). The data gathered via this protocol are applicable to all of these types of models. After formulating or adopting a relevant model, basic parameters may be fitted via dedicated datasets (see Note 22). Remaining parameters can then be fitted to the single-cell dataset(s) and model analyses performed (see Note 23). Single-cell interaction data allow these models to be tested at much higher resolution than was previously feasible.

C.5 Notes

1. Choice of Cell Lines. When choosing cell lines for sender-receiver studies the following must be considered: (1) Properties of the ligand will dictate the suitability of a particular

sender cell line. Consider the disposition of the ligand. Is it secreted or membrane bound? If secreted, does the molecule freely diffuse or is it maintained bound to the local ECM? Such properties will determine the spatial range of ligand activity and will dictate the sender-receiver cell ratios to be determined later in this protocol. If the ligand is membrane bound, it will be important to determine if the ligand is accessible to stimulate receiver cell signaling and if the quantity expressed is capable of promoting detectable changes in signaling. This last consideration is less important for secreted ligands because most are secreted in excess within the microenvironment. Finally, does the ligand, whether membrane bound or secreted, require activation. Some ligands are secreted in an inactive form that requires enzymatic activation. In such cases, if the sender and receiver cells do not express this enzyme, signaling activity may not occur. (2) One must also consider ligand-receptor affinity. For certain high-affinity ligands that stimulate autocrine activation, secreted ligand may bind sender cell receptors, prior to diffusing, leading to weak or no detectable paracrine activity. (3) In choosing a receiver cell, one must consider if the cognate receptor is expressed in the cells. Usually simple confirmation using western blotting to verify receptor expression is sufficient. (4) Confirm that the secreted ligand is not produced by the receiver cell. If the ligand is expressed, one must consider if it is abundant enough to mask the effects of ligand produced by the sender cell. In cases where ligand is expressed at relatively low levels and signaling is weakly activated, one can work around the elevated baseline by adapting the computational methods outlined in this protocol.

2. Choice of Genetically Encoded Reporters. The choice of reporter should be made based on the signaling network of interest and the overall experimental hypothesis. For example, binding of AREG to EGFR results in activation of both Ras-ERK and PI3K-Akt. Since several Akt and ERK reporters exist, either or both can be used depending upon the goals of the experiment. Consideration of FRET-based versus translocation reporters is more nuanced on the technical level and has been discussed elsewhere [14]. However, in general,

translocation reporters are more easily employed, and the same reporter (e.g., ERK-KTR) is available or can be sub-cloned to produce reporters of different colors without effecting function.

3. Image Processing Software. Image processing software for live-cell microscopy is a rapidly evolving industry. At the time of this publication, there are many published implementations and a wide variety of additional techniques under development. Major microscope manufacturers (Nikon, Leica, etc.) and bioscience companies (ThermoFisher, PerkinElmer, etc.) offer image analysis software. Open-source implementations include ImageJ, CellProfiler, BioImageXD, 3D Slicer, Icy, Ilastik, and many others. For those looking to set up a new software pipeline, we recommend performing a search to ensure an up-to-date survey of the field. Include any keywords related to additional complexities of the intended experiments, such as "puncta," "3D," or "mitochondria." As many implementations are now formally distributed, they are accompanied with instructions for installation and use.

4. Considerations for CRISPR Gene Editing. Before proceeding, there are some important considerations that may affect the success of the gene knock-in study. First, we recommend generating knock-in cells prior to adding genetically encoded reporters. This process can be time-consuming, and generation of knock-in lines prior to reporter line generation has added flexibility – allowing for the same lines to be used with many different reporter combinations if desired. Second, we recommend considering the expected expression and dynamics of the POI and what property of protein expression is being studied. Examples of key properties include subcellular translocation, using dynamics of expression (on/off rates), or overall expression. Research prior Western blot, immunofluorescence, or mRNA expression studies to confirm that tagging the gene of interest will reveal useful information. If there is no published work, consider conducting a time course perturbation experiment and measure the expression of the POI via Western blot or immunofluorescence. Third, consider the optimal color of the fluorescent protein (tag) that will be fused to the POI. If

the target cell line will have another reporter integrated, the tag should be spectrally compatible with the reporter. The selected fluorescent protein should be fast folding to ensure the POI expression dynamics remain similar after knock-in. Additionally, the fluorescent protein should have a high quantum yield to allow for a bright signal during live-cell measurements. Furthermore, consider which end (C- or N-terminal) of the POI will be fused to the tag. Some studies suggest the C-terminal fusions are more likely to mimic native localization than N-terminal fusions [35]. In some cases, proteins are cleaved on the C-terminus (e.g., Ras); therefore, N-terminal tagging will be the only option [36]. If available, check the structure of the protein to examine the flanking residues of the POI. If these residues are tucked within the protein, fusing a fluorescent protein to that edge may disrupt proper folding, expression, or localization. In general, C-terminal fusions will be the preferred option; therefore, this protocol will describe a C-terminal tagging attempt. Of note, Koch *et al.* report that about 25% of genes cannot be functionally tagged; therefore, consider pursuing multiple proteins of interest when performing this protocol.

5. Gene Editing Efficiency. It is possible to increase the rate of homology-directed repair to increase knock-in efficiency by using inhibitors of the nonhomologous end joining pathway or activators of HDR [26, 37, 38]. Furthermore, other studies report a minor increase in homozygous insertion using serum starvation and release during the transfection [25].

6. Most fluorescent proteins are about 27 kDa; knock-in cell lines should have protein bands that are heavier than the non-tagged protein. Heterozygous knock-in cells are indicated by two bands (at the native and shifted sizes). Homozygous insertions are indicated by a single band at the shifted size and the absence of the native protein band. Samples should also be probed using a primary antibody specific to the fluorescent protein. Ensure that fluorescent protein-specific band is same size as the shifted POI band. There should not be other bands, which would suggest off-target knock-in events. Use the negative control (non-tagged) cell lines to test for nonspecific bands from the anti-fluorescent protein

antibody.

7. When evaluating PCR product size, heterozygous insertions are indicated by the presence of both the native (non-tagged) size and larger (knock-in) DNA band. The larger band should be about 700 base pairs (length of the fluorescent protein) larger than the native band. Homozygous insertions are indicated by the absence of the native size band and the presence of only the larger band.

8. The choice of fluorescent label(s) for secondary antibodies should be made to allow spectral distinction from the CRISPR-tagged gene(s) and any other reporters expressed in your cell line. Cell fixation and staining can be performed using standard immunofluorescence staining methods.

9. Selection of Reporter Cells. Once reporter cells are generated, a decision has to be made whether clonal or polyclonal populations are more desirable. Generating clonal populations by limited dilution cloning can provide an easy way to generate a population of cells that uniformly express the reporter(s) of interest. If choosing to create clonal populations, one must consider if the cell line is amenable to this process. Some cell lines do not grow well at low densities and may require the addition of conditioned media or half-media changes. Additionally, generating clones will reduce the level of heterogeneity within a cell line and essentially create a derivative cell lineage with altered slightly properties. This is especially true in some cancer cell lines which exhibit high levels of heterogeneity. Our preferred method is flow-based sorting of reporter (+) cell lines. In taking this approach, much of the population-level heterogeneity is preserved, and the vast majority of isolated cells express a moderate level of reporter expression. Since translocation and FRET reporter data is obtained in a ratiometric manner, small fluctuations in reporter expression from cell to cell within these populations does not affect the data interpretation.

10. Extracellular Matrix Choice. The primary goal in choosing a particular ECM for plating is to try and recapitulate the host microenvironment of the cells selected. In our case,

165

we have used collagen I which is abundant in breast cancer stroma or laminin-111 which is a predominant component of normal basement membrane in breast tissue. In our experience, choice of ECM will affect signaling dynamics. For example, we found that laminin results in higher frequency pulsatile EKR dynamics as compared to collagen I in the HMT-3522 cells lines. In designing experiments using this protocol, ECM choice should be made based on considerations of native microenvironment and experimental question.

11. Plating Technique. In our experiments, we prefer to use a "spotting" method as opposed to coating the whole well with ECM and cells. We have found several benefits to the method: (1) The plating area can be more precisely controlled with respect to the placement of cells in the center or the wells as opposed to whole well plating which leads to cell clustering at the edges. (2) Precise cell distribution on the plate results in increased experimental repeatability. This consideration should not be underestimated because it can have a profound impact on plating density variation, formation of a uniform monolayer, and variation from well to well and experiment to experiment and can reduce the need for troubleshooting during data processing, particularly during segmentation steps. (3) Plating a small number of cells relative to the quantity of media present in a well ensures adequate nutrients are provided to the cells for the duration of the experiment. This is an important consideration in longer experiments, such as those lasting ¿48 h, resulting in fewer media changes.

12. Imaging Media. For optimal fluorescent imaging, it is recommended to use imaging media that do not autofluoresence in the spectra of interest. In particular, phenol red, riboflavin, folic acid, and serum often contribute to background fluorescence. Use media lacking for these components to lower background intensity and improve the ability to resolve faint expression. If any of these components are necessary for a cell line of interest, titrate it back into the base imaging media to identify the lowest concentration at which cell behave normally for the duration of the experiment.

13. Baseline Signaling Identification. An important step in reporter line and assay validation is to measure baseline activity of receiver cells. As discussed in Note 1, some receiver cells will have baseline activity of the pathway of interest. This can occur through several mechanisms, including (1) the presence of autocrine signaling in receiver cells resulting from secretion of the same ligand produced by sender cells, but at a relatively low level, and/or (2) activation of alternative pathways that converge on the signaling pathway of interest. For example, ERK can be stimulated by multiple signaling pathways, interactions with the ECM, and cell migration. Baseline signaling can be identified by experiments using a pathway inhibitor. Involvement of particular receptors and ligands can be assayed if suitable inhibitors or competing antibodies are available. When baseline signaling characteristics have been measured, the effects of sender-receiver interactions can be better quantified by comparison with the baseline distribution rather than a theoretical absence of all activity.

14. Regardless of the software platform used, it is advantageous to double-check the quality of the segmentation. Nuclear masks should be consistently within the nucleus, such that average intensities reflect only nuclear pixels. Assume that there will always be some fraction of cells that are not segmented and some rate of poor-quality masks. In many cases, the fraction segmented is not critical, as long as most segmentations are of acceptable quality. However, if the intent is to perform local spatial analyses on a single-cell basis, more complete segmentation is increasingly important, as the analysis relies on knowledge of all nearby cells. It is therefore important to ensure that cultures are free of debris and not overcrowded and that the segmentation marker is distinct.

15. If the different colored markers used to distinguish cell types are fundamentally localized to the nucleus (or cytoplasm), cells of different types may be segmented in two separate processing runs, one for each color marker. Alternatively, the color channels for the two markers may be merged to make a joint segmentation channel. Color channels may be joined in a variety of ways, for example, by summing intensities or using the max of

the two channels per pixel. If the intensities of the two channels differ greatly, they should be normalized so that the resulting joined images are more uniform. The choice of joining function should be made based on contrast in the final image. For example, if debris tend to autofluoresce in both channels, the sum will result in higher debris intensity, and a max projection may be preferred.

16. For cytoplasm sampling from a perinuclear ring, common mask errors can be corrected by avoiding pixels with high values for a nuclear marker, as well as those with background values for a cytoplasmic marker. Depending on the arrangement of colors across two (or more) cell types, these distinctions may or may not be available. Keep in mind that issues with cells overlapping can often be avoided by carefully managing density and plating conditions.

17. In many cases, the clarity of data can be improved via post-processing of signals using calibrations and/or mathematical models of the reporter's function. This is especially true of genetically expressed reporters, as in [39].

18. If the segmentation is relatively poor, the ratio may still be estimated based on the average intensities in the whole frame, provided that neither channel has large amounts of autoflourescent debris. For each channel, estimate the net intensity per cell by taking the sum of all pixels in the masks (or the average intensity per mask times that mask area) and dividing by the number of masks. To estimate the number of each cell type in the frame, divide the sum of the intensity over the entire frame by the intensity per cell.

19. The basic endpoint for effect of density is average signaling level (or gene expression) as a function of the mixing ratio. This endpoint should be considered independently for each cell type; effects on receiver cells reflect their potential to be directly by this paracrine signaling, while effects on sender cells may reflect their reliance of para- or autocrine signaling and how their behavior may change when diluted by different cell types.

20. To be robust to poorer segmentation, estimate local density as a weighted sum of the

intensity of each cell type marker. A typical weighting scheme is a Gaussian function of the distance from the target cell's nucleus. This is equivalent to sampling a Gaussian filtered image.

21. For a more generalized approach considering different features of the signaling response, use a partial least squares regression (PLSR). PLSR allows for simultaneously testing the correlation among many variables (such as the mean, max, and frequency of a signal vs. the local density of two different cell types).

22. Wherever possible, it is recommended to use independent data to determine key parameters (or parameter ranges) in a model. For example, the average decay rate of a protein may be estimated by time series Western blot and that for an mRNA by qPCR. Making these measurements independently allows the main dataset to be used to estimate the more difficult to observe regulatory interactions.

23. Using single-cell data opens opportunities as well as new challenges. From a modeling perspective, we are forced to acknowledge that each individual cell may have a different amount of each protein (receptors, kinases, etc.) and, as a result, different apparent kinetic rates for complex reactions. Therefore, each single-cell trace potentially reflects different parameter values in a model (how different depends on the context of the system). Each cell may also be experiencing a different signaling environment (different amounts of a ligand at any point in time). To make the fullest use of single-cell data, modeling studies should be prepared to estimate different parameter values for each cell. As this can become computationally infeasible with many individual cells, a subset of representative cells may be chosen for explicit modeling (e.g., based on observed clusters in the dataset).

Bibliography

[1] S. Ahmed, K. G. Grant, L. E. Edwards, A. Rahman, M. Cirit, M. B. Goshe, and J. M. Haugh. Data-driven modeling reconciles kinetics of ERK phosphorylation, localization, and activity states. *Mol. Syst. Biol.*, 10:718, Jan. 2014.

[2] T. J. Aikin, A. F. Peterson, M. J. Pokrass, H. R. Clark, and S. Regot. MAPK activity dynamics regulate non-cell autonomous effects of oncogene expression. *Elife*, 9, Sept. 2020.

[3] C. Albanese, J. Johnson, G. Watanabe, N. Eklund, D. Vu, A. Arnold, and R. G. Pestell. Transforming p21ras mutants and c-ets-2 activate the cyclin D1 promoter through distinguishable regions (). *J. Biol. Chem.*, 270(40):23589–23597, Oct. 1995.

[4] J. G. Albeck, G. B. Mills, and J. S. Brugge. Frequency-modulated pulses of ERK activity transmit quantitative proliferation signals. *Mol. Cell*, 49(2):249–261, Jan. 2013.

[5] J. G. Albeck, M. Pargett, and A. E. Davies. Experimental and engineering approaches to intracellular communication. *Essays Biochem.*, 62(4):515–524, Oct. 2018.

[6] B. Alberts, A. Johnson, J. Lewis, D. Morgan, M. Raff, K. Roberts, and P. Walter. *Molecular Biology of the Cell*. Garland Science, Nov. 2014.

[7] G. Altan-Bonnet and R. N. Germain. Modeling T cell antigen discrimination based on feedback control of digital ERK responses. *PLoS Biol.*, 3(11):e356, Nov. 2005.

[8] A. Amaravathi, J. L. Oblinger, D. B. Welling, and others. Neurofibromatosis: molecular pathogenesis and natural compounds as potential treatments. *Frontiers in*, 2021.

[9] I. Amit, A. Citri, T. Shay, Y. Lu, M. Katz, F. Zhang, G. Tarcic, D. Siwak, J. Lahad, J. Jacob-Hirsch, N. Amariglio, N. Vaisman, E. Segal, G. Rechavi, U. Alon, G. B. Mills, E. Domany, and Y. Yarden.

A module of negative feedback regulators defines growth factor signaling. *Nat. Genet.*, 39(4):503–512, Apr. 2007.

[10] S. S. Andrews, W. J. Peria, R. C. Yu, A. Colman-Lerner, and R. Brent. Push-Pull and feedback mechanisms can align signaling system outputs with inputs. *Cell Syst*, 3(5):444–455.e2, Nov. 2016.

[11] Y. E. Antebi, N. Nandagopal, and M. B. Elowitz. An operational view of intercellular signaling pathways. *Curr Opin Syst Biol*, 1:16–24, Feb. 2017.

[12] K. Aoki, Y. Kondo, H. Naoki, T. Hiratsuka, R. E. Itoh, and M. Matsuda. Propagating wave of ERK activation orients collective cell migration. *Dev. Cell*, 43(3):305–317.e5, Nov. 2017.

[13] K. Aoki, Y. Kumagai, A. Sakurai, N. Komatsu, Y. Fujita, C. Shionyu, and M. Matsuda. Stochastic ERK activation induced by noise and cell-to-cell propagation regulates cell density-dependent proliferation. *Mol. Cell*, 52(4):529–540, Nov. 2013.

[14] Y. Arkun and M. Yasemi. Dynamics and control of the ERK signaling pathway: Sensitivity, bistability, and oscillations. *PLoS One*, 13(4):e0195513, Apr. 2018.

[15] Y. Asakura, Y. Kondo, K. Aoki, and H. Naoki. Hierarchical modeling of mechano-chemical dynamics of epithelial sheets across cells and tissue. *Sci. Rep.*, 11(1):4069, Feb. 2021.

[16] M. Barkoulas, J. S. van Zon, J. Milloz, A. van Oudenaarden, and M.-A. Félix. Robustness and epistasis in the c. elegans vulval signaling network revealed by pathway dosage modulation. *Dev. Cell*, 24(1):64–75, Jan. 2013.

[17] A. Beisaw, C. Kuenne, S. Guenther, J. Dallmann, C.-C. Wu, M. Bentsen, M. Looso, and D. Y. R. Stainier. AP-1 contributes to chromatin accessibility to promote sarcomere disassembly and cardiomyocyte protrusion during zebrafish heart regeneration. *Circ. Res.*, 126(12):1760–1778, June 2020.

[18] M. Benary, S. Bohn, M. Lüthen, I. K. Nolis, N. Blüthgen, and A. Loewer. Disentangling pro-mitotic signaling during cell cycle progression using Time-Resolved Single-Cell imaging. *Cell Rep.*, 31(2):107514, Apr. 2020.

[19] G. Bertolin, F. Sizaire, C. Déméautis, C. Chapuis, F. Mérola, M. Erard, and M. Tramier. Optimized FRET pairs and quantification approaches to detect the activation of aurora kinase a at mitosis. *ACS Sens*, 4(8):2018–2027, Aug. 2019.

[20] U. S. Bhalla and R. Iyengar. Emergent properties of networks of biological signaling pathways. *Science*, 283(5400):381–387, Jan. 1999.

[21] Y. Blum, R. D. Fritz, H. Ryu, and O. Pertz. Measuring ERK activity dynamics in single living cells using FRET biosensors. *Methods Mol. Biol.*, 1487:203–221, 2017.

[22] G. Bollag, P. Hirth, J. Tsai, J. Zhang, P. N. Ibrahim, H. Cho, W. Spevak, C. Zhang, Y. Zhang, G. Habets, E. A. Burton, B. Wong, G. Tsang, B. L. West, B. Powell, R. Shellooe, A. Marimuthu, H. Nguyen, K. Y. J. Zhang, D. R. Artis, J. Schlessinger, F. Su, B. Higgins, R. Iyer, K. D'Andrea, A. Koehler, M. Stumm, P. S. Lin, R. J. Lee, J. Grippo, I. Puzanov, K. B. Kim, A. Ribas, G. A. McArthur, J. A. Sosman, P. B. Chapman, K. T. Flaherty, X. Xu, K. L. Nathanson, and K. Nolop. Clinical efficacy of a RAF inhibitor needs broad target blockade in BRAF-mutant melanoma. *Nature*, 467(7315):596–599, Sept. 2010.

[23] D. Boocock, N. Hino, N. Ruzickova, T. Hirashima, and E. Hannezo. Theory of mechanochemical patterning and optimal migration in cell monolayers. *Nat. Phys.*, 17(2):267–274, Sept. 2020.

[24] R. Böttcher, M. Hollmann, K. Merk, V. Nitschko, C. Obermaier, J. Philippou-Massier, I. Wieland, U. Gaul, and K. Förstemann. Efficient chromosomal gene modification with CRISPR/cas9 and PCR-based homologous recombination donors in cultured drosophila cells. *Nucleic Acids Res.*, 42(11):e89, June 2014.

[25] R. Brandt, T. Sell, M. Lüthen, F. Uhlitz, B. Klinger, P. Riemer, C. Giesecke-Thiel, S. Schulze, I. A. El-Shimy, D. Kunkel, B. Fauler, T. Mielke, N. Mages, B. G. Herrmann, C. Sers, N. Blüthgen, and M. Morkel. Cell type-dependent differential activation of ERK by oncogenic KRAS in colon cancer and intestinal epithelium. *Nat. Commun.*, 10(1):2919, July 2019.

[26] M.-A. Bray and A. E. Carpenter. CellProfiler tracer: exploring and validating high-throughput, time-lapse microscopy image data. *BMC Bioinformatics*, 16:368, Nov. 2015.

[27] P. Briand, O. W. Petersen, and B. Van Deurs. A new diploid nontumorigenic human breast epithelial cell line isolated and propagated in chemically defined medium. *In Vitro Cell. Dev. Biol.*, 23(3):181–188, Mar. 1987.

[28] F. A. Brightman and D. A. Fell. Differential feedback regulation of the MAPK cascade underlies the quantitative differences in EGF and NGF signalling in PC12 cells. *FEBS Lett.*, 482(3):169–174, Oct. 2000.

[29] T. Brummer, H. Naegele, M. Reth, and Y. Misawa. Identification of novel ERK-mediated feedback phosphorylation sites at the c-terminus of B-Raf. *Oncogene*, 22(55):8823–8834, Dec. 2003.

[30] A. Brunet, D. Roux, P. Lenormand, S. Dowd, S. Keyse, and J. Pouysségur. Nuclear translocation of p42/p44 mitogen-activated protein kinase is required for growth factor-induced gene expression and cell cycle entry. *EMBO J.*, 18(3):664–674, Feb. 1999.

[31] L. J. Bugaj, A. J. Sabnis, A. Mitchell, J. E. Garbarino, J. E. Toettcher, T. G. Bivona, and W. A. Lim. Cancer mutations and targeted drugs can disrupt dynamic signal encoding by the Ras-Erk pathway. *Science*, 361(6405), Aug. 2018.

[32] P. Burke, K. Schooler, and H. S. Wiley. Regulation of epidermal growth factor receptor signaling by endocytosis and intracellular trafficking. *Mol. Biol. Cell*, 12(6):1897–1910, June 2001.

[33] K. A. Burkhard, F. Chen, and P. Shapiro. Quantitative analysis of ERK2 interactions with substrate proteins: roles for kinase docking domains and activity in determining binding affinity. *J. Biol. Chem.*, 286(4):2477–2485, Jan. 2011.

[34] S. Cagnol and J.-C. Chambard. ERK and cell death: mechanisms of ERK-induced cell death–apoptosis, autophagy and senescence. *FEBS J.*, 277(1):2–21, Jan. 2010.

[35] S. Cagnol, E. Van Obberghen-Schilling, and J.-C. Chambard. Prolonged activation of ERK1,2 induces FADD-independent caspase 8 activation and cell death. *Apoptosis*, 11(3):337–346, Mar. 2006.

[36] X. Cao, R. Mahendran, G. R. Guy, and Y. H. Tan. Detection and characterization of cellular EGR-1 binding to its recognition site. *J. Biol. Chem.*, 268(23):16949–16957, Aug. 1993.

[37] F. Catalanotti, G. Reyes, V. Jesenberger, G. Galabova-Kovacs, R. de Matos Simoes, O. Carugo, and M. Baccarini. A Mek1–Mek2 heterodimer determines the strength and duration of the erk signal. *Nat. Struct. Mol. Biol.*, 16(3):294–303, Feb. 2009.

[38] S. Chavez-Abiega, M. L. B. Grönloh, T. W. J. Gadella, F. J. Bruggeman, and J. Goedhart. Single-cell imaging of ERK and akt activation dynamics and heterogeneity induced by g-protein-coupled receptors. *J. Cell Sci.*, 135(6), Mar. 2022.

[39] J.-Y. Chen, C. Hug, J. Reyes, C. Tian, L. Gerosa, F. Fröhlich, B. Ponsioen, H. J. G. Snippert, S. L. Spencer, A. Jambhekar, P. K. Sorger, and G. Lahav. Multi-range ERK responses shape the proliferative trajectory of single cells following oncogene induction. *Cell Rep.*, 42(3):112252, Mar. 2023.

[40] J.-Y. Chen, J.-R. Lin, K. A. Cimprich, and T. Meyer. A two-dimensional ERK-AKT signaling code for an NGF-triggered cell-fate decision. *Mol. Cell*, 45(2):196–209, Jan. 2012.

[41] W. W. Chen, B. Schoeberl, P. J. Jasper, M. Niepel, U. B. Nielsen, D. A. Lauffenburger, and P. K. Sorger. Input-output behavior of ErbB signaling pathways as revealed by a mass action model trained against dynamic data. *Mol. Syst. Biol.*, 5:239, Jan. 2009.

[42] X. Chen, J. L. Zaro, and W.-C. Shen. Fusion protein linkers: property, design and functionality. *Adv. Drug Deliv. Rev.*, 65(10):1357–1369, Oct. 2013.

[43] R. Cheong, A. Rhee, C. J. Wang, I. Nemenman, and A. Levchenko. Information transduction capacity of noisy biochemical signaling networks. *Science*, 334(6054):354–358, Oct. 2011.

[44] T.-W. W. Chiang, C. le Sage, D. Larrieu, M. Demir, and S. P. Jackson. CRISPR-Cas9D10A nickase-based genotypic and phenotypic screening to enhance genome editing. *Sci. Rep.*, 6(1):24356, Apr. 2016.

[45] R. Choudhury, S. G. Roy, Y. S. Tsai, A. Tripathy, L. M. Graves, and Z. Wang. The splicing activator DAZAP1 integrates splicing control into MEK/Erk-regulated cell proliferation and migration. *Nat. Commun.*, 5:3078, 2014.

[46] L. Ciarloni, S. Mallepell, and C. Brisken. Amphiregulin is an essential mediator of estrogen receptor α function in mammary gland development. *Proceedings of the National Academy of Sciences*, 104(13):5455–5460, 2007.

[47] M. Cirit, C.-C. Wang, and J. M. Haugh. Systematic quantification of negative feedback mechanisms in the extracellular signal-regulated kinase (ERK) signaling network. *J. Biol. Chem.*, 285(47):36736–36744, Nov. 2010.

[48] N. Comandante-Lou, D. G. Baumann, and M. Fallahi-Sichani. AP-1 transcription factor network explains diverse patterns of cellular plasticity in melanoma cells. *Cell Rep.*, 40(5):111147, Aug. 2022.

[49] S. J. Cook, N. Aziz, and M. McMahon. The repertoire of fos and jun proteins expressed during the G1 phase of the cell cycle is determined by the duration of mitogen-activated protein kinase activation. *Mol. Cell. Biol.*, 19(1):330–341, Jan. 1999.

[50] S. Corbalan-Garcia, S. S. Yang, K. R. Degenhardt, and D. Bar-Sagi. Identification of the mitogen-activated protein kinase phosphorylation sites on human sos1 that regulate interaction with grb2. *Mol. Cell. Biol.*, 16(10):5674–5682, Oct. 1996.

[51] S. Cowley, H. Paterson, P. Kemp, and C. J. Marshall. Activation of MAP kinase kinase is necessary and sufficient for PC12 differentiation and for transformation of NIH 3T3 cells. *Cell*, 77(6):841–852, June 1994.

[52] A. Craxton, K. E. Draves, A. Gruppi, and E. A. Clark. BAFF regulates B cell survival by downregulating the BH3-only family member bim via the ERK pathway. *J. Exp. Med.*, 202(10):1363–1374, Nov. 2005.

[53] J. Das, M. Ho, J. Zikherman, C. Govern, M. Yang, A. Weiss, A. K. Chakraborty, and J. P. Roose. Digital signaling and hysteresis characterize ras activation in lymphoid cells. *Cell*, 136(2):337–351, Jan. 2009.

[54] A. E. Davies and J. G. Albeck. Microenvironmental signals and biochemical information processing: Cooperative determinants of intratumoral plasticity and heterogeneity. *Front Cell Dev Biol*, 6:44, Apr. 2018.

[55] A. E. Davies, M. Pargett, S. Siebert, T. E. Gillies, Y. Choi, S. J. Tobin, A. R. Ram, V. Murthy, C. Juliano, G. Quon, M. J. Bissell, and J. G. Albeck. Systems-Level properties of EGFR-RAS-ERK signaling amplify local signals to generate dynamic gene expression heterogeneity. *Cell Syst*, 11(2):161–175.e5, Aug. 2020.

[56] C. de la Cova, R. Townley, S. Regot, and I. Greenwald. A Real-Time biosensor for ERK activity reveals signaling dynamics during c. elegans cell fate specification. *Dev. Cell*, 0(0), Aug. 2017.

[57] A. De Simone, M. N. Evanitsky, L. Hayden, B. D. Cox, J. Wang, V. A. Tornini, J. Ou, A. Chao, K. D. Poss, and S. Di Talia. Control of osteoblast regeneration by a train of erk activity waves. *Nature*, 590(7844):129–133, Feb. 2021.

[58] J. Deathridge, V. Antolović, M. Parsons, and J. R. Chubb. Live imaging of ERK signalling dynamics in differentiating mouse embryonic stem cells. *Development*, 146(12), June 2019.

[59] J. Debnath and J. S. Brugge. Modelling glandular epithelial cancers in three-dimensional cultures. *Nat. Rev. Cancer*, 5(9):675–688, Sept. 2005.

[60] B. Dérijard, M. Hibi, I. H. Wu, T. Barrett, B. Su, T. Deng, M. Karin, and R. J. Davis. JNK1: a protein kinase stimulated by UV light and Ha-Ras that binds and phosphorylates the c-jun activation domain. *Cell*, 76(6):1025–1037, Mar. 1994.

[61] X. Deschênes-Simard, M.-F. Gaumont-Leclerc, V. Bourdeau, F. Lessard, O. Moiseeva, V. Forest, S. Igelmann, F. A. Mallette, M. K. Saba-El-Leil, S. Meloche, F. Saad, A.-M. Mes-Masson, and G. Ferbeyre. Tumor suppressor activity of the ERK/MAPK pathway by promoting selective protein degradation, 2013.

[62] C. Dessauges, J. Mikelson, M. Dobrzyński, M. Jacques, A. Frismantiene, P. A. Gagliardi, M. Khammash, and O. Pertz. Optogenetic actuator – ERK biosensor circuits identify MAPK network nodes that shape ERK dynamics, 2022.

[63] C. Dessauges, J. Mikelson, M. Dobrzyński, M.-A. Jacques, A. Frismantiene, P. A. Gagliardi, M. Khammash, and O. Pertz. Optogenetic actuator/biosensor circuits for large-scale interrogation of ERK dynamics identify sources of MAPK signaling robustness. July 2021.

[64] C. Dessauges, J. Mikelson, M. Dobrzyński, M.-A. Jacques, A. Frismantiene, P. A. Gagliardi, M. Khammash, and O. Pertz. Optogenetic actuator - ERK biosensor circuits identify MAPK network nodes that shape ERK dynamics. *Mol. Syst. Biol.*, 18(6):e10670, June 2022.

[65] C. Dessauges and O. Pertz. Developmental ERK signaling goes digital. *Dev. Cell*, 42(5):443–444, Sept. 2017.

[66] A. DeWitt, T. Iida, H.-Y. Lam, V. Hill, H. S. Wiley, and D. A. Lauffenburger. Affinity regulates spatial range of EGF receptor autocrine ligand binding. *Dev. Biol.*, 250(2):305–316, Oct. 2002.

[67] A. S. Dhillon and E. Tulchinsky. FRA-1 as a driver of tumour heterogeneity: a nexus between oncogenes and embryonic signalling pathways in cancer. *Oncogene*, 34(34):4421–4428, Aug. 2015.

[68] Y. Ding, J. Li, J. R. Enterina, Y. Shen, I. Zhang, P. H. Tewson, G. C. H. Mo, J. Zhang, A. M. Quinn, T. E. Hughes, D. Maysinger, S. C. Alford, Y. Zhang, and R. E. Campbell. Ratiometric biosensors based on dimerization-dependent fluorescent protein exchange. *Nat. Methods*, 12(3):195–198, Mar. 2015.

[69] R. E. Dolmetsch, R. S. Lewis, C. C. Goodnow, and J. I. Healy. Differential activation of transcription factors induced by ca2+ response amplitude and duration. *Nature*, 386(6627):855–858, Apr. 1997.

[70] M. K. Dougherty, J. Müller, D. A. Ritt, M. Zhou, X. Z. Zhou, T. D. Copeland, T. P. Conrads, T. D. Veenstra, K. P. Lu, and D. K. Morrison. Regulation of raf-1 by direct feedback phosphorylation. *Mol. Cell*, 17(2):215–224, Jan. 2005.

[71] M. Ebisuya, K. Kondoh, and E. Nishida. The duration, magnitude and compartmentalization of ERK MAP kinase activity: mechanisms for providing signaling specificity. *J. Cell Sci.*, 118(Pt 14):2997–3002, July 2005.

[72] R. Eferl and E. F. Wagner. AP-1: a double-edged sword in tumorigenesis. *Nat. Rev. Cancer*, 3(11):859–868, Nov. 2003.

[73] M. B. Elowitz, A. J. Levine, E. D. Siggia, and P. S. Swain. Stochastic gene expression in a single cell. *Science*, 297(5584):1183–1186, Aug. 2002.

[74] P. Ender, P. A. Gagliardi, M. Dobrzyński, A. Frismantiene, C. Dessauges, T. Höhener, M.-A. Jacques, A. R. Cohen, and O. Pertz. Spatio-temporal control of ERK pulse frequency coordinates fate decisions during mammary acinar morphogenesis. June 2022.

[75] P. Ender, P. A. Gagliardi, M. Dobrzyński, A. Frismantiene, C. Dessauges, T. Höhener, M.-A. Jacques, A. R. Cohen, and O. Pertz. Spatiotemporal control of ERK pulse frequency coordinates fate decisions during mammary acinar morphogenesis. *Dev. Cell*, 57(18):2153–2167.e6, Sept. 2022.

[76] M. Eriksson, M. Taskinen, and S. Leppä. Mitogen activated protein kinase-dependent activation of c-jun and c-fos is required for neuronal differentiation but not for growth and stress response in PC12 cells. *J. Cell. Physiol.*, 210(2):538–548, Feb. 2007.

[77] L. F. Escobar-Hoyos, A. Penson, R. Kannan, H. Cho, C.-H. Pan, R. K. Singh, L. H. Apken, G. A. Hobbs, R. Luo, N. Lecomte, S. Babu, F. C. Pan, D. Alonso-Curbelo, J. P. Morris, 4th, G. Askan, O. Grbovic-Huezo, P. Ogrodowski, J. Bermeo, J. Saglimbeni, C. D. Cruz, Y.-J. Ho, S. A. Lawrence, J. P. Melchor, G. A. Goda, K. Bai, A. Pastore, S. J. Hogg, S. Raghavan, P. Bailey, D. K. Chang, A. Biankin, K. R. Shroyer, B. M. Wolpin, A. J. Aguirre, A. Ventura, B. Taylor, C. J. Der, D. Dominguez, D. Kümmel, A. Oeckinghaus, S. W. Lowe, R. K. Bradley, O. Abdel-Wahab, and S. D. Leach. Altered RNA splicing by mutant p53 activates oncogenic RAS signaling in pancreatic cancer. *Cancer Cell*, 38(2):198–211.e8, Aug. 2020.

[78] H. Escuin-Ordinas, S. Li, M. W. Xie, L. Sun, W. Hugo, R. R. Huang, J. Jiao, F. M. de Faria, S. Realegeno, P. Krystofinski, A. Azhdam, S. M. D. Komenan, M. Atefi, B. Comin-Anduix, M. Pellegrini, A. J. Cochran, R. L. Modlin, H. R. Herschman, R. S. Lo, W. H. McBride, T. Segura, and A. Ribas. Cutaneous wound healing through paradoxical MAPK activation by BRAF inhibitors. *Nat. Commun.*, 7:12348, Aug. 2016.

[79] T. Evans, E. T. Rosenthal, J. Youngblom, D. Distel, and T. Hunt. Cyclin: a protein specified by maternal mRNA in sea urchin eggs that is destroyed at each cleavage division. *Cell*, 33(2):389–396, June 1983.

[80] Y. Fan and T. Meyer. Molecular control of cell density-mediated exit to quiescence. *Cell Rep.*, 36(4):109436, July 2021.

[81] P. E. Farahani, S. B. Lemke, E. Dine, G. Uribe, J. E. Toettcher, and C. M. Nelson. Substratum stiffness regulates erk signaling dynamics through receptor-level control. *Cell Rep.*, 37(13):110181, Dec. 2021.

[82] P. Ferrara, E. Andermarcher, G. Bossis, C. Acquaviva, F. Brockly, I. Jariel-Encontre, and M. Piechaczyk. The structural determinants responsible for c-fos protein proteasomal degradation differ according to the conditions of expression. *Oncogene*, 22(10):1461–1474, Mar. 2003.

[83] J. E. Ferrell, Jr. Building a cellular switch: more lessons from a good egg. *Bioessays*, 21(10):866–870, Oct. 1999.

[84] J. E. Ferrell, Jr and S. H. Ha. Ultrasensitivity part III: cascades, bistable switches, and oscillators. *Trends Biochem. Sci.*, 39(12):612–618, Dec. 2014.

[85] J. E. Ferrell, Jr and E. M. Machleder. The biochemical basis of an all-or-none cell fate switch in xenopus oocytes. *Science*, 280(5365):895–898, May 1998.

[86] S. Filippi, C. P. Barnes, P. D. W. Kirk, T. Kudo, K. Kunida, S. S. McMahon, T. Tsuchiya, T. Wada, S. Kuroda, and M. P. H. Stumpf. Robustness of MEK-ERK dynamics and origins of Cell-to-Cell variability in MAPK signaling. *Cell Rep.*, 15(11):2524–2535, June 2016.

[87] K. T. Flaherty, I. Puzanov, K. B. Kim, A. Ribas, G. A. McArthur, J. A. Sosman, P. J. O'Dwyer, R. J. Lee, J. F. Grippo, K. Nolop, and P. B. Chapman. Inhibition of mutated, activated BRAF in metastatic melanoma. *N. Engl. J. Med.*, 363(9):809–819, Aug. 2010.

[88] R. Foreman and R. Wollman. Mammalian gene expression variability is explained by underlying cell state. *Mol. Syst. Biol.*, 16(2):e9146, Feb. 2020.

[89] E. Formstecher, J. W. Ramos, M. Fauquet, D. A. Calderwood, J. C. Hsieh, B. Canton, X. T. Nguyen, J. V. Barnier, J. Camonis, M. H. Ginsberg, and H. Chneiweiss. PEA-15 mediates cytoplasmic sequestration of ERK MAP kinase. *Dev. Cell*, 1(2):239–250, Aug. 2001.

[90] D. M. Freed, N. J. Bessman, A. Kiyatkin, E. Salazar-Cavazos, P. O. Byrne, J. O. Moore, C. C. Valley, K. M. Ferguson, D. J. Leahy, D. S. Lidke, and M. A. Lemmon. EGFR ligands differentially stabilize receptor dimers to specify signaling kinetics. *Cell*, 171(3):683–695.e18, Oct. 2017.

[91] R. Fritsche-Guenther, F. Witzel, A. Sieber, R. Herr, N. Schmidt, S. Braun, T. Brummer, C. Sers, and N. Blüthgen. Strong negative feedback from erk to raf confers robustness to MAPK signalling. *Mol. Syst. Biol.*, 7:489, May 2011.

[92] R. D. Fritz, M. Letzelter, A. Reimann, K. Martin, L. Fusco, L. Ritsma, B. Ponsioen, E. Fluri, S. Schulte-Merker, J. van Rheenen, and O. Pertz. A versatile toolkit to produce sensitive FRET biosensors to visualize signaling in time and space. *Sci. Signal.*, 6(285):rs12, July 2013.

[93] B. D. Fulcher and N. S. Jones. hctsa: A computational framework for automated Time-Series phenotyping using massive feature extraction. *Cell Syst*, 5(5):527–531.e3, Nov. 2017.

[94] L. Gabay, R. Seger, and B. Z. Shilo. In situ activation pattern of drosophila EGF receptor pathway during development. *Science*, 277(5329):1103–1106, Aug. 1997.

[95] P. A. Gagliardi, M. Dobrzyński, M.-A. Jacques, C. Dessauges, P. Ender, Y. Blum, R. M. Hughes, A. R. Cohen, and O. Pertz. Collective ERK/Akt activity waves orchestrate epithelial homeostasis by driving apoptosis-induced survival. *Dev. Cell*, May 2021.

[96] L. Gerosa, C. Chidley, F. Fröhlich, G. Sanchez, S. K. Lim, J. Muhlich, J.-Y. Chen, S. Vallabhaneni, G. J. Baker, D. Schapiro, M. I. Atanasova, L. A. Chylek, T. Shi, L. Yi, C. D. Nicora, A. Claas, T. S. C. Ng, R. H. Kohler, D. A. Lauffenburger, R. Weissleder, M. A. Miller, W.-J. Qian, H. S. Wiley, and P. K. Sorger. Receptor-Driven ERK pulses reconfigure MAPK signaling and enable persistence of Drug-Adapted BRAF-Mutant melanoma cells. *Cell Syst*, 11(5):478–494.e9, Nov. 2020.

[97] N. Geva-Zatorsky, E. Dekel, E. Batchelor, G. Lahav, and U. Alon. Fourier analysis and systems identification of the p53 feedback loop. *Proc. Natl. Acad. Sci. U. S. A.*, 107(30):13550–13555, July 2010.

[98] T. E. Gillies, M. Pargett, M. Minguet, A. E. Davies, and J. G. Albeck. Linear integration of ERK activity predominates over persistence detection in fra-1 regulation. *Cell Syst*, Nov. 2017.

[99] T. E. Gillies, M. Pargett, J. M. Silva, C. K. Teragawa, F. McCormick, and J. G. Albeck. Oncogenic mutant RAS signaling activity is rescaled by the ERK/MAPK pathway. *Mol. Syst. Biol.*, 16(10):e9518, Oct. 2020.

[100] C. Giorgi, A. Danese, S. Missiroli, S. Patergnani, and P. Pinton. Calcium dynamics as a machine for decoding signals. *Trends Cell Biol.*, 28(4):258–273, Apr. 2018.

[101] A. G. Goglia, M. Z. Wilson, S. G. Jena, J. Silbert, L. P. Basta, D. Devenport, and J. E. Toettcher. A Live-Cell screen for altered erk dynamics reveals principles of proliferative control. *Cell Syst*, 10(3):240–253.e6, Mar. 2020.

[102] T. Gomard, I. Jariel-Encontre, J. Basbous, G. Bossis, G. Moquet-Torcy, and M. Piechaczyk. Fos family protein degradation by the proteasome. *Biochem. Soc. Trans.*, 36(Pt 5):858–863, Oct. 2008.

[103] Y. Gotoh, E. Nishida, T. Yamashita, M. Hoshi, M. Kawakami, and H. Sakai. Microtubule-associated-protein (MAP) kinase activated by nerve growth factor and epidermal growth factor in PC12 cells. identity with the mitogen-activated MAP kinase of fibroblastic cells. *Eur. J. Biochem.*, 193(3):661–669, Nov. 1990.

[104] Y. Goyal, G. A. Jindal, J. L. Pelliccia, K. Yamaya, E. Yeung, A. S. Futran, R. D. Burdine, T. Schüpbach, and S. Y. Shvartsman. Divergent effects of intrinsically active MEK variants on developmental ras signaling. *Nat. Genet.*, 49(3):465–469, Mar. 2017.

[105] H. M. Green and J. Alberola-Ila. Development of ERK activity sensor, an in vitro, FRET-based sensor of extracellular regulated kinase activity. *BMC Chem. Biol.*, 5:1, July 2005.

[106] O. Grimm, V. Sanchez Zini, Y. Kim, J. Casanova, S. Y. Shvartsman, and E. Wieschaus. Torso RTK controls capicua degradation by changing its subcellular localization. *Development*, 139(21):3962–3968, Nov. 2012.

[107] A. M. Gross, E. Dombi, and B. C. Widemann. Current status of MEK inhibitors in the treatment of plexiform neurofibromas. *Childs. Nerv. Syst.*, 36(10):2443–2452, Oct. 2020.

[108] A. M. Gross, P. L. Wolters, E. Dombi, A. Baldwin, P. Whitcomb, M. J. Fisher, B. Weiss, A. Kim, M. Bornhorst, A. C. Shah, S. Martin, M. C. Roderick, D. C. Pichard, A. Carbonell, S. M. Paul, J. Therrien, O. Kapustina, K. Heisey, D. W. Clapp, C. Zhang, C. J. Peer, W. D. Figg, M. Smith, J. Glod, J. O. Blakeley, S. M. Steinberg, D. J. Venzon, L. A. Doyle, and B. C. Widemann. Selumetinib in children with inoperable plexiform neurofibromas. *N. Engl. J. Med.*, 382(15):1430–1442, Apr. 2020.

[109] J. Gureasko, W. J. Galush, S. Boykevisch, H. Sondermann, D. Bar-Sagi, J. T. Groves, and J. Kuriyan. Membrane-dependent signal integration by the ras activator son of sevenless. *Nat. Struct. Mol. Biol.*, 15(5):452–461, May 2008.

[110] G. Gut, M. D. Herrmann, and L. Pelkmans. Multiplexed protein maps link subcellular organization to cellular states. *Science*, 361(6401), Aug. 2018.

[111] A. Hafner, J. Stewart-Ornstein, J. E. Purvis, W. C. Forrester, M. L. Bulyk, and G. Lahav. p53 pulses lead to distinct patterns of gene expression albeit similar DNA-binding dynamics. *Nat. Struct. Mol. Biol.*, 24(10):840–847, Oct. 2017.

[112] W. B. Hamilton and J. M. Brickman. Erk signaling suppresses embryonic stem cell self-renewal to specify endoderm. *Cell Rep.*, 9(6):2056–2070, Dec. 2014.

[113] W. B. Hamilton, Y. Mosesson, R. S. Monteiro, K. B. Emdal, T. E. Knudsen, C. Francavilla, N. Barkai, J. V. Olsen, and J. M. Brickman. Dynamic lineage priming is driven via direct enhancer regulation by ERK. *Nature*, Nov. 2019.

[114] H. Hanafusa, S. Torii, T. Yasunaga, and E. Nishida. Sprouty1 and sprouty2 provide a control mechanism for the Ras/MAPK signalling pathway. *Nat. Cell Biol.*, 4(11):850–858, Nov. 2002.

[115] A. S. Hansen, N. Hao, and E. K. O'Shea. High-throughput microfluidics to control and measure signaling dynamics in single yeast cells. *Nat. Protoc.*, 10(8):1181–1197, Aug. 2015.

[116] A. S. Hansen and E. K. O'Shea. Promoter decoding of transcription factor dynamics involves a trade-off between noise and control of gene expression. *Mol. Syst. Biol.*, 9:704, Nov. 2013.

[117] A. S. Hansen and E. K. O'Shea. Limits on information transduction through amplitude and frequency regulation of transcription factor activity. *Elife*, 4, May 2015.

[118] A. S. Hansen and E. K. O'Shea. Encoding four gene expression programs in the activation dynamics of a single transcription factor. *Curr. Biol.*, 26(7):R269–71, Apr. 2016.

[119] C. D. Harvey, A. G. Ehrhardt, C. Cellurale, H. Zhong, R. Yasuda, R. J. Davis, and K. Svoboda. A genetically encoded fluorescent sensor of ERK activity. *Proc. Natl. Acad. Sci. U. S. A.*, 105(49):19264–19269, Dec. 2008.

[120] B. S. Hendriks, G. Orr, A. Wells, H. S. Wiley, and D. A. Lauffenburger. Parsing ERK activation reveals quantitatively equivalent contributions from epidermal growth factor receptor and HER2 in human mammary epithelial cells. *J. Biol. Chem.*, 280(7):6157–6169, Feb. 2005.

[121] K. Hettinger, F. Vikhanskaya, M. K. Poh, M. K. Lee, I. de Belle, J.-T. Zhang, S. A. G. Reddy, and K. Sabapathy. c-jun promotes cellular survival by suppression of PTEN. *Cell Death Differ.*, 14(2):218–229, Feb. 2007.

[122] N. Hino, L. Rossetti, A. Marín-Llauradó, K. Aoki, X. Trepat, M. Matsuda, and T. Hirashima. ERK-Mediated mechanochemical waves direct collective cell polarization. *Dev. Cell*, 53(6):646–660.e8, June 2020.

[123] T. Hirashima. Live imaging approach of dynamic multicellular responses in ERK signaling during vertebrate tissue development. *Biochem. J*, 479(2):129–143, Jan. 2022.

[124] E. Hirata, M. R. Girotti, A. Viros, S. Hooper, B. Spencer-Dene, M. Matsuda, J. Larkin, R. Marais, and E. Sahai. Intravital imaging reveals how BRAF inhibition generates drug-tolerant microenvironments with high integrin $\beta 1$/FAK signaling. *Cancer Cell*, 27(4):574–588, Apr. 2015.

[125] T. Hiratsuka, I. Bordeu, G. Pruessner, and F. M. Watt. Regulation of ERK basal and pulsatile activity control proliferation and exit from the stem cell compartment in mammalian epidermis. *Proc. Natl. Acad. Sci. U. S. A.*, 117(30):17796–17807, July 2020.

[126] T. Hiratsuka, Y. Fujita, H. Naoki, K. Aoki, Y. Kamioka, and M. Matsuda. Intercellular propagation of extracellular signal-regulated kinase activation revealed by in vivo imaging of mouse skin. *Elife*, 4:e05178, Feb. 2015.

[127] A. Hoffmann, A. Levchenko, M. L. Scott, and D. Baltimore. The IkappaB-NF-kappaB signaling module: temporal control and selective gene activation. *Science*, 298(5596):1241–1245, Nov. 2002.

[128] C.-H. Hsu, S. J. Altschuler, and L. F. Wu. Patterns of early p21 dynamics determine Proliferation-Senescence cell fate after chemotherapy. *Cell*, 178(2):361–373.e12, July 2019.

[129] C. Hu, C. A. Leche, 2nd, A. Kiyatkin, Z. Yu, S. E. Stayrook, K. M. Ferguson, and M. A. Lemmon. Glioblastoma mutations alter EGFR dimer structure to prevent ligand bias. *Nature*, 602(7897):518–522, Feb. 2022.

[130] C.-H. Huang, M. Tang, C. Shi, P. A. Iglesias, and P. N. Devreotes. An excitable signal integrator couples to an idling cytoskeletal oscillator to drive cell migration. *Nat. Cell Biol.*, 15(11):1307–1316, Nov. 2013.

[131] C. Y. Huang and J. E. Ferrell, Jr. Ultrasensitivity in the mitogen-activated protein kinase cascade. *Proc. Natl. Acad. Sci. U. S. A.*, 93(19):10078–10083, Sept. 1996.

[132] M. Humar, T. Loop, R. Schmidt, A. Hoetzel, M. Roesslein, N. Andriopoulos, H. L. Pahl, K. K. Geiger, and B. H. J. Pannen. The mitogen-activated protein kinase p38 regulates activator protein 1 by direct phosphorylation of c-jun. *Int. J. Biochem. Cell Biol.*, 39(12):2278–2288, July 2007.

[133] J. L. Inman, C. Robertson, J. D. Mott, and M. J. Bissell. Mammary gland development: cell fate specification, stem cells and the microenvironment. *Development*, 142(6):1028–1042, Mar. 2015.

[134] M. Ishii, T. Tateya, M. Matsuda, and T. Hirashima. Retrograde ERK activation waves drive base-to-apex multicellular flow in murine cochlear duct morphogenesis. *Elife*, 10, Mar. 2021.

[135] M.-A. Jacques, M. Dobrzyński, P. A. Gagliardi, R. Sznitman, and O. Pertz. CODEX, a neural network approach to explore signaling dynamics landscapes. *Mol. Syst. Biol.*, 17(4):e10026, Apr. 2021.

[136] E. Janda, K. Lehmann, I. Killisch, M. Jechlinger, M. Herzig, J. Downward, H. Beug, and S. Grünert. Ras and TGFβ cooperatively regulate epithelial cell plasticity and metastasis dissection of ras signaling pathways. *J. Cell Biol.*, 156(2):299–314, Jan. 2002.

[137] K. A. Janes, J. G. Albeck, S. Gaudet, P. K. Sorger, D. A. Lauffenburger, and M. B. Yaffe. A systems model of signaling identifies a molecular basis set for cytokine-induced apoptosis. *Science*, 310(5754):1646–1653, Dec. 2005.

[138] K. A. Janes, H. C. Reinhardt, and M. B. Yaffe. Cytokine-induced signaling networks prioritize dynamic range over signal strength. *Cell*, 135(2):343–354, Oct. 2008.

[139] K. A. Janes, C.-C. Wang, K. J. Holmberg, K. Cabral, and J. S. Brugge. Identifying single-cell molecular programs by stochastic profiling. *Nat. Methods*, 7(4):311–317, Apr. 2010.

[140] K. Jaqaman, D. Loerke, M. Mettlen, H. Kuwata, S. Grinstein, S. L. Schmid, and G. Danuser. Robust single-particle tracking in live-cell time-lapse sequences. *Nat. Methods*, 5(8):695–702, July 2008.

[141] S. G. Jena, C. Yu, and J. E. Toettcher. Dynamics and heterogeneity of erk-induced immediate-early gene expression. Apr. 2021.

[142] K.-S. Jeng, S.-J. Lu, C.-H. Wang, and C.-F. Chang. Liver fibrosis and inflammation under the control of ERK2. *Int. J. Mol. Sci.*, 21(11), May 2020.

[143] G. A. Jindal, Y. Goyal, K. Yamaya, A. S. Futran, I. Kountouridis, C. A. Balgobin, T. Schüpbach, R. D. Burdine, and S. Y. Shvartsman. In vivo severity ranking of ras pathway mutations associated with developmental disorders. *Proc. Natl. Acad. Sci. U. S. A.*, 114(3):510–515, Jan. 2017.

[144] H. E. Johnson, Y. Goyal, N. L. Pannucci, T. Schüpbach, S. Y. Shvartsman, and J. E. Toettcher. The spatiotemporal limits of developmental erk signaling. *Dev. Cell*, 40(2):185–192, Jan. 2017.

[145] H. E. Johnson and J. E. Toettcher. Signaling dynamics control cell fate in the early drosophila embryo. *Dev. Cell*, 48(3):361–370.e3, Feb. 2019.

[146] S. M. Jones and A. Kazlauskas. Growth-factor-dependent mitogenesis requires two distinct phases of signalling. *Nat. Cell Biol.*, 3(2):165–172, Feb. 2001.

[147] J. Joung, S. Konermann, J. S. Gootenberg, O. O. Abudayyeh, R. J. Platt, M. D. Brigham, N. E. Sanjana, and F. Zhang. Genome-scale CRISPR-Cas9 knockout and transcriptional activation screening. *Nat. Protoc.*, 12(4):828–863, Apr. 2017.

[148] J. Jumper, R. Evans, A. Pritzel, T. Green, M. Figurnov, O. Ronneberger, K. Tunyasuvunakool, R. Bates, A. Žídek, A. Potapenko, A. Bridgland, C. Meyer, S. A. A. Kohl, A. J. Ballard, A. Cowie, B. Romera-Paredes, S. Nikolov, R. Jain, J. Adler, T. Back, S. Petersen, D. Reiman, E. Clancy, M. Zielinski, M. Steinegger, M. Pacholska, T. Berghammer, S. Bodenstein, D. Silver, O. Vinyals, A. W. Senior, K. Kavukcuoglu, P. Kohli, and D. Hassabis. Highly accurate protein structure prediction with AlphaFold. *Nature*, 596(7873):583–589, Aug. 2021.

[149] R. Kalluri and R. A. Weinberg. The basics of epithelial-mesenchymal transition. *J. Clin. Invest.*, 119(6):1420–1428, June 2009.

[150] Y. Kamioka, K. Sumiyama, R. Mizuno, Y. Sakai, E. Hirata, E. Kiyokawa, and M. Matsuda. Live imaging of protein kinase activities in transgenic mice expressing FRET biosensors. *Cell Struct. Funct.*, 37(1):65–73, Jan. 2012.

[151] Y. Kamioka, S. Yasuda, Y. Fujita, K. Aoki, and M. Matsuda. Multiple decisive phosphorylation sites for the negative feedback regulation of SOS1 via ERK. *J. Biol. Chem.*, 285(43):33540–33548, Oct. 2010.

[152] S. Kao, R. K. Jaiswal, W. Kolch, and G. E. Landreth. Identification of the mechanisms regulating the differential activation of the mapk cascade by epidermal growth factor and nerve growth factor in PC12 cells. *J. Biol. Chem.*, 276(21):18169–18177, May 2001.

[153] P. A. Kenny and M. J. Bissell. Targeting TACE-dependent EGFR ligand shedding in breast cancer. *J. Clin. Invest.*, 117(2):337–345, Feb. 2007.

[154] J. Keyes, A. Ganesan, O. Molinar-Inglis, A. Hamidzadeh, J. Zhang, M. Ling, J. Trejo, A. Levchenko, and J. Zhang. Signaling diversity enabled by rap1-regulated plasma membrane ERK with distinct temporal dynamics. *Elife*, 9, May 2020.

[155] B. N. Kholodenko. Negative feedback and ultrasensitivity can bring about oscillations in the mitogen-activated protein kinase cascades, 2000.

[156] B. N. Kholodenko, O. V. Demin, G. Moehren, and J. B. Hoek. Quantification of short term signaling by the epidermal growth factor receptor. *J. Biol. Chem.*, 274(42):30169–30181, Oct. 1999.

[157] B. N. Kholodenko, J. F. Hancock, and W. Kolch. Signalling ballet in space and time. *Nat. Rev. Mol. Cell Biol.*, 11(6):414–426, June 2010.

[158] H. K. Kim, S. Min, M. Song, S. Jung, J. W. Choi, Y. Kim, S. Lee, S. Yoon, and H. h. Kim. Deep learning improves prediction of CRISPR–Cpf1 guide RNA activity. *Nat. Biotechnol.*, 36(3):239–241, Jan. 2018.

[159] S.-J. Kim, Y.-S. Kim, J. H. Kim, H. Y. Jang, D. D. Ly, R. Das, and K.-S. Park. Activation of ERK1/2-mTORC1-NOX4 mediates TGF-β1-induced epithelial-mesenchymal transition and fibrosis in retinal pigment epithelial cells. *Biochem. Biophys. Res. Commun.*, 529(3):747–752, Aug. 2020.

[160] C. Kime, M. A. Mandegar, D. Srivastava, S. Yamanaka, B. R. Conklin, and T. A. Rand. Efficient CRISPR/Cas9-Based genome engineering in human pluripotent stem cells. *Curr. Protoc. Hum. Genet.*, 88:21.4.1–21.4.23, Jan. 2016.

[161] A. Kiyatkin, I. K. van Alderwerelt van Rosenburgh, D. E. Klein, and M. A. Lemmon. Kinetics of receptor tyrosine kinase activation define ERK signaling dynamics. *Sci. Signal.*, 13(645), Aug. 2020.

[162] L. B. Kleiman, T. Maiwald, H. Conzelmann, D. A. Lauffenburger, and P. K. Sorger. Rapid phospho-turnover by receptor tyrosine kinases impacts downstream signaling and drug binding. *Mol. Cell*, 43(5):723–737, Sept. 2011.

[163] E. Kobrinsky, D. E. Mager, S. A. Bentil, S.-I. Murata, D. R. Abernethy, and N. M. Soldatov. Identification of plasma membrane macro- and microdomains from wavelet analysis of FRET microscopy. *Biophys. J.*, 88(5):3625–3634, May 2005.

[164] B. Koch, B. Nijmeijer, M. Kueblbeck, Y. Cai, N. Walther, and J. Ellenberg. Generation and validation of homozygous fluorescent knock-in cells using CRISPR–Cas9 genome editing. *Nat. Protoc.*, 13(6):1465–1487, May 2018.

[165] M. Kochańczyk, P. Kocieniewski, E. Kozłowska, J. Jaruszewicz-Błońska, B. Sparta, M. Pargett, J. G. Albeck, W. S. Hlavacek, and T. Lipniacki. Relaxation oscillations and hierarchy of feedbacks in MAPK signaling. *Sci. Rep.*, 7:38244, Jan. 2017.

[166] P. Kocieniewski and T. Lipniacki. MEK1 and MEK2 differentially control the duration and amplitude of the ERK cascade response. *Phys. Biol.*, 10(3):035006, June 2013.

[167] N. Kokhlikyan, V. Miglani, M. Martin, E. Wang, B. Alsallakh, J. Reynolds, A. Melnikov, N. Kliushkina, C. Araya, S. Yan, and O. Reblitz-Richardson. Captum: A unified and generic model interpretability library for PyTorch. Sept. 2020.

[168] N. Komatsu, K. Aoki, M. Yamada, H. Yukinaga, Y. Fujita, Y. Kamioka, and M. Matsuda. Development of an optimized backbone of FRET biosensors for kinases and GTPases. *Mol. Biol. Cell*, 22(23):4647–4656, Dec. 2011.

[169] R. L. Kortum, M. R. Fernandez, D. L. Costanzo-Garvey, H. J. Johnson, K. W. Fisher, D. J. Volle, and R. E. Lewis. Caveolin-1 is required for kinase suppressor of ras 1 (KSR1)-mediated extracellular signal-regulated kinase 1/2 activation, H-RasV12-induced senescence, and transformation. *Mol. Cell. Biol.*, 34(18):3461–3472, Sept. 2014.

[170] N. Kosaisawe, B. Sparta, M. Pargett, C. K. Teragawa, and J. G. Albeck. Transient phases of OXPHOS inhibitor resistance reveal underlying metabolic heterogeneity in single cells. *Cell Metab.*, 33(3):649–665.e8, Mar. 2021.

[171] B. A. Kramer, J. Sarabia del Castillo, and L. Pelkmans. Multimodal perception links cellular state to decision making in single cells. *Science*, July 2022.

[172] D. Kraus, S. Khoury, A. Fendyur, S. G. Kachalsky, T. Abu-Hatoum, and R. Rahamimoff. Intracellular calcium dynamics–sparks of insight. *J. Basic Clin. Physiol. Pharmacol.*, 11(4):331–365, 2000.

[173] H. B. Krause, H. Bondarowicz, A. L. Karls, M. N. McClean, and P. K. Kreeger. Design and implementation of a microfluidic device capable of temporal growth factor delivery reveal filtering capabilities of the EGFR/ERK pathway. *APL Bioengineering*, 5(4):046101, Dec. 2021.

[174] T. Kudo, S. Jeknić, D. N. Macklin, S. Akhter, J. J. Hughey, S. Regot, and M. W. Covert. Live-cell measurements of kinase activity in single cells using translocation reporters. *Nat. Protoc.*, 13(1):155–169, Jan. 2018.

[175] T. Kunath, M. K. Saba-El-Leil, M. Almousailleakh, J. Wray, S. Meloche, and A. Smith. FGF stimulation of the erk1/2 signalling cascade triggers transition of pluripotent embryonic stem cells from self-renewal to lineage commitment. *Development*, 134(16):2895–2902, Aug. 2007.

[176] Y. Kwon, S. Mehta, M. Clark, G. Walters, Y. Zhong, H. N. Lee, R. K. Sunahara, and J. Zhang. Non-canonical β-adrenergic activation of ERK at endosomes. *Nature*, pages 1–7, Oct. 2022.

[177] S. Lamouille, J. Xu, and R. Derynck. Molecular mechanisms of epithelial-mesenchymal transition. *Nat. Rev. Mol. Cell Biol.*, 15(3):178–196, Mar. 2014.

[178] F. Lanner and J. Rossant. The role of FGF/Erk signaling in pluripotent cells. *Development*, 137(20):3351–3360, Oct. 2010.

[179] H. Lavoie, J. Gagnon, and M. Therrien. ERK signalling: a master regulator of cell behaviour, life and fate. *Nat. Rev. Mol. Cell Biol.*, June 2020.

[180] M. J. Lazzara, K. Lane, R. Chan, P. J. Jasper, M. B. Yaffe, P. K. Sorger, T. Jacks, B. G. Neel, and D. A. Lauffenburger. Impaired SHP2-mediated extracellular signal-regulated kinase activation contributes to gefitinib sensitivity of lung cancer cells with epidermal growth factor receptor-activating mutations. *Cancer Res.*, 70(9):3843–3850, May 2010.

[181] T. D. Lebedev, E. R. Khabusheva, S. R. Mareeva, K. A. Ivanenko, A. V. Morozov, P. V. Spirin, P. M. Rubtsov, A. V. Snezhkina, A. V. Kudryavtseva, M. I. Sorokin, A. A. Buzdin, and V. S. Prassolov. Identification of cell type-specific correlations between ERK activity and cell viability upon treatment with ERK1/2 inhibitors. *J. Biol. Chem.*, 298(8):102226, Aug. 2022.

[182] M. A. Lemmon, D. M. Freed, J. Schlessinger, and A. Kiyatkin. The dark side of cell signaling: Positive roles for negative regulators. *Cell*, 164(6):1172–1184, Mar. 2016.

[183] J. H. Levine, Y. Lin, and M. B. Elowitz. Functional roles of pulsing in genetic circuits. *Science*, 342(6163):1193–1200, Dec. 2013.

[184] H. Li, X. Wang, N. Li, J. Qiu, Y. Zhang, and X. Cao. hPEBP4 resists TRAIL-induced apoptosis of human prostate cancer cells by activating akt and deactivating ERK1/2 pathways. *J. Biol. Chem.*, 282(7):4943–4950, Feb. 2007.

[185] Q.-J. Li, S.-H. Yang, Y. Maeda, F. M. Sladek, A. D. Sharrocks, and M. Martins-Green. MAP kinase phosphorylation-dependent activation of elk-1 leads to activation of the co-activator p300. *EMBO J.*, 22(2):281–291, Jan. 2003.

[186] X. Li, Y. Huang, J. Jiang, and S. J. Frank. ERK-dependent threonine phosphorylation of EGF receptor modulates receptor downregulation and signaling. *Cell. Signal.*, 20(11):2145–2155, Nov. 2008.

[187] B. Lim, C. J. Dsilva, T. J. Levario, H. Lu, T. Schüpbach, I. G. Kevrekidis, and S. Y. Shvartsman. Dynamics of inductive ERK signaling in the drosophila embryo. *Curr. Biol.*, 25(13):1784–1790, June 2015.

[188] S. Lin, D. Hirayama, G. Maryu, K. Matsuda, N. Hino, E. Deguchi, K. Aoki, R. Iwamoto, K. Terai, and M. Matsuda. Redundant roles of EGFR ligands in the ERK activation waves during collective cell migration. *Life Sci Alliance*, 5(1), Jan. 2022.

[189] M. Linkert, C. T. Rueden, C. Allan, J.-M. Burel, W. Moore, A. Patterson, B. Loranger, J. Moore, C. Neves, D. Macdonald, A. Tarkowska, C. Sticco, E. Hill, M. Rossner, K. W. Eliceiri, and J. R. Swedlow. Metadata matters: access to image data in the real world. *J. Cell Biol.*, 189(5):777–782, May 2010.

[190] P. Lito, C. A. Pratilas, E. W. Joseph, M. Tadi, E. Halilovic, M. Zubrowski, A. Huang, W. L. Wong, M. K. Callahan, T. Merghoub, J. D. Wolchok, E. de Stanchina, S. Chandarlapaty, P. I. Poulikakos, J. A. Fagin, and N. Rosen. Relief of profound feedback inhibition of mitogenic signaling by RAF inhibitors attenuates their activity in BRAFV600E melanomas. *Cancer Cell*, 22(5):668–682, Nov. 2012.

[191] H. Lodish, A. Berk, S. L. Zipursky, P. Matsudaira, D. Baltimore, and J. Darnell. Molecular cell biology 4th edition. *National Center for Biotechnology Information, Bookshelf*, 9, 2000.

[192] S. Löffek, O. Schilling, and C.-W. Franzke. Biological role of matrix metalloproteinases: a critical balance. *Eur. Respir. J.*, 38(1):191–208, July 2011.

[193] N. C. Luetteke, T. H. Qiu, S. E. Fenton, K. L. Troyer, R. F. Riedel, A. Chang, and D. C. Lee. Targeted inactivation of the EGF and amphiregulin genes reveals distinct roles for EGF receptor ligands in mouse mammary gland development. *Development*, 126(12):2739–2750, June 1999.

[194] X. Ma, H. Chen, and L. Chen. A dual role of erk signaling in embryonic stem cells. *Exp. Hematol.*, 44(3):151–156, Mar. 2016.

[195] S. K. Madala, S. Schmidt, C. Davidson, M. Ikegami, S. Wert, and W. D. Hardie. MEK-ERK pathway modulation ameliorates pulmonary fibrosis associated with epidermal growth factor receptor activation. *Am. J. Respir. Cell Mol. Biol.*, 46(3):380–388, Mar. 2012.

[196] G. Maik-Rachline, A. Hacohen-Lev-Ran, and R. Seger. Nuclear ERK: Mechanism of translocation, substrates, and role in cancer. *Int. J. Mol. Sci.*, 20(5), Mar. 2019.

[197] I. Manolaridis, K. Kulkarni, R. B. Dodd, S. Ogasawara, Z. Zhang, G. Bineva, N. O. Reilly, S. J. Hanrahan, A. J. Thompson, N. Cronin, S. Iwata, and D. Barford. Mechanism of farnesylated CAAX protein processing by the intramembrane protease rce1. *Nature*, 504(7479):301–305, Dec. 2013.

[198] S. P. H. Mao, M. Park, R. M. Cabrera, J. R. Christin, G. S. Karagiannis, M. H. Oktay, D. M. W. Zaiss, S. I. Abrams, W. Guo, J. S. Condeelis, P. A. Kenny, and J. E. Segall. Loss of amphiregulin reduces myoepithelial cell coverage of mammary ducts and alters breast tumor growth. *Breast Cancer Res.*, 20(1):131, Oct. 2018.

[199] D. R. Marenda, A. D. Vrailas, A. B. Rodrigues, S. Cook, M. A. Powers, J. A. Lorenzen, L. A. Perkins, and K. Moses. MAP kinase subcellular localization controls both pattern and proliferation in the developing drosophila wing. *Development*, 133(1):43–51, Jan. 2006.

[200] S. M. Margarit, H. Sondermann, B. E. Hall, B. Nagar, A. Hoelz, M. Pirruccello, D. Bar-Sagi, and J. Kuriyan. Structural evidence for feedback activation by Ras.GTP of the ras-specific nucleotide exchange factor SOS. *Cell*, 112(5):685–695, Mar. 2003.

[201] N. I. Markevich, J. B. Hoek, and B. N. Kholodenko. Signaling switches and bistability arising from multisite phosphorylation in protein kinase cascades. *J. Cell Biol.*, 164(3):353–359, Feb. 2004.

[202] C. J. Marshall. Specificity of receptor tyrosine kinase signaling: transient versus sustained extracellular signal-regulated kinase activation. *Cell*, 80(2):179–185, Jan. 1995.

[203] G. Maryu, M. Matsuda, and K. Aoki. Multiplexed fluorescence imaging of ERK and akt activities and cell-cycle progression. *Cell Struct. Funct.*, 41(2):81–92, July 2016.

[204] I. Matos, A. Asare, J. Levorse, T. Ouspenskaia, J. de la Cruz-Racelis, L.-N. Schuhmacher, and E. Fuchs. Progenitors oppositely polarize WNT activators and inhibitors to orchestrate tissue development. *Elife*, 9, Apr. 2020.

[205] Y. Matsubayashi, M. Ebisuya, S. Honjoh, and E. Nishida. ERK activation propagates in epithelial cell sheets and regulates their migration during wound healing. *Curr. Biol.*, 14(8):731–735, Apr. 2004.

[206] S. Mehta, Y. Zhang, R. H. Roth, J.-F. Zhang, A. Mo, B. Tenner, R. L. Huganir, and J. Zhang. Single-fluorophore biosensors for sensitive and multiplexed detection of signalling activities. *Nat. Cell Biol.*, 20(10):1215–1225, Oct. 2018.

[207] D. R. Meier, M. A. Girtman, K. A. Lofgren, and P. A. Kenny. Amphiregulin deletion strongly attenuates the development of estrogen receptor-positive tumors in p53 mutant mice. *Breast Cancer Res. Treat.*, 179(3):653–660, Feb. 2020.

[208] E. Meijering. Cell segmentation: 50 years down the road [life sciences]. *IEEE Signal Process. Mag.*, 29(5):140–145, Sept. 2012.

[209] S. Meloche, K. Seuwen, G. Pagès, and J. Pouysségur. Biphasic and synergistic activation of p44mapk (ERK1) by growth factors: correlation between late phase activation and mitogenicity. *Mol. Endocrinol.*, 6(5):845–854, May 1992.

[210] M. C. Mendoza, E. E. Er, W. Zhang, B. A. Ballif, H. L. Elliott, G. Danuser, and J. Blenis. ERK-MAPK drives lamellipodia protrusion by activating the WAVE2 regulatory complex. *Mol. Cell*, 41(6):661–671, Mar. 2011.

[211] M. C. Mendoza, M. Vilela, J. E. Juarez, J. Blenis, and G. Danuser. ERK reinforces actin polymerization to power persistent edge protrusion during motility. *Sci. Signal.*, 8(377):ra47, May 2015.

[212] I. Michailovici, H. A. Harrington, H. H. Azogui, Y. Yahalom-Ronen, A. Plotnikov, S. Ching, M. P. H. Stumpf, O. D. Klein, R. Seger, and E. Tzahor. Nuclear to cytoplasmic shuttling of ERK promotes differentiation of muscle stem/progenitor cells. *Development*, 141(13):2611–2620, July 2014.

[213] C. Michaloglou, L. C. W. Vredeveld, M. S. Soengas, C. Denoyelle, T. Kuilman, C. M. A. M. van der Horst, D. M. Majoor, J. W. Shay, W. J. Mooi, and D. S. Peeper. BRAFE600-associated senescence-like cell cycle arrest of human naevi. *Nature*, 436(7051):720–724, Aug. 2005.

[214] M. Min, Y. Rong, C. Tian, and S. Spencer. Temporal integration of mitogen history in mother cells controls proliferation of daughter cells. *Science*, Apr. 2020.

[215] E. Moreno, L. Valon, F. Levillayer, and R. Levayer. Competition for space induces cell elimination through Compaction-Driven ERK downregulation. *Curr. Biol.*, 29(1):23–34.e8, Jan. 2019.

[216] K. Muroya, S. Hattori, and S. Nakamura. Nerve growth factor induces rapid accumulation of the GTP-bound form of p21ras in rat pheochromocytoma PC12 cells. *Oncogene*, 7(2):277–281, Feb. 1992.

[217] L. O. Murphy, J. P. MacKeigan, and J. Blenis. A network of immediate early gene products propagates subtle differences in mitogen-activated protein kinase signal amplitude and duration. *Mol. Cell. Biol.*, 24(1):144–153, Jan. 2004.

[218] L. O. Murphy, S. Smith, R.-H. Chen, D. C. Fingar, and J. Blenis. Molecular interpretation of ERK signal duration by immediate early gene products. *Nat. Cell Biol.*, 4(8):556–564, Aug. 2002.

[219] Y. Muta, Y. Fujita, K. Sumiyama, A. Sakurai, M. M. Taketo, T. Chiba, H. Seno, K. Aoki, M. Matsuda, and M. Imajo. Composite regulation of ERK activity dynamics underlying tumour-specific traits in the intestine. *Nat. Commun.*, 9(1):2174, June 2018.

[220] S. K. Muthuswamy, D. Li, S. Lelievre, M. J. Bissell, and J. S. Brugge. ErbB2, but not ErbB1, reinitiates proliferation and induces luminal repopulation in epithelial acini. *Nat. Cell Biol.*, 3(9):785–792, Sept. 2001.

[221] T. Nagashima, N. Inoue, N. Yumoto, Y. Saeki, S. Magi, N. Volinsky, A. Sorkin, B. N. Kholodenko, and M. Okada-Hatakeyama. Feedforward regulation of mRNA stability by prolonged extracellular signal-regulated kinase activity. *FEBS J.*, 282(4):613–629, Feb. 2015.

[222] T. Nakakuki, M. R. Birtwistle, Y. Saeki, N. Yumoto, K. Ide, T. Nagashima, L. Brusch, B. A. Ogunnaike, M. Okada-Hatakeyama, and B. N. Kholodenko. Ligand-specific c-fos expression emerges from the spatiotemporal control of ErbB network dynamics. *Cell*, 141(5):884–896, May 2010.

[223] A. Nakamura, Y. Goto, Y. Kondo, and K. Aoki. Shedding light on developmental ERK signaling with genetically encoded biosensors. *Development*, 148(18), Sept. 2021.

[224] K. Nakayama, T. Satoh, A. Igari, R. Kageyama, and E. Nishida. FGF induces oscillations of hes1 expression and Ras/ERK activation. *Curr. Biol.*, 18(8):R332–4, Apr. 2008.

[225] T. S. Nambiar, P. Billon, G. Diedenhofen, S. B. Hayward, A. Taglialatela, K. Cai, J.-W. Huang, G. Leuzzi, R. Cuella-Martin, A. Palacios, A. Gupta, D. Egli, and A. Ciccia. Stimulation of CRISPR-mediated homology-directed repair by an engineered RAD18 variant. *Nat. Commun.*, 10(1):3395, July 2019.

[226] M. Navandar, A. Garding, S. K. Sahu, A. Pataskar, S. Schick, and V. K. Tiwari. ERK signalling modulates epigenome to drive epithelial to mesenchymal transition. *Oncotarget*, 8(17):29269–29281, Apr. 2017.

[227] R. Nazarian, H. Shi, Q. Wang, X. Kong, R. C. Koya, H. Lee, Z. Chen, M.-K. Lee, N. Attar, H. Sazegar, T. Chodon, S. F. Nelson, G. McArthur, J. A. Sosman, A. Ribas, and R. S. Lo. Melanomas acquire resistance to B-RAF(V600E) inhibition by RTK or N-RAS upregulation. *Nature*, 468(7326):973–977, Dec. 2010.

[228] T. S. Netterfield, G. J. Ostheimer, A. R. Tentner, P. K. Sorger, K. A. Janes, D. A. Lauffenburger, and M. B. Yaffe. Biphasic JNK–Erk signaling separates induction and maintenance of cell senescence after DNA damage. June 2022.

[229] T. T. Nguyen, J. C. Scimeca, C. Filloux, P. Peraldi, J. L. Carpentier, and E. Van Obberghen. Co-regulation of the mitogen-activated protein kinase, extracellular signal-regulated kinase 1, and the 90-kda ribosomal S6 kinase in PC12 cells. distinct effects of the neurotrophic factor, nerve growth factor, and the mitogenic factor, epidermal growth factor. *J. Biol. Chem.*, 268(13):9803–9810, May 1993.

[230] T. T. Nguyen, J. C. Scimeca, C. Filloux, P. Peraldi, J. L. Carpentier, and E. Van Obberghen. Co-regulation of the mitogen-activated protein kinase, extracellular signal-regulated kinase 1, and the 90-kda ribosomal S6 kinase in PC12 cells. distinct effects of the neurotrophic factor, nerve growth factor, and the mitogenic factor, epidermal growth factor. *J. Biol. Chem.*, 268(13):9803–9810, 1993.

[231] M. Niepel, S. L. Spencer, and P. K. Sorger. Non-genetic cell-to-cell variability and the consequences for pharmacology. *Curr. Opin. Chem. Biol.*, 13(5-6):556–561, Dec. 2009.

[232] H. Nunns and L. Goentoro. Signaling pathways as linear transmitters. *Elife*, 7:e33617, Sept. 2018.

[233] Y. Ogura, F.-L. Wen, M. M. Sami, T. Shibata, and S. Hayashi. A switch-like activation relay of EGFR-ERK signaling regulates a wave of cellular contractility for epithelial invagination. *Dev. Cell*, 46(2):162–172.e5, July 2018.

[234] K. S. Okuda, M. S. Keyser, D. B. Gurevich, C. Sturtzel, E. A. Mason, S. Paterson, H. Chen, M. Scott, N. D. Condon, P. Martin, M. Distel, and B. M. Hogan. Live-imaging of endothelial erk activity reveals dynamic and sequential signalling events during regenerative angiogenesis. *Elife*, 10, May 2021.

[235] R. J. Orton, O. E. Sturm, A. Gormand, W. Wolch, and D. R. Gilbert. Computational modelling reveals feedback redundancy within the epidermal growth factor receptor/extracellular-signal regulated kinase signalling pathway. *IET Syst. Biol.*, 2(4):173–183, July 2008.

[236] R. J. Orton, O. E. Sturm, V. Vyshemirsky, M. Calder, D. R. Gilbert, and W. Kolch. Computational modelling of the receptor-tyrosine-kinase-activated MAPK pathway. *Biochem. J*, 392(Pt 2):249–261, Dec. 2005.

[237] E. Palmer and T. Freeman. Investigation into the use of C- and n-terminal GFP fusion proteins for subcellular localization studies using reverse transfection microarrays. *Comp. Funct. Genomics*, 5(4):342–353, 2004.

[238] M. Pargett and J. G. Albeck. Live-Cell imaging and analysis with multiple genetically encoded reporters. *Curr. Protoc. Cell Biol.*, 78(1):4.36.1–4.36.19, Mar. 2018.

[239] M. Pargett, T. E. Gillies, C. K. Teragawa, B. Sparta, and J. G. Albeck. Single-Cell imaging of ERK signaling using fluorescent biosensors. *Methods Mol. Biol.*, 1636:35–59, 2017.

[240] K. Peeters, F. Van Leemputte, B. Fischer, B. M. Bonini, H. Quezada, M. Tsytlonok, D. Haesen, W. Vanthienen, N. Bernardes, C. B. Gonzalez-Blas, V. Janssens, P. Tompa, W. Versées, and J. M. Thevelein. Fructose-1,6-bisphosphate couples glycolytic flux to activation of ras. *Nat. Commun.*, 8(1):922, Oct. 2017.

[241] N. Peláez, A. Gavalda-Miralles, B. Wang, H. T. Navarro, H. Gudjonson, I. Rebay, A. R. Dinner, A. K. Katsaggelos, L. A. N. Amaral, and R. W. Carthew. Dynamics and heterogeneity of a fate determinant during transition towards cell differentiation. *Elife*, 4:e08924, Nov. 2015.

[242] M. J. Pokrass, K. A. Ryan, T. Xin, B. Pielstick, W. Timp, V. Greco, and S. Regot. Cell-Cycle-Dependent ERK signaling dynamics direct fate specification in the mammalian preimplantation embryo. *Dev. Cell*, 55(3):328–340.e5, Nov. 2020.

[243] B. Ponsioen, J. B. Post, J. R. Buissant des Amorie, D. Laskaris, R. L. van Ineveld, S. Kersten, A. Bertotti, F. Sassi, F. Sipieter, B. Cappe, S. Mertens, I. Verlaan-Klink, S. F. Boj, R. G. J. Vries, H. Rehmann, P. Vandenabeele, F. B. Riquet, L. Trusolino, J. L. Bos, and H. J. G. Snippert. Quantifying single-cell ERK dynamics in colorectal cancer organoids reveals EGFR as an amplifier of oncogenic MAPK pathway signalling. *Nat. Cell Biol.*, 23(4):377–390, Apr. 2021.

[244] P. M. D. Potey, A. G. Rossi, C. D. Lucas, and D. A. Dorward. Neutrophils in the initiation and resolution of acute pulmonary inflammation: understanding biological function and therapeutic potential. *J. Pathol.*, 247(5):672–685, Apr. 2019.

[245] P. I. Poulikakos, C. Zhang, G. Bollag, K. M. Shokat, and N. Rosen. RAF inhibitors transactivate RAF dimers and ERK signalling in cells with wild-type BRAF. *Nature*, 464(7287):427–430, Feb. 2010.

[246] B. J. Pulverer, J. M. Kyriakis, J. Avruch, E. Nikolakaki, and J. R. Woodgett. Phosphorylation of c-jun mediated by MAP kinases. *Nature*, 353(6345):670–674, Oct. 1991.

[247] J. E. Purvis, K. W. Karhohs, C. Mock, E. Batchelor, A. Loewer, and G. Lahav. p53 dynamics control cell fate. *Science*, 336(6087):1440–1444, June 2012.

[248] D. Raina, A. Bahadori, A. Stanoev, M. Protzek, A. Koseska, and C. Schröter. Cell-cell communication through FGF4 generates and maintains robust proportions of differentiated cell types in embryonic stem cells. *Development*, 148(21), Nov. 2021.

[249] D. Raina, F. Fabris, L. G. Morelli, and C. Schröter. Intermittent ERK oscillations downstream of FGF in mouse embryonic stem cells. Dec. 2020.

[250] M. Raman, W. Chen, and M. H. Cobb. Differential regulation and properties of MAPKs. *Oncogene*, 26(22):3100–3112, May 2007.

[251] K. A. Rauen, S. M. Huson, E. Burkitt-Wright, D. G. Evans, S. Farschtschi, R. E. Ferner, D. H. Gutmann, C. O. Hanemann, B. Kerr, E. Legius, L. F. Parada, M. Patton, J. Peltonen, N. Ratner, V. M. Riccardi, T. van der Vaart, M. Vikkula, D. H. Viskochil, M. Zenker, and M. Upadhyaya. Recent developments in neurofibromatoses and RASopathies: management, diagnosis and current and future therapeutic avenues. *Am. J. Med. Genet. A*, 167A(1):1–10, Jan. 2015.

[252] P. T. Ravindran, S. McFann, R. H. Thornton, and J. E. Toettcher. A synthetic gene circuit for imaging-free detection of signaling pulses. *Cell Syst*, 13(2):131–142.e13, Feb. 2022.

[253] P. T. Ravindran, M. Z. Wilson, S. G. Jena, and J. E. Toettcher. Engineering combinatorial and dynamic decoders using synthetic immediate-early genes. *Commun Biol*, 3(1):436, Aug. 2020.

[254] S. Regot, J. J. Hughey, B. T. Bajar, S. Carrasco, and M. W. Covert. High-sensitivity measurements of multiple kinase activities in live single cells. *Cell*, 157(7):1724–1734, June 2014.

[255] D. A. Ritt, D. M. Monson, S. I. Specht, and D. K. Morrison. Impact of feedback phosphorylation and raf heterodimerization on normal and mutant B-Raf signaling. *Mol. Cell. Biol.*, 30(3):806–819, 2010.

[256] A. Rizki, V. M. Weaver, S.-Y. Lee, G. I. Rozenberg, K. Chin, C. A. Myers, J. L. Bascom, J. D. Mott, J. R. Semeiks, L. R. Grate, I. S. Mian, A. D. Borowsky, R. A. Jensen, M. O. Idowu, F. Chen, D. J. Chen, O. W. Petersen, J. W. Gray, and M. J. Bissell. A human breast cell model of preinvasive to invasive transition. *Cancer Res.*, 68(5):1378–1387, Mar. 2008.

[257] K. Roepstorff, M. V. Grandal, L. Henriksen, S. L. J. Knudsen, M. Lerdrup, L. Grøvdal, B. M. Willumsen, and B. van Deurs. Differential effects of EGFR ligands on endocytic sorting of the receptor. *Traffic*, 10(8):1115–1127, Aug. 2009.

[258] H. Ryu, M. Chung, M. Dobrzyński, D. Fey, Y. Blum, S. S. Lee, M. Peter, B. N. Kholodenko, N. L. Jeon, and O. Pertz. Frequency modulation of ERK activation dynamics rewires cell fate. *Mol. Syst. Biol.*, 11(11):838, Nov. 2015.

[259] W. Sabbagh, Jr, L. J. Flatauer, A. J. Bardwell, and L. Bardwell. Specificity of MAP kinase signaling in yeast differentiation involves transient versus sustained MAPK activation. *Mol. Cell*, 8(3):683–691, Sept. 2001.

[260] M. Saha, A. Carriere, M. Cheerathodi, X. Zhang, G. Lavoie, J. Rush, P. P. Roux, and B. A. Ballif. RSK phosphorylates SOS1 creating 14-3-3-docking sites and negatively regulating MAPK activation. *Biochem. J*, 447(1):159–166, Oct. 2012.

[261] T. H. Saito, S. Uda, T. Tsuchiya, Y.-I. Ozaki, and S. Kuroda. Temporal decoding of MAP kinase and CREB phosphorylation by selective immediate early gene expression. *PLoS One*, 8(3):e57037, Mar. 2013.

[262] S. D. M. Santos, P. J. Verveer, and P. I. H. Bastiaens. Growth factor-induced MAPK network topology shapes erk response determining PC-12 cell fate. *Nat. Cell Biol.*, 9(3):324–330, Mar. 2007.

[263] C. J. Sarkisian, B. A. Keister, D. B. Stairs, R. B. Boxer, S. E. Moody, and L. A. Chodosh. Dose-dependent oncogene-induced senescence in vivo and its evasion during mammary tumorigenesis. *Nat. Cell Biol.*, 9(5):493–505, May 2007.

[264] S. Sasagawa, Y.-I. Ozaki, K. Fujita, and S. Kuroda. Prediction and validation of the distinct dynamics of transient and sustained ERK activation. *Nat. Cell Biol.*, 7(4):365–373, Apr. 2005.

[265] U. Schmidt, M. Weigert, C. Broaddus, and G. Myers. Cell detection with Star-Convex polygons. In *Medical Image Computing and Computer Assisted Intervention – MICCAI 2018*, pages 265–273. Springer International Publishing, 2018.

[266] B. Schoeberl, C. Eichler-Jonsson, E. D. Gilles, and G. Müller. Computational modeling of the dynamics of the MAP kinase cascade activated by surface and internalized EGF receptors. *Nat. Biotechnol.*, 20(4):370–375, Apr. 2002.

[267] J. Selimkhanov, B. Taylor, J. Yao, A. Pilko, J. Albeck, A. Hoffmann, L. Tsimring, and R. Wollman. Systems biology. accurate information transmission through dynamic biochemical signaling networks. *Science*, 346(6215):1370–1373, Dec. 2014.

[268] L. Sepe, M. C. Ferrari, C. Cantarella, F. Fioretti, and G. Paolella. Ras activated ERK and PI3K pathways differentially affect directional movement of cultured fibroblasts. *Cell. Physiol. Biochem.*, 31(1):123–142, Jan. 2013.

[269] S. M. Shaffer, M. C. Dunagin, S. R. Torborg, E. A. Torre, B. Emert, C. Krepler, M. Beqiri, K. Sproesser, P. A. Brafford, M. Xiao, E. Eggan, I. N. Anastopoulos, C. A. Vargas-Garcia, A. Singh, K. L. Nathanson, M. Herlyn, and A. Raj. Rare cell variability and drug-induced reprogramming as a mode of cancer drug resistance. *Nature*, 546(7658):431–435, June 2017.

[270] H. Shankaran, D. L. Ippolito, W. B. Chrisler, H. Resat, N. Bollinger, L. K. Opresko, and H. Steven Wiley. Rapid and sustained nuclear–cytoplasmic ERK oscillations induced by epidermal growth factor. *Mol. Syst. Biol.*, 5(1):332, Jan. 2009.

[271] H. Shankaran and H. S. Wiley. Oscillatory dynamics of the extracellular signal-regulated kinase pathway. *Curr. Opin. Genet. Dev.*, 20(6):650–655, Dec. 2010.

[272] C. Sheridan, G. Brumatti, and S. J. Martin. Oncogenic B-RafV600E inhibits apoptosis and promotes ERK-dependent inactivation of bad and bim. *J. Biol. Chem.*, 283(32):22128–22135, Aug. 2008.

[273] T. Shi, M. Niepel, J. E. McDermott, Y. Gao, C. D. Nicora, W. B. Chrisler, L. M. Markillie, V. A. Petyuk, R. D. Smith, K. D. Rodland, P. K. Sorger, W.-J. Qian, and H. S. Wiley. Conservation of protein abundance patterns reveals the regulatory architecture of the EGFR-MAPK pathway. *Sci. Signal.*, 9(436):rs6, July 2016.

[274] S. Shin, G. R. Buel, M. J. Nagiec, M.-J. Han, P. P. Roux, J. Blenis, and S.-O. Yoon. ERK2 regulates epithelial-to-mesenchymal plasticity through DOCK10-dependent Rac1/FoxO1 activation. *Proc. Natl. Acad. Sci. U. S. A.*, 116(8):2967–2976, Feb. 2019.

[275] S. Y. Shvartsman, C. B. Muratov, and D. A. Lauffenburger. Modeling and computational analysis of EGF receptor-mediated cell communication in drosophila oogenesis. *Development*, 129(11):2577–2589, June 2002.

[276] S. Sigismund, E. Argenzio, D. Tosoni, E. Cavallaro, S. Polo, and P. P. Di Fiore. Clathrin-mediated internalization is essential for sustained EGFR signaling but dispensable for degradation. *Dev. Cell*, 15(2):209–219, Aug. 2008.

[277] C. S. Simon, S. Rahman, D. Raina, C. Schröter, and A.-K. Hadjantonakis. Live visualization of ERK activity in the mouse blastocyst reveals Lineage-Specific signaling dynamics. *Dev. Cell*, 55(3):341–353.e5, Nov. 2020.

[278] F. Sipieter, B. Cappe, A. Leray, E. De Schutter, J. Bridelance, P. Hulpiau, G. Van Camp, W. Declercq, L. Héliot, P. Vincent, P. Vandenabeele, and F. B. Riquet. Characteristic ERK1/2 signaling dynamics distinguishes necroptosis from apoptosis. *iScience*, 24(9):103074, Sept. 2021.

[279] A. Sorkin and L. K. Goh. Endocytosis and intracellular trafficking of ErbBs. *Exp. Cell Res.*, 314(17):3093–3106, Oct. 2008.

[280] B. Sparta, M. Pargett, M. Minguet, K. Distor, G. Bell, and J. G. Albeck. Receptor level mechanisms are required for epidermal growth factor (EGF)-stimulated extracellular signal-regulated kinase (ERK) activity pulses. *J. Biol. Chem.*, 290(41):24784–24792, Oct. 2015.

[281] S. L. Spencer, S. D. Cappell, F.-C. Tsai, K. W. Overton, C. L. Wang, and T. Meyer. The proliferation-quiescence decision is controlled by a bifurcation in CDK2 activity at mitotic exit. *Cell*, 155(2):369–383, Oct. 2013.

[282] S. L. Spencer, S. Gaudet, J. G. Albeck, J. M. Burke, and P. K. Sorger. Non-genetic origins of cell-to-cell variability in TRAIL-induced apoptosis. *Nature*, 459(7245):428–432, May 2009.

[283] M. Srivastava, M. Nambiar, S. Sharma, S. S. Karki, G. Goldsmith, M. Hegde, S. Kumar, M. Pandey, R. K. Singh, P. Ray, R. Natarajan, M. Kelkar, A. De, B. Choudhary, and S. C. Raghavan. An inhibitor of nonhomologous end-joining abrogates double-strand break repair and impedes cancer progression. *Cell*, 151(7):1474–1487, Dec. 2012.

[284] W. Stallaert, S. R. Taylor, K. M. Kedziora, C. D. Taylor, H. K. Sobon, C. L. Young, J. C. Limas, J. Varblow Holloway, M. S. Johnson, J. G. Cook, and J. E. Purvis. The molecular architecture of cell cycle arrest. *Mol. Syst. Biol.*, 18(9):e11087, Sept. 2022.

[285] C. Starbuck and D. A. Lauffenburger. Mathematical model for the effects of epidermal growth factor receptor trafficking dynamics on fibroblast proliferation responses. *Biotechnol. Prog.*, 8(2):132–143, Mar. 1992.

[286] J. Stewart-Ornstein and G. Lahav. Dynamics of CDKN1A in single cells defined by an endogenous fluorescent tagging toolkit. *Cell Rep.*, 14(7):1800–1811, Feb. 2016.

[287] R. C. Stone, I. Pastar, N. Ojeh, V. Chen, S. Liu, K. I. Garzon, and M. Tomic-Canic. Epithelial-mesenchymal transition in tissue repair and fibrosis. *Cell Tissue Res.*, 365(3):495–506, Sept. 2016.

[288] J. Strasen, U. Sarma, M. Jentsch, S. Bohn, C. Sheng, D. Horbelt, P. Knaus, S. Legewie, and A. Loewer. Cell-specific responses to the cytokine TGFβ are determined by variability in protein levels. *Mol. Syst. Biol.*, 14(1):e7733, Jan. 2018.

[289] C. Stringer, T. Wang, M. Michaelos, and M. Pachitariu. Cellpose: a generalist algorithm for cellular segmentation. *Nat. Methods*, 18(1):100–106, Jan. 2021.

[290] O. E. Sturm, R. Orton, J. Grindlay, M. Birtwistle, V. Vyshemirsky, D. Gilbert, M. Calder, A. Pitt, B. Kholodenko, and W. Kolch. The mammalian MAPK/ERK pathway exhibits properties of a negative feedback amplifier. *Sci. Signal.*, 3(153):ra90, Dec. 2010.

[291] R. Suderman, J. A. Bachman, A. Smith, P. K. Sorger, and E. J. Deeds. Fundamental trade-offs between information flow in single cells and cellular populations. *Proc. Natl. Acad. Sci. U. S. A.*, 114(22):5755–5760, May 2017.

[292] Q. Sun, D. Novak, L. Hüser, J. Poelchen, H. Wu, K. Granados, A. Federico, K. Liu, T. Steinfass, M. Vierthaler, V. Umansky, and J. Utikal. FOXD1 promotes dedifferentiation and targeted therapy resistance in melanoma by regulating the expression of connective tissue growth factor. *Int. J. Cancer*, 149(3):657–674, Aug. 2021.

[293] M. Sundararajan, A. Taly, and Q. Yan. Axiomatic attribution for deep networks. In D. Precup and Y. W. Teh, editors, *Proceedings of the 34th International Conference on Machine Learning*, volume 70 of *Proceedings of Machine Learning Research*, pages 3319–3328. PMLR, 2017.

[294] W. L. Tam, H. Lu, J. Buikhuisen, B. S. Soh, E. Lim, F. Reinhardt, Z. J. Wu, J. A. Krall, B. Bierie, W. Guo, X. Chen, X. S. Liu, M. Brown, B. Lim, and R. A. Weinberg. Protein kinase C α is a central signaling node and therapeutic target for breast cancer stem cells. *Cancer Cell*, 24(3):347–364, Sept. 2013.

[295] Y. Tang, A. Adelaja, F. X.-F. Ye, E. Deeds, R. Wollman, and A. Hoffmann. Quantifying information accumulation encoded in the dynamics of biochemical signaling. *Nat. Commun.*, 12(1):1272, Feb. 2021.

[296] R. Tany, Y. Goto, Y. Kondo, and K. Aoki. Quantitative live-cell imaging of GPCR downstream signaling dynamics. *Biochem. J*, 479(8):883–900, Apr. 2022.

[297] D. Teis, W. Wunderlich, and L. A. Huber. Localization of the MP1-MAPK scaffold complex to endosomes is mediated by p14 and required for signal transduction. *Dev. Cell*, 3(6):803–814, Dec. 2002.

[298] M. Therrien, N. R. Michaud, G. M. Rubin, and D. K. Morrison. KSR modulates signal propagation within the MAPK cascade. *Genes Dev.*, 10(21):2684–2695, Nov. 1996.

[299] C. Tian, C. Yang, and S. L. Spencer. EllipTrack: A Global-Local Cell-Tracking pipeline for 2D fluorescence Time-Lapse microscopy. *Cell Rep.*, 32(5):107984, Aug. 2020.

[300] W. E. Tidyman and K. A. Rauen. The RASopathies: developmental syndromes of Ras/MAPK pathway dysregulation. *Curr. Opin. Genet. Dev.*, 19(3):230–236, June 2009.

[301] J. E. Toettcher, O. D. Weiner, and W. A. Lim. Using optogenetics to interrogate the dynamic control of signal transmission by the Ras/Erk module. *Cell*, 155(6):1422–1434, Dec. 2013.

[302] A. Tomasso, K. Bartscherer, and A. W. Seifert. An ERK-dependent molecular switch antagonizes fibrosis and promotes regeneration in spiny mice (acomys). June 2022.

[303] S. Traverse, N. Gomez, H. Paterson, C. Marshall, and P. Cohen. Sustained activation of the mitogen-activated protein (MAP) kinase cascade may be required for differentiation of PC12 cells. comparison of the effects of nerve growth factor and epidermal growth factor. *Biochem. J*, 288 (Pt 2)(Pt 2):351–355, Dec. 1992.

[304] M. Tresini, A. Lorenzini, C. Torres, and V. J. Cristofalo. Modulation of replicative senescence of diploid human cells by nuclear ERK signaling. *J. Biol. Chem.*, 282(6):4136–4151, Feb. 2007.

[305] J. Tsoi, L. Robert, K. Paraiso, C. Galvan, K. M. Sheu, J. Lay, D. J. L. Wong, M. Atefi, R. Shirazi, X. Wang, D. Braas, C. S. Grasso, N. Palaskas, A. Ribas, and T. G. Graeber. Multi-stage differentiation defines melanoma subtypes with differential vulnerability to Drug-Induced Iron-Dependent oxidative stress. *Cancer Cell*, 33(5):890–904.e5, May 2018.

[306] D. A. Tuveson, A. T. Shaw, N. A. Willis, D. P. Silver, E. L. Jackson, S. Chang, K. L. Mercer, R. Grochow, H. Hock, D. Crowley, S. R. Hingorani, T. Zaks, C. King, M. A. Jacobetz, L. Wang, R. T. Bronson, S. H. Orkin, R. A. DePinho, and T. Jacks. Endogenous oncogenic K-ras(G12D) stimulates proliferation and widespread neoplastic and developmental defects. *Cancer Cell*, 5(4):375–387, Apr. 2004.

[307] F. Uhlitz, A. Sieber, E. Wyler, R. Fritsche-Guenther, J. Meisig, M. Landthaler, B. Klinger, and N. Blüthgen. An immediate–late gene expression module decodes ERK signal duration. *Mol. Syst. Biol.*, 13(5):928, May 2017.

[308] E. B. Ünal, F. Uhlitz, and N. Blüthgen. A compendium of ERK targets. *FEBS Lett.*, 591(17):2607–2615, Sept. 2017.

[309] L. Valon, A. Davidović, F. Levillayer, A. Villars, M. Chouly, F. Cerqueira-Campos, and R. Levayer. Robustness of epithelial sealing is an emerging property of local ERK feedback driven by cell elimination. *Dev. Cell*, 56(12):1700–1711.e8, June 2021.

[310] M. van Rosmalen, M. Krom, and M. Merkx. Tuning the flexibility of Glycine-Serine linkers to allow rational design of multidomain proteins. *Biochemistry*, 56(50):6565–6574, Dec. 2017.

[311] P. Vandame, C. Spriet, F. Riquet, D. Trinel, K. Cailliau-Maggio, and J.-F. Bodart. Optimization of ERK activity biosensors for both ratiometric and lifetime FRET measurements. *Sensors*, 14(1):1140–1154, Jan. 2014.

[312] H. N. Vasudevan, P. Mazot, F. He, and P. Soriano. Receptor tyrosine kinases modulate distinct transcriptional programs by differential usage of intracellular pathways. *Elife*, 4, May 2015.

[313] H. N. Vasudevan and P. Soriano. Chapter Twenty-Three-A thousand and one receptor tyrosine kinases: Wherein the specificity? *Curr. Top. Dev. Biol.*, 117:393–404, 2016.

[314] J. D. Wade, X.-K. Lun, N. Zivanovic, E. O. Voit, and B. Bodenmiller. Mechanistic model of signaling dynamics across an epithelial mesenchymal transition. *Front. Physiol.*, 11:579117, Nov. 2020.

[315] C.-C. Wang, S. S. Bajikar, L. Jamal, K. A. Atkins, and K. A. Janes. A time- and matrix-dependent TGFBR3-JUND-KRT5 regulatory circuit in single breast epithelial cells and basal-like premalignancies. *Nat. Cell Biol.*, 16(4):345–356, Apr. 2014.

[316] W. Wang, Y. Zhang, P. Dettinger, A. Reimann, T. Kull, D. Loeffler, M. G. Manz, C. Lengerke, and T. Schroeder. Cytokine combinations for human blood stem cell expansion induce cell type- and cytokine-specific signaling dynamics. *Blood*, May 2021.

[317] H. Waterman, I. Sabanai, B. Geiger, and Y. Yarden. Alternative intracellular routing of ErbB receptors may determine signaling potency. *J. Biol. Chem.*, 273(22):13819–13827, May 1998.

[318] V. M. Weaver, O. W. Petersen, F. Wang, C. A. Larabell, P. Briand, C. Damsky, and M. J. Bissell. Reversion of the malignant phenotype of human breast cells in three-dimensional culture and in vivo by integrin blocking antibodies. *J. Cell Biol.*, 137(1):231–245, Apr. 1997.

[319] W. Wei, J. Jin, S. Schlisio, J. W. Harper, and W. G. Kaelin, Jr. The v-jun point mutation allows c-jun to escape GSK3-dependent recognition and destruction by the fbw7 ubiquitin ligase. *Cancer Cell*, 8(1):25–33, July 2005.

[320] R. A. Weinberg. The retinoblastoma protein and cell cycle control. *Cell*, 81(3):323–330, May 1995.

[321] A. Wells, J. B. Welsh, C. S. Lazar, H. S. Wiley, G. N. Gill, and M. G. Rosenfeld. Ligand-induced transformation by a noninternalizing epidermal growth factor receptor. *Science*, 247(4945):962–964, Feb. 1990.

[322] J. F. Wiesen, P. Young, Z. Werb, and G. R. Cunha. Signaling through the stromal epidermal growth factor receptor is necessary for mammary ductal development. *Development*, 126(2):335–344, Jan. 1999.

[323] H. S. Wiley. Decoding signal processing at the Single-Cell level. *Cell Syst*, 5(6):542–543, Dec. 2017.

[324] H. S. Wiley, J. J. Herbst, B. J. Walsh, D. A. Lauffenburger, M. G. Rosenfeld, and G. N. Gill. The role of tyrosine kinase activity in endocytosis, compartmentation, and down-regulation of the epidermal growth factor receptor. *J. Biol. Chem.*, 266(17):11083–11094, June 1991.

[325] H. S. Wiley, S. Y. Shvartsman, and D. A. Lauffenburger. Computational modeling of the EGF-receptor system: a paradigm for systems biology. *Trends Cell Biol.*, 13(1):43–50, Jan. 2003.

[326] M. Z. Wilson, P. T. Ravindran, W. A. Lim, and J. E. Toettcher. Tracing information flow from erk to target gene induction reveals mechanisms of dynamic and combinatorial control. *Mol. Cell*, 67(5):757–769.e5, Sept. 2017.

[327] R. Wisdom, R. S. Johnson, and C. Moore. c-jun regulates cell cycle progression and apoptosis by distinct mechanisms. *EMBO J.*, 18(1):188–197, Jan. 1999.

[328] I. Wortzel and R. Seger. The ERK cascade: Distinct functions within various subcellular organelles. *Genes Cancer*, 2(3):195–209, Mar. 2011.

[329] T. Yamamoto, M. Ebisuya, F. Ashida, K. Okamoto, S. Yonehara, and E. Nishida. Continuous ERK activation downregulates antiproliferative genes throughout G1 phase to allow cell-cycle progression. *Curr. Biol.*, 16(12):1171–1182, June 2006.

[330] C. Yang, C. Tian, T. E. Hoffman, N. K. Jacobsen, and S. L. Spencer. Melanoma subpopulations that rapidly escape MAPK pathway inhibition incur DNA damage and rely on stress signalling. *Nat. Commun.*, 12(1):1747, Mar. 2021.

[331] H. Yang, R. C. Adam, Y. Ge, Z. L. Hua, and E. Fuchs. Epithelial-Mesenchymal micro-niches govern stem cell lineage choices. *Cell*, 169(3):483–496.e13, Apr. 2017.

[332] J.-M. Yang, S. Bhattacharya, H. West-Foyle, C.-F. Hung, T.-C. Wu, P. A. Iglesias, and C.-H. Huang. Integrating chemical and mechanical signals through dynamic coupling between cellular protrusions and pulsed ERK activation. *Nat. Commun.*, 9(1):4673, Nov. 2018.

[333] S.-H. Yang, P. Shore, N. Willingham, J. H. Lakey, and A. D. Sharrocks. The mechanism of phosphorylation-inducible activation of the ETS-domain transcription factor elk-1. *EMBO J.*, 18(20):5666–5674, Oct. 1999.

[334] K. Yeung, T. Seitz, S. Li, P. Janosch, B. McFerran, C. Kaiser, F. Fee, K. D. Katsanakis, D. W. Rose, H. Mischak, J. M. Sedivy, and W. Kolch. Suppression of raf-1 kinase activity and MAP kinase signalling by RKIP. *Nature*, 401(6749):173–177, Sept. 1999.

[335] R. D. York, H. Yao, T. Dillon, C. L. Ellig, S. P. Eckert, E. W. McCleskey, and P. J. Stork. Rap1 mediates sustained MAP kinase activation induced by nerve growth factor. *Nature*, 392(6676):622–626, Apr. 1998.

[336] Y. Yu, X. Wang, X. Zhang, Y. Zhai, X. Lu, H. Ma, K. Zhu, T. Zhao, J. Jiao, Z.-A. Zhao, and L. Li. ERK inhibition promotes neuroectodermal precursor commitment by blocking self-renewal and primitive streak formation of the epiblast. *Stem Cell Res. Ther.*, 9(1):2, Jan. 2018.

[337] M. Zarrabi, E. Afzal, M. H. Asghari, M. Mohammad, H. A. Es, and M. Ebrahimi. Inhibition of MEK/ERK signalling pathway promotes erythroid differentiation and reduces HSCs engraftment in ex vivo expanded haematopoietic stem cells. *J. Cell. Mol. Med.*, 22(3):1464–1474, Mar. 2018.

[338] E. R. Zhang, S. Liu, L. F. Wu, S. J. Altschuler, and M. H. Cobb. Chemoattractant concentration–dependent tuning of ERK signaling dynamics in migrating neutrophils. *Sci. Signal.*, 9(458):ra122–ra122, 2016.

[339] J. Zheng, Z. Shi, P. Yang, Y. Zhao, W. Tang, S. Ye, Z. Xuan, C. Chen, C. Shao, Q. Wu, and H. Sun. ERK-Smurf1-RhoA signaling is critical for TGFβ-drived EMT and tumor metastasis. *Life Sci Alliance*, 5(10), Oct. 2022.

[340] Y. Zwang, A. Sas-Chen, Y. Drier, T. Shay, R. Avraham, M. Lauriola, E. Shema, E. Lidor-Nili, J. Jacob-Hirsch, N. Amariglio, Y. Lu, G. B. Mills, G. Rechavi, M. Oren, E. Domany, and Y. Yarden. Two phases of mitogenic signaling unveil roles for p53 and EGR1 in elimination of inconsistent growth signals. *Mol. Cell*, 42(4):524–535, May 2011.